Applying the Kolmogorov equation to the problem of subgrid modeling for Large-Eddy Simulation of turbulence

Le Fang

Année 2009

Thèse

pour obtenir

le titre de DOCTORAT

de

L'UNIVERSITE DE LYON

délivré par

L'ECOLE CENTRALE DE LYON

par

Le FANG

Applying the Kolmogorov equation to the problem of subgrid modeling for Large-Eddy Simulation of turbulence

---

Soutenance le 23 Juillet devant la Commission d'Examen

Jury:

M.	J.-P. Bertoglio	LMFA	- *Directeur de thèse*
M.	L. Shao	LMFA	
M.	P. Sagaut	Université Paris 6	- *Rapporteur*
M.	E. Levêque	ENS Lyon	- *Rapporteur*
Mme.	G. Cui	Université Tsinghua	

Abstract

The aim of the current work is to investigate a series of new subgrid models by employing the Kolmogorov equation of filtered quantities (KEF), which is an exact relation of turbulence in physical space.

Different formulations of KEF are derived, including the forms in velocity field (homogeneous isotropic turbulence, inhomogeneous anisotropic turbulence, homogeneous shear turbulence, homogeneous rotating turbulence), in scalar turbulence and in magnetohydrodynamic turbulence. The corresponding subgrid models are then formulated, for example:

- The multi-scale improvement of CZZS model.
- A new anisotropic eddy-viscosity model in homogeneous shear turbulence.
- The improved velocity increment model (IVI).
- The rapid-slow analysis and model application in inhomogeneous anisotropic scalar turbulence.
- The attempt in magnetohydrodynamic (MHD) turbulence.

Besides, there are also other important conclusions in this thesis:

- The anisotropic effect of mean shear in physical space is analyzed.
- Analytical corrections to the scaling of the second-order structure function in isotropic turbulence in introduced.
- It is shown that the two-point distance of velocity increment must be much larger than the filter size, in order to satisfy the classical scaling law. Otherwise, the classical scaling law can not be directly applied in subgrid modeling.
- A thought-experiment is described to analyse the time-reversibility problem of subgrid models.
- A rapid algorithm for Tophat filter operator in discrete field is introduced.

Acknowledgements

There are many people without whom this work would not have been possible. I would first like to thank my supervisor, Jean-Pierre Bertoglio, for taking me on as his student and allowing me to pursue my research interests, and for his support and friendship during the course of this thesis. He is, without question, a great master with genuine knowledge on turbulence. I would also like to thank my co-supervisor Liang Shao, who has quite good ideas for helping me improve my work. Besides I wish to thank him for teaching me a lot on the attitude of research. I would like to give a special thanks to Wouter. J. T. Bos, who helped me very much in both the work and the language. I'm really quite grateful for his kindness.

I want to thank the two referees of my manuscript, professor Pierre Sagaut and Dr. Emmanuel Levêque for the time and energy they have put in reading my manuscript and their interesting and valuable comments on my work.

Also I would like to thank professor Guixiang Cui, professor Zhaoshun Zhang and professor Chunxiao Xu. They helped me on both the work and the life when I was in Tsinghua University of China, and they are also concerned with my thesis. I am also grateful to professor Cui for accepting to be members of the jury.

Madam Benedicte Cuenot accpeted to be a member of the jury, but a serious illness prevents her from visiting Lyon. I really wish that she will recover soon.

I would like to thank my collaborators Chunhong Pan, professor Stephane Cotin, Dr. Hongtao Wang, Ying Wang and Yiyi Wei. The projects extend my vision and my undertanding of fluid mechanics.

My former classmates Xiaozhou Zhou and Yunke Yang helped me on some problems of my thesis. Wei Ma gave me lots of help with my articles. Aurelien Hemon corrected my french language in the abstract. Dr. Jérome Boudet helped me on the finite volumn method of large-eddy simulation.

Thanks also to the friends from Lyon, with a special mentioning of Dabing Luo and Chuantao Yin. They are the most close friends of mine, and they made the life in Lyon more than pleasant.

The most special thanks to my girl friend (and will be my wife soon) Jieying Hong, for her support in these three years, thank you. And of course to my parents, I dedicate this thesis to them.

Contents

List of Figures

Nomenclature

$\vec{b}, b_i$	Magnetic induction
C_f	Coefficient in velocity increment model
C_m	Coefficient in Matais-Lesieur model
C_s	Coefficient in Smagorinsky model
$\mathscr{D}$	Laplace operator in a moving coordinate system
D_{ll}	Second-order structure function of non-filtered velocity
$D_{ll}^<$	Second-order structure function of filtered velocity
D_{lll}	Third-order structure function of non-filtered velocity
$D_{lll}^<$	Third-order structure function of filtered velocity
$D_{\theta\theta}^<$	Second-order structure function of filtered scalar
$\mathscr{D}_{ii}^<$	Compensating structure function of filtered velocity
$E(k)$	Energy spectrum
$F(k)$	Forcing term in spectral space
F_n	n^{th} order structure function
$\mathscr{F}(k)$	Forcing term in physical space
G	Mean scalar gradient
$G(\vec{x})$	Filter kernel
h	Grid size
$J_{ij}^<$	Strain rate of resolved scale magnetic field
k, p, q	Wave number
k_c	Cut-off wave number
k_p	Characteristic wave number in von-Karman energy spectrum
L	Integrated scale
L_{ij}	Leonard stress tensor
n	Scaling exponent of the second-order structure function
$\vec{n}, n_i$	Unit vector in the normal dirction of the surface
p	Pressure
Pr	Prandtl number
Pr_t	Turbulent Prandtl number
Q_{ij}	Filtered velocity increment tensor
r	Two-point distance
R_{ij}	Correlation function of filtered velocity
Re	Renolds number
Ro	Rossby number
S	Surface of a local sphere
S_k	Skewness
$S_{ij}^<$	Strain rate of resolved scale turbulence
t	Temporal variable

$T(k)$	Energy transfer spectrum
$T_{l,ll}$	Subgrid energy transfer term in KEF
U	Mean velocity
$\vec{u}, u_i$	Velocity
V	Volumn of a local sphere
$\vec{x}, x_i$	Spatial variable
y	Coordinate in the normal direction of channel
y^+, Y^+	Normalized coordinate in the normal direction of channel
$\vec{z}, z_i$	Elsässer variable
γ	Mean shear
Δ	Filter size (except in chapter 5)
Δ	Grid size (only in chapter 5)
Δ'	Two-point distance used in velocity increment model
Δ_f	Filter size
$\delta\vec{u}$	Velocity increment
δ_{ij}	Kronecker Delta
ϵ_{ijk}	Levi-Civita symbol
ε	Total dissipation
$\varepsilon^<$	Resolved dissipation
ε_f	Subgrid dissipation
$\vec{\zeta}, \zeta_i$	Spatial variable in a moving coordinate system
$\zeta(n)$	Scaling exponent of n^{th} order structure function
η	Kolmogorov scale (except in chapter 6)
η	Magnetic diffusivity (only in chapter 6)
θ	Scalar (except in Sec. 2.4.3)
κ	Molecular diffusivity
κ_t	Eddy diffusivity
ν	Molecular viscosity
ν_t	Eddy viscosity
ξ, ξ_i	Two-point distance in KEF
τ	Temporal variable in a moving coordinate system
$\tau_{ij}^<, \tau_{ij}$	Subgrid stress tensor
τ_{ij}^b	Subgrid stress tensor in magnetic field of MHD
τ_{ij}^u	Subgrid stress tensor in velocity field of MHD
$\tau_{\theta j}$	Subgrid scalar flux
Ω	Rotating rate

Chapter 1

Introduction

The large-eddy-simulation (LES) technique of turbulent flows is now recognized as a powerful tool, and the applications in several engineering fields are becoming more and more frequent. This technique has been developed during the past 40 years, aiming at solving the large-scale structures by employing a subgrid-scale (SGS) model. Large and small scales are isolated by a filtering operation, which can either be in physical or spectral space. The filtered velocity field represents the motion of large eddies, and the subgrid motions are denoted by the SGS stress tensor in the filtered Navier-Stokes equations. [1, 2]

The spirit of LES is to model the subgrid motion by using the information contained in the resolved quantities, so as to calculate the resolved part by direct numerical simulation (DNS) and calculate the subgrid part by using SGS models. In this thesis, we consider each subgrid modeling has two steps:

1. Any subgrid model must be based on a certain assumption on the subgrid motion, *i.e.* assume a formulation for subgrid quantities (especially, subgrid stress). However, there are always undetermined factors in this assumption.

2. A complete subgrid model must employ a certain method to determine the unknown factors mentioned in the first step.

Various assumptions for subgrid tensor were introduced, such as the eddy-viscosity assumption [3], the formulation of scale-similarity [4], the gradient diffusion assumption [5] and the formulation of velocity increment [6]. The details of these assumptions will be shown at the beginning of chapter 4. What should an assumption aim at?

As we know, it is impossible to simulate the "correct" subgrid motion in each discrete point. Usually the subgrid assumptions focus on two physical behaviors: first, a proper dissipation, which could represent the strong dissipative effect at small scales, is a direct conclusion of the kinetic energy equation, and is also quite important for numerical stability [7]; second, some physical mechanism, *i.e.* the interaction between resolved and subgrid scales, usually representing some self-similarity behaviors in inertial subrange, which can accurately describe the physical properties in high Reynolds number turbulence [8, 9]. However, few subgrid assumptions can satisfy both these conditions. For instance, the scale-similarity assumption [4] has very good relativity, but it does not generate enough subgrid dissipation. Other pure dissipative models, such as the implicit model (MILES) [10], could not satisfy the correct physical mechanism. In chapter 3 of this thesis, we utilize the eddy-viscosity assumption since it usually dissipates well. Besides, the velocity increment assumption, which denotes a two-point self-similarity between scales, is employed in chapter 4 of this thesis.

From many existed assumptions, we can find that each assumption could assume a relation between subgrid and resolved motions, but the subgrid motion could not be completely fixed by this assumption. For example, in eddy-viscosity assumption the subgrid eddy viscosity can not be determined, and in velocity increment assumption the dynamic coefficient can not be determined. It indicates that a certain method must be applied to achieve closure. Thus, a complete "pure" subgrid modeling should contain both the assumption and the method.

The concepts of "method" and "model" are usually confused in many researches. In this thesis, we would like to point out that the "methods", which could determine the coefficients of an assumption, can not be considered as complete "models". For instance, the coefficient of eddy-viscosity assumption could be estimated by using either EDQNM theory [8] or Germano procedure [11], and they should only be considered as different "methods". One method can also be applied in different assumptions, for instance both the eddy viscosity and the coefficient of velocity increment assumption can be determined by Germano procedure [6, 11].

Many "methods" are already available and will be introduced as a background in the next section, including mathematical methods and the physical methods in spectral and physical spaces. In Sec. 1.1.1 we review various mathematical methods

employed in practical LES modeling [12–14]. Besides, the physical theory in spectral space, introduced by Kraichnan [15, 16] and employed in many spectral SGS models, will be introduced in Sec. 1.1.2. In addition, we review the Kolmogorov's theory in physical space. The original K41 theory is available for homogeneous isotropic turbulence for non-filtered field [9]. Furthermore, Meneveau's work showed that it is possible to apply the Kolmogorov's theory in SGS modeling, since the Kolmogorov equation describes a physical law that should be satisfied in LES [17]. However, few works are proposed to derive subgrid models in physical space from Kolmogorov's theory. In section 1.1.3 we will introduce the existed works.

1.1 Background

1.1.1 Mathematical methods in large-eddy simulation

The Galilean invariance for the spatial filtering approach was employed to determine the unknown coefficient of scale-similarity model [4]. Although the result is corrected in later works [18, 19], this method could be considered as an important attempt of mathematical methods in LES.

One of the most famous mathematical tools in subgrid modeling is the Germano procedure based on Germano identity [12]. It is based on the decomposition of filter operations. When applied at two filters, it can be named as the multiplicative Germano identity [20]. It can also be extended to the case of N filter levels, *i.e.* the multilevel Germano identity [21]. Germano identity represents the characteristics of filters and provides a dynamic method to determine the undetermined factors.

There are also researchers who introduced other mathematical methods to provide subgrid models. For example, a series of regularized methods are introduced by Holm *et al.* [14, 22]. The regularization is achieved by imposing an energy penalty which damps the scales smaller than a threshold scale α, while still allowing for non linear sweeping of the small scales by the largest ones. The regularization appears as a non-linearly dispersive modification of the convection term in the Navier-Stokes equations.

Generally speaking, these mathematical methods try to provide mathematical approach in subgrid modeling. The lack of physical background is an obvious disadvantage, which may lead to numerical unstability. For instance as discussed in Lesieur [8], the Germano procedure can yield strongly varying coefficient value and

the corresponding model may be unstable. Many researchers believe that a well-performing subgrid model should be derived from physical properties, so as to ensure the turbulent behavior. In these studies, the most widely applied method is Kraichnan's theory in spectral space.

1.1.2 Kraichnan's spectral theory in LES

The spirit Kraichnan's original theory is the triad interaction between three wave vectors, which causes the energy transfer between scales. When employ this theory in LES, different types of triad interactions in subgrid transfer should be considered: local triads and non-local triads. Local triads correspond to interactions among wave vectors of neighboring modules, and therefore to interactions among scales of slightly different sizes. In contrast, non-local triads are all those other interactions, i.e. interactions among scales of widely differing sizes.

Another important result of this Kraichnan's theory is the energy backscatter, which corresponds to non-local triad of the R type according to Waleffe's classification [23]. It denotes a backward kinetic energy cascade, which is not mentioned from Kolmogorov 1941 (K41) theory. Waleffe refines the analysis of this phenomenon: a very large part of the energy is transferred locally from the intermediate wave number located just ahead of the cutoff toward the larger wave number just after it, and the remaining fraction of energy is transferred to the smaller wave number. The energy backscatter has also been verified in numerical cases [24–26]. In the research of large-eddy simulation, it is also important to evaluate the backscatter properties of subgrid models.

Kraichnan's theory was further developed by Orszag [27] as an analytical closure, named as Eddy-Damped Quasi Normal Markovian (EDQNM). In LES, the EDQNM theory can also help us in subgrid modeling. In spectral space, Chollet and Lesieur proposed an effective viscosity model using the results of EDQNM, i.e. the spectral eddy-viscosity model [28]. The asymptotic value of the effective viscosity is extended to the case of spectra of slope $-m$ by Metais and Lesieur [29]. Bertoglio proposed a spectral stochastic subgrid model based on the EDQNM analysis, which could represent the backward energy transfer [30]. The spectral result could also be employed

into physical space, for instance the structure function model proposed by Metais and Lesieur [29].

In general, with a certain assumption, for example by assuming eddy-viscosity, we could employ spectral analysis to determine the unknown subgrid statistical quantities dynamically. Especially with the help of EDQNM theory in spectral space, great success has been obtained in subgrid modeling. However, the formulations of these models are in spectral space, and there are few researches in physical space. Therefore, in the next section, we introduce one of the most important turbulent theories in physical space and its applications in large-eddy simulation.

1.1.3 Kolmogorov's theory of physical space and applications in LES

Kolmogorov's theory (K41) [9] was introduced much earlier than Kraichnan's spectral theory. The spirit of K41 theory is the four-fifth law, which represents the energy transfer property between two points. This four-fifth law could be written as a formulation of Kolmogorov equation. There are already lots of work on extending this theory. For instance, it was extended into passive scalar by Yaglom [31]. In addition, in K41 theory, the two-point statistical quantities, *i.e.* the structure functions, require the recognition of scaling law, which also attracted lots of researchers [32–37]. However, most these works focus on non-filtered fields, and few works are done for the filtered fields in LES.

The importance of Kolmogorov equation in LES is emphasized by Meneveau [17]. He derived the formulation of Kolmogorov equation of filtered velocity, and regarded it as a necessary condition in LES. It can also be considered as a method for evaluating two-point subgrid model behaviors.

The first attempt in subgrid modeling by employing Kolmogorov equation is the CZZS model by Cui *et al.* [38]. With eddy-viscosity assumption, the eddy viscosity could be determined dynamically. Furthermore, the simplification of CZZS model yields the skewness-based models [39]. However, these methods are still new and have not been well developed. In this thesis, we continue this method and have published more results [40–43]. The main structure of the thesis is described in the next section.

1.2 Structure of the thesis

As introduced in the last section, the SGS modeling methods in physical space has not been well developed yet. Therefore, in this thesis, we primarily aim at summarizing and investigating new modeling methods in physical space, by employing the Kolmogorov equation for the filtered quantities (KEF).

In chapter 2, various formulations of KEF for different cases of flows are derived. The formulation in homogeneous isotropic turbulence, introduced by Meneveau [17] and Cui *et al.* [38], is analyzed mainly on the energy budget with different filter sizes and two-point distances. The formulation in inhomogeneous anisotropic turbulence contains rapid and slow terms, which could be considered as a complete form of KEF, but too complex to be applied in subgrid modeling. Two more simple cases are the homogeneous shear flow and the rotating turbulence, the former in which is analyzed particularly. Comparing with the classical analysis for the correlation functions in spectral space, we investigate the shear effect in physical space. The anisotropic properties of structure function between different directions are emphasized. Besides, in order to employ the classical scaling law, we study the behavior of filtered structure functions, in physical and spectral spaces, respectively.

In chapter 3, we employ KEF on eddy-viscosity models. With homogeneous isotropic assumption, the CZZS model is further discussed. Various subgrid models are proposed and verified in numerical cases. Similar as Germano procedure, another dynamic method is introduced to determine the coefficient of Smagorinsky model, which is much less expensive in terms of computational cost and has clear physical background. In homogeneous anisotropic turbulence, for instance the rotating turbulence and wall-bounded shear turbulence, a new anisotropic model is derived. *A Posteriori* tests are made to evaluate this model. The most important advantage is that the mean velocity is explicitly contained in the formulation of subgrid eddy viscosity.

In chapter 4, another assumption of subgrid stress is introduced, i.e. the velocity increment assumption. Comparing with eddy-viscosity assumption, this two-point assumption is easier to be combined with KEF, which is also a two-point equation. The improved increment model (IVI) is then derived, by employing KEF to determine the model coefficient dynamically. In real flow, when scales are not well separated,

the model coefficient has a dynamic form; in ideal high Reynolds number turbulence, we could obtain a constant coefficient. This model is extremely simple and low cost. The IVI model is verified in *A Priori* and *A Posteriori* tests.

In chapter 5, KEF is employed in anisotropic eddy-diffusivity models of passive scalar. The transfer processes of scalar energy and scalar flux are mainly investigated. We split the subgrid scalar flux into rapid and slow parts, and do *A Priori* tests on them in a channel Couette flow. The new anisotropic eddy-diffusivity model based on KEF is then verified for its properties of reproducing subgrid scalar dissipation. As a side result, we also analyze the ability of the scale-similarity model to properly reproduce the rapid part of the subgrid term, extending the approach of Shao *et al.* to the case of a scalar field.

In chapter 6, dynamic subgrid models in magnetohydrodynamic turbulence are derived by employing KEF. The magnetic field is coupled with velocity field, but the similar Kolmogorov equation could be obtained. Thus the subgrid eddy viscosity and magnetic diffusivity could be determined by various methods. The models are verified in A Posteriori tests of homogeneous decaying turbulence.

In chapter 7, we give the conclusion.

Chapter 2

Formulations of Kolmogorov equation of filtered velocity (KEF)

This chapter primarily focus on the basic concepts and equations of the Kolmogorov equation of filtered velocity (KEF). In Sec. 2.1, the concepts of filter and ensemble average are introduced. From Sec. 2.2 to 2.5 we derive the different formulations of KEF: the formulation in homogeneous isotropic turbulence is shown in Sec. 2.2 and the formulation in general inhomogeneous anisotropic turbulence is shown in Sec. 2.3; however the general anisotropic formula is too complicated, and two simplified cases are discussed in Sec. 2.4 and 2.5 respectively. Besides, the scaling law of filtered velocity is discussed, which could be employed to simplify the isotropic formulation in the following chapters.

2.1 Filter and ensemble average

In this thesis, the operators of filter and ensemble average should be clarified. They could be applied to any physical variable ϕ. A filter operator divides the variable into two parts:

$$\phi = \phi^{<} + \phi^{>} \tag{2.1}$$

in which $\phi^{<}$ is the grid-scale (GS) part (or resolved part) and $\phi^{>}$ is the subgrid-scale (SGS) part. In this thesis we only consider the spatial filters, and do not consider time-dependent temporal filters. A filter in physical space can be represented by introducing a filter kernel

$$\int G(\vec{x} - \vec{x}')d\vec{x}' = 1, \tag{2.2}$$

and the GS part ($\phi^<$) could be denoted as

$$\phi^<(\vec{x}) = \int G(\vec{x} - \vec{x}')\phi(\vec{x}')d\vec{x}'. \tag{2.3}$$

In general, the filter operator has the following properties:

$$\begin{aligned} (\phi + \psi)^< =& \phi^< + \psi^<, \\ \left(\frac{\partial \phi}{\partial t}\right)^< =& \frac{\partial \phi^<}{\partial t}. \end{aligned} \tag{2.4}$$

Besides, $\phi^{<<} \neq \phi^<, (\phi^<)^> \neq 0$ except when filter is performed with a spectral cutoff filter, which is an exact low-pass filter in spectral space.

By contraries, the ensemble average operator is defined in full-developed turbulence. Every physical variable can be divided into the mean part and the fluctuating part:

$$\phi = \langle \phi \rangle + \phi' \tag{2.5}$$

in which the symbol $\langle\rangle$ is the arithmetic mean from experiments.

Comparing with the filter operator, the ensemble average has different properties:

$$\begin{aligned} \langle \phi + \psi \rangle =& \langle \phi \rangle + \langle \psi \rangle \\ \left\langle \frac{\partial \phi}{\partial s} \right\rangle =& \frac{\partial \langle \phi \rangle}{\partial s}, s = \vec{x}, t \\ \langle \langle \phi \rangle \rangle =& \langle \phi \rangle \\ \langle \phi' \rangle =& 0 \end{aligned} \tag{2.6}$$

The symbol $\langle\rangle$ represents a linear operation, thus the following commutations can be obtained:

$$\langle \phi \rangle^< = \langle \phi^< \rangle, \left\langle \frac{\partial \phi}{\partial x_i} \right\rangle = \frac{\partial \langle \phi \rangle}{\partial x_i}. \tag{2.7}$$

However, filtering and differentiation do not commute when the filter width is nonuniform in space [44]. A general class of commutative filters was introduced by Vasilyev [45] and Marsden [46] to decrease the commutation error in LES equations, especially for inhomogeneous filter width. Leonard et al. [47] studied the commutation error with time-dependent filter width. In this thesis, we assume that the meshes are homogeneous, so that the filtering and differentiation could commute:

$$\left(\frac{\partial \phi}{\partial x_i}\right)^< = \frac{\partial \phi^<}{\partial x_i} \tag{2.8}$$

2.2 KEF in homogeneous isotropic turbulence

The formulation of KEF in homogeneous isotropic turbulence was derived by Meneveau [17] and Cui [38]. The process of deviation in details is shown in appendix A. From the filtered Navier-Stokes (N-S) equation and with only the assumptions of isotropy and homogeneity, we can obtain the original Karman-Howarth equation of filtered velocity:

$$\frac{\partial\langle(u_1^<)^2\rangle}{\partial t}-\frac{1}{2}\frac{\partial D_{ll}^<}{\partial t}=\frac{1}{6\xi^4}\frac{\partial}{\partial\xi}(\xi^4 D_{lll}^<)-\frac{\nu}{\xi^4}\frac{\partial}{\partial\xi}\left(\xi^4\frac{\partial D_{ll}^<}{\partial\xi}\right)-\frac{1}{\xi^4}\frac{\partial}{\partial\xi}(\xi^4 T_{l,ll}), \tag{2.9}$$

in which the subscript l denotes a component in the direction of the two-point distance $\vec{\xi}$. Notice that in homogeneous isotropic turbulence, $\vec{u}=\vec{u}'$, thus the primes are ignored. Define the velocity increment $\delta\vec{u}(\vec{x},\vec{\xi})=\vec{u}(\vec{x}+\vec{\xi})-\vec{u}(\vec{x})$. In equation (2.9), $D_{ll}^<(\xi)=\langle\delta u_1^<(\xi)\delta u_1^<(\xi)\rangle$ is the second order longitudinal structure function, $D_{lll}^<(\xi)=\langle\delta u_1^<(\xi)\delta u_1^<(\xi)\delta u_1^<(\xi)\rangle$ is the third order longitudinal structure function, and $T_{l,ll}(\xi)=\langle u_1^<(x_1)\tau_{11}^<(x_1+\xi)\rangle$ is the subgrid energy transfer.

In order to simplify the first term in equation (2.9), we write the filtered N-S equation:

$$\frac{\partial u_i^<}{\partial t}+u_j^<\frac{\partial u_i^<}{\partial x_j}=-\frac{1}{\rho}\frac{\partial p^<}{\partial x_i}+\nu\frac{\partial^2 u_i^<}{\partial x_j\partial x_j}-\frac{\partial\tau_{ij}^<}{\partial x_j}, \tag{2.10}$$

in which the subgrid stress is defined in a implicit form:

$$\tau_{ij}^<=(u_iu_j)^<-u_i^<u_j^<. \tag{2.11}$$

The decay of turbulent kinetic energy in resolved scale turbulence could be represented as

$$\frac{\partial(u_i^<)^2}{\partial t}+u_j^<\frac{\partial(u_i^<)^2}{\partial x_j}=-2\nu\frac{\partial u_i^<}{\partial x_j}\frac{\partial u_i^<}{\partial x_j}+2\tau_{ij}^<S_{ij}^<+\frac{\partial}{\partial x_j}\left(\nu\frac{\partial(u_i^<)^2}{\partial x_j\partial x_j}-2\tau_{ij}^<u_i^<-\frac{2}{\rho}p^<u_j^<\right), \tag{2.12}$$

where $S_{ij}^<$ the strain rate of resolved scale turbulence

$$S_{ij}^<=\frac{1}{2}\left(\frac{\partial u_i^<}{\partial x_j}+\frac{\partial u_j^<}{\partial x_i}\right). \tag{2.13}$$

After ensemble averaging in homogeneous isotropic turbulence, this becomes

$$\frac{\partial\langle(u_1^<)^2\rangle}{\partial t}=-\frac{2}{3}\varepsilon^<+\frac{2}{3}\langle\tau_{ij}^<S_{ij}^<\rangle, \tag{2.14}$$

where $\varepsilon^{<} = \nu \left\langle \frac{\partial u_i^{<}}{\partial x_j} \frac{\partial u_i^{<}}{\partial x_j} \right\rangle$ is the resolved dissipation. $-\langle \tau_{ij}^{<} S_{ij}^{<} \rangle$ is the subgrid dissipation, denoted as ε_f.

Substituting equation (2.14) into equation (2.9) and integrating it over ξ, and neglecting the time-dependent term with the assumption of steadiness of the small scale turbulence in the classic Kolmogorov equation, we obtain the formulation of KEF in homogeneous isotropic turbulence:

$$-\frac{4}{5}\varepsilon_f \xi - \frac{4}{5}\varepsilon^{<}\xi = D_{lll}^{<} - 6T_{l,ll} - 6\nu \frac{\partial D_{ll}^{<}}{\partial \xi}. \tag{2.15}$$

When Reynolds number is high, the molecular viscosity could be neglected, therefore the KEF in high Reynolds number turbulence reads:

$$-\frac{4}{5}\varepsilon_f \xi = D_{lll}^{<} - 6T_{l,ll}. \tag{2.16}$$

In order to represent this equation by using only 11 component, we propose Meneveau's method [17]. Neglecting the molecular terms in equation (2.9) leads to

$$\frac{\partial \langle (u_1)^{<2} \rangle}{\partial t} = \frac{1}{6\xi^4} \frac{\partial}{\partial \xi} (\xi^4 D_{lll}^{<}) - \frac{1}{\xi^4} \frac{\partial}{\partial \xi} (\xi^4 T_{l,ll}). \tag{2.17}$$

In this equation, the following relations are satisfied:

$$\begin{aligned}
D_{lll}|_{\xi=0} &= 0, \\
\frac{D_{lll}}{\xi}|_{\xi\to 0} &\propto \xi^2 = 0, \\
\frac{\partial D_{lll}}{\partial \xi}|_{\xi=0} &\propto \xi^2 = 0, \\
T_{l,ll}|_{\xi=0} &= 0, \\
\frac{T_{l,ll}}{\xi}|_{\xi\to 0} &= \frac{T_{lll}(\xi) - T_{lll}(0)}{\xi}|_{\xi\to 0} = -\langle S_{11}^{<} \tau_{11} \rangle, \\
\frac{\partial T_{l,ll}}{\partial \xi}|_{\xi=0} &= -\langle S_{11}^{<}(x_1) \tau_{11}(x_1+\xi) \rangle |_{\xi=0} = -\langle S_{11}^{<} \tau_{11}^{<} \rangle .
\end{aligned} \tag{2.18}$$

From equation (2.17) and (2.18), we could obtain

$$\frac{\partial \langle (u_1)^{<2} \rangle}{\partial t} = 5 \langle S_{11}^{<} \tau_{11}^{<} \rangle . \tag{2.19}$$

Therefore, the formulation of KEF could also be written as

$$6\,\langle S_{11}^{<}\tau_{11}^{<}\rangle\,\xi = D_{lll}^{<} - 6T_{l,ll}. \tag{2.20}$$

In homogeneous isotropic turbulence, if we select the two-point distance ξ in x_1 direction, the equation is simplified to denote the behavior in one direction, that is

$$6\,\langle S_{11}^{<}\tau_{11}^{<}\rangle\,\xi = D_{111}^{<} - 6T_{1,11}. \tag{2.21}$$

Note that $T_{l,ll}$ is a correlation term between $u_1(x)$ and $\tau_{11}(x+\xi)$, it tends to 0 when ξ is large. From scaling law, we can also obtain $T_{l,ll} = 0$ in inertial subrange [17]. As will be discussed in Sec. 2.6, when $\xi \gg \Delta$, this term could vanish and the KEF formulation is

$$-\frac{4}{5}\varepsilon_f\xi = D_{lll}^{<}. \tag{2.22}$$

This quite simple formulation is applied in the ideal modeling analysis in this thesis.

2.2.1 Energy budget and error analysis in physical space

In order to show the two-point energy budget in physical space, two DNS cases of homogeneous isotropic turbulence with spectral method are used for *A Priori* test. The computation domain has 256^3 grid points. The grid size is denoted as h. The two different Reynolds numbers Re_λ are 50 and 70. The description in detail will be shown in section 4.3.1 and in the appendix.

We apply the Kolmogorov equation at the filter size, i.e. $\xi = \Delta = \pi/k_c$, to find where the equation is well satisfied. The energy budget with different filter sizes is shown in Fig. 2.1(a). The error of energy transfer is defined as

$$T^{\mathrm{error}} = D_{lll}^{<} - 6T_{l,ll} + \frac{4}{5}\varepsilon_f\xi, \tag{2.23}$$

which is shown in Fig. 2.1(b), normalized by the subgrid dissipation term. The minimum error occurs in the region where the filter Δ/η is neither too large nor too small, with η being the Kolmogorov scale. This region could be considered as the inertial subrange. It is about $10 < \Delta/\eta < 30$. However, because the Reynolds numbers are not large enough, this region is not obvious to distinguish, and the energy transfer equation is not quite well satisfied. The compensated energy spectra of DNS cases are shown in Fig. 2.2, where the plateaus represent the inertial subrange

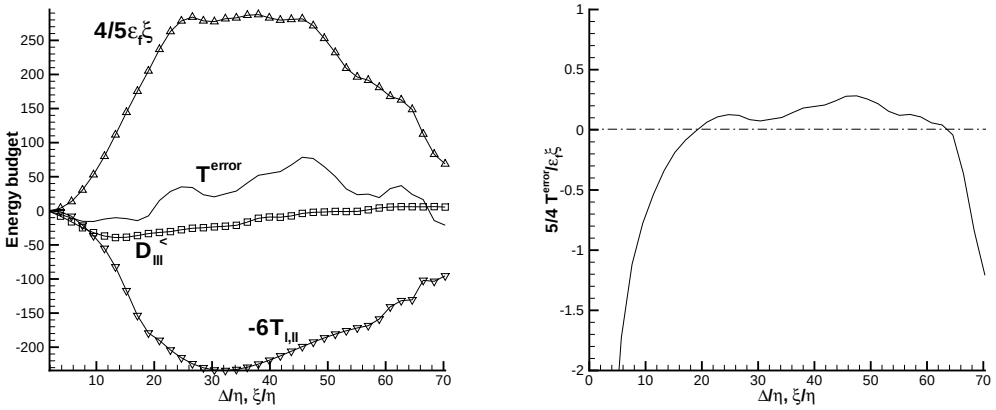

(a) (b)

Figure 2.1: Exact two-point energy transfer budget in homogeneous isotropic turbulence. Filter size $\Delta = \xi$. Solid line: $Re_\lambda = 50$; dashed line: $Re_\lambda = 70$. (a) Verification of each term in Kolmogorov equation of filtered velocity. (b) Error of subgrid energy transfer, normalized by the subgrid dissipation term.

in spectral space. Although not obvious, the corresponding wave number is about $0.1 < k_c\eta < 0.3$. According to the two cases, the region is wider when Reynolds number is higher. In addition, the integrated scale $L \sim 70\eta$ in the two cases, thus we could reasonably consider that $\Delta = \xi \ll L$ in the region of minimum error. Anyway, the inertial subrange exists when $\eta \ll \Delta = \xi \ll L$. If the filter is in the dissipative range, the resolved dissipation can not be neglected; if the filter size is larger than 30η, the error is still acceptable from Fig. 2.3(b), however, the filter size is not small enough compared with the integrated scale, and we can not easily consider it the inertial subrange.

Notice that ξ and Δ are independent. Thus we can fix a filter size Δ, and search for a suitable two-point distance ξ to minimize the error. The filter size is given as $\Delta = 8h$, which is about 15.2η when $\mathrm{Re}_\lambda = 50$, and 26.3η when $\mathrm{Re}_\lambda = 70$. Both filter sizes are much greater than Kolmogorov scale and do not need a correction. The budget of the two-point energy transfer with different two-point distances is shown in Fig. 2.3(a). The minimum error occurs in the region where the two-point distance $\xi \sim \Delta$. Thus with a suitable filter size $10 < \Delta/\eta < 30$, it seems reasonable to apply $\xi = \Delta$. This minimized error strongly supports the corresponding subgrid modeling.

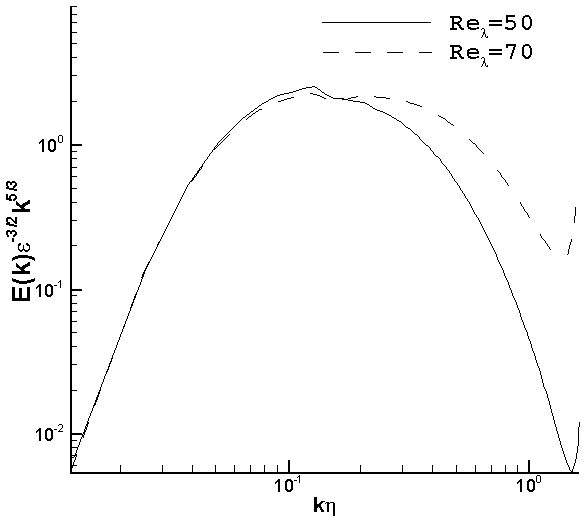

Figure 2.2: Compensate energy spectrum in homogeneous isotropic turbulence. Solid line: $\mathrm{Re}_\lambda = 50$; dashed line: $\mathrm{Re}_\lambda = 70$.

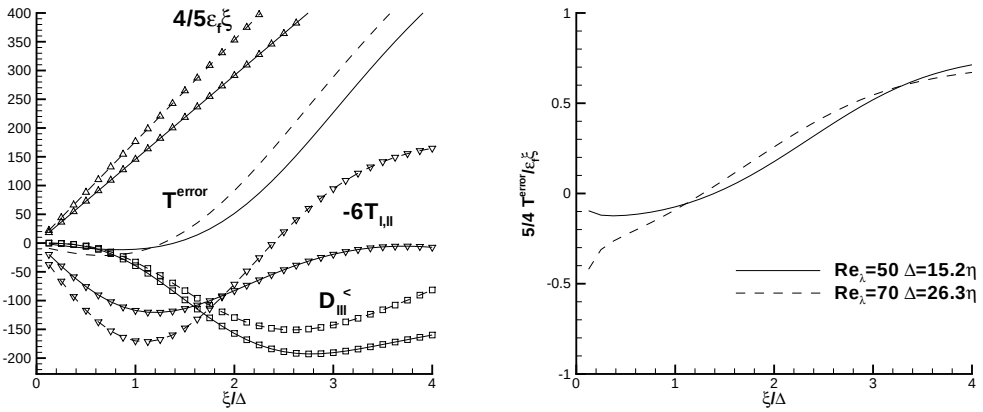

(a) (b)

Figure 2.3: Exact two-point energy transfer budget in homogeneous isotropic turbulence. Filter size $\Delta = 8h$. Solid line: $Re_\lambda = 50$, $\Delta = 15.2\eta$; dashed line: $Re_\lambda = 70$, $\Delta = 26.3\eta$. (a) Verification of each term in Kolmogorov equation of filtered velocity. (b) Error of subgrid energy transfer, normalized by the subgrid dissipation term.

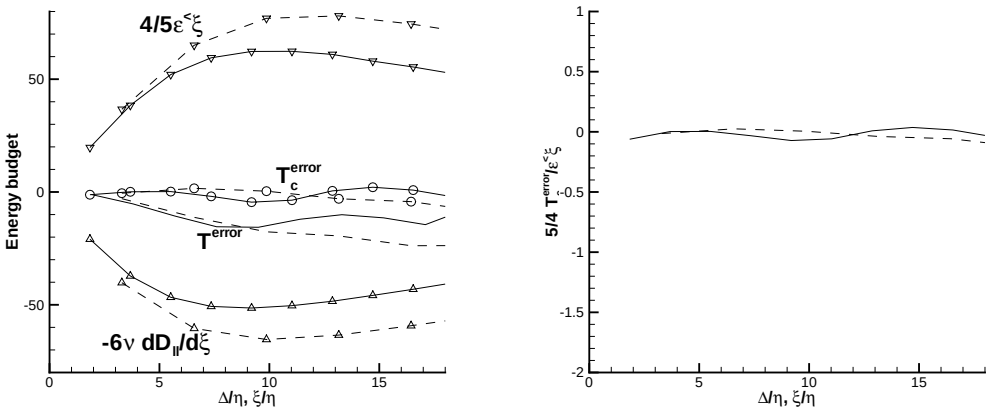

(a) (b)

Figure 2.4: Exact two-point energy transfer with small filter size budget in homogeneous isotropic turbulence. Filter size $\Delta = \xi$. Solid line: $Re_\lambda = 50$; dashed line: $Re_\lambda = 70$. (a) Verification of the correction terms in Eq. (2.15). (b) Corrected error of two-point energy transfer, normalized by the resolved dissipation term.

In Fig. 2.1, we find that the great error in the region $\Delta/\eta < 15$ can be corrected by considering the viscous effects of the resolved part. From equation (2.15), the corrected error value can then be calculated as

$$T_c^{\text{error}} = D_{lll}^{<} - 6T_{l,ll} + \frac{4}{5}\varepsilon_f\xi - 6\nu\frac{\partial D_{ll}^{<}}{\partial\xi} + \frac{4}{5}\varepsilon^{<}\xi. \tag{2.24}$$

The last two terms and the corrected error value are shown in Fig. 2.4, in the region $\Delta/\eta < 15$. The error is obviously reduced, comparing with the original T^{error} term in Fig. 2.4(a). And in Fig. 2.4(b), the nondimensional value is approximately zero. It means that the Kolmogorov equation of filtered velocity for LES (2.15) can only fit for a filter size much greater than Kolmogorov scale. Otherwise, viscous corrections are necessary.

In fact the analysis in this section is very rough, while there are lots of errors: low Reynolds number, forcing, statistical samples ... However the analysis also shows that there is a region where the KEF is satisfied, thus we can employ KEF in subgrid modeling in this region. Also in this region, even when we neglect the molecular viscosity at low Reynolds number, the two-point distance $\xi = \Delta$ can be acceptable in subgrid modeling.

2.2.2 Energy budget analysis in spectral space

In order to analyze the Kolmogorov equation in spectral space, in forced turbulence we can write the energy transfer equation as

$$\frac{dE(k)}{dt} = -2\nu k^2 E(k) + T(k) + F(k) = 0, \tag{2.25}$$

in which $E(k)$ is the energy spectrum, $T(k)$ is the energy transfer spectrum, and we force the system by keeping the energy constant for $k < k_f$, i.e. the forcing term is

$$F(k) = \begin{cases} 2\nu k^2 E(k) - T(k), & k < k_f, \\ 0, & k \geq k_f. \end{cases} \tag{2.26}$$

Also we can write the equation for the second-order structure function in forced turbulence:

$$D^<_{ll}(\xi) - 6T_{l,ll}(\xi) - 6\nu \frac{dD^<_{ll}(\xi)}{dr} + \mathscr{F}^<(\xi) = 0, \tag{2.27}$$

where $\mathscr{F}(\xi)$ is the corresponding forcing term, which can be represented as the dissipative terms and time-dependent terms in decaying turbulence. In order to calculate the terms in Eq. 2.27, we have the following relations:

$$\begin{aligned} D^<_{ll}(\xi) =& 12\xi \int_0^\infty T^<(k) g(k\xi) dk, \\ \frac{dD^<_{ll}(\xi)}{d\xi} =& 4 \int_0^\infty k E^<(k) f(k\xi) dk, \\ \mathscr{F}^<(\xi) =& 12\xi \int_0^\infty F^<(k) g(k\xi) dk, \\ T_{l,ll}(\xi) =& \frac{1}{6}\left(D^<_{ll}(\xi) - 6\nu \frac{dD^<_{ll}(\xi)}{d\xi} + \mathscr{F}^<(\xi) \right), \end{aligned} \tag{2.28}$$

in which

$$\begin{aligned} f(k\xi) =& -\frac{\sin(k\xi)}{(k\xi)^2} - \frac{3\cos(k\xi)}{(k\xi)^3} + \frac{3\sin(k\xi)}{(k\xi)^4}, \\ g(k\xi) =& \frac{3\sin(k\xi) - 3kr\cos(k\xi) - (k\xi)^2 \sin(k\xi)}{(k\xi)^5}. \end{aligned} \tag{2.29}$$

The spectra of $E(k)$ and $T(k)$ are generated using EDQNM calculation by W.J.T. Bos. The corresponding terms in very high Reynolds number turbulence are shown

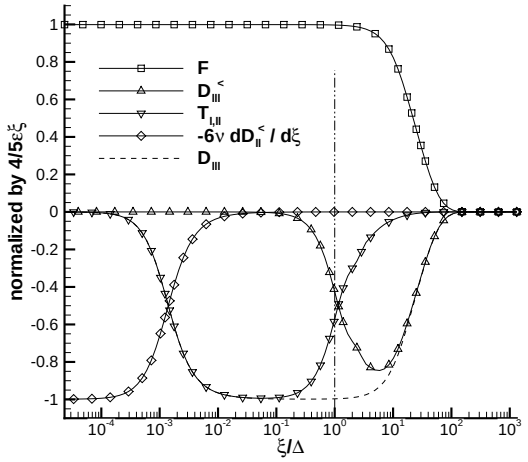

Figure 2.5: Normalized two-point energy budget of forced turbulence for filtered ($<$) and full velocity field (without $<$). EDQNM calculation. The vertical line indicates the location of filter size.

in Fig. (2.5). The symbol r is the same as the two-point distance ξ. The vertical line indicates the location of the filter size Δ. The forcing term is almost equal to $4/5\varepsilon\xi$, or say $4/5\varepsilon^{<}\xi$ because of high Reynolds number. The $T_{l,ll}$ term is the same order as $D^{<}_{lll}$ when $\xi = \Delta$, and tends to zero when ξ is large. The viscosity term only takes effect at very small distance, and can be neglected when ξ is the same magnitude as Δ. Another fact is shown that there is only quite short range in which the scaling law $D^{<}_{lll}(\xi) \propto \xi$ is satisfied, since no obvious plateau of $D^{<}_{lll}(\xi)/\xi$ is shown in this figure. This fact will also be discussed in Sec. 2.6 for more details.

2.3 KEF in inhomogeneous anisotropic turbulence

In inhomogeneous anisotropic turbulence, the mean velocity is not zero and should should be focused on. The N-S equation of velocity fluctuation can be written as

$$\frac{\partial u_i'}{\partial t} + \frac{\partial u_i' \langle u_j \rangle}{\partial x_j} + \frac{\partial \langle u_i \rangle u_j'}{\partial x_j} = -\frac{1}{\rho}\frac{\partial p'}{\partial x_i} + \nu \frac{\partial^2 u_i'}{\partial x_j \partial x_j} - \frac{\partial}{\partial x_j}(u_i' u_j' - \langle u_i' u_j' \rangle). \tag{2.30}$$

When the filter is applied, the resolved scale equation of the velocity fluctuation is obtained:

$$\frac{\partial u_i'^{<}}{\partial t} + \frac{\partial (u_i' \langle u_j \rangle)^{<}}{\partial x_j} + \frac{\partial (\langle u_i \rangle u_j')^{<}}{\partial x_j} = -\frac{1}{\rho}\frac{\partial p'^{<}}{\partial x_i} + \nu \frac{\partial^2 u_i'^{<}}{\partial x_j \partial x_j} - \frac{\partial}{\partial x_j}\left((u_i' u_j')^{<} - \langle u_i' u_j' \rangle^{<} \right). \tag{2.31}$$

We could also write equation (2.31) in another point $\vec{x}^*$, where $\vec{x} = \vec{x}^* + \vec{\xi}$:

$$\frac{\partial u_i'^{<*}}{\partial t}+\frac{\partial(u_i'^*\langle u_j^*\rangle)^<}{\partial x_j^*}+\frac{\partial(\langle u_i^*\rangle u_j'^*)^<}{\partial x_j^*} = -\frac{1}{\rho}\frac{\partial p'^{<*}}{\partial x_i^*}+\nu\frac{\partial^2 u_i'^{<*}}{\partial x_j^*\partial x_j^*}-\frac{\partial}{\partial x_j^*}\left((u_i'^*u_j'^*)^< - \langle u_i'^*u_j'^*\rangle^<\right). \tag{2.32}$$

Subtracting equation (2.32) from (2.31), and defining $\delta u_i = u_i - u_i^*$, we obtain:

$$\begin{aligned}\frac{\partial \delta u_i'^<}{\partial t}&+\frac{\partial(u_i'\langle u_j\rangle)^<}{\partial x_j} - \frac{\partial(u_i'^*\langle u_j^*\rangle)^<}{\partial x_j^*} + \frac{\partial(\langle u_i\rangle u_j')^<}{\partial x_j} - \frac{\partial(\langle u_i^*\rangle u_j'^*)^<}{\partial x_j^*}\\ &= -\frac{1}{\rho}\frac{\partial p'^<}{\partial x_i} + \frac{1}{\rho}\frac{\partial p'^{<*}}{\partial x_i^*} + \nu\frac{\partial^2 u_i'^<}{\partial x_j\partial x_j} - \nu\frac{\partial^2 u_i'^{<*}}{\partial x_j^*\partial x_j^*}\\ &\quad -\frac{\partial}{\partial x_j}\left((u_i'u_j')^< - \langle u_i'u_j'\rangle^<\right) + \frac{\partial}{\partial x_j^*}\left((u_i'^*u_j'^*)^< - \langle u_i'^*u_j'^*\rangle^<\right).\end{aligned} \tag{2.33}$$

Because $\vec{\xi} = \vec{x} - \vec{x}^*$, the following relations are satisfied:

$$\frac{\partial u_i}{\partial x_i^*} = 0, \frac{\partial u_i^*}{\partial x_i} = 0, \frac{\partial}{\partial x_i} = \frac{\partial}{\partial \xi_i}, \frac{\partial}{\partial x_i'} = -\frac{\partial}{\partial \xi_i}, \frac{\partial^2}{\partial x_i\partial x_i} = \frac{\partial^2}{\partial x_i'\partial x_i'} = \frac{\partial^2}{\partial \xi_i\partial \xi_i}. \tag{2.34}$$

Note that the average operator $\langle\rangle$ can not reduce the variable $\vec{x}$, and each term of equation (2.33) is always a function of two variables: $\vec{x}$ and $\vec{\xi}$. Multiplying equation (2.33) by $\delta u_i'^<$, and employing the ensemble average, the first term becomes

$$\left\langle \delta u_i'^<\frac{\partial \delta u_i'^<}{\partial t}\right\rangle = \left\langle \frac{1}{2}\frac{\partial(\delta u_i'^<\delta u_i'^<)}{\partial t}\right\rangle = \frac{1}{2}\frac{\partial D_{ii}^<(\vec{x})}{\partial t}, \tag{2.35}$$

in which $D_{ii}^<(\vec{x}) = \langle \delta u_i'^<\delta u_i'^<\rangle$.

The terms involving pressure on the right hand side could be simplified as

$$\begin{aligned}\left\langle \delta u_i'^<\left(-\frac{1}{\rho}\frac{\partial p'^<}{\partial x_i}+\frac{1}{\rho}\frac{\partial p'^{<*}}{\partial x_i^*}\right)\right\rangle &= -\frac{1}{\rho}\frac{\partial\langle \delta u_i'^<\delta p'^<\rangle}{\partial x_i} - \frac{1}{\rho}\frac{\partial\langle \delta u_i'^<\delta p'^<\rangle}{\partial x_i^*}\\ &= -\frac{1}{\rho}\frac{\partial\langle \delta u_i'^<\delta p'^<\rangle(\vec{x})}{\partial \xi_i} + \frac{1}{\rho}\frac{\partial\langle \delta u_i'^<\delta p'^<\rangle(\vec{x^*})}{\partial \xi_i}\\ &= -\delta\left(\frac{1}{\rho}\frac{\partial\langle \delta u_i'^<\delta p'^<\rangle}{\partial \xi_i}\right)(\vec{x}),\end{aligned} \tag{2.36}$$

and the viscosity terms read:

$$\begin{aligned}\left\langle \delta u_i'^<\left(\nu\frac{\partial^2 u_i'^<}{\partial x_j\partial x_j} - \nu\frac{\partial^2 u_i'^{<*}}{\partial x_j^*\partial x_j^*}\right)\right\rangle =&\nu\frac{\partial D_{ii}^<(\vec{x})}{\partial \xi_j\partial \xi_j} - 2\varepsilon^<(\vec{x})\\ &-\frac{\nu}{2}\delta\left(\frac{\partial D_{ii}^<}{\partial \xi_j\partial \xi_j}\right)(\vec{x}) + \delta\varepsilon^<(\vec{x}),\end{aligned} \tag{2.37}$$

in which $\varepsilon^<(\vec{x}) = \nu \left\langle \frac{\partial u_i^<}{\partial x_j} \frac{\partial u_i^<}{\partial x_j} \right\rangle$.

Following Shao [48], we define the slow subgrid stress

$$\tau_{ij}^{slow<} = u_i'^< u_j'^< - (u_i' u_j')^<, \tag{2.38}$$

and obtain a two-point equation:

$$\begin{aligned}
&\frac{1}{2}\frac{\partial D_{ii}^<}{\partial t} + \left\langle \delta u_i'^< \left(\frac{\partial (u_i' \langle u_j \rangle)^<}{\partial x_j} - \frac{\partial (u_i'^* \langle u_j^* \rangle)^<}{\partial x_j^*} + \frac{\partial (\langle u_i \rangle u_j')^<}{\partial x_j} - \frac{\partial (\langle u_i^* \rangle u_j'^*)^<}{\partial x_j^*} \right) \right\rangle \\
&\qquad + \left\langle \delta u_i'^< \left(\frac{\partial (u_i'^< u_j'^<)}{\partial x_j} - \frac{\partial (u_i'^{<*} u_j'^{<*})}{\partial x_j^*} \right) \right\rangle \\
&\qquad - \left\langle \delta u_i'^< \left\langle \frac{\partial (u_i'^< u_j'^<)}{\partial x_j} - \frac{\partial (u_i'^{<*} u_j'^{<*})}{\partial x_j^*} \right\rangle \right\rangle \\
&= -\delta \left(\frac{1}{\rho} \frac{\partial \langle \delta u_i'^< \delta p'^< \rangle}{\partial \xi_i} \right)(\vec{x}) + \nu \frac{\partial D_{ii}^<}{\partial \xi_j \partial \xi_j} - 2\varepsilon^< - \frac{\nu}{2} \delta \left(\frac{\partial D_{ii}^<}{\partial \xi_j \partial \xi_j} \right)(\vec{x}) + \delta \varepsilon^<(\vec{x}) \\
&\qquad + \left\langle \delta u_i'^< \left(\frac{\partial \tau_{ij}^{slow<}}{\partial x_j} - \frac{\partial \tau_{ij}^{slow<*}}{\partial x_j^*} \right) \right\rangle - \left\langle \delta u_i'^< \left\langle \frac{\partial \tau_{ij}^{slow<}}{\partial x_j} - \frac{\partial \tau_{ij}^{slow<*}}{\partial x_j^*} \right\rangle \right\rangle.
\end{aligned} \tag{2.39}$$

Applying the property called Reynolds rule

$$\langle \langle \phi \rangle \psi \rangle = \langle \phi \rangle \langle \psi \rangle, \tag{2.40}$$

the terms in equation (2.39) read

$$\begin{aligned}
&\left\langle \delta u_i'^< \left\langle \frac{\partial (u_i'^< u_j'^<)}{\partial x_j} - \frac{\partial (u_i'^{<*} u_j'^{<*})}{\partial x_j^*} \right\rangle \right\rangle = \langle \delta u_i'^< \rangle \left\langle \frac{\partial (u_i'^< u_j'^<)}{\partial x_j} - \frac{\partial (u_i'^{<*} u_j'^{<*})}{\partial x_j^*} \right\rangle = 0 \\
&\left\langle \delta u_i'^< \left\langle \frac{\partial \tau_{ij}^{slow<}}{\partial x_j} - \frac{\partial \tau_{ij}^{slow<*}}{\partial x_j^*} \right\rangle \right\rangle = \langle \delta u_i'^< \rangle \left\langle \frac{\partial \tau_{ij}^{slow<}}{\partial x_j} - \frac{\partial \tau_{ij}^{slow<*}}{\partial x_j^*} \right\rangle = 0.
\end{aligned} \tag{2.41}$$

The convection term on the left hand side is written as

$$\begin{aligned}
\left\langle \delta u_i'^< \left(\frac{\partial (u_i'^< u_j'^<)}{\partial x_j} - \frac{\partial (u_i'^{<*} u_j'^{<*})}{\partial x_j^*} \right) \right\rangle &= \frac{1}{2} \left\langle \frac{\partial (u_j'^< \delta u_i'^< \delta u_i'^<)}{\partial x_j} + \frac{\partial (u_j'^{<*} \delta u_i'^< \delta u_i'^<)}{\partial x_j^*} \right\rangle \\
&= \frac{1}{2} \frac{\partial D_{iij}^<}{\partial \xi_j}(\vec{x}) - \frac{1}{2} \delta \left(\frac{\partial D_{iij}^<}{\partial \xi_j} \right)(\vec{x}),
\end{aligned} \tag{2.42}$$

in which $D^{<}_{iij}(\vec{x}) = \langle \delta u_j'^{<} \delta u_i'^{<} \delta u_i'^{<} \rangle$ is the third order structure function.

Next, consider the four terms in equation (2.39). Define the rapid subgrid stress

$$\tau_{ij}^{rapid<} = \langle u_i \rangle^{<} u_j'^{<} - \left(\langle u_i \rangle u_j' \right)^{<} + \langle u_j \rangle^{<} u_i'^{<} - \left(\langle u_j \rangle u_i' \right)^{<}, \tag{2.43}$$

equation (2.39) reads

$$\begin{aligned}
&\frac{1}{2}\frac{\partial D^{<}_{ii}}{\partial t} + \frac{1}{2}\frac{\partial D^{<}_{iij}}{\partial \xi_j} - \frac{1}{2}\delta\left(\frac{\partial D^{<}_{iij}}{\partial \xi_j}\right)(\vec{x}) \\
&\quad + \left\langle \delta u_i'^{<} \left(\frac{\partial (u_i'^{<} \langle u_j \rangle^{<})}{\partial x_j} - \frac{\partial (u_i'^{<*} \langle u_j^{*} \rangle^{<})}{\partial x_j^{*}} + \frac{\partial (\langle u_i \rangle^{<} u_j'^{<})}{\partial x_j} - \frac{\partial (\langle u_i \rangle^{<*} u_j'^{<*})}{\partial x_j^{*}} \right) \right\rangle \\
&\quad = -\delta\left(\frac{1}{\rho} \frac{\partial \langle \delta u_i'^{<} \delta p'^{<} \rangle}{\partial \xi_i} \right)(\vec{x}) + \nu \frac{\partial D^{<}_{ii}}{\partial \xi_j \partial \xi_j} - 2\varepsilon^{<} - \frac{\nu}{2}\delta\left(\frac{\partial D^{<}_{ii}}{\partial \xi_j \partial \xi_j} \right)(\vec{x}) + \delta\varepsilon^{<}(\vec{x}) \\
&\quad + \left\langle \delta u_i'^{<} \left(\frac{\partial \tau_{ij}^{slow<}}{\partial x_j} - \frac{\partial \tau_{ij}^{slow<*}}{\partial x_j^{*}} \right) \right\rangle + \left\langle \delta u_i'^{<} \left(\frac{\partial \tau_{ij}^{rapid<}}{\partial x_j} - \frac{\partial \tau_{ij}^{rapid<*}}{\partial x_j^{*}} \right) \right\rangle .
\end{aligned} \tag{2.44}$$

Employing the Reynolds rule (2.40), we obtain

$$\begin{aligned}
&\left\langle \delta u_i'^{<} \left(\frac{\partial (u_i'^{<} \langle u_j \rangle^{<})}{\partial x_j} - \frac{\partial (u_i'^{<*} \langle u_j^{*} \rangle^{<})}{\partial x_j^{*}} \right) \right\rangle \\
&= \frac{1}{2}\langle u_j \rangle^{<} \left\langle \frac{\partial (\delta u_i'^{<} \delta u_i'^{<})}{\partial x_j} \right\rangle + \frac{1}{2}\langle u_j \rangle^{<*} \left\langle \frac{\partial (\delta u_i'^{<} \delta u_i'^{<})}{\partial x_j^{*}} \right\rangle \\
&= \frac{1}{2}\langle u_j \rangle^{<} \frac{\partial D^{<}_{ii}}{\partial \xi_j}(\vec{x}) - \frac{1}{2}\langle u_j \rangle^{<*} \frac{\partial D^{<}_{ii}}{\partial \xi_j}(\vec{x^{*}}) \\
&= \frac{1}{2}\delta\langle u_j \rangle^{<} \frac{\partial D^{<}_{ii}}{\partial \xi_j}(\vec{x}) - \frac{1}{2}\langle u_j \rangle^{<*} \delta\left(\frac{\partial D^{<}_{ii}}{\partial \xi_j} \right)(\vec{x}) \\
&= \frac{1}{2}\delta\langle u_j \rangle^{<} \frac{\partial D^{<}_{ii}}{\partial \xi_j}(\vec{x}) - \frac{1}{2}\langle u_j \rangle^{<} \delta\left(\frac{\partial D^{<}_{ii}}{\partial \xi_j} \right)(\vec{x}) + \frac{1}{2}\delta\langle u_j \rangle^{<} \delta\left(\frac{\partial D^{<}_{ii}}{\partial \xi_j} \right)(\vec{x}).
\end{aligned} \tag{2.45}$$

Because

$$\left\langle \delta u_i'^{<} \frac{\partial (\langle u_i \rangle^{<} u_j'^{<})}{\partial x_j} \right\rangle = \left\langle u_j'^{<} \delta u_i'^{<} \frac{\partial \delta \langle u_i \rangle^{<}}{\partial \xi_j} \right\rangle = \left\langle u_j'^{<} \delta u_i'^{<} \right\rangle \frac{\partial \delta \langle u_i \rangle^{<}(\vec{x})}{\partial \xi_j}, \tag{2.46}$$

and similarly

$$\left\langle \delta u_i'^{<} \frac{\partial (\langle u_i \rangle^{<*} u_j'^{<*})}{\partial x_j^{*}} \right\rangle = \left\langle u_j'^{<*} \delta u_i'^{<} \right\rangle \frac{\partial \delta \langle u_i \rangle^{<}(\vec{x^{*}})}{\partial \xi_j}, \tag{2.47}$$

thus from equation (2.46) - (2.47):

$$\begin{aligned}
&\left\langle \delta u_i'^{<} \frac{\partial \langle u_i\rangle^{<} u_j'^{<}}{\partial x_j} \right\rangle - \left\langle \delta u_i'^{<} \frac{\partial \langle u_i\rangle^{<*} u_j'^{<*}}{\partial x_j^*} \right\rangle \\
&= \left\langle \delta u_i'^{<} \delta u_j'^{<} \right\rangle \frac{\partial \delta \langle u_i\rangle^{<}}{\partial \xi_j} + \left\langle u_j'^{<*} \delta u_i'^{<} \right\rangle \delta \left(\frac{\partial \delta \langle u_i\rangle^{<}}{\partial \xi_j} \right)(\vec{x}) \\
&= \left\langle \delta u_i'^{<} \delta u_j'^{<} \right\rangle \frac{\partial \delta \langle u_i\rangle^{<}}{\partial \xi_j} + \left\langle u_j'^{<} \delta u_i'^{<} \right\rangle \delta \left(\frac{\partial \delta \langle u_i\rangle^{<}}{\partial \xi_j} \right)(\vec{x}) - \left\langle \delta u_i'^{<} \delta u_j'^{<} \right\rangle \delta \left(\frac{\partial \delta \langle u_i\rangle^{<}}{\partial \xi_j} \right)(\vec{x}) \\
&= \frac{\partial \delta \langle u_i\rangle^{<}}{\partial \xi_j} D_{ij}^{<}(\vec{x}) + \left\langle u_j'^{<} \delta u_i'^{<} \right\rangle \delta \left(\frac{\partial \delta \langle u_i\rangle^{<}}{\partial \xi_j} \right)(\vec{x}) - \delta \left(\frac{\partial \delta \langle u_i\rangle^{<}}{\partial \xi_j} \right)(\vec{x}) D_{ij}^{<}(\vec{x}).
\end{aligned} \tag{2.48}$$

Equation (2.44) becomes

$$\begin{aligned}
&\frac{1}{2}\frac{\partial D_{ii}^{<}}{\partial t} + \frac{1}{2}\frac{\partial D_{iij}^{<}}{\partial \xi_j} - \frac{1}{2}\delta \left(\frac{\partial D_{iij}^{<}}{\partial \xi_j} \right)(\vec{x}) \\
&\quad + \frac{1}{2}\delta\langle u_j\rangle^{<} \frac{\partial D_{ii}^{<}}{\partial \xi_j} - \frac{1}{2}\langle u_j\rangle^{<} \delta \left(\frac{\partial D_{ii}^{<}}{\partial \xi_j} \right)(\vec{x}) + \frac{1}{2}\delta\langle u_j\rangle^{<} \delta \left(\frac{\partial D_{ii}^{<}}{\partial \xi_j} \right)(\vec{x}) \\
&\quad + \frac{\partial \delta \langle u_i\rangle^{<}}{\partial \xi_j} D_{ij}^{<} + \left\langle u_j'^{<} \delta u_i'^{<} \right\rangle \delta \left(\frac{\partial \delta \langle u_i\rangle^{<}}{\partial \xi_j} \right)(\vec{x}) - \delta \left(\frac{\partial \delta \langle u_i\rangle^{<}}{\partial \xi_j} \right)(\vec{x}) D_{ij}^{<}(\vec{x}) \\
&\quad = -\delta \left(\frac{1}{\rho} \frac{\partial \langle \delta u_i'^{<} \delta p'^{<} \rangle}{\partial \xi_i} \right)(\vec{x}) + \nu \frac{\partial D_{ii}^{<}}{\partial \xi_j \partial \xi_j} - 2\varepsilon^{<} - \frac{\nu}{2}\delta \left(\frac{\partial D_{ii}^{<}}{\partial \xi_j \partial \xi_j} \right)(\vec{x}) + \delta\varepsilon^{<}(\vec{x}) \\
&\quad + \left\langle \delta u_i'^{<} \left(\frac{\partial \tau_{ij}^{slow<}}{\partial x_j} - \frac{\partial \tau_{ij}^{slow<*}}{\partial x_j^*} \right) \right\rangle + \left\langle \delta u_i'^{<} \left(\frac{\partial \tau_{ij}^{rapid<}}{\partial x_j} - \frac{\partial \tau_{ij}^{rapid<*}}{\partial x_j^*} \right) \right\rangle.
\end{aligned} \tag{2.49}$$

In fact, we could define the terms which are caused by the inequality $\langle\varphi\rangle \neq \langle\varphi^*\rangle$:

$$\begin{aligned}
H^{rapid}(\vec{x}) =& \frac{1}{2}\langle u_j\rangle^{<} \delta \left(\frac{\partial D_{ii}^{<}}{\partial \xi_j} \right)(\vec{x}) - \frac{1}{2}\delta\langle u_j\rangle^{<} \delta \left(\frac{\partial D_{ii}^{<}}{\partial \xi_j} \right)(\vec{x}) \\
&+ \delta \left(\frac{\partial \delta \langle u_i\rangle^{<}}{\partial \xi_j} \right)(\vec{x}) D_{ij}^{<}(\vec{x}) \\
H^{slow}(\vec{x}) =& \frac{1}{2}\delta \left(\frac{\partial D_{iij}^{<}}{\partial \xi_j} \right)(\vec{x}) - \left\langle u_j'^{<} \delta u_i'^{<} \right\rangle \delta \left(\frac{\partial \delta \langle u_i\rangle^{<}}{\partial \xi_j} \right)(\vec{x}) \\
&- \delta \left(\frac{1}{\rho} \frac{\partial \langle \delta u_i'^{<} \delta p'^{<} \rangle}{\partial \xi_i} \right)(\vec{x}) - \frac{\nu}{2}\delta \left(\frac{\partial D_{ii}^{<}}{\partial \xi_j \partial \xi_j} \right)(\vec{x}) + \delta\varepsilon^{<}(\vec{x})
\end{aligned} \tag{2.50}$$

Equation (2.49) could be written as

$$\begin{aligned}
&\frac{1}{2}\frac{\partial D_{ii}^{<}}{\partial t}+\frac{1}{2}\frac{\partial D_{iij}^{<}}{\partial \xi_j}+\frac{1}{2}\delta\langle u_j\rangle^{<}\frac{\partial D_{ii}^{<}}{\partial \xi_j}+\frac{\partial \delta\langle u_i\rangle^{<}}{\partial \xi_j}D_{ij}^{<} \\
&\quad =H^{rapid}(\vec{x})+H^{slow}(\vec{x})+\nu\frac{\partial D_{ii}^{<}}{\partial \xi_j \partial \xi_j}-2\varepsilon^{<} \\
&\quad +\left\langle \delta u_i'^{<}\left(\frac{\partial \tau_{ij}^{slow<}}{\partial x_j}-\frac{\partial \tau_{ij}^{slow<*}}{\partial x_j^*}\right)\right\rangle+\left\langle \delta u_i'^{<}\left(\frac{\partial \tau_{ij}^{rapid<}}{\partial x_j}-\frac{\partial \tau_{ij}^{rapid<*}}{\partial x_j^*}\right)\right\rangle
\end{aligned} \tag{2.51}$$

If we consider the local homogeneous assumption, there will be $\langle\varphi\rangle = \langle\varphi^*\rangle$, thus $H^{rapid}(\vec{x}) = H^{slow}(\vec{x}) = 0$, the previous equation will become much more simple. It will be discussed in the next section, and will be applied to build new subgrid models.

2.4 KEF in homogeneous shear turbulence

With constant shear, the formulation of KEF can be simplified. In this section, we first write the formulation in a general fixed coordinate system in Sec. 2.4.1, and introduce the classical analysis in spectral space in Sec. 2.4.2; then in Sec. 2.4.3 we rewrite the formula of KEF in a moving coordinate system, in order to explain the effect of the coordinate-depended term; in Sec. 2.4.4 the assumption of local isotropy is studied, and proved to be not satisfied in homogeneous shear turbulence; finally in Sec. 2.4.5 we introduce the concept of skewness and find it approximately satisfies local isotropy in shear turbulence.

2.4.1 Equation formulation

In homogeneous shear turbulence, we assume $\langle u_i\rangle = \gamma x_2\delta_{i1} = \langle u_i\rangle^{<}$, and two terms in equation (2.51) could be written as

$$\frac{1}{2}\delta\langle u_j\rangle^{<}\frac{\partial D_{ii}^{<}}{\partial \xi_j}=\frac{\gamma\xi_2}{2}\frac{\partial D_{ii}^{<}}{\partial \xi_1}, \tag{2.52}$$

$$\frac{\partial \delta\langle u_i\rangle^{<}}{\partial \xi_j}D_{ij}^{<}=\frac{\gamma}{2}D_{12}^{<}. \tag{2.53}$$

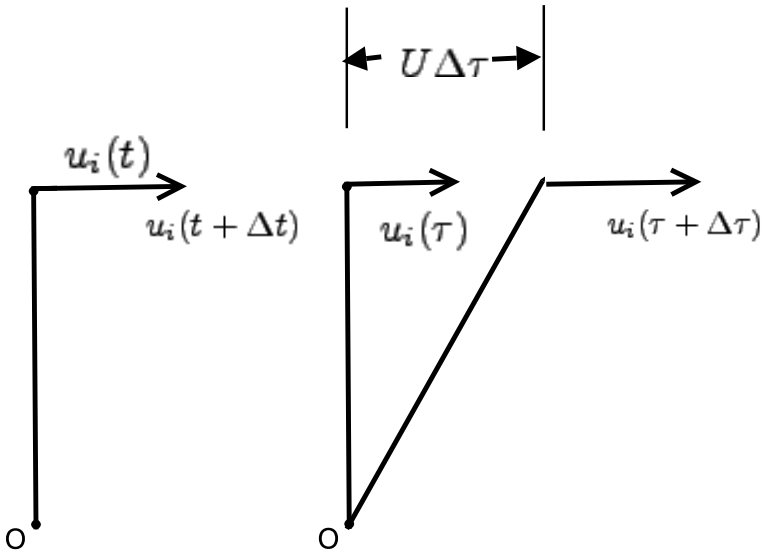

(a) (b)

Figure 2.6: Time develop in numerical simulation, in different coordinate systems. (a) Fixed coordinate system. (b) Moving coordinate system.

As discussed in the last section, in homogeneous turbulence $H^{rapid}(\vec{x}) = H^{slow}(\vec{x}) = 0$. Therefore, equation (2.51) can be simplified:

$$\begin{aligned} &\frac{1}{2}\frac{\partial D_{ii}^{<}}{\partial t}+\frac{1}{2}\frac{\partial D_{iij}^{<}}{\partial \xi_j}+\frac{\gamma\xi_2}{2}\frac{\partial D_{ii}^{<}}{\partial \xi_1}+\frac{\gamma}{2}D_{12}^{<} \\ &=\nu\frac{\partial D_{ii}^{<}}{\partial \xi_j \partial \xi_j}-2\varepsilon^{<}+\left\langle \delta u_i'^{<}\left(\frac{\partial \tau_{ij}^{<}}{\partial x_j}-\frac{\partial \tau_{ij}^{<}*}{\partial x_j^*}\right)\right\rangle, \end{aligned} \tag{2.54}$$

in which $\tau_{ij}^{<} = \tau_{ij}^{rapid<} + \tau_{ij}^{slow<}$ corresponds to the total SGS stress in homogeneous shear turbulence. The detailed process can be found in the paper of Cui *et al.* [40].

2.4.2 Analysis of the shear effect in spectral space

There are already lots of researches on the two-point correlation equation in spectral space. Since the correlation function could be translated from Fourier transform easily, we follow Hinze's method and finally write the governing equation for two-point correlation functions:

$$\begin{aligned} &\frac{\partial R_{ij}^{<}}{\partial t}+\gamma\left(\delta_{i1}R_{2j}^{<}+\delta_{j1}R_{i2}^{<}+\xi_2\frac{\partial}{\partial \xi_1}R_{ij}^{<}\right) \\ &=\text{transfer}+\text{pressure}+\text{dissipation}+\text{subgrid}, \end{aligned} \tag{2.55}$$

in which $R_{ij}^{<}(\vec{\xi}) = \langle u_i^{<}(\vec{x}) u_j^{<}(\vec{x}+\vec{\xi})\rangle$. In order to clarify the effect by mean flow, we mainly note the terms related with γ. Contraction of equation (2.55) vanishes the pressure terms and yields

$$\begin{aligned} &\frac{\partial R_{ii}^{<}}{\partial t} + \gamma\left(2R_{12}^{<} + \xi_2 \frac{\partial}{\partial \xi_1} R_{ii}^{<}\right) \\ &= \text{transfer} + \text{dissipation} + \text{subgrid}, \end{aligned} \tag{2.56}$$

in which the two shear terms $2\gamma R_{12}^{<}$ and $\gamma\xi_2 \dfrac{\partial}{\partial \xi_1} R_{ii}^{<}$ are similar as the terms in equation 2.54.

The two-point correlation function could be expressed in spectral space:

$$R_{ij}^{<}(\vec{\xi}) = \iiint \mathrm{S}_{ij}^{<} e^{\iota \vec{\xi}\cdot\vec{k}} d\vec{k}, \tag{2.57}$$

where $\mathrm{S}_{ij}^{<}$ is the filtered correlation tensor in spectral space. Thus the shear terms read

$$\begin{aligned} 2\gamma R_{12}^{<}(\vec{\xi}) &= 2\gamma \iiint \mathrm{S}_{12}^{<} e^{\iota \vec{\xi}\cdot\vec{k}} d\vec{k}, \\ \gamma\xi_2 \frac{\partial}{\partial \xi_1} R_{ii}^{<} &= -\iiint k_1 \frac{\partial \mathrm{S}_{ii}^{<}}{\partial k_2} e^{\iota \vec{\xi}\cdot\vec{k}} d\vec{k}. \end{aligned} \tag{2.58}$$

The term $2\gamma \mathrm{S}_{12}^{<}$ is regarded as a production term. The term $-k_1 \dfrac{\partial \mathrm{S}_{ii}^{<}}{\partial k_2}$ is a energy transfer term which does not generate or dissipate, since integrated over all wavenumbers it yields a zero integral contribution:

$$\iiint k_1 \frac{\partial \mathrm{S}_{ii}^{<}}{\partial k_2} = 0, \tag{2.59}$$

since it is equal to

$$\lim_{\xi_2 \to 0} \xi_2 \frac{\partial R_{ii}^{<}}{\partial \xi_1} = 0. \tag{2.60}$$

Batchelor [49] suggested doing the same in a anisotropic but homogeneous turbulence by averaging the correlation and spectrum functions over all directions of $\vec{\xi}$ and $\vec{k}$ in the corresponding spaces, thus the mean effect on a sphere face could be evaluated. However, there is also a turning effect caused by the mean shear [50]. Any flow of an incompressible fluid, whose velocity distribution is a linear function of the space coordinates, can be decomposed into a pure rotation and a pure deformation. For instance the simple case $\langle u_i \rangle = \gamma x_2 \delta_{i1}$, the flow consists of a bodily rotation

with angular speed $-\frac{1}{2}\gamma$, and a pure deformation with a maximum strain rate $+\frac{1}{2}\gamma$ along the principal axis in the direction $\pi/4$, and a minimum strain rate $-\frac{1}{2}\gamma$ (i.e. a compression) in the direction $3\pi/4$ [51].

Lumley [52, 53] calculates the energy budget of shear flow in spectral space. The shear terms are found to be obvious in small wave numbers, i.e. in large scales. Thus this large-scale region is considered to be anisotropic. Also, direct interaction between the smaller eddies in the equilibrium range and the mean motion, resulting in direct energy transfer from the mean motion to these eddied, is negligibly small.

These works were done many years ago, which explained the shear effect in spectral space. In the following parts, we shall analyze the shear effect in physical space, mainly on the evolution and anisotropy of structure functions.

2.4.3 KEF in a moving coordinate system

We could also study the two-point behavior in a moving coordinate system. Following Rogallo [54] and Gualtieri [55], a coordinate transformation is introduced that

$$\zeta_1 = x_1 - \gamma x_2 t, \zeta_2 = x_2, \zeta_3 = x_3, \tau = t, \tag{2.61}$$

hence the $(\vec{\zeta}, \tau)$ coordinate system is moving with the mean flow. The different coordinate systems are shown in Fig. (2.6). Compared with the origin coordinate system $(\vec{x}, t)$, the relations of derivatives are satisfied:

$$\frac{\partial}{\partial x_j} = \frac{\partial}{\partial \zeta_j} - \gamma\tau\delta_{j2}\frac{\partial}{\partial \zeta_1}, \quad \frac{\partial}{\partial t} = \frac{\partial}{\partial \tau} - \gamma\zeta_2\frac{\partial}{\partial \zeta_1}. \tag{2.62}$$

N-S equations in the moving coordinate system are

$$\frac{\partial u_i}{\partial \zeta_i} = \gamma\tau\frac{\partial u_2}{\partial \zeta_1}, \tag{2.63}$$

$$\frac{\partial u_i}{\partial \tau} + u_j\frac{\partial u_i}{\partial \zeta_j} = -\frac{\partial p}{\partial \zeta_j} + \gamma\tau\delta_{j2}\frac{\partial p}{\partial \zeta_1} + \nu\mathscr{D}u_i + \gamma\tau u_2\frac{\partial u_i}{\partial \zeta_1} - \gamma u_2\delta_{i1}, \tag{2.64}$$

where $\mathscr{D} = \frac{\partial^2}{\partial \zeta_j \partial \zeta_j} - 2\gamma\tau\frac{\partial^2}{\partial \zeta_1 \partial \zeta_2} + \gamma^2\tau^2\frac{\partial^2}{\partial \zeta_1 \zeta_1}$.

If the variable of time τ is given as 0, the equations become:

$$\begin{aligned} \frac{\partial u_i}{\partial \zeta_i} &= 0, \\ \frac{\partial u_i}{\partial \tau} + u_j\frac{\partial u_i}{\partial \zeta_j} &= -\frac{\partial p}{\partial \zeta_j} + \nu\frac{\partial^2 u_i}{\partial \zeta_j \partial \zeta_j} - \gamma u_2\delta_{i1}. \end{aligned} \tag{2.65}$$

If the filter operator is defined in the moving coordinate system, in order to derive the formulation of KEF, the filter operator should commute with the time derivative. In physical space it means that the filter should remain its shape, for instance in Fig. 2.7, if at time $\tau = 0$ the filter is a circle at A_1, after $\Delta\tau$ it locates at A_2 but should remain a circle. Thus the filter operators are the same between the fixed and moving coordinate systems, and we could obtain the KEF formulation by applying a similar method. It leads to:

$$\frac{1}{2}\frac{\partial D_{ii}^{<}}{\partial \tau} + \frac{1}{2}\frac{\partial D_{iij}^{<}}{\partial \varsigma_j} + \frac{\gamma}{2}D_{12}^{<} = \nu\frac{\partial D_{ii}^{<}}{\partial \varsigma_j \partial \varsigma_j} - 2\varepsilon^{<} + \left\langle \delta u_i'^{<}\left(\frac{\partial \tau_{ij}^{<}}{\partial \zeta_j} - \frac{\partial \tau_{ij}^{<*}}{\partial \zeta_j^*}\right)\right\rangle, \tag{2.66}$$

in which $\vec{\varsigma} = \vec{\zeta} - \vec{\zeta}^*$ is the two-point distance in the moving coordinate system. If the time τ is considered as 0, the filter operator is the same as in the fixed coordinate system in this moment. From equation (2.62), we could also write

$$\frac{\partial}{\partial x_j} = \frac{\partial}{\partial \zeta_j}, \quad \frac{\partial}{\partial \xi_j} = \frac{\partial}{\partial \varsigma_j} \tag{2.67}$$

in this $\tau = 0$ moment. Thus the differences between equation (2.54) and (2.66) are the time-depending term and the shear term $\frac{\gamma\xi_2}{2}\frac{\partial D_{ii}^{<}}{\partial \xi_1}$. In order to analyze the effect of this shear term, we substract (2.54) from (2.66), and obtain

$$\gamma\xi_2\frac{\partial D_{ii}^{<}}{\partial \xi_1} = \frac{\partial D_{ii}^{<}(\text{moving})}{\partial \tau} - \frac{\partial D_{ii}^{<}(\text{fixed})}{\partial t} \tag{2.68}$$

This equation means that the shear term $\frac{\gamma\xi_2}{2}\frac{\partial D_{ii}^{<}}{\partial \xi_1}$ denotes the differences of time development of second order structure function of filtered velocity $D_{ii}^{<}$. As shown in Fig. (2.6), if we apply the moving coordinate system in numerical computing, the discrete difference has to be employed between two points of two moments (τ and $\tau + \Delta\tau$). It could be treated as a kind of Lagrange description [51, 56, 57], but the equation is written with mean flow (not with a real particle).

We could write the shear term $\frac{\gamma\xi_2}{2}\frac{\partial D_{ii}^{<}}{\partial \xi_1}$ in a spherical coordinate system to verify its anisotropy. The spherical coordinate is introduced as (see Fig. 2.8):

$$\xi_1 = r\cos\theta, \xi_2 = r\sin\theta\cos\varphi, \xi_3 = r\sin\theta\sin\varphi. \tag{2.69}$$

The gradient operation of $D_{ii}^{<}$ is then written as

$$\nabla D_{ii}^{<} = \frac{\partial D_{ii}^{<}}{\partial r}\vec{e}_r + \frac{1}{r}\frac{\partial D_{ii}^{<}}{\partial \theta}\vec{e}_\theta + \frac{1}{r\sin\theta}\frac{\partial D_{ii}^{<}}{\partial \varphi}\vec{e}_\varphi, \tag{2.70}$$

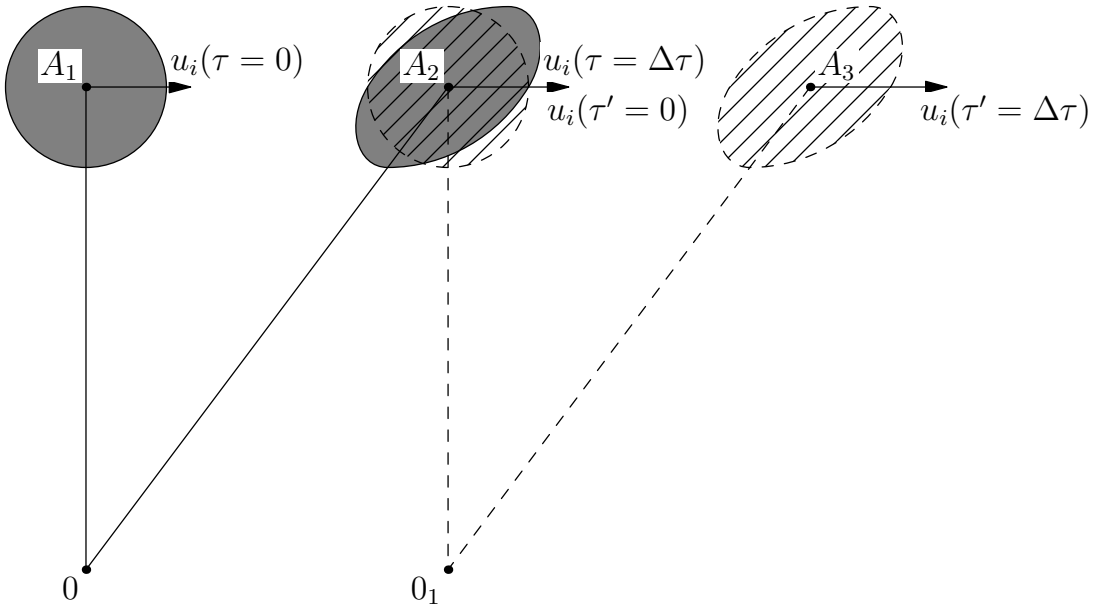

Figure 2.7: Filter operator in physical space, in moving coordinate system.

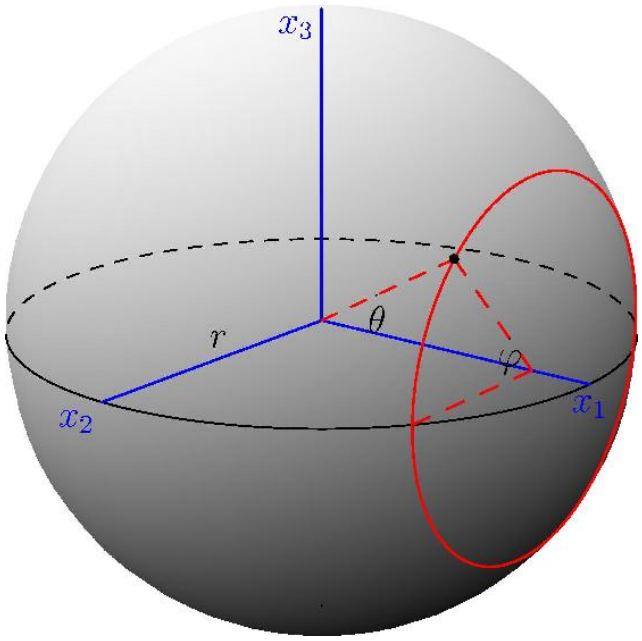

Figure 2.8: Sphere coordinate system used for analyzing the anisotropy of the shear term.

and the component in x_1 direction reads:

$$\frac{\partial D_{ii}^{<}}{\partial \xi_1} = \cos\left(\frac{1}{r}\frac{\partial D_{ii}^{<}}{\partial \theta}\right)\frac{\partial D_{ii}^{<}}{\partial r}. \tag{2.71}$$

The integration of the shear term from 0 to radius r is:

$$\begin{aligned}\int_0^r -\frac{1}{2}\gamma\xi_2\frac{\partial D_{ii}^{<}}{\partial \xi_1}dr &= -\frac{1}{2}\gamma\int_0^r r\sin\theta\cos\varphi\cos\left(\frac{1}{r}\frac{\partial D_{ii}^{<}}{\partial \theta}\right)\frac{\partial D_{ii}^{<}}{\partial r}dr \\ &= -\frac{1}{2}\gamma\sin\theta\cos\varphi\left[r\cos\left(\frac{1}{r}\frac{\partial D_{ii}^{<}}{\partial \theta}\right)D_{ii}^{<} - \int_0^r D_{ii}^{<}\cos\left(\frac{1}{r}\frac{\partial D_{ii}^{<}}{\partial \theta}\right)dr\right. \\ &\quad \left. - \int_0^r \frac{1}{r}D_{ii}^{<}\sin\left(\frac{1}{r}\frac{\partial D_{ii}^{<}}{\partial \theta}\right)\frac{\partial D_{ii}^{<}}{\partial \theta}dr\right].\end{aligned} \tag{2.72}$$

If local isotropy is satisfied, $D_{ii}^{<}$ is only a function of r, thus $\dfrac{\partial D_{ii}^{<}}{\partial \theta} = 0$, and the integral value is simplified as

$$\int_0^r -\frac{1}{2}\gamma\xi_2\frac{\partial D_{ii}^{<}}{\partial \xi_1}dr = \frac{1}{2}\gamma\sin\theta\cos\varphi\left(rD_{ii}^{<} - \int_0^r D_{ii}^{<}dr\right). \tag{2.73}$$

The value verifies with the coordinates θ and φ (see Fig. 2.9). It means this shear term is anisotropic in the radius r sphere. In fact, the anisotropic property might also affect the local isotropy assumption of $D_{ii}^{<}$. Although the problem of local isotropy has no direct relation with our SGS model designing, we want to have a simple discussion on it. The assumption of local isotropy is queried on.

2.4.4 Doubt on the assumption of local isotropy

Local isotropy was introduced by Kolmogorov [9] as homogeneity plus isotropy of the small scales of turbulent motions, and it remained an implicit assumption in his refinements [58]. It is a cornerstone of the theory of universal self-similarity, closely connected with the assumption of complete independence of the small-scale structure of the turbulent field from its large-scale structure and mean shears, and also with the random character of the energy cascade. Obukhov [59] and Corrsin [60] have extended the assumption to the small scales of scalar fields mixed by turbulence, apparently as a consequence of their properties as passive contaminants.

Although some scientists had doubt about the assumption in shear flow [61–63], Mestayer thought that there are at least four reasons that these hypotheses are true [64]:

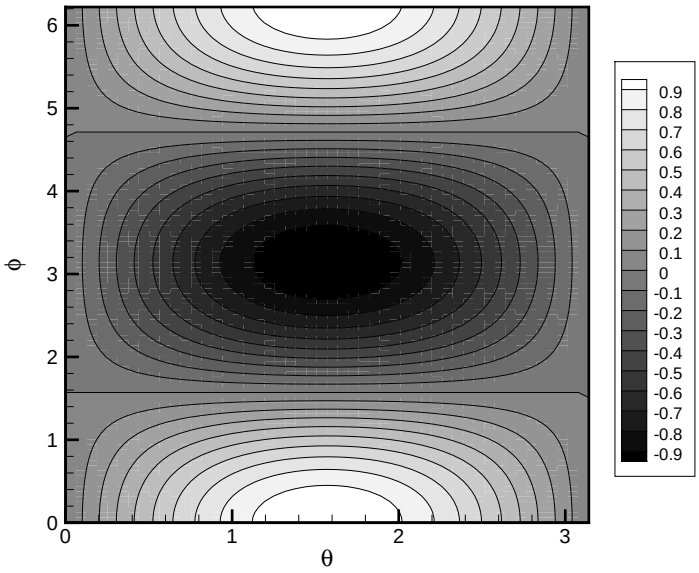

Figure 2.9: $\sin\theta\cos\varphi$ against different angles θ and φ, in a sphere coordinate system.

1. The hypotheses seem necessary for the self-similarity theory to hold - and this theory seem too coherent and efficient to be wrong.

2. Local isotropy brings such great simplifications in equations, and also in the experimental estimation of some operators like the dissipation rates of kinetic energy and of scalar variances that could perhaps not be estimated otherwise.

3. In numerous fluid-mechanics problems isotropy has been proved to be a very efficient first approximation.

4. There seems to be little experimental evidence against the hypotheses.

Mestayer' experiments show that the local isotropy assumption of moment spectrum is satisfied only at the scales less than 20 times of Kolmogorov scale η, but not in the inertial subrange. For the scalar field (the temperature field in Mestayer's experiments), the local isotropy assumption is not satisfied in almost all scales. Most of the later researches are based on group theory [65, 66]. Numerical and experimental results are analyzed to verify the local isotropy and anisotropy of high-order structure functions [67–69]. However, the physical mechanism leading to local isotropy and anisotropy has not been clarified yet. Uberoi thought that the vorticity should

be highest and lowest in the direction of contraction. These directions are at $\pm 45°$ to the mean flow for parallel or nearly parallel flows. In most of the studies, turbulence is regarded as 2-D, where only the streamwise direction and normal direction are considered. The spanwise direction was considered to be homogeneous, which is the same as the streamwise direction. However, the following analysis shows the anisotropy among the three directions of 3-D turbulence.

In homogeneous shear flow, if the local isotropy assumption is satisfied, there should be:

$$D_{ii}(\xi_1) = D_{ii}(\xi_2) = D_{ii}(\xi_3) \tag{2.74}$$

for non-filtered velocity.

If the filter is isotropic (such as in the fixed coordinate system, shown in Fig. 2.7), we could also write:

$$D^{<}_{ii}(\xi_1) = D^{<}_{ii}(\xi_2) = D^{<}_{ii}(\xi_3) \tag{2.75}$$

for the filtered velocity.

We discuss the case of non-filtered velocity as an example. If the filter size tends to zero, equation (2.54) could be rewritten to represent the structure functions of non-filtered velocity:

$$\frac{1}{2}\frac{\partial D_{ii}}{\partial t} + \frac{1}{2}\frac{\partial D_{iij}}{\partial \xi_j} + \frac{\gamma \xi_2}{2}\frac{\partial D_{ii}}{\partial \xi_1} + \frac{\gamma}{2} D_{12} = \nu \frac{\partial D_{ii}}{\partial \xi_j \partial \xi_j} - 2\varepsilon. \tag{2.76}$$

If the assumption of local isotropy is satisfied, we could write this equation in the directions of x_1 and x_3, respectively:

$$\frac{1}{2}\frac{\partial D_{ii}(\xi_1)}{\partial t} + \frac{1}{2}\frac{\partial D_{iij}(\xi_1)}{\partial \xi_j} + \frac{\gamma}{2} D_{12}(\xi_1) = \nu \frac{\partial D_{ii}(\xi_1)}{\partial \xi_j \partial \xi_j} - 2\varepsilon, \tag{2.77}$$

$$\frac{1}{2}\frac{\partial D_{ii}(\xi_3)}{\partial t} + \frac{1}{2}\frac{\partial D_{iij}(\xi_3)}{\partial \xi_j} + \frac{\gamma}{2} D_{12}(\xi_3) = \nu \frac{\partial D_{ii}(\xi_3)}{\partial \xi_j \partial \xi_j} - 2\varepsilon. \tag{2.78}$$

The terms of D_{ii} and $\partial D_{iij}/\partial \xi_j$ should then be isotropic, thus one can obtain $D_{12}(\xi_1) = D_{12}(\xi_3)$. However, notice that $D_{12}(\xi_1)$ is a correlation function between the longitudinal and transverse velocities, while $D_{12}(\xi_3)$ is a correlation function between two transverse velocities. A difference might exist. The longitudinal-transverse correlation function was studied by Kurien [68]. It should be zero in isotropic turbulence, but Kurien's experiments show that $D_{12}(\xi_1) \propto \xi_1^{1.22}$ in inertial subrange. However, there is no further research on the transverse-transverse correlation function $D_{12}(\xi_3)$.

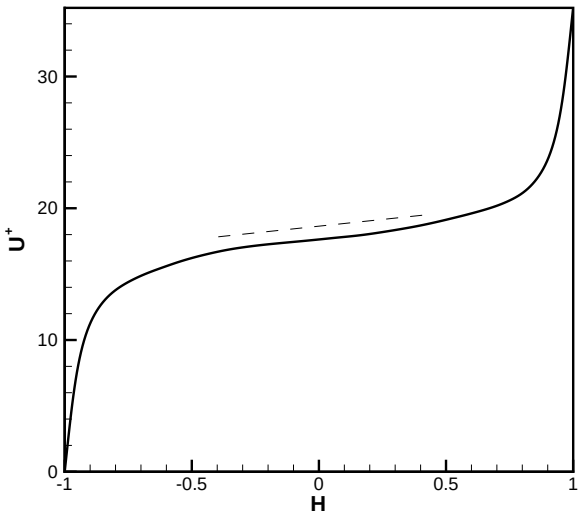

Figure 2.10: Velocity profile in turbulent Couette flow.

An *A Priori* test in turbulent Couette flow is done. The DNS database is calculated in Tsinghua university of China. A pseudo-spectral method is used. The Reynolds number $\mathrm{Re}_H = 3200$, based on the center velocity U_m and channel half-width H. The grid number is $196 \times 196 \times 128$. The computation domain is $4\pi H$, $2H$ and $2\pi H$ in streamwise, normal and spanwise directions. The mean velocity is shown in Fig. 2.10. In the center of the channel, the mean velocity could be considered to be linear, thus we calculate the $D_{12}(\vec{\xi})$ when ξ are in three axis directions respectively, by making statistics in this linear region. The values are normalized by the second-order moment $R_{12} = \langle u_1^< u_2^< \rangle$. The results are shown in Fig. 2.11. There is the difference between $D_{12}(x_3)$ and the others. However, in the $10 < \xi/\eta < 20$ range, the 1.22 scaling is approximately satisfied for all three quantities. Another anisotropic behavior is the different scaling law in dissipative range, i.e. $\xi/\eta < 10$. The structure function in normal direction is not the same as the other two. In this thesis we attempt to explain it, but unfortunately the database is not fine enough, and we could not obtain more information in the dissipative range.

We consider the effect of the shear term mentioned in the last section. As analyzed, the shear term has an effect of distortion. If the two-point distance is in x_2 direction,

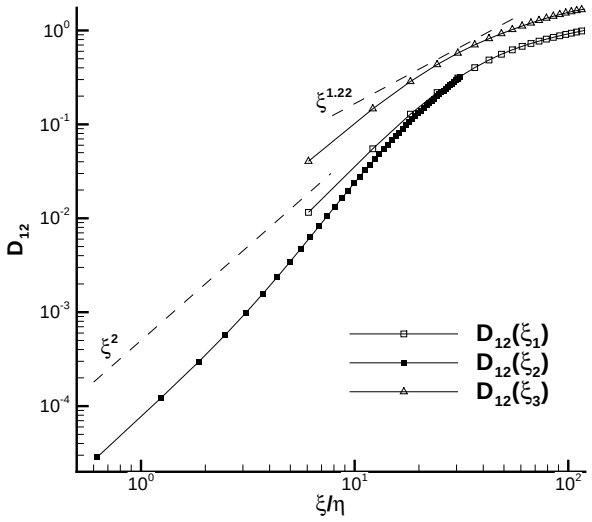

Figure 2.11: Structure function D_{12} in different directions of two-point distance.

we can write both the equations in fixed and moving coordinate systems:

$$\begin{aligned}
&\frac{1}{2}\frac{\partial D_{ii}}{\partial t}+\frac{1}{2}\frac{\partial D_{iij}}{\partial \xi_j}+\frac{\gamma\xi_2}{2}\frac{\partial D_{ii}}{\partial \xi_1}+\frac{\gamma}{2}D_{12}=\nu\frac{\partial D_{ii}}{\partial \xi_j\partial \xi_j}-2\varepsilon,\\
&\frac{1}{2}\frac{\partial D_{ii}}{\partial \tau}+\frac{1}{2}\frac{\partial D_{iij}}{\partial \varsigma_j}+\frac{\gamma}{2}D_{12}=\nu\frac{\partial D_{ii}}{\partial \varsigma_j\partial \varsigma_j}-2\varepsilon.
\end{aligned} \tag{2.79}$$

There is no reason to assume that the shear term $\frac{\gamma\xi_2}{2}\frac{\partial D_{ii}}{\partial \xi_1}$ is isotropic. Comparing with equation (2.77), it is more probable that the local isotropy between x_1 and x_2 directions exists in the moving coordinate system only. This effect is obvious when the two-point distance is large and the mean velocity gradient is strong.

Various interactions of mean shear with turbulent fluctuations cause the anisotropy of structure function. The second-order longitudinal structure functions in different directions are shown in Fig. 2.12. The values are normalized by the second-order longitudinal moment $R_{ll}=\langle u_l^< u_l^<\rangle$. Similarly, the third-order longitudinal structure functions in different directions are shown in Fig. 2.13. The values are normalized by the third-order longitudinal moment $R_{lll}=\langle u_l^< u_l^< u_l^<\rangle$. Difference always exists among the three directions. Noting the relation between the second- and third-order structure functions, we will analyze the properties of skewness in section 2.4.5.

The analyses for filtered velocity are also similar. However, there are more terms of the subgrid stress. In many subgrid models, the subgrid stress is assumed to

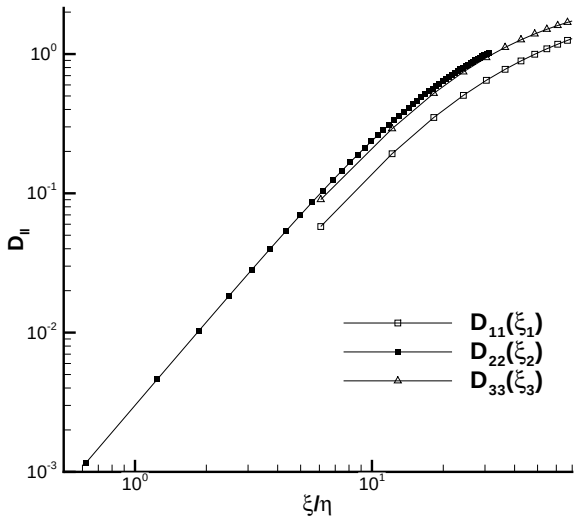

Figure 2.12: Second-order longitudinal structure function D_{ll} in different directions of two-point distance.

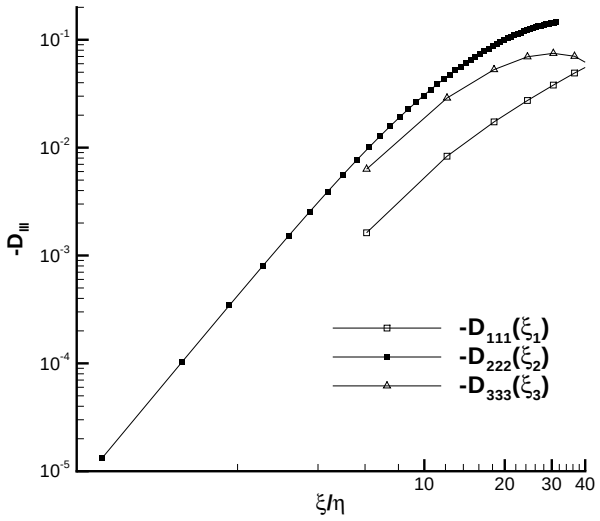

Figure 2.13: Third-order longitudinal structure function D_{lll} in different directions of two-point distance.

be isotropic, and is represented only with the velocity fluctuations. For example, the Shear-Improved Smagorinsky Model (SISM [70]) is a great improvement of the original Smagorinsky model, by considering the fluctuation parts. However, more and more works show that the mean velocity also has a contribution on subgrid scales, although it is difficult to be modelled [40,48]. We believe that it is the similar problem as the querying of local isotropy. More analyses of the SGS stress in homogeneous shear flow will be shown in the next chapter.

Therefore, the assumption of local isotropy is queried. It is not completely satisfied for the second-order structure function in homogeneous shear flow.

2.4.5 Analysis of two-point skewness

Skewness is an important physical quantity of turbulence analysis in physical space. The one-point skewness of a non-filtered isotropic velocity field is defined as

$$S_k^{\text{one point}} = \frac{\left\langle \left(\frac{\partial u_1}{\partial x_1} \right)^3 \right\rangle}{\left\langle \left(\frac{\partial u_1}{\partial x_1} \right)^2 \right\rangle^{\frac{3}{2}}}. \tag{2.80}$$

From EDQNM theory, the value of $S_k^{\text{one point}}$ is about -0.457 [8]. It has been verified in experiments and numerical simulations [71, 72]. Results show that the skewness is not just -0.457, but depends slightly on the Reynolds numbers.

Similarly, the two-point longitudinal skewness of a non-filtered isotropic velocity field is defined as

$$S_k^{\text{two point}}(\xi) = \frac{\left\langle (u_1(x_1+\xi) - u_1(x_1))^3 \right\rangle}{\left\langle (u_1(x_1+\xi) - u_1(x_1))^2 \right\rangle^{\frac{3}{2}}}. \tag{2.81}$$

In the dissipative range for small ξ, Taylor expansion can be employed, that $u_1(x_1 + \xi) - u_1(x_1) \approx \xi \frac{\partial u_1}{\partial x_1}$, thus the two-point definition equals the Eq. (2.80). However, the experiments of P. Tabeling [73] show that the two-point longitude skewness is not constant for different two-point distances ξ. When ξ increases, this value decreases, and it is $-0.3 \sim -0.2$ in the inertial subrange. It is also in agreement with Cerutti's experiment [74].

In large-eddy simulation, the skewness is defined as

$$S_k^{<\text{two point}}(\xi) = \frac{D_{lll}^{<}(\xi)}{(D_{ll}^{<}(\xi))^{\frac{3}{2}}}. \tag{2.82}$$

when the filter size Δ is much less than the two-point distance ξ, it could be considered as the same as in non-filtered velocity field. This will be proved in section 2.6.

The extended self-similarity theory (ESS) also strongly supports constant two-point skewness. ESS theory is not a scaling law, but a self-similarity result between second-order and high-order structure functions. It is well satisfied in different regions. From ESS theory, the skewness value (equation 2.82) is a constant, in both dissipative range and inertial subrange. However, in anisotropic turbulence, the isotropy of skewness should be verified.

In anisotropic turbulence, the two-point skewness of filtered velocity in an axis direction x_i is defined as (without summation convention):

$$S_k^{<\text{two point}}(\xi_i) = \frac{\left\langle (u_i^{<}(x_i+\xi) - u_i^{<}(x_i))^3 \right\rangle}{\left\langle (u_i^{<}(x_i+\xi) - u_i^{<}(x_i))^2 \right\rangle^{\frac{3}{2}}}. \tag{2.83}$$

In the center region of Couette flow (the database was described in section 2.4.4), the two-point skewness values in different directions are calculated (Fig. 2.14). Comparing with the second- and third-order structure functions mentioned in section 2.4.4, the skewness values are almost the same among the three directions. The value is approximately between -0.3 and -0.2, and it decreases when ξ increases. They are in agreement with P. Tabeling's experiments.

Since the mean velocity increment vanishes, $S_k^{<\text{two point}} < 0$ implies that the p.d.f $p(\delta u_l^{<})$ is skewed, with negative $\delta u_l^{<}$ occurring less frequently than positive values but reaching larger amplitude. The second-order structure function denotes energy, and the third-order structure function denotes the transfer, thus skewness could be considered as a property of energy transfer between resolved and subgrid scales. Batchelor thought that the skewness can represent the non-linear transfer and dissipation of the contribution of small structures [49]. Therefore, in the modeling applications, we attempt to employ the skewness, to represent the local-isotropic behavior in subgrid scale.

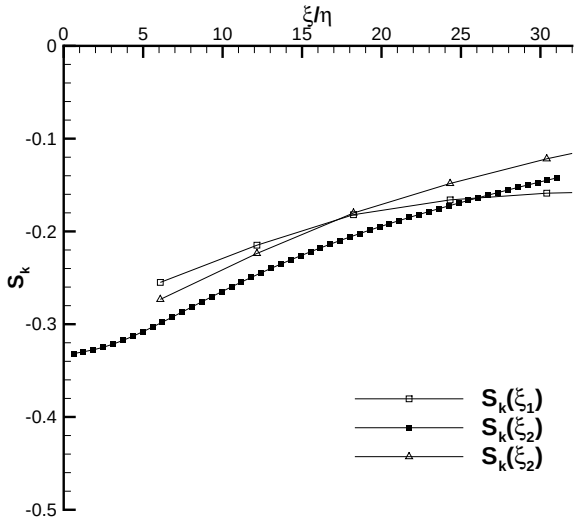

Figure 2.14: Two-point skewness $S_k^{<\text{two point}}$ in different directions of two-point distance.

2.5 KEF in homogeneous rotating turbulence

Rotating turbulence is a typical case of anisotropic turbulence with practical interest in geophysical and astrophysical flows, as well as turbulent flows in turbomachinery. Considerable efforts have been made to investigate the behavior of rotating turbulence and its structure by numerical simulation [75], experimental measurements [76] and theoretical analyses [77]. A number of peculiar properties of rotating turbulence have been revealed. The transfer of kinetic energy from large scales to small ones is reduced; consequently energy dissipation is decreasing with increasing rotating rates. It has also been found that the energy spectrum shows a steeper slope than the Kolmogorov $-5/3$ law, approaching a spectral exponent of -3 asymptotically at infinite Reynolds number and zero Rossby number. It is possible that the feature of rotating turbulence results from anisotropic nonlinear transfer of turbulent kinetic energy among velocity fluctuation components.

The governing equation of LES for homogeneous rotating turbulence can be written as

$$\frac{\partial u_i'^{<}}{\partial t} + u_j'^{<}\frac{\partial u_i'^{<}}{\partial x_j} = -\frac{1}{\rho}\frac{\partial p'^{<}}{\partial x_i} + \nu\frac{\partial^2 u_i'^{<}}{\partial x_j \partial x_j} + 2\epsilon_{ij3}\Omega u_j'^{<} - \frac{\partial \tau_{ij}^{<}}{\partial x_j}, \tag{2.84}$$

in which Ω is the rotation rate in x_3 direction, and ε_{ijk} is the Levi-Civita symbol. In order to derive the formulation of KEF, we could use the same method as described in section 2.3. Most of the processes are similar. Note that

$$\epsilon_{ij3} = -\epsilon_{ji3}, \tag{2.85}$$

this property vanish the rotating term, which could mean that the rotation effect is implicitly involved in the energy transfer. The details can be found in Shao's paper [78]. Finally the formulation of KEF is similar as equation (2.54), but without any forcing term or shear term :

$$\frac{1}{2}\frac{\partial D_{ii}^{<}}{\partial t} + \frac{1}{2}\frac{\partial D_{iij}^{<}}{\partial \xi_j} = \nu\frac{\partial D_{ii}^{<}}{\partial \xi_j \partial \xi_j} - 2\varepsilon^{<} + \left\langle \delta u_i'^{<}\left(\frac{\partial \tau_{ij}^{slow<}}{\partial x_j} - \frac{\partial \tau_{ij}^{slow<*}}{\partial x_j^*}\right)\right\rangle. \tag{2.86}$$

2.6 The scaling law of filtered velocity

From the KEF equations in different turbulence, the structure functions of filtered velocity always play important roles. In fact, among many other different analyses which may eventually be performed [79–82], the statistical properties of homogeneous isotropic turbulence are usually investigated by studying the velocity structure functions

$$F_n(r) = \langle \delta u(r)^n \rangle, \tag{2.87}$$

where $\delta u(r) = u_1(x+r) - u_1(x)$ is the increment of non-filtered velocity. At high Reynolds number, one observes that there exists a range in r, called the inertial subrange, where $F_n(r)$ has a power law behavior that is

$$F_n(r) \propto r^{\zeta(n)}. \tag{2.88}$$

The inertial subrange corresponds to length scales where viscosity effects are negligible, i.e. to an interval $\eta \ll r \ll L$, where $\eta = (\nu^3/\varepsilon)^{1/4}$ is the Kolmogorov dissipation scale, ε is the mean energy dissipation rate and L is the integral scale of motion. The Kolmogorov theory [9] predicts that the statistical properties of $\delta u(r)$ depend only on ε and r. It then follows by dimensional analysis that

$$\zeta(n) = n/3. \tag{2.89}$$

In fact, many experiments and numerical results in high Reynolds number turbulence have shown that the $n/3$ scaling law is not satisfied completely. A few models [32–37] have been proposed in order to explain the effect of intermittency on the scaling exponents of the structure functions. Two analytical solutions of the scaling exponent are also provied in the appendix D. However, these models are usually complex and not easy to be employed in real practice. The corrections for $n = 2$ and 3 with respect to K41 are usually very small. These orders are the most important in predicting the large scale behavior of turbulent flows. In this thesis, we therefore apply the classical scaling law theory (2.89) in inertial subrange.

The following problem is that the scaling law of filtered velocity might not be the same as the non-filtered velocity. In the following part, we analyze the behavior of structure function of filtered velocity, in physical space and spectral space respectively.

2.6.1 Analysis in physical space

In order to investigate the difference, a filter in physical space is represented by introducing the kernel

$$\int G(\vec{x} - \vec{x}')d\vec{x}' = 1, \tag{2.90}$$

and the velocity increment $\delta u_i^<(\vec{x}) = u_i^<(\vec{x} + \vec{r}) - u_1^<(\vec{x})$ can be written as

$$\delta u_i^<(\vec{x}) = \int G(\vec{x} - \vec{x}')\delta u_i(\vec{x}')d\vec{x}'. \tag{2.91}$$

Following Germano [83], it is easy to verify that

$$\begin{aligned}\delta u_i^< \delta u_j^< =& (\delta u_i \delta u_j)^< \\ &-\frac{1}{2}\int\int G(\vec{x} - \vec{x}')G(\vec{x} - \vec{x}'')\left(u_i(\vec{x}') - u_i(\vec{x}'')\right)\left(u_j(\vec{x}') - u_j(\vec{x}'')\right)d\vec{x}'d\vec{x}''.\end{aligned} \tag{2.92}$$

Using the same coordinate transformation as Germano, and assuming that the filter is Gaussian with filter size Δ, finally we obtain

$$\begin{aligned}\left\langle \delta u_i^< \delta u_j^< \right\rangle =& \left\langle (\delta u_i \delta u_j)^< \right\rangle \\ &-\frac{1}{2}\int\int G(\vec{s}; \sqrt{2}\Delta)\left\langle \left(\delta u_i(\vec{s}) - \delta u_i(\vec{0})\right)\left(\delta u_j(\vec{s}) - \delta u_j(\vec{0})\right)\right\rangle d\vec{r}.\end{aligned} \tag{2.93}$$

Because of the effect of filter kernel $G(\vec{s};\sqrt{2}\Delta)$, the last term of equation (2.93) is mostly effective when $s \lesssim \Delta$. When $\Delta \ll r$, the production of the velocity increments in the last term could be evaluated that

$$\left\langle \left(\delta u_i(\vec{s}) - \delta u_i(\vec{0})\right)\left(\delta u_j(\vec{s}) - \delta u_j(\vec{0})\right)\right\rangle \ll \left\langle \left(\delta u_i(\vec{r}) - \delta u_i(\vec{0})\right)\left(\delta u_j(\vec{r}) - \delta u_j(\vec{0})\right)\right\rangle . \tag{2.94}$$

Notice that the right hand side is at most the same order of magnitude as the second order structure function

$$\left\langle \left(\delta u_i(\vec{r}) - \delta u_i(\vec{0})\right)\left(\delta u_j(\vec{r}) - \delta u_j(\vec{0})\right)\right\rangle \lesssim \left\langle \left(u_i(\vec{r}) - u_i(\vec{0})\right)\left(u_j(\vec{r}) - u_j(\vec{0})\right)\right\rangle , \tag{2.95}$$

thus it could be then estimated approximately:

$$\left\langle \left(\delta u_i(\vec{r}) - \delta u_i(\vec{0})\right)\left(\delta u_j(\vec{r}) - \delta u_j(\vec{0})\right)\right\rangle \ll \langle \delta u_i \delta u_j \rangle . \tag{2.96}$$

In homogeneous turbulence, the first term in the right-hand side of equation (2.93) is

$$\left\langle (\delta u_i \delta u_j)^{<}\right\rangle = \langle \delta u_i \delta u_j \rangle^{<} = \langle \delta u_i \delta u_j \rangle , \tag{2.97}$$

Therefore when $\Delta \ll r$, there is the approximate relation that

$$\left\langle \delta u_i^{<} \delta u_j^{<}\right\rangle \approx \langle \delta u_i \delta u_j \rangle , \tag{2.98}$$

which means the properties of second-order structure functions are approximately the same between filtered and non-filtered velocities.

In homogeneous isotropic turbulence, we extend this conclusion onto higher-order structure functions, that

$$\langle (\delta u_1^{<})^n \rangle \approx F_n(r) \tag{2.99}$$

when $\Delta \ll r$.

And generally, in inhomogeneous anisotropic turbulence, there is the conclusion that

$$\left\langle (\delta u_{i_1}^{<} \delta u_{i_2}^{<} \ldots \delta u_{i_n}^{<})\right\rangle \approx \langle (\delta u_{i_1} \delta u_{i_2} \ldots \delta u_{i_n}) \rangle \tag{2.100}$$

when $\Delta \ll r$.

Therefore, in equation (2.21) if $\Delta \ll \xi$, the third-order structure function term will be

$$D_{111}^{<}(\xi) \propto \xi. \tag{2.101}$$

The dissipation term has the same trend that $6\langle S_{11}^{<}\tau_{11}^{<}\rangle\xi \propto \xi$. The subgrid transfer term in the right hand side $6T_{1,11} = 6\langle u_1^{<}(x_1)\tau_{11}^{<}(x_1+\xi)\rangle$ is a two-point correlation function, which would tend to zero when ξ is large. Thus the balance of magnitude in equation (2.21) is proved to be satisfied.

For the two-point skewness mentioned in section 2.4.5, if $\Delta \ll \xi$, we could obtain

$$D_{lll}^{<}(\xi) \approx \left\langle (u_1(x_1+\xi) - u_1(x_1))^3 \right\rangle, \qquad D_{ll}^{<}(\xi) \approx \left\langle (u_1(x_1+\xi) - u_1(x_1))^2 \right\rangle, \quad (2.102)$$

thus the skewness values of filtered and non-filtered velocity field could be considered the same.

2.6.2 Analysis in spectral space

A statistically homogeneous velocity field can be represented in spectral space:

$$\vec{u}(\vec{x}) = \left(\frac{1}{2\pi}\right)^3 \int \widehat{\vec{u}}(\vec{k}) \mathrm{e}^{-\iota\vec{k}\cdot\vec{x}} d\vec{k}. \quad (2.103)$$

A cut-off filter in spectral space is defined as

$$\widehat{\vec{u}}(\vec{k})^{<} = \begin{cases} \widehat{\vec{u}}(\vec{k}), & |\vec{k}| \le k_c, \\ 0, & |\vec{k}| > k_c, \end{cases} \quad (2.104)$$

where k_c is the cut-off wave number.

If the turbulence is isotropic, the summation of structure function could thus be denoted as [51,84]:

$$D_{ii}^{<}(\xi) = 4\int_0^\infty E(k)^{<} \left[1 - \frac{\sin k\xi}{k\xi}\right] dk, \quad (2.105)$$

where $E(k)$ is the energy spectrum and $E(k)^{<}$ represents a cut-off filter applied. Approximately, we could assume a von-Karman energy spectrum that

$$E(k) = E(k_p) 2^{17/6} \frac{(k/k_p)^4}{[1+(k/k_p)^2]^{17/6}}, \quad (2.106)$$

in which we fix $E(k) = 1.0$ and $k_p = 1.0$ (see Fig. 2.15). Suppose that $k_{c0} = 500$ corresponds with a grid size h of DNS, we have $h = 1/k_{c0} = 0.002$. When the filter size is $2h, 4h, ..., nh$, the corresponding cut-off wave numbers are $k_{c0}/2, k_{c0}/4, ..., k_{c0}/n$.

With the filter sizes $\Delta = h, 2h, 4h, 8h, 16h$ and $32h$, the summation of structure functions of filtered velocity $D_{ii}^{<}$ are calculated and shown in Fig. 2.16(a). The $\xi^{2/3}$

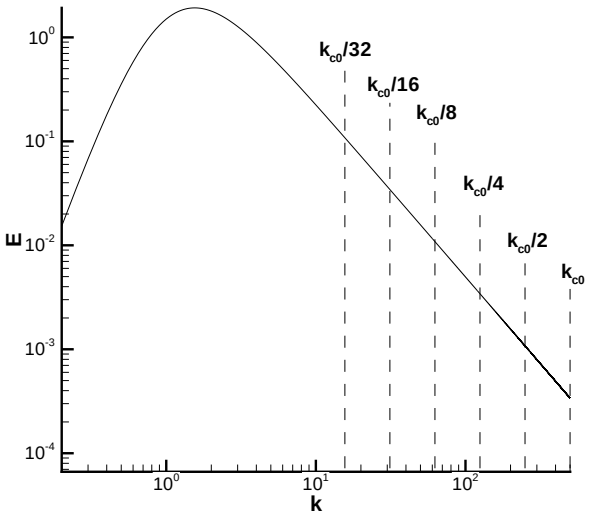

Figure 2.15: Von-Karman energy spectrum, with $E(k) = 1.0$, $k_p = 1.0$.

range is obvious when Δ is small, and it is less obvious when Δ is large (for instance $\Delta = 32h$). In order to investigate the behavior clearly, we define the compensating structure function:

$$\mathscr{D}_{ii}^{<}(\xi) = \xi^{-2/3} D_{ii}^{<}(\xi), \tag{2.107}$$

which are shown in Fig. 2.16(b). The plateau corresponds to the range which satisfies the $\xi^{2/3}$ scaling law. It becomes more narrow when Δ increase. Furthermore, note that with each filter size Δ, the start point of the corresponding plateau is about $\xi \simeq 10\Delta$. This phenomenon is in agreement with the analysis in physical space (section 2.6.1), that $\xi \gg \Delta$ should be satisfied to obtain the classical scaling law.

Note that in this section only the summation of structure function is discussed. The Fourier transforms of the components of structure function tensor are much more complex (see P. 206 in Hinze's book [51]). In fact, as long as the isotropic behavior is satisfied in each section of wave number (i.e. in each scale), the similar results for the tensor components are doubtless. In order to employ the classical scaling law in LES simulation, this behavior should be noticed and we propose the two-point distance is much larger than filter size, i.e. $\xi \gg \Delta$.

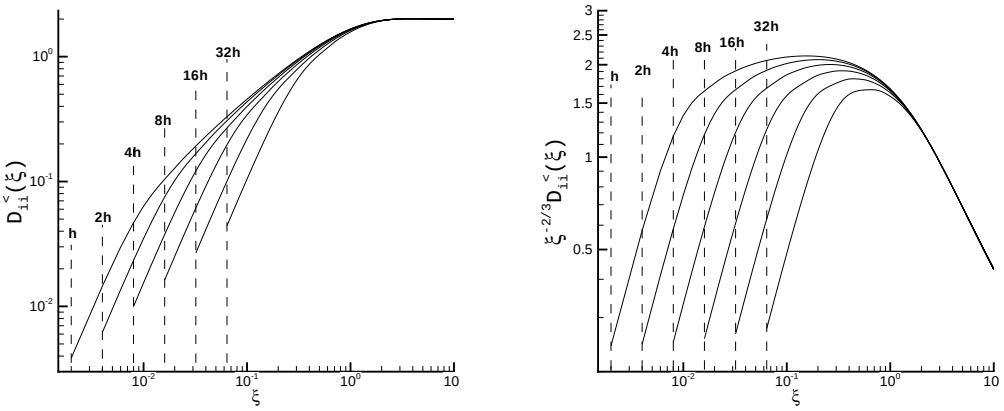

(a) (b)

Figure 2.16: Summation of structure functions of filtered velocity, with different cut-off filters of a von-Karman energy spectrum. In each figure from left to right: $\Delta = h, 2h, 4h, 8h, 16h,$ and $32h$. (a) Structure functions. (b) Compensating structure functions.

Chapter 3

Applying KEF on eddy-viscosity models

In this chapter, KEF is applied in eddy-viscosity modeling. From the eddy-viscosity assumption, the SGS stress tensor is aligned with the resolved strain rate tensor, i.e.:

$$\tau_{ij}^{<} - \frac{1}{3}\tau_{mm}^{<}\delta_{ij} = -2\nu_t S_{ij}^{<}, \tag{3.1}$$

where ν_t is the SGS eddy-viscosity coefficient. $S_{ij}^{<}$ is the strain rate for resolved scale turbulence:

$$S_{ij}^{<} = \frac{1}{2}\left(\frac{\partial u_i^{<}}{\partial x_j} + \frac{\partial u_j^{<}}{\partial x_i}\right). \tag{3.2}$$

When applied in anisotropic turbulence, the strain rates can be defined using the fluctuation parts of the velocity:

$$S_{ij}^{<} = \frac{1}{2}\left(\frac{\partial u_i'^{<}}{\partial x_j} + \frac{\partial u_j'^{<}}{\partial x_i}\right). \tag{3.3}$$

There is already lots of research on determining the eddy viscosity. In spectral space, models are all effective viscosity models drawing upon the analyses of Kraichnan. The subgrid viscosity is a function of wave number k. From Fourier transformation, introducing a cut-off wave number k_c, ν_t could be represented as

$$\nu_t(k|k_c) = -\frac{1}{2}\frac{T_{sgs}(k|k_c)}{2k^2E(k)}, \tag{3.4}$$

where $E(k)$ is the kinetic energy (the superscript $\bullet^*$ denotes the conjugation operation, and $S(\vec{k}$ is a spherical shell of radius k):

$$E(k) = \frac{1}{2}\int \widehat{\vec{u}}(\vec{k}) \cdot \widehat{\vec{u}}^{\,*}(\vec{k}) dS(\vec{k}), \tag{3.5}$$

and $T_{sgs}(k|k_c)$ is the subgrid energy transfer term [16].

Chollet and Lesieur proposed an effective viscosity model using the results of the EDQNM closure on the canonical case of isotropic turbulence [28]. The model formulation is obtained by approximating the exact solution with a law of exponential form:

$$\nu_t(k|k_c) = [1 + 34.59\exp(-3.03k_c/k)]\sqrt{\frac{E(k_c)}{k_c}}. \tag{3.6}$$

This form makes it possible to obtain an effective viscosity that is nearly independent of k for wave numbers that are small compared with k_c, with a finite increase near the cutoff. Another simplified form of the effective viscosity could be derived independently of the wave number k [85]. By averaging the effective viscosity along k and assuming that the subgrid modes are in a state of energy balance, we could obtain:

$$\nu_t(k|k_c) = \frac{2}{3}K_0^{-3/2}\sqrt{\frac{E(k_c)}{k_c}}. \tag{3.7}$$

In physical space, various subgrid viscosity models are available. The well-known Smagorinsky model is very simple to implement [3]. It is generally used in a local form in physical space, in order to be more adaptable to the flow being calculated. This model can be expressed as:

$$\nu_t = (C_s\Delta)^2|S^<|, \tag{3.8}$$

in which the constant theoretical value C_s should be determined. Using an isotropic energy spectrum, we could obtain $C_s = 0.17$ [86]. Clark uses $C_s = 0.2 \sim 0.22$ for a case of isotropic homogeneous turbulence [87], while Deardoff uses $C_s = 0.1$ for a plane channel flow [88]. Studies of shear flows using experimental data yield similar evaluations that $C_s \simeq 0.1 \sim 0.12$ [17, 89].

In order to determine the model coefficient, a dynamic method is to employ the Germano Identity [11, 12]. The dynamic method depend on two filters: the filtered part at mesh scale Δ is denoted as $\widetilde{\bullet}$, the corresponding subgrid stress is $\tau_{ij}^{\Delta} = \widetilde{u_iu_j} - \widetilde{u}_i\widetilde{u}_j$; the filtered part as a test scale $\alpha\Delta\,(\alpha > 1)$ is denoted as $\overline{\bullet}$, the corresponding subgrid stress is $\tau_{ij}^{\alpha\Delta} = \overline{u_iu_j} - \overline{u}_i\,\overline{u}_j$. A subgrid stress tensor is defined with the two filters $L_{ij} = \overline{\widetilde{u}_i\widetilde{u}_j} - \overline{\widetilde{u}_i}\,\overline{\widetilde{u}_j}$. Germano assumes:

$$L_{ij} = \tau_{ij}^{\alpha\Delta} - \tau_{ij}^{\Delta}. \tag{3.9}$$

Consider that the subgrid stress could be formulated by using Smagorinsky model (3.8), we could obtain the following equation:

$$L_{ij} - \frac{1}{3} L_{kk}\delta_{ij} = (C_s^{\Delta})^2 M_{ij}, \tag{3.10}$$

where $M_{ij} = -2\Delta^2 \left[\alpha^2 \left(\frac{C_s^{\alpha\Delta}}{C_s^{\Delta}} \right)^2 |\widetilde{\overline{S}}|\widetilde{\overline{S}}_{ij} - \widetilde{\overline{|\overline{S}|\overline{S}_{ij}}} \right]$. If the model coefficient is independent with grid size, i.e. $C_s^{\alpha\Delta} = C_s^{\Delta}$, employing the least-squares procedure, and the model coefficient could be solved dynamically:

$$(C_s)^2 = \frac{\langle L_{ij} M_{ij} \rangle}{\langle M_{ij} M_{ij} \rangle}. \tag{3.11}$$

The dynamic Smagorinsky model is widely applied in numerical simulation. It could yield good result, especially on the near-wall behavior. However, this method is a mathematical closure, but not a physical method, there is no physical relation implied.

When applied in anisotropic shear turbulence, the classical Smagorinsky model can not well represent the shear effect. Levêque *et al.* introduced a shear-improved model, which is based on results concerning mean-shear effects in wall-bounded turbulence [70]. The Smagorinsky eddy-viscosity is modified as

$$\nu_t = (C_s\Delta)^2 (|S^<| - |\langle S \rangle^<|), \tag{3.12}$$

where the magnitude of the mean shear $|\langle S \rangle^<|$ is subtracted from the magnitude of the instantaneous resolved rate-of-strain tensor $|S^<|$. Thus the shear-improved Smagorinsky model could represent the slow part of energy transfer equation.

The structure function model is a transposition of Metais and Lesieur's constant effective viscosity model into physical space, and can consequently be interpreted as a model based on the energy at the cutoff, expressed in physical space [29]. The second-order structure function is defined as

$$D_{ll}(\vec{x}, r) = \int_{|\vec{x}'|=r} \left[\vec{u}(\vec{x}) - \vec{u}(\vec{x} + \vec{x}') \right]^2 d^3\vec{x}', \tag{3.13}$$

and the structure function model takes the form:

$$\nu_t(r) = A(r/\delta)\Delta\sqrt{D_{ll}(r)}, \tag{3.14}$$

in which

$$A(x) = \frac{2K_0^{-3/2}}{3\pi^{4/3}\sqrt{9/5\Gamma(1/3)}} x^{-4/3} \left(1 - x^{-2/3} H_{sf}(x)\right)^{-1/2}. \tag{3.15}$$

In the case where $r = \Delta$, the model takes the simplified form:

$$\nu_t(\Delta) = 0.105\Delta\sqrt{D_{ll}(\Delta)}. \tag{3.16}$$

In addition, there are other viscosity models which are introduced in different ways [90, 91]. In this chapter, we introduce the CZZS model (*i.e.* the "third-order structure function model" [2]), which is the first modeling attempt by employing the homogeneous isotropic KEF. The simplifications and variations of CZZS model are discussed in Sec. 3.1. The KEF can also been applied in determining the coefficient of Smagorinsky model in Sec. 3.2. Besides, this model is extended into homogeneous shear turbulence and rotating turbulence in Sec. 3.3. In shear turbulence, the subgrid viscosity is affected by the mean shear. The anisotropic model is verified in large-eddy simulation. The corresponding work has been published in *Journal of Fluid Mechanics* [40].

3.1 Discussions on CZZS model

In section 2.2, we have obtained the homogeneous isotropic formulation of KEF:

$$-\frac{4}{5}\varepsilon_f \xi = D_{lll}^{<} - 6T_{l,ll}. \tag{3.17}$$

Employing the eddy-viscosity assumption (3.1), The isotropic part of subgrid stress can be included in the pressure of kinetic equation and $T_{l,ll}$ in equation (3.17) could be evaluated as

$$\begin{aligned} T_{l,ll} =& -2\nu_t \left\langle u^{<}(x) \frac{\partial u^{<}}{\partial x}(x+\xi) \right\rangle \\ =& -2\nu_t \frac{\partial}{\partial \xi} \left\langle u^{<}(x) u^{x}(x+\xi) \right\rangle \\ =& -2\nu_t \frac{\partial R_{ll}}{\partial \xi}. \end{aligned} \tag{3.18}$$

Since $D_{ll}^{<} = 2\langle u^{<^2} \rangle - 2R_{ll}$, we could write

$$T_{l,ll} = \nu_t \frac{\partial D_{ll}^{<}}{\partial \xi}. \tag{3.19}$$

The dissipation rate of resolved scale turbulence ε_f equals $-\langle\tau_{ij}^{<}S_{ij}^{<}\rangle$, and in the case of constant subgrid eddy viscosity, we have

$$\varepsilon_f = 2\nu_t\langle S_{ij}^{<}S_{ij}^{<}\rangle. \tag{3.20}$$

Inserting equations (3.19) and (3.20) into equation (3.17) one obtains the formulation for subgrid eddy viscosity [38]

$$\nu_t = \frac{-5D_{lll}^{<}}{8\langle S_{ij}^{<}S_{ij}^{<}\rangle\xi - 30\dfrac{\partial D_{ll}^{<}}{\partial\xi}}. \tag{3.21}$$

Introducing the skewness S_k (discussed in section 2.4.5):

$$S_k = \frac{D_{lll}^{<}}{(D_{ll}^{<})^{3/2}}, \tag{3.22}$$

the subgrid model could be expressed as

$$\nu_t = \frac{-5S_k(D_{ll}^{<})^{1/2}}{8\dfrac{\langle S_{ij}^{<}S_{ij}^{<}\rangle}{D_{ll}^{<}}\xi - \dfrac{30}{D_{ll}^{<}}\dfrac{\partial D_{ll}^{<}}{\partial\xi}}. \tag{3.23}$$

As discussed in the last chapter, the $T_{l,ll}$ vanish when $\xi \gg \Delta$. Thus the following discuss contain two parts: the one-scale models when $\xi = \Delta$, and the multi-scale models when $\xi \gg \Delta$.

3.1.1 One-scale models

The second-order structure function can be approximated by the scaling law:

$$D_{ll}^{<}(\xi) \propto \xi^n, \tag{3.24}$$

where n is the scaling exponent. As discussed in section 2.6, the classical scaling law could not be applied when $\xi = \Delta$. However, from Eq. (3.24) we can obtain

$$\frac{\partial D_{ll}^{<}}{\partial\xi} = \frac{nD_{ll}^{<}}{\xi}. \tag{3.25}$$

For small ξ, the second invariant of the strain rate tensor $S_{ij}^{<}S_{ij}^{<}$ could be evaluated in isotropic turbulence as

$$S_{ij}^{<}S_{ij}^{<} = \frac{15}{2}\left\langle\left(\frac{\partial u_1^{<}}{\partial x_1}\right)^2\right\rangle \approx \frac{15D_{ll}^{<}}{2\xi^2}. \tag{3.26}$$

Inserting (3.25) and (3.26) into the subgrid eddy viscosity formulation (3.23), we have a similar formulation to Smagorinsky model:

$$\nu_t = (C_s\Delta)^2\sqrt{2\langle S_{ij}^{<}S_{ij}^{<}\rangle}, \tag{3.27}$$

where

$$C_s = \sqrt{-\frac{S_k}{(12-6n)\sqrt{15}}}. \tag{3.28}$$

If $S_k = -0.457$ and $n = 2/3$ are accepted then the equivalent Smagorinsky coefficient $C_s \approx 0.12$. In fact, the ideal values maybe not correct for this problem. In Fig. 2.14 we have the two-point skewness $-0.3 < S_k < -0.2$. From section 2.6 the classical scaling law is not satisfied, thus we have $2/3 < n < 2$. Therefore, the coefficient C_s has dynamic values $C_s > 0.08$. These values are in magnitudal agreement with the classical coefficient values.

The subgrid eddy viscosity can also be written as

$$\nu_t = -\frac{S_k}{12-6n}\sqrt{D_{ll}^{<}}\xi. \tag{3.29}$$

Since $\xi = \Delta$, it is in the same formulation as Metais and Lesieur's structure function model:

$$\nu_t = C_m\sqrt{D_{ll}^{<}}\xi. \tag{3.30}$$

If $-0.3 < S_k < -0.2$ and $2/3 < n < 2$, the model coefficient $C_m > 0.025$. In this range, it depends on different mesh scales, and it's also in magnitudal agreement with Metais and Lesieur's result $C_m = 0.105$.

Both the simplified CZZS formulations (3.28) and (3.29) are expressed by the two-point skewness S_k. An advantage is that the skewness is approximately isotropic in homogeneous shear flow (as analyzed in section 2.4.5). It is also a direct result from the ESS theory, which has been verified to be more universal than the classical scaling law. Thus it might be better in LES applications than the structure function $D_{ll}^{<}$.

A Posteriori tests are performed in channel turbulence. Two numerical methods, one is the spectral method and the other is the finite volume method, are employed. The spectral method utilizes the Chebyshev polynomial. The mesh contains $32\times64\times32$ grids, in streamwise, normal and spanwise directions respectively. The numerical

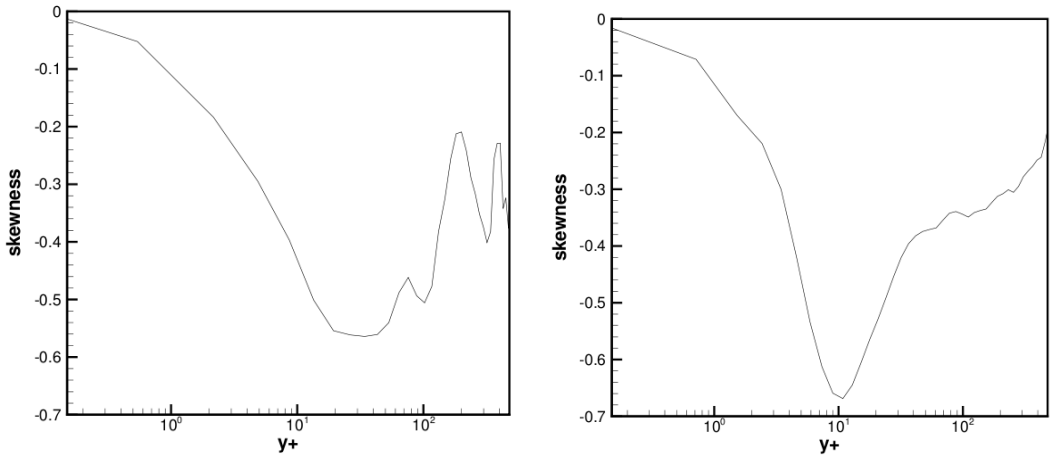

(a) Spectral method (b) Finite volume method

Figure 3.1: *A Posteriori* two-point skewness values, in normal direction of channel flow.

details are shown in the appendix. The finite volume code utilizes a precision of spatial resolution, which is 4^{th} order in homogeneous directions (i.e. streamwise and spanwise directions), and is 3^{th} order in normal direction. The temporal proceed is the 3^{th} order Runge-Kutta method. The mesh contains $48 \times 64 \times 48$ grids. The Reynolds number $\mathrm{Re}_H = 7000$, based on the bulk velocity U_m and channel half-width H.

The subgrid model employed in spectral method is the skewness-based CZZS model of Smagorinsky formulation (3.28). Let $n = 2/3$, the model could be represented as

$$C_s = \sqrt{-\frac{S_k}{8\sqrt{15}}}. \tag{3.31}$$

The finite volume method utilizes the Shear-Improved Smagorinsky Model (SISM):

$$\nu_t = (C_s\Delta)^2(|S^<| - |\langle S\rangle^<|), \tag{3.32}$$

where $C_s = 0.16$ according to EDQNM theory.

The skewness values in normal direction are shown in Fig. 3.1. In the center of channel, the value is about -0.3, which is in agreement with Cerutti's experiment [74]. In the region $10 < y^+ < 20$, the skewness is found to be about -0.7 in both cases, but the peak location is not exactly the same. The skewness values tend to zero in near-wall region in the two cases.

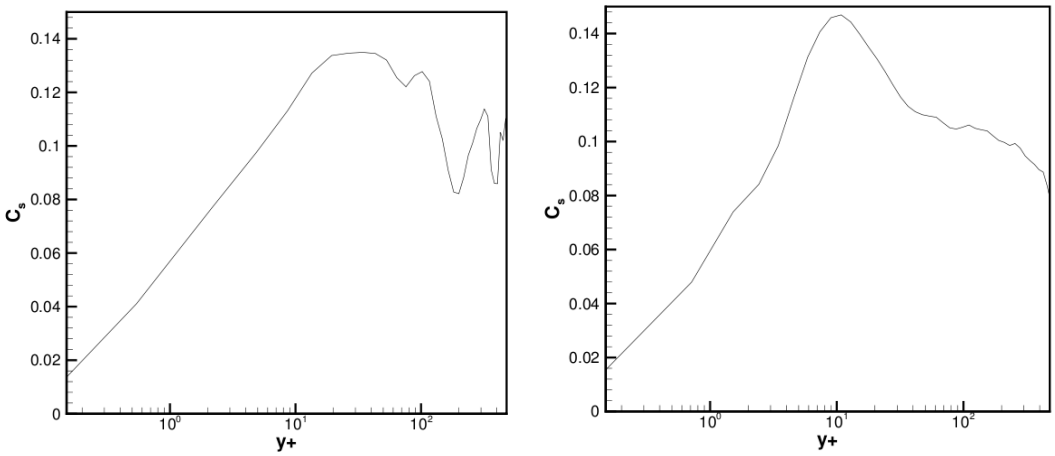

(a) Spectral method (b) Finite volume method

Figure 3.2: *A Posteriori* values of Smagorinsky coefficient C_s, in normal direction of channel flow.

The corresponding coefficient values of the Smagorinsky model is calculated by using equation (3.31). The values in both the two cases are also in agreement. In the center of channel, the values are about 0.1, which in in agreement with Deardoff's proposition [88]. The values tend to zero in near-wall region, which is the correct wall behavior.

A Posteriori statistical results of spectral method are shown in Fig. 3.3, compared with Moser's DNS results [92], LES results using classical Smagorinsky model (SM) and the dynamic Smagorinsky model (DSM). The behavior of the present subgrid model, i.e. Eq. (3.31), is as good as the DSM, and is much better than SM.

3.1.2 Multi-scale models in inertial subrange

According to eddy-viscosity assumption, we can obtain the multi-scale models, if all scales are in the inertial subrange. From equation (3.25), we have

$$T_{l,ll}(\xi) \propto \xi^{n-1}, \tag{3.33}$$

where n is the scaling exponent of second-order structure function. Especially if $n = 2/3$ we have

$$T_{l,ll}(\xi) \propto \xi^{-1/3}. \tag{3.34}$$

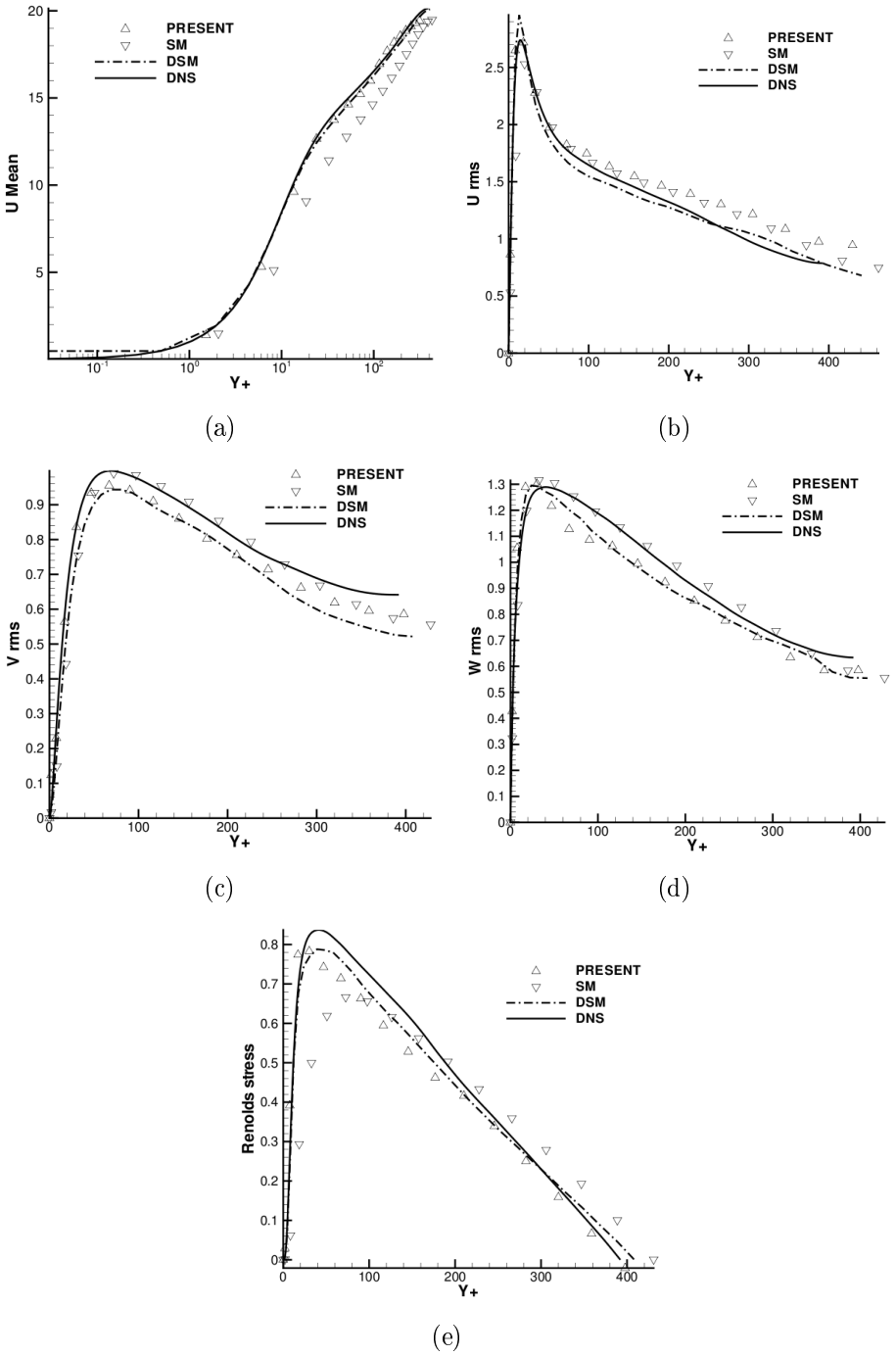

Figure 3.3: *A Posteriori* statistical results of channel flow. LES cases are using Eq. (3.31), Smagorinsky model (SM), dynamic Smagorinsky model (DSM), respectively. (a) Mean velocity profile. (b) Turbulence intensity in streamwise direction. (c) Turbulence intensity in normal direction. (d) Turbulence intensity in spanwise direction. (e) Reynolds stress profile.

Therefore, if two space increments ξ_1 and ξ_2 both satisfy this scaling law, we obtain the multi-scale relation [39]:

$$\frac{0.8\varepsilon_f\xi_1 + D^<_{ll}(\xi_1)}{0.8\varepsilon_f\xi_2 + D^<_{ll}(\xi_2)} = \left(\frac{\xi_1}{\xi_2}\right)^{-1/3}. \tag{3.35}$$

Thus the subgrid viscosity is denoted as

$$\nu_t = \frac{D^<_{ll}(\xi_1) - \left(\frac{\xi_1}{\xi_2}\right)^{-1/3} D^<_{ll}(\xi_2)}{-0.4|S^<|^2\left(1 - \left(\frac{\xi_1}{\xi_2}\right)^{4/3}\right)\xi_1}. \tag{3.36}$$

Furthermore, we can derive a similar formulation with three or more scales in the inertial subrange. Suppose three space increments ξ_1, ξ_2 and ξ_3 all satisfy the scaling law (3.34), we have

$$\frac{T_{l,ll}(\xi_1)}{T_{l,ll}(\xi_2)}\left(\frac{\xi_1}{\xi_2}\right)^{-1/3} = \frac{T_{l,ll}(\xi_2)}{T_{l,ll}(\xi_3)}\left(\frac{\xi_2}{\xi_3}\right)^{-1/3}. \tag{3.37}$$

The subgrid viscosity is the root of the following equation:

$$(A\alpha_2^2 - \alpha_1\alpha_3)\nu_t^2 + (A\alpha_2\beta_2 - \alpha_1\beta_3 - \alpha_3\beta_1)\nu_t + A\beta_2^2 - \beta_1\beta_3 = 0, \tag{3.38}$$

in which

$$\alpha_i = \frac{4}{5}|S^<|\xi_i,\ \beta_i = D^<_{ll}(\xi_i),\ A = \left(\frac{\xi_2^2}{\xi_1\xi_3}\right)^{-1/3}. \tag{3.39}$$

These multi-scale models are attempts to obtain a relative relation between different scales. However, the same scaling exponents are not exactly satisfied when ξ_i is of the same magnitude as Δ. Therefore, another multi-scale model is proposed, considering two separated scales.

3.1.3 Multi-scale model with separated scales

In the simplifications of CZZS model (section 3.1.1), both the scaling law and the Taylor expansion are employed. However, the scaling law should be applied in inertial subrange, and the Taylor expansion should be used in very small two-point distance. Thus in this section, we consider that the filter size Δ and the two-point distance ξ in KEF are separated, i.e $\Delta \ll \xi$. Assume that ξ is in inertial subrange and the scaling law is satisfied:

$$D^<_{ll}(\xi) \propto \xi^{2/3}. \tag{3.40}$$

Then, the subgrid transfer term could be written by employing scaling law:

$$\frac{\partial D_{ll}^{<}}{\partial \xi} = \frac{2D_{ll}^{<}(\xi)}{3\xi}. \tag{3.41}$$

And the dissipation term could be expressed by employing Taylor expansion at small scale Δ:

$$S_{ij}^{<}S_{ij}^{<} = \frac{15}{2}\left\langle \left(\frac{\partial u_1^{<}}{\partial x_1}\right)^2 \right\rangle \approx \frac{15D_{ll}^{<}(\Delta)}{2\Delta^2}. \tag{3.42}$$

Therefore, the formulation of this multi-scale subgrid model could be:

$$\nu_t = \frac{-D_{lll}^{<}(\xi)}{12\dfrac{\xi}{\Delta^2}D_{ll}^{<}(\Delta) - 4\dfrac{D_{ll}^{<}(\xi)}{\xi}}. \tag{3.43}$$

Furthermore, when ξ is large, the second term in the denominator can be negelcted by comparing with the first term, and we can obtain a simple expression:

$$\nu_t = \frac{-\Delta^2 D_{lll}^{<}(\xi)}{12\xi D_{ll}^{<}(\Delta)}. \tag{3.44}$$

In LES applications, we could consider Δ as the same as grid size h, and the two-point distance ξ much larger than h, to calculate the subgrid viscosity dynamically.

3.2 A new dynamic method to determine the coefficient of Smagorinsky model

The KEF can not only be employed to bring up new subgrid models (such as the CZZS model), but also applied to determine the model coefficients. In this section we determine the coefficient of Smagorinsky model by using the homogeneous isotropic formulation of KEF.

In homogeneous isotropic turbulence, considering that $\xi \gg \Delta$, the subgrid transfer term $T_{l,ll}$ in equation (2.16) vanishes. Employing the formulation of the Smagorinsky model (3.8), the subgrid dissipation can be represented as

$$\begin{aligned} \varepsilon_f =& -\langle \tau_{ij}^{<} S_{ij}^{<} \rangle \\ =& 2\langle \nu_t S_{ij}^{<} S_{ij}^{<} \rangle \\ =& 2(C_s\Delta)^2 (S_{kl}^{<}S_{kl}^{<})^{1/2} S_{ij}^{<} S_{ij}^{<}. \end{aligned} \tag{3.45}$$

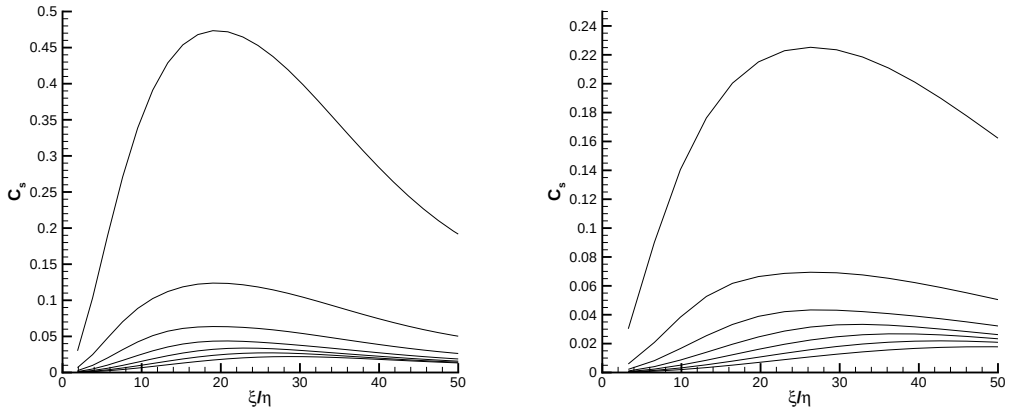

(a) $Re_\lambda = 50$ (b) $Re_\lambda = 70$

Figure 3.4: Dynamic values of the coefficient of Smagorinsky model. From top to bottom: $\Delta = h, 2h, ..., 7h$.

Thus from equation (2.16), we solve the dynamic coefficient C_s as

$$C_s^2 = \frac{-5D_{lll}^{<}(\xi)}{8\xi\Delta^2\langle(S_{ij}^{<}S_{ij}^{<})^{3/2}\rangle}. \tag{3.46}$$

Thus the coefficient is determined dynamically. Note that we should let $\xi \gg \Delta$ in order to neglect the $T_{l,ll}$ term. This formulation is similar with Canuto's result [93]:

$$C_s^2 \propto \frac{q_{sgs}^2}{\varepsilon|S^{<}|\Delta^2}. \tag{3.47}$$

In order to evaluate the behavior of this new method, *A Priori* numerical tests are made. The two DNS cases of homogeneous isotropic turbulence with spectral method are utilized. The filter scale Δ and the increment distance ξ are selected independently. The filter scales are between 1 and 7 times of grid size h. Results are shown in Fig. 3.4. It shows that the values are of the same magnitude as the classical theory. When Δ is not large (for instance $\Delta = 2h$) and $10 < \xi < 30$ is in the inertial subrange, we could obtain $C_s \approx 0.1$ and 0.06, when $\mathrm{Re}_\lambda = 50$ and 70, respectively. Both these values could be applied in numerical simulation. It also shows the trend that the coefficient value decreases when filter size increases.

In conclusion, in this section we propose another dynamic method to determine the coefficient of Smagorinsky model. The results show the correct magnitude and scale behavior. As long as we select the appropriate filter size Δ and increment

distance ξ, this method might be applied in large-eddy-simulation. It is much less costly than the dynamic Smagorinsky model based on Germano identity [11], and it has clear physical background.

3.3 SGS models for homogeneous anisotropic turbulence

The governing equations for both homogeneous rotating turbulence and shear turbulence can be written in a unified form for convenient derivation of subgrid eddy viscosity as follows

$$\begin{aligned} \frac{\partial u_i'}{\partial t} + U\frac{\partial u_i'}{\partial x_1} + u_j'\frac{\partial u_i'}{\partial x_j} =& -\frac{1}{\rho}\frac{\partial p'}{\partial x_i} + \nu\frac{\partial^2 u_i'}{\partial x_j \partial x_j} + s_i, \\ \frac{\partial u_i'}{\partial x_i} =& 0, \end{aligned} \tag{3.48}$$

in which $U = \gamma x_2, s_i = -\gamma u_2' \delta_{i1}$ for homogeneous shear turbulence, and $U = 0, s_i = 2\epsilon_{ij3}\Omega u_j'$ in homogeneous rotating turbulence. It should be emphasized that the reference frames for rotating turbulence and shear turbulence are different, although their governing equations are written in same formulae. This indicates that the subgrid eddy viscosity for rotating turbulence is reconstructed in a rotating frame whereas it is in an inertial frame for homogeneous shear turbulence.

From equation (2.54) and (2.86), the general formulation of KEF can be written as

$$\begin{aligned} &\frac{\partial D_{ii}^<}{\partial t} + \frac{\partial D_{iij}^<}{\partial \xi_j} + \frac{\partial (\delta U D_{ii}^<)}{\partial \xi_1} - 2\langle \delta u_i'^< \delta s_i^< \rangle \\ &\quad = 2\nu \frac{\partial D_{ii}^<}{\partial \xi_j \partial \xi_j} - 4\varepsilon^< + 2\left\langle \delta u_i'^< \left(\frac{\partial \tau_{ij}^<}{\partial x_j} - \frac{\partial \tau_{ij}^{<*}}{\partial x_j^*} \right) \right\rangle. \end{aligned} \tag{3.49}$$

Note that the SGS stress $\tau_{ij}^<$ contains both the homogeneous rapid part and the slow part.

The last two subgrid terms can be represented as

$$\begin{aligned} &\left\langle \delta u_i'^< \left(\frac{\partial \tau_{ij}^<}{\partial x_j} - \frac{\partial \tau_{ij}^{<*}}{\partial x_j^*} \right) \right\rangle \\ &= \left\langle \frac{\partial \delta u_i'^< \tau_{ij}^<}{\partial x_j} - \frac{\partial \delta u_i'^< \tau_{ij}^{<*}}{\partial x_j^*} \right\rangle - \left\langle \tau_{ij}^< \frac{\partial \delta u_i'^<}{\partial x_j} - \tau_{ij}^{<*} \frac{\partial \delta u_i'^<}{\partial x_j^*} \right\rangle. \end{aligned} \tag{3.50}$$

Introducing the eddy-viscosity assumption (3.1), where the strain rate is defined as the fluctuation part, i.e. equation (3.3), the first two terms on the right-hand side of equation (3.50) can be derived as

$$\begin{aligned}\frac{\partial\langle\delta u_i'^{<}\tau_{ij}^{<}\rangle}{\partial x_j}-\frac{\partial\langle\delta u_i'^{<}\tau_{ij}^{<*}\rangle}{\partial x_j^*}=&\frac{\partial\langle\delta u_i'^{<}\tau_{ij}^{<}\rangle}{\partial\xi_j}+\frac{\partial\langle\delta u_i'^{<}\tau_{ij}^{<*}\rangle}{\partial\xi_j}\\ =&\nu_t\frac{\partial^2\langle\delta u_i^{<}\delta u_i^{<}\rangle}{\partial\xi_j\partial\xi_j}+2\nu_t\frac{\partial^2\langle\delta u_j^{<}\delta u_i^{<}\rangle}{\partial\xi_j\partial\xi_i}.\end{aligned}\tag{3.51}$$

The last term of the above equation is equal to zero in homogeneous turbulence as can be proved as follows

$$\begin{aligned}\nu_t\frac{\partial^2\langle\delta u_j'^{<}\delta u_i'^{<}\rangle}{\partial\xi_j\partial\xi_i}=&\nu_t\frac{\partial^2\langle\delta u_j'^{<}\delta u_i'^{<}\rangle}{\partial x_j\partial x_i}=\nu_t\left\langle\frac{\partial^2(\delta u_j'^{<}\delta u_i'^{<})}{\partial x_j\partial x_i}\right\rangle\\ =&\nu_t\left\langle\frac{\partial\delta u_k'^{<}}{\partial x_i}\frac{\partial\delta u_i'^{<}}{\partial x_k}\right\rangle=\nu_t\left\langle\frac{\partial u_k'^{<}}{\partial x_i}\frac{\partial u_i'^{<}}{\partial x_k}\right\rangle=\nu_t\frac{\partial^2\langle u_k'^{<}u_i'^{<}\rangle}{\partial x_k\partial x_i}.\end{aligned}\tag{3.52}$$

Since the turbulence is homogeneous, the derivatives of one-point statistics are equal to zero, i.e.

$$\nu_t\frac{\partial^2\langle\delta u_j'^{<}\delta u_i'^{<}\rangle}{\partial\xi_j\partial\xi_i}=\nu_t\frac{\partial^2\langle u_k'^{<}u_i'^{<}\rangle}{\partial x_k\partial x_i}=0.\tag{3.53}$$

The first two terms in (3.50) are then simplified as

$$\frac{\partial\langle\delta u_i'^{<}\tau_{ij}^{<}\rangle}{\partial x_j}-\frac{\partial\langle\delta u_i'^{<}\tau_{ij}^{<*}\rangle}{\partial x_j^*}=\nu_t\frac{\partial^2\langle\delta u_i'^{<}\delta u_i'^{<}\rangle}{\partial\xi_i\partial\xi_i}=\nu_t\frac{\partial D_{ii}^{<}}{\partial\xi_i\partial\xi_i}.\tag{3.54}$$

The last two terms of (3.50) are manipulated as follows

$$\begin{aligned}&-\left\langle\tau_{ij}^{<}\frac{\partial\delta u_i'^{<}}{\partial x_j}-\tau_{ij}^{<*}\frac{\partial\delta u_i'^{<}}{\partial x_j^*}\right\rangle\\ =&-\left\langle\left(\frac{\partial u_i'^{<}}{\partial x_j}+\frac{\partial u_j'^{<}}{\partial x_i}\right)\frac{\partial\delta u_i'^{<}}{\partial x_j}\right\rangle+\left\langle\left(\frac{\partial u_i'^{<*}}{\partial x_j^*}+\frac{\partial u_j'^{<*}}{\partial x_i^*}\right)\frac{\partial\delta u_i'^{<}}{\partial x_j^*}\right\rangle\\ =&-\left\langle\left(\frac{\partial u_i'^{<}}{\partial x_j}+\frac{\partial u_j'^{<}}{\partial x_i}\right)\frac{\partial u_i'^{<}}{\partial x_j}\right\rangle+\left\langle\left(\frac{\partial u_i'^{<*}}{\partial x_j^*}+\frac{\partial u_j'^{<*}}{\partial x_i^*}\right)\frac{\partial u_i'^{<*}}{\partial x_j^*}\right\rangle\\ =&-2\nu_t\left\langle\frac{\partial u_i'^{<}}{\partial x_k}\frac{\partial u_i'^{<}}{\partial x_k}\right\rangle,\end{aligned}\tag{3.55}$$

in which $\varepsilon_f=\nu_t\left\langle\frac{\partial u_i'^{<}}{\partial x_k}\frac{\partial u_i'^{<}}{\partial x_k}\right\rangle$ is the subgrid dissipation.

Therefore, the KEF (3.49) could be rewritten as

$$\begin{aligned}&\frac{\partial D_{ii}^{<}}{\partial t}+\frac{\partial D_{iij}^{<}}{\partial \xi_j}+\frac{\partial(\delta U D_{ii}^{<})}{\partial \xi_1}-2\langle \delta u_i^{<}\delta s_i^{<}\rangle \\ =&2(\nu+\nu_t)\frac{\partial D_{ii}^{<}}{\partial \xi_j \partial \xi_j}-4\varepsilon^{<}-4\varepsilon_f.\end{aligned} \tag{3.56}$$

Following the classic theory that the time derivative of $D_{ll}^{<}$ and the molecular viscosity diffusion can be neglected in the dynamic equation of structure functions for high-Reynolds-number flows [94], the final formula of the generalized Kolmogorov equation for anisotropic resolved scale turbulence is then written as

$$\frac{\partial D_{iij}^{<}}{\partial \xi_j}+\frac{\partial(\delta U D_{ii}^{<})}{\partial \xi_1}-2\langle \delta u_i^{<}\delta s_i^{<}\rangle=2\nu_t\frac{\partial D_{ii}^{<}}{\partial \xi_j \partial \xi_j}-4\varepsilon_f. \tag{3.57}$$

In order to obtain the eddy viscosity for homogeneous turbulence, we take the local volume average in displacement space as Hill [95] and Casciola [96] did, as follows

$$\begin{aligned}&\int_V\left(\frac{\partial D_{iij}^{<}}{\partial \xi_j}+\frac{\partial \delta U D_{ii}^{<}}{\partial \xi_1}\right)dv \\ =&\int_V\left(2\nu_t\frac{\partial^2 D_{ii}^{<}}{\partial \xi_j \partial \xi_j}-4\nu_t\left\langle\frac{\partial u_i'^{<}}{\partial x_j}\frac{\partial u_i'^{<}}{\partial x_j}\right\rangle+2\langle \delta u_i'^{<}\delta s_i^{<}\rangle\right)dv.\end{aligned} \tag{3.58}$$

The volume integration on the left-hand side can be transferred to surface integration by the Gauss formula such that

$$\begin{aligned}\int_v\frac{\partial D_{iij}^{<}}{\partial \xi_j}dv&=\int_S D_{iij}^{<}n_j dA,\\ \int_v\frac{\partial \delta U D_{ii}^{<}}{\partial \xi_1}dv&=\int_S \delta U D_{ii}^{<}n_1 dA.\end{aligned} \tag{3.59}$$

The first term on right-hand side can also be transferred to surface integration such that

$$\int_V 2\nu_t\frac{\partial^2 D_{ii}^{<}}{\partial \xi_j \partial \xi_j}dv=2\nu_t\int_S\frac{\partial D_{ii}^{<}}{\partial \xi_k}n_k dA. \tag{3.60}$$

The linear size of the integration volume should be within the inertial subrange. In practice, it is equal to twice the mesh length in the following computational cases. Define the local volume average and surface average, respectively, as

$$\begin{aligned}Q^V=&\frac{1}{V}\int_V Q dv,\\ Q^S=&\frac{1}{S}\int_S Q dA.\end{aligned} \tag{3.61}$$

Equation (3.58) is then rewritten as

$$\begin{aligned} &S(D^{<}_{iij}n_j)^S+S(\delta UD^{<}_{ii}n_1)^S \\ &\quad =S\nu_t\left(\frac{\partial D^{<}_{ii}}{\partial \xi_j}n_j\right)^S-4\nu_t V\left\langle\frac{\partial u_i'^{<}}{\partial x_j}\frac{\partial u_i'^{<}}{\partial x_j}\right\rangle^V+2V\langle\delta u_i'^{<}\delta s_i^{<}\rangle^V. \end{aligned} \tag{3.62}$$

Finally, the subgrid eddy viscosity is equal to

$$\nu_t=\frac{(D^{<}_{iij}n_j)^S+(\delta UD^{<}_{ii}n_1)^S+2V/S\langle\delta u_i'^{<}\delta s_i^{<}\rangle^V}{2\left(\frac{\partial D^{<}_{ii}}{\partial \xi_j}n_j\right)^S-4V/S\left\langle\frac{\partial u_i'^{<}}{\partial x_j}\frac{\partial u_i'^{<}}{\partial x_j}\right\rangle^V}. \tag{3.63}$$

The structure functions $D^{<}_{ii}, D^{<}_{iij}$ are the ensemble average of the products of velocity increment in physical space, in practice the ensemble average can be taken in homogeneous directions; hence, the structure functions are independent of x and varying with displacement $\vec{\xi}$. The local volume average is taken in displacement space $\vec{\xi}$ which is independent of physical space $\vec{x}$. After local space averaging, the terms involving structure functions are constants both in physical and displacement spaces and, finally, the subgrid eddy viscosity is a constant in homogeneous turbulence. In practice, the local volume-average method is dependent on the flow geometry so that it can be taken in a sphere for homogeneous rotating turbulence or in a rectangular box for plane shear flow.

In homogeneous rotating turbulence $\delta U=0$ and $\langle\delta u_i'^{<}\delta s_i^{<}\rangle=2\epsilon_{ij3}\langle\delta u_i'^{<}\delta u_j'^{<}\Omega\rangle=0$. The subgrid eddy viscosity for homogeneous rotating flow is then equal to

$$\nu_t=\frac{(D^{<}_{iij}n_j)^S}{2\left(\frac{\partial D^{<}_{ii}}{\partial \xi_j}n_j\right)^S-4V/S\left\langle\frac{\partial u_i'^{<}}{\partial x_j}\frac{\partial u_i'^{<}}{\partial x_j}\right\rangle^V}. \tag{3.64}$$

Note that the rotation rate does not appear explicitly in the formula of eddy viscosity. It is not surprising because the solid rotation does not contribute directly to the total transfer of turbulent kinetic energy; neither does it to the transfer of velocity increment variance. However, rotation can redistribute kinetic energy among fluctuating velocity components and the turbulence becomes anisotropic. Equation (3.64) represents correct transfer of kinetic energy in anisotropic resolved scale turbulence through the local volume average of transfer and dissipation terms.

In homogeneous shear turbulence, $\delta U = \gamma \xi_2$ and $\langle \delta u_i'^{<} \delta s_i^{<} \rangle = \gamma D_{12}^{<}$. The subgrid eddy viscosity becomes

$$\nu_t = \frac{(D_{iij}^{<} n_j)^S + (\gamma \xi D_{ii}^{<} n_1)^S - 2\gamma V/S (D_{12}^{<})^V}{2\left(\dfrac{\partial D_{ii}^{<}}{\partial \xi_j} n_j\right)^S - 4V/S \left\langle \dfrac{\partial u_i'^{<}}{\partial x_j} \dfrac{\partial u_i'^{<}}{\partial x_j} \right\rangle^V}. \tag{3.65}$$

3.3.1 Model applications in rotating turbulence

In this section, we are trying to simulate rotating turbulence numerically by LES. The traditional subgrid models fail to predict rotating turbulence since they do not consider the anisotropic effect of turbulence in the model. Yang [97] used truncated Navier–Stokes (TNS) as a model for large-eddy simulation of homogeneous rotating turbulence with considerable success; for instance, they obtained a k^{-3} energy spectrum at high Reynolds numbers and small Rossby numbers. The idea of TNS is to try to model the energy transfer from large (non-truncated) to small-scale (truncated) turbulence by the estimation method. The new model presented here is different from theirs in that we formulate the eddy-viscosity model with the correct turbulent energy transfer from the Navier–Stokes equation without any assumptions on the velocity fluctuations, with the exception of homogeneity. Moreover, we will give more significant and critical statistical properties of rotating turbulence, such as the skewness of the velocity derivative, which was not given in Yang's paper.

The numerical simulation of homogeneous rotating turbulence is performed in a rotating frame by the pseudo-spectrum method with rotation in the x_3 direction. The initial turbulence field is generated by the method proposed by Rogallo [54] with a von-Karman spectrum. The computational domain is a rectangular box which is four times longer in the rotating direction than in the horizontal direction, since the turbulence scale is increasing greatly in the rotating direction. A fourth-order Runge–Kutta integration is used for time advancement. The time step is set to be small enough to resolve the inertial waves. The flow Reynolds number is assumed to be infinite by prescribing zero molecular viscosity.

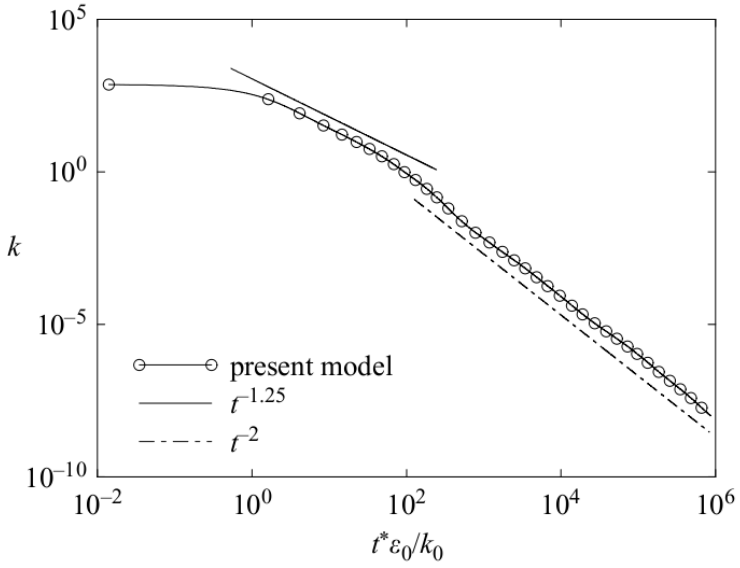

Figure 3.5: Decay of turbulent kinetic energy in isotropic turbulence with 64^3 LES.

In homogeneous rotating turbulence, the local average is taken in a sphere with radius r and the subgrid eddy viscosity is derived from (3.64) so that

$$\nu_t = \frac{3(D_{iir}^{<})^{S_r}}{6\left(\dfrac{\partial D_{ii}^{<}}{\partial r}\right)^{S_r} - 4\left\langle \dfrac{\partial u_i'^{<}}{\partial x_j}\dfrac{\partial u_i'^{<}}{\partial x_j}\right\rangle^{V_r} r}. \tag{3.66}$$

In practical computation, the local volume average is taken in a sphere circumscribing a cube with twice the mesh length.

The first test case is a decaying isotropic turbulence without rotation with 64^3 grids in order to validate the model and numerical method. The simulation is run for more than 10^6 initial turn-over time and the classic decaying law, t^{-n}, is found in a short time with $n \approx 1.25$, which is in agreement with previous numerical and experiment results. The exponent of the decaying law approaches -2 at the final stage of decay (Fig. 3.5), and this result is consistent with the experimental study by Skrbek [98], and the numerical analysis of Touil *et al.* [99].

To perform large-eddy simulation of decaying rotating turbulence at high Reynolds number, a purely decaying turbulence without rotation was computed for sufficient time and a solid-body rotation was then switched on when the time decay of large-scale kinetic energy k reached a reliable power law in pre-computation. Figure 3.6 shows the time variation of the large-scale turbulence kinetic energy for different rotation

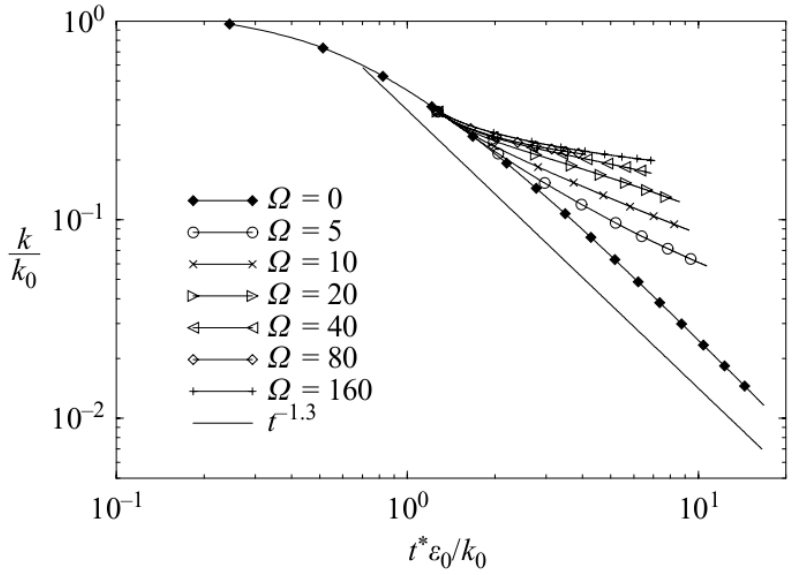

Figure 3.6: Time variation of large-scale kinetic energy for different rotating rates, grids: $64 \times 64 \times 256$.

rates. The numerical grid is $64 \times 64 \times 256$ in spectral space. As the rotation reduces the spectral energy transfer, the decay of the turbulent kinetic energy is becoming slower. This phenomenon is pronounced when the rotating rate is increasing.

The critical examination of the applicability of the new model is to check the variation of the derivative skewness with time. The derivative skewness, i.e. equation (2.80), represents the balance between transfer of turbulent kinetic energy and its dissipation. The direct comparison of the derivative skewness between DNS and LES results is meaningless, but the variation of S_k/S_{k0} with time under the influence of rotation indicates the capability of the self-adjustment of a subgrid model to the rotation effect. In decaying turbulence, Cambon [75] proposed a scaling law of S_k/S_{k0} versus Rossby number, as follows:

$$\frac{S_k(t)}{S_{k0}} = \frac{1}{\left(1 + 2\left(\mathrm{Ro}^{\Omega}(t)\right)^{-2}\right)^{1/2}}, \tag{3.67}$$

in which $\mathrm{Ro}^{\Omega} = (\varepsilon/k\Omega)/(k^2/\nu\varepsilon)^{1/2}$ is based on the Taylor micro scale and called the micro Rossby number. In LES, the turbulent dissipation ε and molecular viscosity ν are replaced by ε_f and ν_t , respectively, and k is the large-scale turbulence kinetic energy. This replacement is valid so that the governing equation of LES for homogeneous turbulence with constant eddy viscosity is in a similar form to DNS with

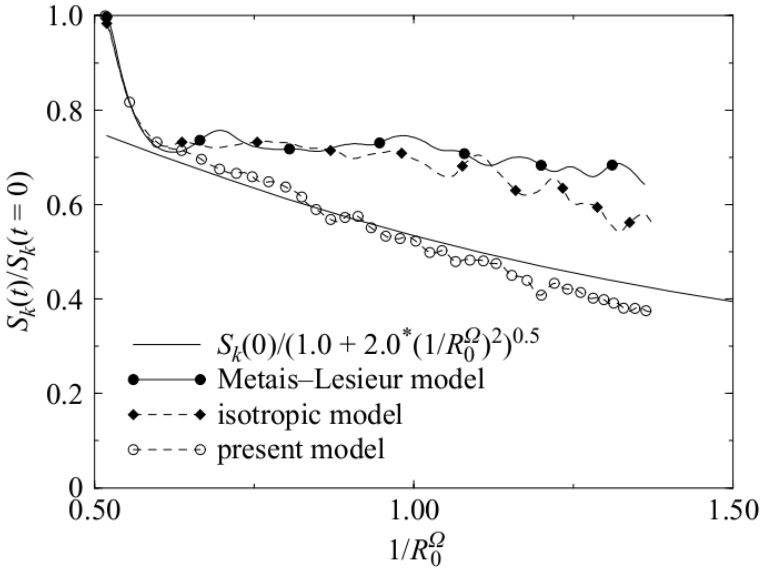

Figure 3.7: Skewness variation versus micro Rossby number at rotating rate $\Omega = 10$.

replacement of molecular viscosity by eddy viscosity. Following the same deduction procedure as was performed by Cambon [75], it is reasonable to accept the above parameters in scale law (3.67). Comparison of the predicted results among different subgrid models is presented in Fig. 3.7. The initial micro Rossby number is equal to 1.82 at $\Omega = 10$ and drops to 0.72 at the end of computation. All models produce a sudden reduction of derivative skewness to the level predicted by (3.67) at the beginning when rotation is applied and the Rossby number is relatively high. However, the later development differs greatly between the new model and the others. The Metais–Lesieur model [29] and the CZZS model cannot predict the reduction of skewness after a sudden reduction. The Metais–Lesieur mode predicts nearly constant level of skewness, whereas the CZZS model shows a small reduction of skewness. In contrast, the skewness predicted by the new model, which involves the anisotropic transfer of kinetic energy, fits the scaling law (3.67) very well, particularly at Rossby number around 1.

A finer grid with $96 \times 96 \times 384$ nodes was used to check the resolution influence. The micro Rossby number is nearly 2.0 in the initial state and reaches 0.22 at the end of computation. The result is shown in Fig. 3.8 and is much better than in the lower resolution run.

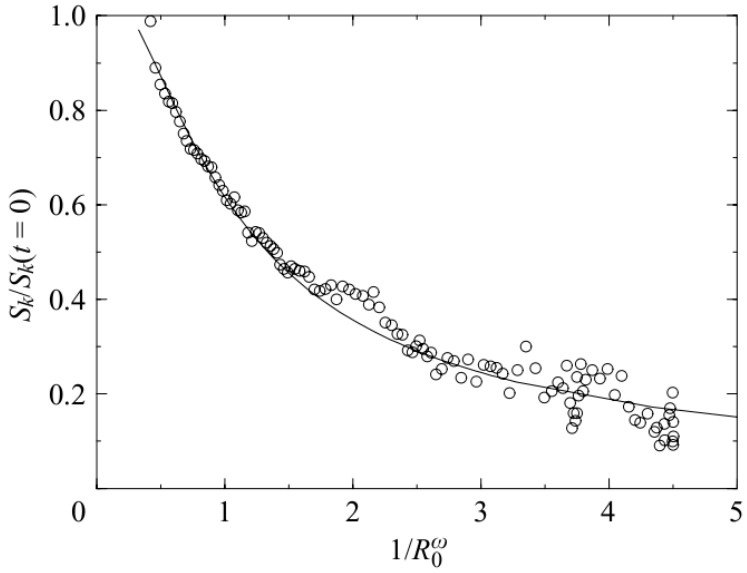

Figure 3.8: Skewness versus micro Rossby number with finer grids $96 \times 96 \times 384$. Line: Cambon et al. (1997); symbols: anisotropic model.

The energy spectrum $E(k)$ is checked and presented in Fig. 3.9 for rotating rates of 10 and 100. The initial micro Rossby numbers are nearly 2.22 and 0.222 and approaching to 0.222 and 0.0667 at the end of computation. Once the rotation is switched on, the spectral slope shifts gradually from $-5/3$ to -3 as shown in Figs. 3.9(a) and (b). In Figs. 3.9(c) and (d), the compensated spectra for both cases are plotted at the end of computation time. The plateau is shown clearly in both figures.

3.3.2 Model applications in wall-bounded shear turbulence

The proposed new model is based on the assumption of homogeneous turbulence. The homogeneity of turbulence can be accepted approximately in the major part of wall-bounded turbulence, with the exception of the near-wall region. The proposed new model has correct asymptotic behavior in the near-wall region where ν_t is proportional to y^3; hence, the molecular viscosity is dominant there and the computation of wall-bounded turbulence can be performed by LES properly with fine normal resolution to the wall with the proposed new model. In fact, the previous CZZS model is capable of predicting turbulent channel flow in fairly good agreement with DNS results [38]. Here, we will show that the proposed new model improves the prediction precision considerably.

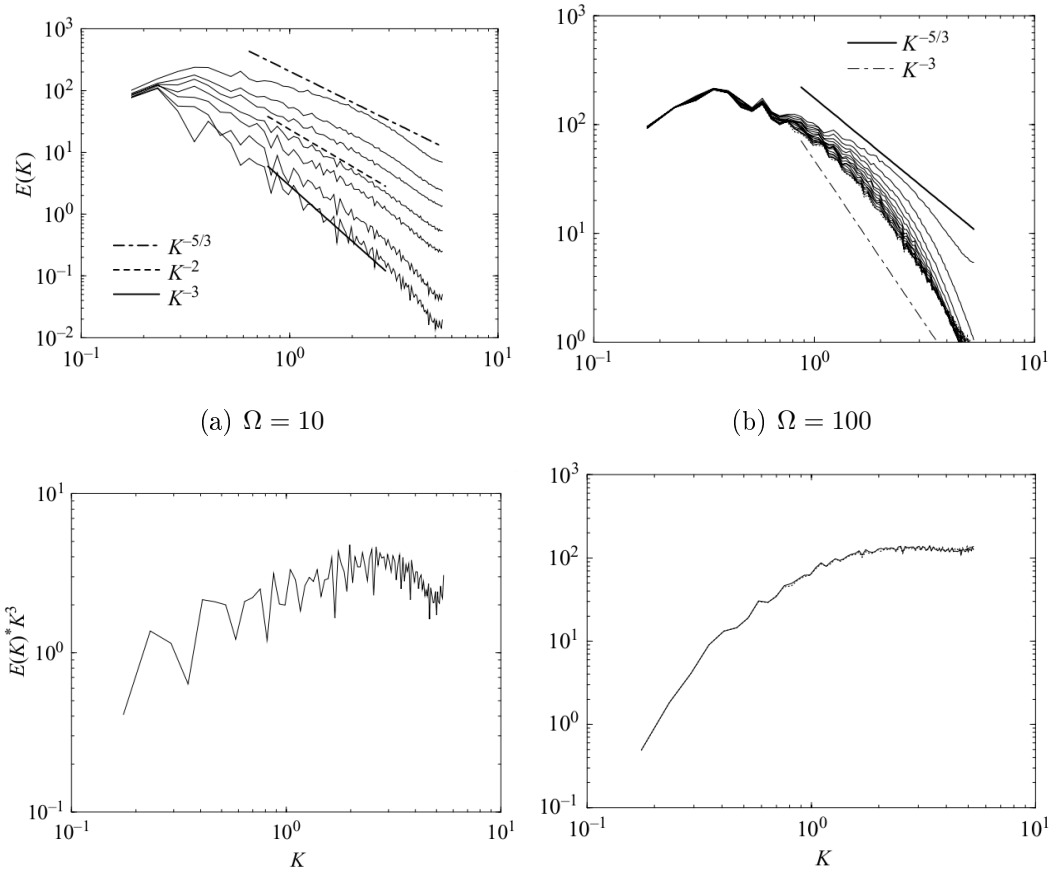

(a) $\Omega = 10$ (b) $\Omega = 100$

(c) compensated $\Omega = 10$ (d) compensated $\Omega = 100$

Figure 3.9: Evolution of energy spectrum with grids $96 \times 96 \times 384$.

In plane wall-bounded turbulent flows, the local volume average is taken in a rectangular element volume. The terms of local volume average, (3.63) can be

$$\begin{aligned}(D^{<}_{iij}n_j)^S =&\frac{1}{S}\left(\iint\limits_{S^+_{23}} D^{<}_{ii1}d\xi_2d\xi_3-\iint\limits_{S^-_{23}} D^{<}_{ii1}d\xi_2d\xi_3+\iint\limits_{S^+_{13}} D^{<}_{ii2}d\xi_1d\xi_3\right.\\ &\left.-\iint\limits_{S^-_{13}} D^{<}_{ii2}d\xi_1d\xi_3+\iint\limits_{S^+_{12}} D^{<}_{ii3}d\xi_1d\xi_2-\iint\limits_{S^-_{12}} D^{<}_{ii3}d\xi_1d\xi_2\right),\\ \left(\frac{\partial D^{<}_{ii}}{\partial\xi_j}n_j\right)^S =&\frac{1}{S}\left(\iint\limits_{S^+_{23}} \frac{\partial D^{<}_{ii}}{\partial\xi_1}d\xi_2d\xi_3-\iint\limits_{S^-_{23}} \frac{\partial D^{<}_{ii}}{\partial\xi_1}d\xi_2d\xi_3+\iint\limits_{S^+_{13}} \frac{\partial D^{<}_{ii}}{\partial\xi_2}d\xi_1d\xi_3\right.\\ &\left.-\iint\limits_{S^-_{13}} \frac{\partial D^{<}_{ii}}{\partial\xi_2}d\xi_1d\xi_3+\iint\limits_{S^+_{12}} \frac{\partial D^{<}_{ii}}{\partial\xi_3}d\xi_1d\xi_2-\iint\limits_{S^-_{12}} \frac{\partial D^{<}_{ii}}{\partial\xi_3}d\xi_1d\xi_2\right),\end{aligned} \tag{3.68}$$

in which

$$S=2(\Delta x_1\Delta x_2+\Delta x_1\Delta x_3+\Delta x_2\Delta x_3). \tag{3.69}$$

Since the turbulence is homogeneous in the x_1 and x_3 directions in plane wall-bounded flows (x_2 is assumed to be normal to the wall), two surface integrals on the element perpendicular to x_1 , i.e. on S^+_{23} and S^-_{23}, cancel each other; the same results are obtained on S^+_{12} and S^-_{12} . Therefore, these terms can be simplified as

$$\begin{aligned}(D^{<}_{iij}n_j)^S =&\frac{1}{S}\left(\iint\limits_{S^+_{13}} D^{<}_{ii2}d\xi_1d\xi_3-\iint\limits_{S^-_{13}} D^{<}_{ii2}d\xi_1d\xi_3\right),\\ \left(\frac{\partial D^{<}_{ii}}{\partial\xi_j}n_j\right)^S =&\frac{1}{S}\left(\iint\limits_{S^+_{13}} \frac{\partial D^{<}_{ii}}{\partial\xi_2}d\xi_1d\xi_3-\iint\limits_{S^-_{13}} \frac{\partial D^{<}_{ii}}{\partial\xi_2}d\xi_1d\xi_3\right).\end{aligned} \tag{3.70}$$

The integrals $(D^{<}_{iij}n_j)^S$ and $\left(\frac{\partial D^{<}_{ii}}{\partial\xi_j}n_j\right)^S$ are then denoted by $(D^{<}_{ii2})^{A_{13}}$ and $(\partial D^{<}_{ii}/\partial\xi_2)^{A_{13}}$, respectively. The ratio of the local volume to its surface area is equal to

$$\begin{aligned}\frac{V}{S}=&\frac{\Delta x_1\Delta x_2\Delta x_3}{2(\Delta x_1\Delta x_2+\Delta x_1\Delta x_3+\Delta x_2\Delta x_3)}\\ =&\frac{\Delta x_2}{2(\Delta x_2/\Delta x_3+\Delta x_2/\Delta x_1+1)}.\end{aligned} \tag{3.71}$$

It can be expressed as $V/S = c_y \Delta x_2$ with $c_y \approx 0.5$ near the wall, and $c_y \approx 1/6$ at the central part of the channel when we used the Gauss-Lobatto collocation in the normal direction. With similar manipulation of the other volume average terms, the subgrid eddy viscosity can be written as

$$\nu_t = \frac{(D^<_{ii2})^{A_{13}} + 2\gamma (D^<_{12})^V c_y \Delta_y}{(\frac{\partial D^<_{ii}}{\partial \xi_2})^{A_{13}} - 4 \left\langle \frac{\partial u_i'^<}{\partial x_j} \frac{\partial u_i'^<}{\partial x_j} \right\rangle^V c_y \Delta_y}, \tag{3.72}$$

in which $\Delta_y = 2\Delta x_2$ is twice the local normal mesh length and $\gamma = dU/dy$ is the local mean strain rate. Since the magnitude of the velocity has asymptotic estimations at the wall in incompressible flows, as

$$u_1'^< \propto y, \; u_2'^< \propto y^2, \; u_3'^< \propto y, \tag{3.73}$$

it is easy to show that (3.72) leads to $\nu_t \propto y^3$ in the near-wall region, and this is correct asymptotic behavior for eddy viscosity. Note that the third and second structure functions are $D^<_{ii2}$ and $D^<_{12}$ in the numerator of (3.72). This means that the kinetic energy is transferred by normal velocity fluctuations which is a correct mechanism in the near-wall region.

The numerical method used in simulating turbulent plane Couette flow and channel flow is a pseudospectral method with Fourier decomposition in the x_1 and x_3 directions and Chebyshev polynomial in the normal direction since the turbulence is homogeneous in the x_1 and x_3 directions. The details of the numerical method is described in appendix.

3.3.2.1 The results of plane Couette flow

The plane Couette flow is a good test case of the subgrid eddy-viscosity model for the homogeneous shear flow, since it has almost constant shear in the major part of the flow, apart from the near-wall region, which is a thin layer at high Reynolds number. The flow Reynolds number is defined as UH/ν in which U is the moving speed of the upper plate and $Re = 3200$ is accepted in the numerical simulation which is equivalent to a Reynolds number of 12800 in Kawamura's DNS results [100]. The grid points are $32 \times 64 \times 32$ in the streamwise, normal and spanwise directions, respectively. The predicted mean velocity profile by the proposed new model is shown

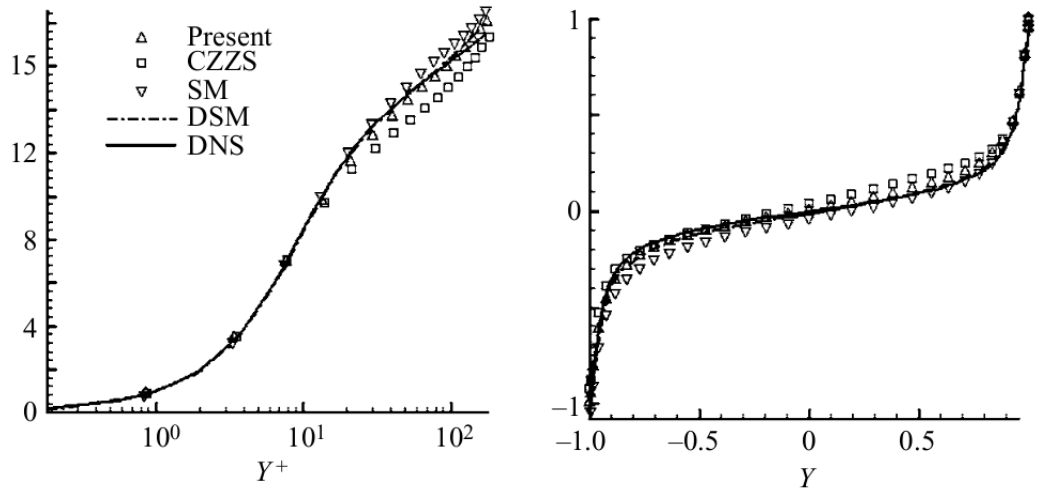

(a) Y^+ scaled by wall units

(b) Y scaled by H

Figure 3.10: Mean velocity profile for plane Couette flow with grids $32 \times 64 \times 32$.

in Fig. 3.10 together with the DNS results by Kawamura, the Smagorinsky model, the dynamic Smagorinsky model and the CZZS model. In the computation with the Smagorinsky model, we use model coefficient $C_s = 0.08$ and the van Driest damping function in the near-wall region.

Figure 3.11 shows the distribution of turbulent kinetic energy and Reynolds stress between two plates. In the plots, both turbulent kinetic energy and Reynolds stress include subgrid counterparts with the corrections given by Pope [1]. The results show that the new model is better than the others.

3.3.2.2 The results of plane Poiseuille flow

Turbulent Poiseuille flow is another case for which to examine the applicability of the proposed model. The turbulent channel is inhomogeneous in the direction normal to the wall; however, the mean shear rate is proportional to $1/y^+$ in the logarithmic layer which is not so large, and the mean shear rate is much less above the logarithmic layer. Therefore, local homogeneity would be a good approximation in the major part of the channel flow. In the near-wall region, the model has the correct asymptotic behavior as proved before, and it is expected that the proposed model is applicable in turbulent channel flows.

The flow Reynolds number is defined as $U_m H/\nu$, in which U_m is the bulk velocity in the channel and it is unchanged during the computation so that we use the constant-

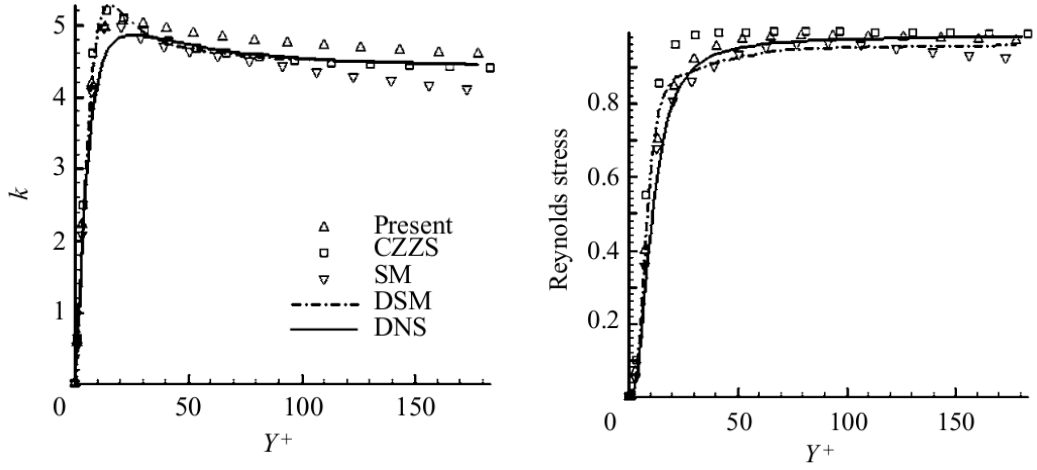

(a) Turbulent kinetic energy (b) Reynolds stress

Figure 3.11: Distribution of turbulent statistics with grids $32 \times 64 \times 32$.

flow-rate condition in numerical simulation [101]. Two test cases are computed at Reynolds numbers of 7000 and 10000, which are equivalent to $Re_\tau = 395, 590$, respectively, in DNS performed by Moser *et al.* [92] with constant pressure gradients. The grid points are $32 \times 64 \times 32$ in the streamwise, normal and spanwise directions, respectively, for $Re = 7000$ and $32 \times 96 \times 32$ for $Re = 10000$. Although the CZZS model predicts fairly good statistics in turbulent channel flow [38], the new model gives better results. This indicates that the inclusion of anisotropic transfer of turbulent kinetic energy is necessary and, indeed, improves the prediction.

Figure 3.12 presents the mean velocity profiles in which the prediction by the present subgrid model fits the DNS results well at both Reynolds numbers, and is better than previous CZZS model. Figure 3.13 shows the distribution of turbulent kinetic energy in which the correction of subgrid counterpart is added. The improvement of the present new model is evident; in particular, the location of the peak is close to that for the DNS results. Figure 3.14 shows the distribution of Reynolds stress in which the correction is also added. All results show that the proposed model is the best.

3.3.2.3 Discussion

The present model is established based on the homogeneity of turbulence, and is then applied to non-uniform shear turbulence. The extension of the homogeneous

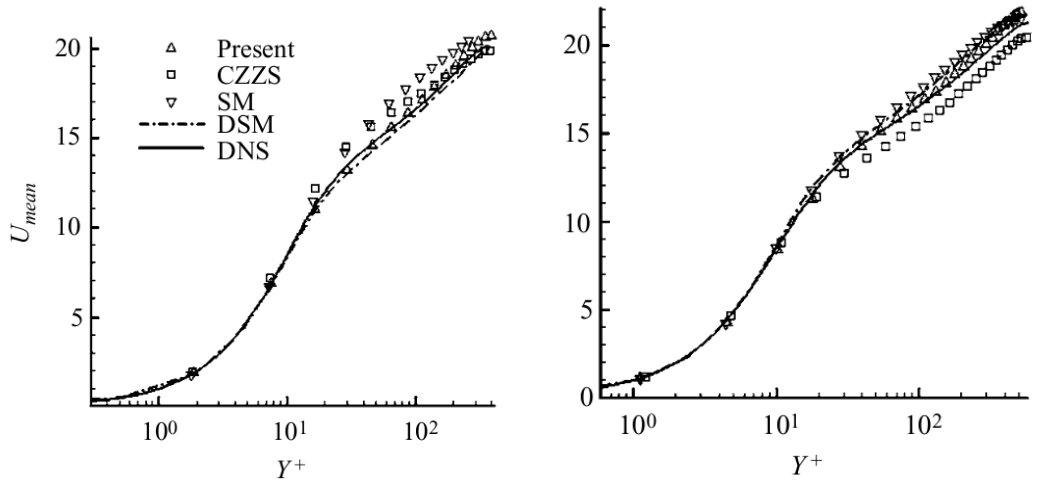

(a) $32 \times 64 \times 32$ for $Re = 7000$ (b) $32 \times 96 \times 32$ for $Re = 10000$

Figure 3.12: *A Posteriori* results of mean velocity profile in channel Poiseuille flow.

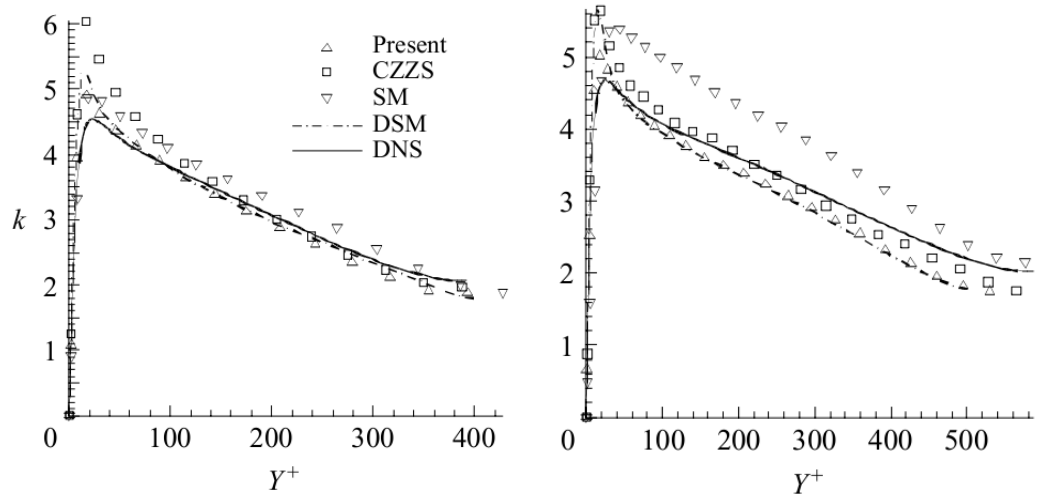

(a) $32 \times 64 \times 32$ for $Re = 7000$ (b) $32 \times 96 \times 32$ for $Re = 10000$

Figure 3.13: *A Posteriori* results of turbulent kinetic energy in channel Poiseuille flow.

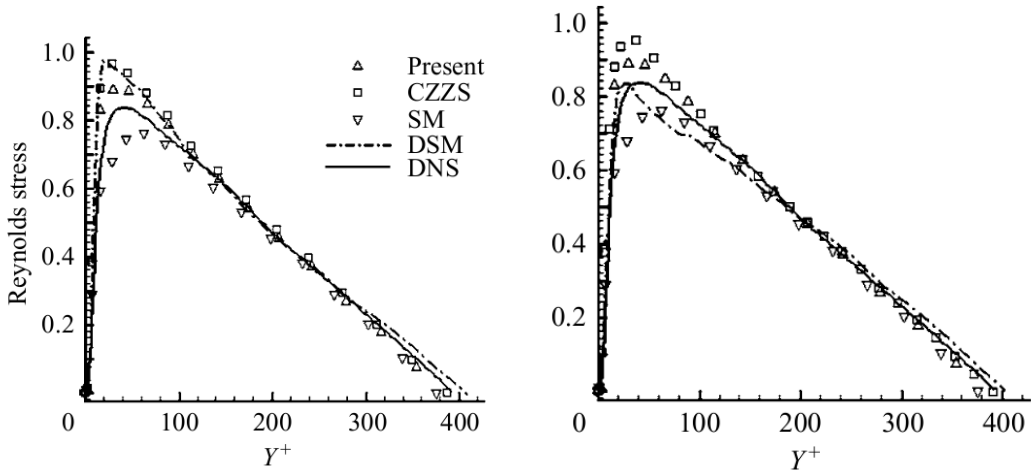

(a) $32 \times 64 \times 32$ for $Re = 7000$ (b) $32 \times 96 \times 32$ for $Re = 10000$

Figure 3.14: *A Posteriori* results of Reynolds stress in channel Poiseuille flow.

model, i.e. constant subgrid eddy viscosity, to non-uniform shear turbulence is reasonable when the flow can be considered to be locally homogeneous, and the eddy viscosity is accepted as locally constant. In a large part of the wall shear layer, the mean shear rates are small so that in the logarithm layer the mean shear rate is proportional to $1/y^+$ and it is much smaller above the logarithm layer. Therefore, the derivative of the mean shear rate is small and the local homogeneity can be acceptable. In the near-wall region, the proposed new model has correct asymptotic behavior, i.e. $\nu_t \propto y^3$, and it can be used in the wall shear layer without any damping functions or wall models. The good predicted results from the present model in plane Couette and channel flows indicate that local constant subgrid eddy viscosity, which is a function of the normal distance to the wall, is acceptable, at least for the attached wall shear turbulence.

In rotating turbulence, the transformation property of the subgrid stress model should be concerned between the inertial frame and the rotating frame [102]. The present model is established for homogeneous rotating flow in a rotating frame by use of an isotropic filter and it can be proved that the generalized Kolmogorov equations for resolved scale turbulence of the homogeneous fluctuating motion are the same in both inertial and rotational frames. Therefore, the present subgrid-stress model satisfies the transformation property. In practice, some errors might be introduced by any slightly non-isotropic operations in numerical computation, but the errors are

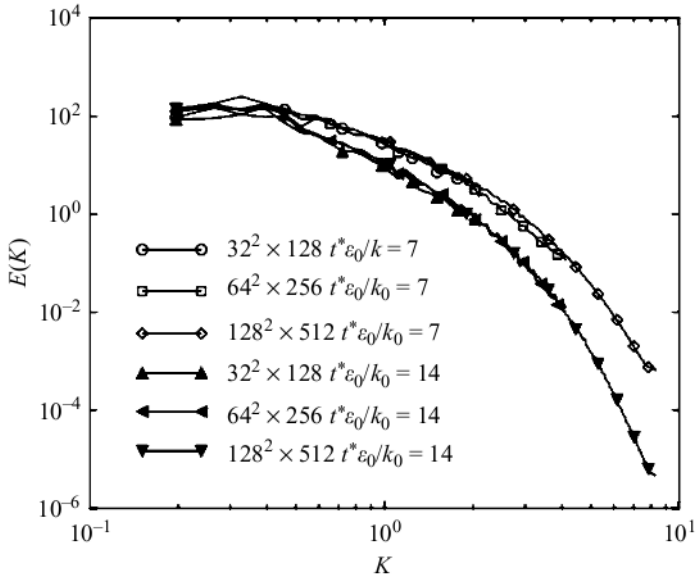

Figure 3.15: Comparison of energy spectrum between DNS ($128^2 \times 512$) and LES

expected to be small, at least smaller than the modeling errors. To make sure that the influence of the practical numerical method on LES results is negligible, we compare the LES with DNS results at lower Reynolds number $Re_\lambda = 50$ and rotating rate at 10 rad s^{-1} . The comparison of energy spectrum is shown in Fig. 3.15 in which DNS is performed with grid number $128^2 \times 512$ and LES is computed with coarse grids. The rotation is switched on at $t = 2k_0/\varepsilon_0 = 2$ and the energy spectra shown in Fig. 3.15 are at time $t = 2k_0/\varepsilon_0 = 7$ and 14, respectively. The results of the LES are in good agreement with DNS.

In practical computation, the initial condition of velocity fluctuations is important in DNS and LES. For the new model, we need approximately correct initial structure functions, in particular $(D^{\leq}_{iij}n_j)^S$. Numerical computation with an improper initial fluctuating field is bound to fail. There is no problem for homogeneous turbulence, since the initial structure function is approximately correct if we use some well-known spectrum as the initial condition, e.g. Comte-Bellot spectrum or von-Karman spectrum. During the time advancement, the spectrum will automatically evolve into the correct spectrum. For the wall-bounded turbulence, we have already checked from DNS and LES results that the skewness of the velocity increment, or the third-order structure function, is negative across the channel (see section 2.4.5). Various ways can be applied to satisfy this condition in practical computation. One possible way is to

use the data bank of lower-Reynolds-number cases as the initial condition for higher-Reynolds-flows in a channel with a non-dimensional correction. This is what we have done in test cases for turbulent plane Couette and channel flows. Another way is to start the computation by use of an easily accessible subgrid model, for instance the Smagorinsky model, and the new model will be switched on when the turbulent flow becomes nearly fully developed. We have tested this method and obtained results as good as by the first method. There may be other ways in practice, since the initial condition for LES, also in DNS, is a technical issue.

In numerical computation, the length of the local average volume, equivalent to the filter length, is equal to twice the mesh lengths h in the test cases. It has been proved that $\Delta/h = 2$ is approximately optimum in numerical errors see [1, 103]. For homogeneous rotating turbulence, the grid resolution depends on the turbulent Rossby number rather than on the Reynolds number. For instance, the $64 \times 64 \times 256$ grids are adequate for $\mathrm{Ro}^{\omega} < 0.5$ whereas $98 \times 98 \times 384$ grids are marginally adequate for $\mathrm{Ro}^{\omega} \approx 0.2$ (Figs. 3.7 and 3.8). As far as the wall turbulent shear flows are concerned, higher spatial resolution is required in the wall-normal direction than in the horizontal directions for adequate simulation of the near-wall behaviors without wall model. For instance, 64 non-uniform grid points are enough for channel flow at $Re = 7000$, whereas at least 96 non-uniform grid points are required at $Re = 10000$. The requirement of resolution in streamwise and spanwise directions, i.e. in homogeneous directions, is not as serious as in normal direction, 32 uniform gird points are enough in LES, whereas at least 256 grid points are required in DNS for $Re = 7000$ to 10000. To check the effectiveness of the SGS stress in the computation, the comparison of the the predicted results between the new model and no model has been made (Figs. 3.16 and 3.17). The deviation of no model results is obvious from the DNS results in the mean velocity profiles and the deviation is great in the Reynolds stress.

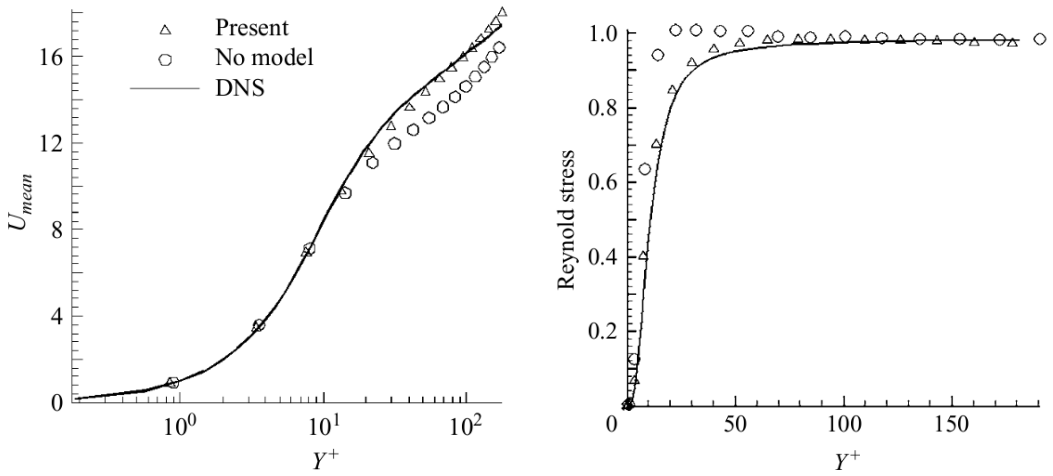

(a) mean velocity profiles (b) Reynolds stress profiles

Figure 3.16: Comparison of the statistical properties of turbulent plane Couette flow between the new model and no model, $Re = 3200$, grid $32 \times 64 \times 32$.

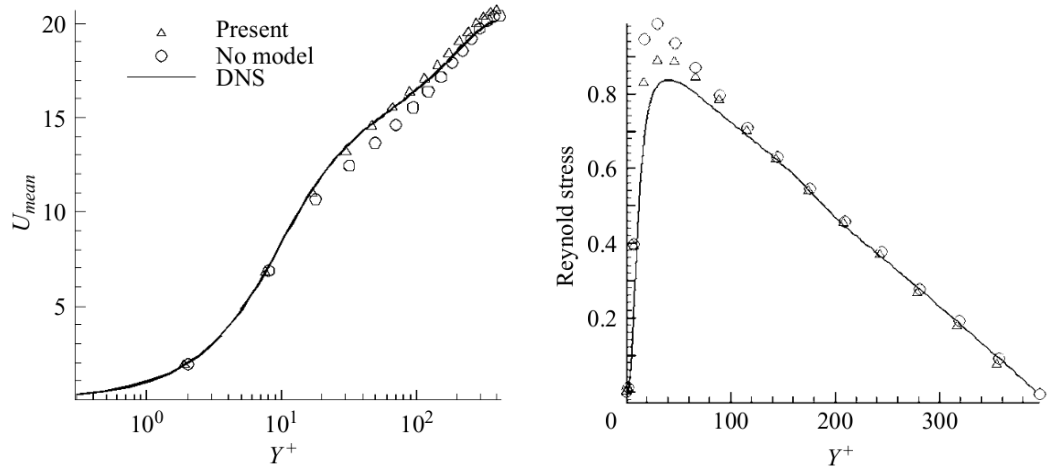

(a) mean velocity profiles (b) Reynolds stress profiles

Figure 3.17: Comparison of the statistical properties of turbulent plane Poiseuille flow between the new model and no model, $Re = 7000$, grid $32 \times 64 \times 32$.

Chapter 4

Improved velocity increment model (IVI)

In the last chapter, the eddy-viscosity models assume that the SGS stress tensor is aligned with the strain rate tensor. A less classical approach consists in modeling the SGS stress tensor on the basis of a tensor which possesses a higher level of correlation with $\tau_{ij}^{<}$ than the strain rate tensor $S_{ij}^{<}$. Such models are developed on the basis of scale invariance properties of turbulent flows [7]. The original scale similarity formulation is related to the Leonard stress tensor $L_{ij} = \left(u_i^{<} u_j^{<}\right)^{<} - u_i^{<} u_j^{<}$. The only limitation of this approach lies in the necessity of an explicit filtering procedure. Indeed, the use of a specific filter yields specific effects of the SGS model. This is demonstrated in *A Priori* tests with various local filters [18, 104, 105]. The reconstruction of L_{ij} based on Taylor expansions yields the gradient diffusion model [5, 106, 107]. Another scale similarity formulation is related to the Reynolds type stress tensor $R_{ij} = u_i'^{<} u_j'^{<}$ based on the statistical velocity fluctuation $u_i' = u_i - \langle u_i \rangle$.

One of the recent attempts is considering the velocity increment in SGS modeling. Metais and Lesieur [29] have transposed the spectral eddy-viscosity concept to physical space on the basis of the second order velocity structure function which represents the energy of the flow stored at the mesh size Δ (i.e. the filter scale in spectral space). The dimension of an eddy-viscosity requires two scales, a lengthscale $\xi = \Delta$ and a velocity scale $\delta u_1^{<} = u_1(x_1 + \xi) - u_1(x_1)$. However, the spirit of this model is based on eddy-viscosity assumption, which might be not good in some areas. From spectral analysis, there is weak energy backscatter in homogeneous isotropic turbulence [9]. This phenomenon is obvious in some complex turbulence [24–26]. Brun proposed an

increment model (VI), in which the subgrid stress in formulated by using the filtered velocity increment [6]:

$$\tau_{ij}^{<} = fQ_{ij}, \qquad Q_{ij} = \delta u_i^{<} \delta u_j^{<}. \tag{4.1}$$

This model has good performance of tensor correlation. With this model, the forward and backward scatters could be both simulated. However, some arbitrariness remains in the model, for example the model coefficient was not determined physically.

In this chapter, we further discuss the tensor formulations of the filtered velocity increment Q_{ij}. Then KEF is applied to determine the coefficient values, in isotropic turbulence and shear flow respectively. The improved SGS models are tested in homogeneous isotropic turbulence and anisotropic channel flow. The corresponding work has been published in *Physics of Fluids* [42].

4.1 Formulations of the filtered velocity increment tensor

Brun has defined a formulation of filtered velocity increment, that

$$\delta u_i^{<}(\vec{x}) = \sum_{k=1}^{3} \left[u_i^{<}\left(\vec{x} + \frac{1}{2} r_k \vec{e}_k\right) - u_i^{<}\left(\vec{x} - \frac{1}{2} r_k \vec{e}_k\right) \right]. \tag{4.2}$$

Thus the tensor Q_{ij} is defined as

$$\begin{aligned} Q_{ij} &= \delta u_i^{<} \delta u_j^{<} \\ &= \left[\sum_{k=1}^{3} \left[u_i^{<}\left(\vec{x} + \frac{1}{2} r_k \vec{e}_k\right) - u_i^{<}\left(\vec{x} - \frac{1}{2} r_k \vec{e}_k\right) \right] \right] \left[\sum_{k=1}^{3} \left[u_j^{<}\left(\vec{x} + \frac{1}{2} r_k \vec{e}_k\right) - u_j^{<}\left(\vec{x} - \frac{1}{2} r_k \vec{e}_k\right) \right] \right], \end{aligned} \tag{4.3}$$

where $\vec{r}$ is a given distance vector. In fact, this definition concludes the relations among four points: $\vec{x}$, $\vec{x} + 1/2 r_1 \vec{e}_1$, $\vec{x} + 1/2 r_2 \vec{e}_2$ and $\vec{x} + 1/2 r_3 \vec{e}_3$.

In numerical applications, if the filters and grids are homogeneous, i.e. $\Delta_1 = \Delta_2 = \Delta_3 = h$ in the three axis directions, Brun suggested that the distance vector is taken as

$$\vec{r} = \sum_{k=1}^{3} 2h \vec{e}_k, \tag{4.4}$$

and the filtered increment velocity reads

$$\delta u_i^< = \sum_{k=1}^{3} \left[u_i^<(x_k + h) - u_i^<(x_k - h) \right]. \tag{4.5}$$

When h is small, Taylor expansion is employed, and this model could be written as

$$\tau_{ij}^< = f h_k h_l \frac{\partial u_i^<}{\partial x_k} \frac{\partial u_j^<}{\partial x_l}. \tag{4.6}$$

Comparing with Leonard's subgrid model [5]:

$$\tau_{ij}^< = C_n h^2 \frac{\partial u_i^<}{\partial x_k} \frac{\partial u_j^<}{\partial x_k}, \tag{4.7}$$

Brun's increment model contains more terms. It is in agreement with the results of Taylor expansion of filters. Considering a three-dimensional low-pass filter with the characteristics $[\Delta x_k, a_{(k)}, b_{(kl)}]$, where Δx_k is the filter width, $a_{(k)}\Delta x_k$ and $b_{(kl)}\Delta x_k \Delta x_l$ are the first and second moments of filter, respectively, we could obtain an expansion of the filtered variable:

$$h^<(\vec{x}) = h(\vec{x}) + a_{(k)}\Delta x_k \frac{\partial h}{\partial x_k}(\vec{x}) + b_{(kl)}\Delta x_k \Delta x_l \frac{\partial^2 h}{\partial x_k \partial x_l}(\vec{x}) + o(\Delta x_k^2), \tag{4.8}$$

where $o(\Delta x_k^2)$ is small compared with Δx_k^2.

However, this analysis of Taylor expansion is opposed by Frisch [108] and Borue [107]. They proposed a "fractal" Taylor expansion to correct it. There are still arguments, thus we could not evaluate a subgrid model by using the Taylor expansion simply. The expansion results are only given for comparison purposes.

In order to further simplify Brun's formulation, equation (4.6) is written on a normal component specially, in isotropic turbulence:

$$\langle \tau_{11}^< \rangle = f h^2 \left(\left\langle \frac{\partial u_1^<}{\partial x_1} \frac{\partial u_1^<}{\partial x_1} \right\rangle + 2 \left\langle \frac{\partial u_1^<}{\partial x_2} \frac{\partial u_1^<}{\partial x_2} \right\rangle + 4 \left\langle \frac{\partial u_1^<}{\partial x_1} \frac{\partial u_1^<}{\partial x_2} \right\rangle + 2 \left\langle \frac{\partial u_1^<}{\partial x_2} \frac{\partial u_1^<}{\partial x_3} \right\rangle \right). \tag{4.9}$$

In homogeneous isotropic turbulence, both the last two terms equal zero. Besides, the following incompressible condition is satisfied:

$$\left\langle \frac{\partial u_1^<}{\partial x_2} \frac{\partial u_1^<}{\partial x_2} \right\rangle = 2 \left\langle \frac{\partial u_1^<}{\partial x_1} \frac{\partial u_1^<}{\partial x_1} \right\rangle. \tag{4.10}$$

It means that the right hand side of equation (4.9) could be treated by simply consider the first term $\left\langle \frac{\partial u_1^<}{\partial x_1} \frac{\partial u_1^<}{\partial x_1} \right\rangle$. This simplification also agrees with the classical eddy-viscosity assumption, that the 11 component of subgrid stress could be formulated

by only the $S_{11}^{<}$ component of resolved strain rate. Therefore, the simplified tensor of velocity increment in 11 direction reads

$$Q_{11}(x_1, h) = \left[u_1^{<}\left(x_1 + \frac{1}{2}h\right) - u_1^{<}\left(x_1 - \frac{1}{2}h\right)\right]^2. \tag{4.11}$$

In order to further simplify the calculations, another formulation is written at a given distance Δ':

$$Q_{11}(x_1, \Delta') = \frac{1}{2}\left[\delta u_1^{<}(x_1 - \Delta', \Delta')\delta u_1^{<}(x_1 - \Delta', \Delta') + \delta u_1^{<}(x_1, \Delta')\delta u_1^{<}(x_1, \Delta')\right], \tag{4.12}$$

where $\delta\vec{u}(\vec{x}, \vec{\xi}) = \vec{u}(\vec{x} + \vec{\xi}) - \vec{u}(\vec{x})$. This final formulation is used in this thesis, and the tensor is defined as

$$\begin{aligned} Q_{ij}(\vec{x}, \Delta') =& \frac{1}{2}\left[(u_i^{<}(\vec{x} + \Delta'\vec{e}_i) - u_i^{<}(\vec{x}))\left(u_j^{<}(\vec{x} + \Delta'\vec{e}_j) - u_j^{<}(\vec{x})\right)\right. \\ &\left. + (u_i^{<}(\vec{x}) - u_i^{<}(\vec{x} - \Delta'\vec{e}_i))\left(u_j^{<}(\vec{x}) - u_j^{<}(\vec{x} - \Delta'\vec{e}_j)\right)\right]. \end{aligned} \tag{4.13}$$

Although different from Brun's definition, it also satisfies the tensor symmetry

$$Q_{ij}(\vec{x}, \Delta') = Q_{ij}(\vec{x}, -\Delta'), \;\; Q_{ij} = Q_{ji}. \tag{4.14}$$

Comparing with Brun's definition, it is simplified by omitting the transverse components. The main problem of this simplification is that the subgrid stress vanishes when the flow is locally characterized by a pure shear flow $u_1^{<}(x_2)$ somewhere. However, in this situation, the effect of dissipation are the same between definitions (4.14) and (4.3), both of them yield the zero subgrid dissipation $-\tau_{ij}^{<}S_{ij}^{<} = 0$. This behavior can also be explicitly achieved in the Clark model [109]. In the KEF formulation (2.21), all terms can be represented by the longitude components. Thus it could be appropriate to characterize the energy transfer using the longitude components, in homogeneous isotropic turbulence.

The formulation of the velocity increment model could be written as

$$\tau_{ij}^{<}(\vec{x}, \Delta) = C_f(\Delta')Q_{ij}(\vec{x}, \Delta'), \tag{4.15}$$

where C_f is the dynamic model coefficient, depending on another distance Δ'. In Brun's paper [6], he assumed $\Delta' = \Delta$. However, in this thesis we analyze the relations, which could bring good result in inertial subrange.

4.2 Improved velocity increment model

The KEF formulation in homogeneous isotropic turbulence is discussed in section 2.2. We only concern the longitudinal components, thus from equation (2.21), (4.11), (4.15), and isotropy assumption, the subgrid dissipation could be denoted as:

$$\begin{aligned} -\frac{4}{5}\varepsilon_f\xi &= 6C_f \left\langle Q_{11}(\Delta')S_{11}^{<}\right\rangle \xi \\ &= 6C_f \left\langle \delta u_1^{<}(\Delta')\delta u_1^{<}(\Delta')\frac{\partial u_1^{<}}{\partial x_1}\right\rangle \xi \\ &= 6C_f \left\langle \delta u_1^{<}(\Delta')\delta u_1^{<}(\Delta')\frac{\partial \delta u_1^{<}(\Delta')}{\partial \Delta'}\right\rangle \xi \\ &= 2C_f\xi \left.\frac{\partial D_{lll}^{<}(r)}{\partial r}\right|_{r=\Delta'}, \end{aligned} \tag{4.16}$$

and the the subgrid transfer term reads:

$$-6T_{l,ll}(\xi) = -6C_f \left\langle u_1^{<}(x_1)Q_{11}(x_1+\xi,\Delta')\right\rangle . \tag{4.17}$$

Therefore, equation (2.21) could be written:

$$2C_f\xi \left.\frac{\partial D_{lll}^{<}(r)}{\partial r}\right|_{r=\Delta'} = D_{lll}^{<}(\xi) - 6C_f \left\langle u_1^{<}(x_1)Q_{11}(x_1+\xi,\Delta')\right\rangle , \tag{4.18}$$

and the model coefficient is:

$$C_f = \frac{D_{lll}^{<}(\xi)}{2\xi \left.\frac{\partial D_{lll}^{<}(r)}{\partial r}\right|_{r=\Delta'} + 6\left\langle u_1^{<}(x_1)Q_{11}(x_1+\xi,\Delta')\right\rangle} \tag{4.19}$$

Three different scales implied in this result should be clarified: the physical quantities are filtered at a filter size Δ; VI model assumes C_f and Q_{ij} at a distance Δ'; and the equation itself is based on a distance ξ. In the following parts, the three scales will be analyzed primarily in an ideal high Reynolds number turbulence, and then in a real flow.

4.2.1 Model analysis in high Reynolds number turbulence

In section 2.6, the scaling law of filtered velocity is discussed. If the scaling law is satisfied, the first term of the denominator in equation (4.19) could be simplified

when $\Delta \ll \Delta'$ and Δ' is in inertial subrange:

$$2\xi \left.\frac{\partial D_{lll}^{<}(r)}{\partial r}\right|_{r=\Delta'} = \frac{2\xi}{\Delta'} D_{lll}^{<}(\Delta'). \tag{4.20}$$

If ξ is also in inertial subrange, we could obtain:

$$2\xi \left.\frac{\partial D_{lll}^{<}(r)}{\partial r}\right|_{r=\Delta'} = 2D_{lll}^{<}(\xi). \tag{4.21}$$

The second term of the denominator in equation (4.19) corresponds to the transfer term of KEF. According to Meneveau's analysis [17], it tends to zero when ξ is large. In fact, it is a correlation function between velocity $u_1^<$ and velocity increment Q_{11} at distance Δ', thus it tends to zero when ξ is large. From equation (4.11) and (4.17), we could also easily evaluate the magnitude when $\Delta' \ll \xi$:

$$\langle u_1^<(x_1) Q_{11}(x_1+\xi, \Delta')\rangle \sim \langle \delta u_1^<(\xi) \delta u_1^<(\Delta') \Delta u_1^<(\Delta')\rangle \ll D_{lll}^<(\xi). \tag{4.22}$$

Thus the transfer term in equation (4.19) could be neglected, and the coefficient is

$$C_f = \frac{D_{lll}^<(\xi)}{2D_{lll}^<(\xi)} = \frac{1}{2}. \tag{4.23}$$

The value does not depend on ξ. It agrees with the model assumption (4.15), where C_f is only a function of Δ and Δ'. Notice that this result is satisfied only when the inertial subrange is wide enough, and Δ' and ξ are both in inertial subrange. Besides, in order to neglect the molecular terms in original KEF (Cui *et al.* [38]), the filter size of LES should be much larger than the dissipation scale η. Therefore, we could write the combined multi-scale relation:

$$\eta \ll \Delta \ll \Delta' \ll \xi \ll L, \tag{4.24}$$

where L is the integrated scale.

4.2.2 Model analysis in moderate Reynolds number turbulence

In the numerical simulation of LES, the Reynolds number might not be high enough, and the inertial subrange is not wide enough. Equation (4.24) is difficult to be satisfied, thus we fix the scales as $\Delta = \Delta' = \xi$, and simplify the form of VI model in another way. The subgrid energy transfer $T_{l,ll}$ could be represented by using

velocity increment. In homogeneous turbulence, it is only a function of ξ, and does not depend on the location x_1. It could be represented as:

$$\begin{aligned}
T_{l,ll}(\xi) =& \langle u_1^<(x_1)\tau_{11}^<(x_1+\xi)\rangle \\
=& C_f \langle u_1^<(x_1)Q_{11}(x_1,2\xi)\rangle \\
=& \frac{1}{2}C_f \left[\left\langle u_1^{<3}\right\rangle - 2\langle u_1^<(x_1)u_1^<(x_1)u_1^<(x_1+\xi)\rangle + 2\langle u_1^<(x_1)u_1^<(x_1+\xi)u_1^<(x_1+\xi)\rangle \right. \\
& \left. + \langle u_1^<(x_1)u_1^<(x_1+2\xi)u_1^<(x_1+2\xi)\rangle - 2\langle u_1^<(x_1)u_1^<(x_1+\xi)u_1^<(x_1+2\xi)\rangle\right].
\end{aligned} \tag{4.25}$$

The third order moment of velocity $\left\langle u_1^{<3}\right\rangle = 0$. The last term in the right hand side of equation (4.25) could be proved to be zero in isotropic turbulence:

$$\begin{aligned}
\langle u_1^<(x_1)u_1^<(x_1+\xi)u_1^<(x_1+2\xi)\rangle =& \langle u_1^<(x_1-\xi)u_1^<(x_1)u_1^<(x_1+\xi)\rangle \\
=& -\langle u_1^<(x_1+\xi)u_1^<(x_1)u_1^<(x_1-\xi)\rangle \\
=& -\langle u_1^<(x_1)u_1^<(x_1+\xi)u_1^<(x_1+2\xi)\rangle .
\end{aligned} \tag{4.26}$$

Define the third order correlations

$$\begin{aligned}
R_{l,ll}(2\xi) =& \langle u_1^<(x_1)u_1^<(x_1+2\xi)u_1^<(x_1+2\xi)\rangle , \\
R_{ll,l}(2\xi) =& \langle u_1^<(x_1)u_1^<(x_1)u_1^<(x_1+2\xi)\rangle .
\end{aligned} \tag{4.27}$$

In isotropic turbulence $R_{l,ll}(2\xi) = -R_{ll,l}(2\xi)$. The subgrid energy transfer $T_{l,ll}$ reads:

$$T_{l,ll}(\xi) = -2C_f R_{ll,l}(\xi) - \frac{1}{2}C_f R_{ll,l}(2\xi). \tag{4.28}$$

Since in isotropic turbulence $D_{lll}^< = 6R_{ll,l}$, the term of two-point subgrid energy transfer

$$T_{l,ll}(\xi) = -\frac{1}{3}C_f D_{lll}^<(\xi) - \frac{1}{12}C_f D_{lll}^<(2\xi). \tag{4.29}$$

It is interesting to notice that the energy transfer has a linear relation with the third order structure function. In equation (4.16) and (4.29) there might be energy backscatter because of the third order structure function $D_{lll}^<$, which will be further analyzed in the next section.

However, notice that in CZZS model, the eddy viscosity subgrid dissipation is always positive. The subgrid energy transfer depends on the gradient of the second order structure function, that is:

$$T_{l,ll}(\xi) = \nu_t \frac{\partial D^<_{ll}(\xi)}{\partial \xi}. \tag{4.30}$$

From the classical scaling law $\dfrac{\partial D^<_{ll}}{\partial \xi} > 0$ and the eddy viscosity $\nu_t > 0$, it implies $T_{l,ll} > 0$ is purely dissipative.

From equation (2.21), (4.16) and (4.29), the coefficient C_f could be obtained:

$$C_f = \frac{2D^<_{lll}(\xi)}{4\xi \left.\dfrac{\partial D^<_{lll}(r)}{\partial r}\right|_{r=\xi} - 4D^<_{lll}(\xi) - D^<_{lll}(2\xi)}. \tag{4.31}$$

In applications, if the scaling law $D^<_{lll}(\xi) \propto \xi^n$ is satisfied, we could obtain:

$$\left.\frac{\partial D^<_{lll}(r)}{\partial r}\right|_{r=\xi} = n\frac{D^<_{lll}(\xi)}{\xi}, \tag{4.32}$$

finally the dynamic form of IVI model could be

$$C_f = \frac{2D^<_{lll}(\xi)}{4(n-1)D^<_{lll}(\xi) - D^<_{lll}(2\xi)}. \tag{4.33}$$

When Δ, Δ', ξ tend to zero, the scaling exponent $n \to 3$. Also we have $D^<_{lll}(2\xi) = 8D^<_{lll}(\xi)$, thus the denominator tends to zero. It agrees with the conclusion of Meneveau [17] that $-T_{l,ll}(\xi) = \langle \tau^<_{11} S^<_{11} \rangle \, \xi$ in small ξ. However, notice that n depends on ξ, thus n is not a constant, and we could not have the relation $D^<_{lll}(2\xi) = 2^n D^<_{lll}(\xi)$. In real practice, the scaling exponent n could be calculated by any numerical difference methods. However, we suggest to fix $n = 2.5$ in real practices, since it is simple and numerical stable, and is verified in *A Priori* cases, which will be discussed in Sec. 4.4.

When $\Delta = \Delta' = \xi$, the ideal inertial subrange condition (4.24) is not satisfied, thus we should use the dynamic model form (4.33) instead of the constant model form (4.23). However, the low-cost constant model form is more convenient in calculation. In order to check whether the constant model form could be applied approximately in this case, different model forms are then verified by *A Priori* and *A Posteriori* tests in the next section.

4.3 Numerical verifications

4.3.1 A Priori analysis in homogeneous isotropic turbulence

Two DNS cases of homogeneous isotropic turbulence are used for *A Priori* test. In these two cases, spectral method is applied, and a deterministic forcing method is employed to simulate a statistically stationary turbulence. The computation domain has 256^3 grid. The grid size is denoted as h. Reynolds numbers Re_λ are 50 and 70 respectively. The compensate energy spectrums of DNS cases were shown in Fig. 2.2, where the plateaus represent the inertial subrange in spectral space. The corresponding wave number of the plateaus is about $0.1 < k_c\eta < 0.3$. The relevant filter size is $10 < \Delta/\eta < 30$. In addition, the integrated scale $L \sim 70\eta$ in the two cases. Thus we could reasonably consider that $\eta \ll \Delta = \xi \ll L$, which could minimize the model error mentioned in section 2.2.1. The plateau in the case $\mathrm{Re}_\lambda = 70$ is wider than $\mathrm{Re}_\lambda = 50$.

In homogeneous isotropic turbulence, the exact subgrid stress is calculated with different cut-off wave numbers. The coefficient of VI model is calculated as

$$C_f = \frac{\langle \tau_{11}^{<} S_{11}^{<} \rangle}{\langle Q_{11} S_{11}^{<} \rangle}. \tag{4.34}$$

The dynamic value of IVI model (4.33) is compared with the exact value (4.34) in Fig. 4.1, where the scaling exponent n is calculated by using the first-order central difference method. It shows that the exact coefficient value increases with Δ and ξ, and it is about 1/2 when $10 < \xi/\eta \lesssim 18$, which is a small region of inertial subrange. Moreover, the dynamic model value is also in good agreement in this region. Therefore, in a practical LES case, if the filter size Δ and the two-point distance ξ are fixed in this region, the constant form (4.23) of IVI model might be applied to obtain the low cost in calculation. When ξ is small, the constant form is in disagreement. It stems from the effect of molecular viscosity, which is neglected in KEF. When ξ is too large, the error is also obvious.

4.3.2 A Priori analysis on isotropy in homogeneous shear flow

As analyzed in section 2.4.4, the isotropy of third-order structure function might not be satisfied in homogeneous shear turbulence. Thus, the anisotropy of C_f should

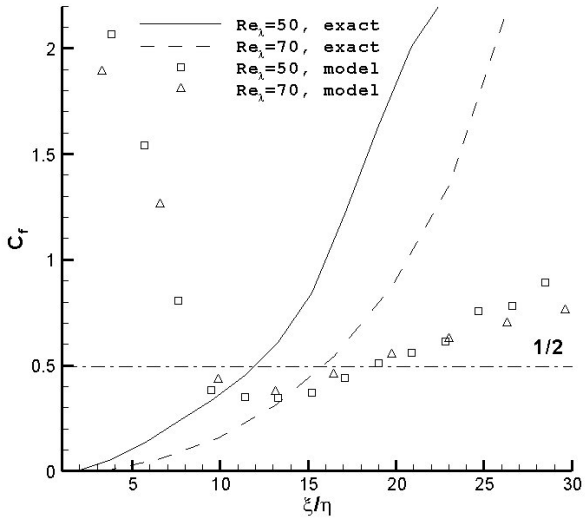

Figure 4.1: Comparison between exact value and dynamic model value of C_f, against different filter sizes and two-point distances $\Delta = \xi$, in homogeneous isotropic turbulence. Solid line with symbols: $Re_\lambda = 50$; dashed line with symbols: $Re_\lambda = 70$. The horizontal line is the theoretical value.

be verified. The DNS database is the center region of Couette flow, which was described in section 2.4.4. The dynamic coefficient C_f is calculated with different two-point direction, and different two-point distance length. Since it is not easy to change filter size Δ, we fixed it as the grid size, i.e. $\Delta = h$, only to investigate the anisotropy among three directions. Here the scale condition $\Delta = \xi$ is not satisfied, thus the results could only show a trend. As shown in Fig. 4.2, the values are not the same among different directions. Therefore, in applications of shear flow, the anisotropic properties should be noticed. In the following cases using dynamic model form, we simply set the coefficient value as the average of three axis directions.

4.3.3 A Priori analysis on wall behavior in wall-bounded flow

KEF is based on homogeneous isotropic turbulence, but in wall-bounded shear flow, the local isotropy could also be satisfied by considering the slow parts [38, 48]. In a local region, the two-point velocity increment is considered as a slow part for subgrid modeling, which provides a good near-wall property [70]. A DNS case of channel flow is used for *A Priori* test. The pseudo-spectral method is applied. The

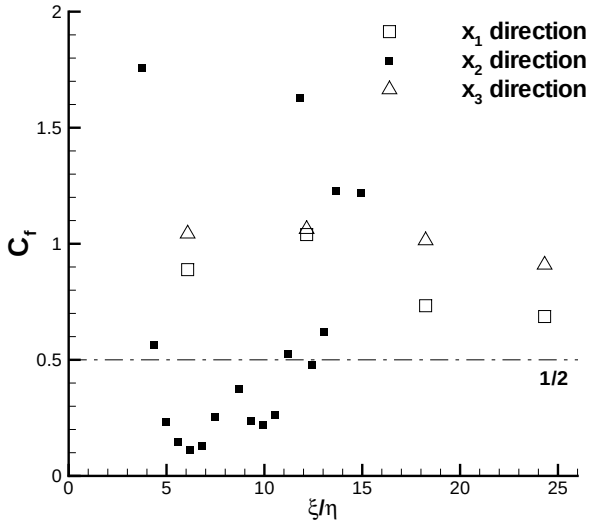

Figure 4.2: Dynamic model value of C_f, against different two-point distance, in homogeneous shear turbulence. Filter size is fixed as grid size. The horizontal line is the theoretical value.

Reynolds number $\mathrm{Re}_H = 7000$, based on the bulk velocity U_m and channel half-width H. The grid number is $128 \times 128 \times 64$. The computation domain is $4\pi H$, $2H$ and $2\pi H$ in streamwise, normal and spanwise directions. The DNS grid size is denoted by h. The filter size of LES and the two-point distance in VI model are the same: $\Delta = \xi = 2h$. This size is compared with the Kolmogorov scale and the integrated scale respectively, which are shown in Fig. 4.3. According to the prior result in homogeneous isotropic turbulence, this two-point distance, which satisfies $\eta \ll \xi \ll L$ in most of the channel region, could be applied to minimize the error of two-pointer energy transfer.

In IVI model, the effective eddy viscosity ν_t could be defined as $\tau_{ij}^{<} = -2\nu_t S_{ij}^{<}$, in which the prime means the fluctuated part without mean flow. To compare with other models, it could be calculated as:

$$\nu_t = -C_f \frac{\left\langle Q'_{ij} S'^{<}_{ij} \right\rangle}{2 \left\langle S'^{<}_{ij} S'^{<}_{ij} \right\rangle}, \tag{4.35}$$

where C_f is regarded as a constant 1/2. The other SGS models used for comparison are the original Smagorinsky model (SM) with model constant $C_s = 0.1$, the Germano Dynamic Smagorinsky model (DSM), the Smagorinsky model with van Driest

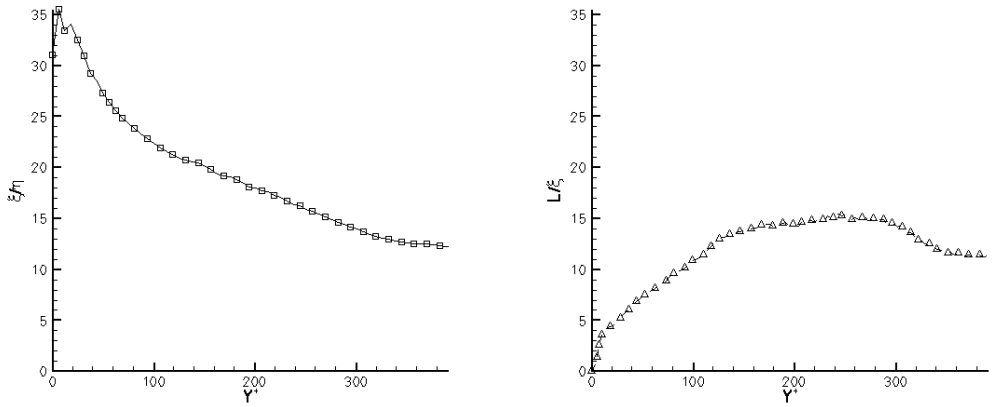

Figure 4.3: Filter size / two-point distance $\Delta = \xi = 2h$ in different position of normal direction in channel flow. (a) Compared with Kolmogorov scale. (b) Compared with integrated scale.

damping function in near-wall region (SM Damping) and the CZZS model. *A Priori* test of the magnitude of eddy viscosity is done, with the filter size $\Delta = 2h$. Results are shown in Fig. 4.4. The original Smagorinsky model causes a false viscosity at the wall, which does not tend to zero. An empirical method for solving this problem is to use van Driest damping function. An alternative mathematical way is the Germano dynamic model, which depends on the use of a test filter and a reference model. However, it doesn't fit well for the empirical location of peak $Y^+ \simeq 25$ [70]. In contrast, with KEF applied in SGS models, the near-wall property is naturally satisfied and the location of peak is well captured.

The relation between the two-point distance and the effective eddy viscosity of IVI model is then analyzed. Figure 4.5(a) shows the effective ν_t with ξ from h to $6h$, under the condition $\Delta = \xi$. Only when $\xi \leq 2h$, the near-wall region (about $10 < Y^+ < 50$) has a large eddy viscosity, which satisfies the empirical peak location. In fact, when $\xi > 2h$, in this region we could not consider $\xi \ll L$ approximately (see Fig. 4.3(b)). It means that the two-point energy transfer could only be satisfied in a proper two-point distance. Additionally, the near-wall Y^{+3} law is satisfied well, which is shown in Fig. 4.5(b).

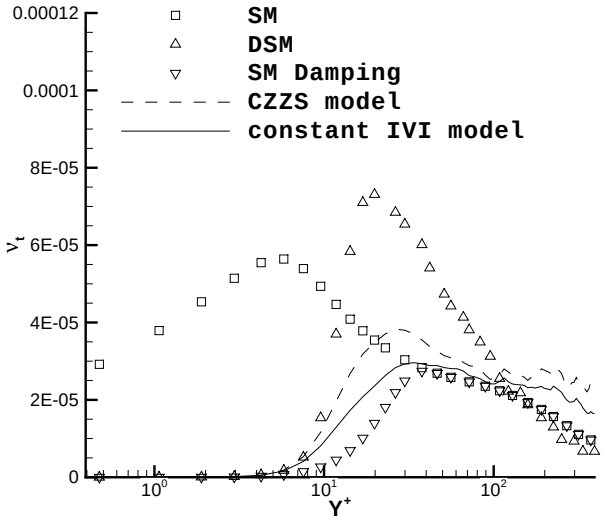

Figure 4.4: *A Priori* test of the eddy viscosity by using different SGS models in channel flow, with filter size $\Delta = 2h$. Symbols: Smagorinsky model with or without different corrections; lines: models based on KEF.

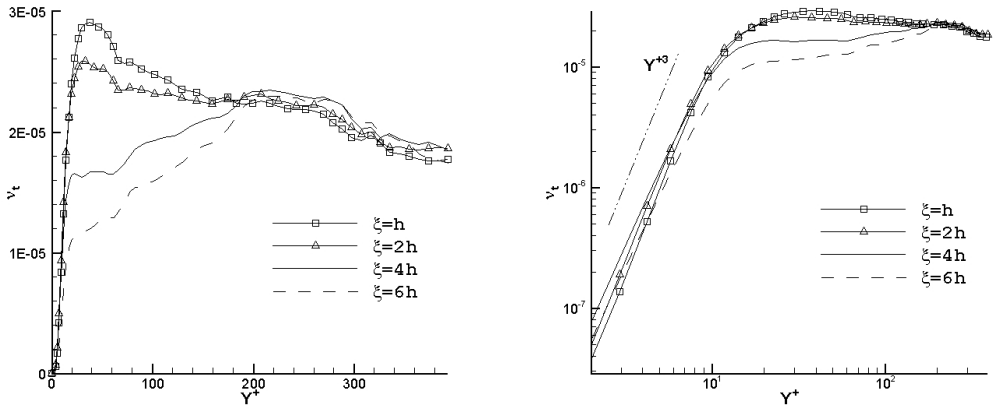

(a) (b)

Figure 4.5: *A Priori* effective ν_t in channel flow, by using IVI model. Two-point distances $\xi = h, 2h, 4h$, and $6h$. Filter size $\Delta = \xi$. (a) Original coordinate. (b) Log-log coordinate.

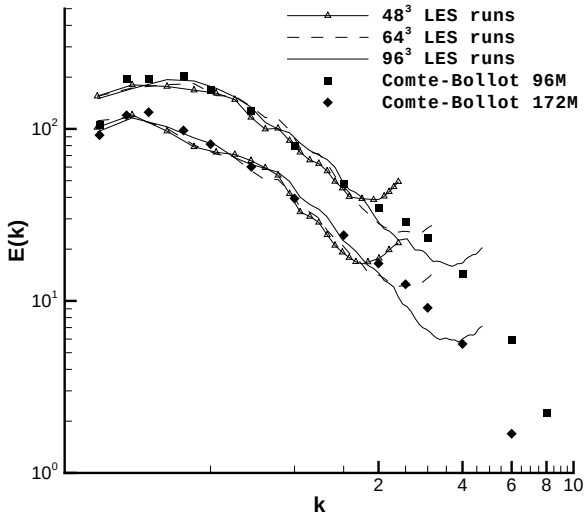

Figure 4.6: Energy spectrum in decaying isotropic turbulence. Squares: Comte-Bellot 96 M; diamonds: Comte-Bellot 172 M; lines with triangles: 48^3 LES runs; dashed lines: 64^3 LES runs; solid lines: 96^3 LES runs.

4.3.4 A Posteriori tests in homogeneous isotropic turbulence

Two *A Posteriori* tests are tried in this section. Firstly, we employ IVI model in LES of homogeneous isotropic turbulence. Our LES cases correspond to the decay turbulence at low Reynolds number, similar to the results of Comte-Bellot experiment [110]. These simulations are run on 48^3, 64^3 and 96^3 grids respectively. The initial field is generated by using Rogallo's method [54] with randomly distributed velocity phases. Figure 4.6 shows the spectrum in comparison with experiment data (the filled symbols) at 96 and 172 M. All cases are calculated with the constant coefficient, i.e., equation (4.23), and give satisfactory results.

In these calculations, the energy backscatter is omitted in spectral space. In applications, too strong backscatter will cause the flow instability. The study in detail is discussed in section 4.3.6.

4.3.5 A Posteriori tests in Poiseuille channel turbulence

Secondly, another attempt is done in channel flow. The parameters of Reynolds number, computation domain and numerical method are the same as those in our DNS channel case. The grid numbers and subgrid models are shown in Table 4.1.

Case	Grid	Model
DNS case	$128 \times 128 \times 64$	-
No model case	$32 \times 48 \times 32$	-
Dynamic IVI model case	$32 \times 48 \times 32$	Equation (4.33)
Constant IVI model case	$32 \times 48 \times 32$	Equation (4.23)

Table 4.1: The parameters implemented in *A Posteriori* tests

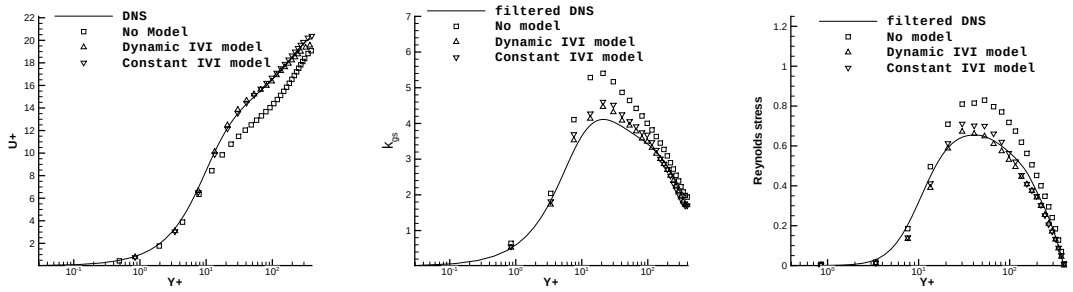

(a) (b) (c)

Figure 4.7: *A Posteriori* statistical results using different models (Table 4.1) in channel flow. (a) Mean velocity. (b) Resolved-scale turbulence kinetic energy. (c) Resolved-scale Reynolds stress.

The DNS case is already introduced in the last section. The "no model case" applies the "DNS" method at a coarse grid ($32 \times 48 \times 32$), which is compared with the LES cases to shown the model effect. Two LES cases are also executed at $32 \times 48 \times 32$ grid, with the dynamic IVI model formulation (4.33) and the constant IVI model formulation (4.23), respectively. The scaling exponent is given as $n = 2.5$ in Eq. (4.33). *A Posteriori* results are shown in Fig. 4.7.

In Fig. 4.7(a), the two SGS models both yield good agreement with DNS velocity profile, they are better than the "no model" case. In Figs. 4.7(b,c), the DNS results are filtered to the $32 \times 48 \times 32$ resolution, in order to be compared with others at the same grid scale. Both the two LES cases show quite better performances than the "no model" case. There are only slight differences between these two LES cases. The dynamic IVI model case is in slightly better agreement with the filtered DNS results in near-wall region. The peak locations of the kinetic energy and the Reynolds stress are a little better simulated in the dynamic IVI model case. However, the constant IVI model works quite well. Compared with other works, the results are as good as other

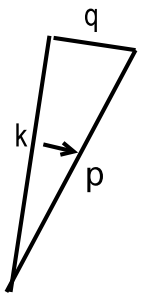

Figure 4.8: Triad interaction causing energy backscatter (R-type triad according to Waleffe's classification).

dynamic subgrid models (the same channel flow were calculated using other models in Refs. [38,40]), and all these models are much better than the original Smagorinsky model, especially in near-wall region. Therefore, the most valuable improvement in IVI model is not the accurate dynamic formulation, but is the constant coefficient introduced. It has as good performance as the other dynamic subgrid models, and the constant formulation is also greatly low-cost. In addition, in the engineering projects of complicated geometries, it is difficult to calculate the structure functions using spatial average, but the constant coefficient value will be appropriate.

4.3.6 Energy backscatter in homogeneous isotropic turbulence

Energy backscatter in homogeneous isotropic turbulence could be analyzed in spectral space. Both DIA and EDQNM theories point out that in distant triad interaction, when $k \sim p, q \ll k_c$, k_c is the cut-off wave number, there could be energy backscatter [2,8,111]. Backward transfer of energy is from wave numbers p and q to k (Fig. 4.8). The backscatter is k^4 magnitude at small wave numbers, and could be reasonably well approximated be a k^4 term [30,112,113]. Analysis shows that energy backscatter only takes effect at very small wave numbers.

The subgrid energy could be represented as

$$\varepsilon_f = -\langle \tau_{ij}^{<} S_{ij}^{<} \rangle = -3\langle \tau_{11}^{<} S_{11}^{<} \rangle - 6\langle \tau_{12}^{<} S_{12}^{<} \rangle. \tag{4.36}$$

The normal component could be denoted as $\varepsilon_f^{norm} = -\langle \tau_{11}^{<} S_{11}^{<} \rangle$, and the deviatonic component is $\varepsilon_f^{devi} = -\langle \tau_{12}^{<} S_{12}^{<} \rangle$. Thus at any moment the instant energy backscater

could be obtained by calculating the negative dissipation points [24]:

$$\begin{aligned}\varepsilon_f^{norm}(\text{backscater}) =&\langle \min(-\tau_{11}^{<} S_{11}^{<}, 0)\rangle,\\ \varepsilon_f^{devi}(\text{backscater}) =&\langle \min(-\tau_{12}^{<} S_{12}^{<}, 0)\rangle.\end{aligned} \tag{4.37}$$

The energy backscatter values in homogeneous isotropic turbulence are shown in Fig. 4.9. Two DNS cases ($Re_\lambda = 50, 70$) are employed in *A Priori* tests. The filter size is given as $\Delta = 2h, 4h, 8h, 12h$, respectively. At small wave numbers, the k^4 law are all satisfied well. However, when the wave number is large, there is also strong effect of energy backscatter. It might cause the instability in LES calculation. This is the reason that we have to omit the energy backscatter in numerical simulation of homogeneous isotropic turbulence. In order to improve this model, the model properties in spectral space must be further analyzed. However, they are not mentioned in this thesis.

4.3.7 Energy backscatter in Poiseuille channel turbulence

Further analysis is on the forward and backward flux of energy transfer in Poiseuille channel turbulence. The SGS dissipation ε_f represents the energy transfer between resolved and subgrid scales [24]. The contributions of the components of SGS dissipation were analyzed by Hartel *et al.* [26], where the interactions between fluctuating stresses and fluctuating rates of strain are studied. From their analysis, the SGS energy is dissipated in streamwise and normal direction, and the backscatter of SGS energy is in spanwise direction. While C_f is always positive, the nondimensionalized subgrid dissipation tensor components $\varepsilon_{f\,ij}^{+}$ caused by fluctuations could be calculated as (without summation convention)

$$\varepsilon_{f\,ij}^{+} = \frac{-\left\langle \tau_{ij}^{\prime <} S_{ij}^{\prime <} \right\rangle}{\text{rms}(\tau_{ij}^{\prime <})\text{rms}(S_{ij}^{\prime <})} = \frac{-\left\langle Q_{ij}^{\prime} S_{ij}^{\prime <} \right\rangle}{\text{rms}(Q_{ij}^{\prime})\text{rms}(S_{ij}^{\prime <})}. \tag{4.38}$$

The components of SGS dissipation are shown in Fig. 4.10. *A Priori* results are from our DNS case of channel flow, and *A Posteriori* results are from the fine grid case 1. In these figures, positive value means SGS energy dissipation, i.e. forward scatter; negative value represents the energy backscatter. Though the Reynolds numbers are different ($\text{Re}_\tau = 395$ in our case and $\text{Re}_\tau = 180$ in the work of Hartel *et al.*), the results can be qualitatively compared. Among the normal components, $\varepsilon_{f\,11}$ is the

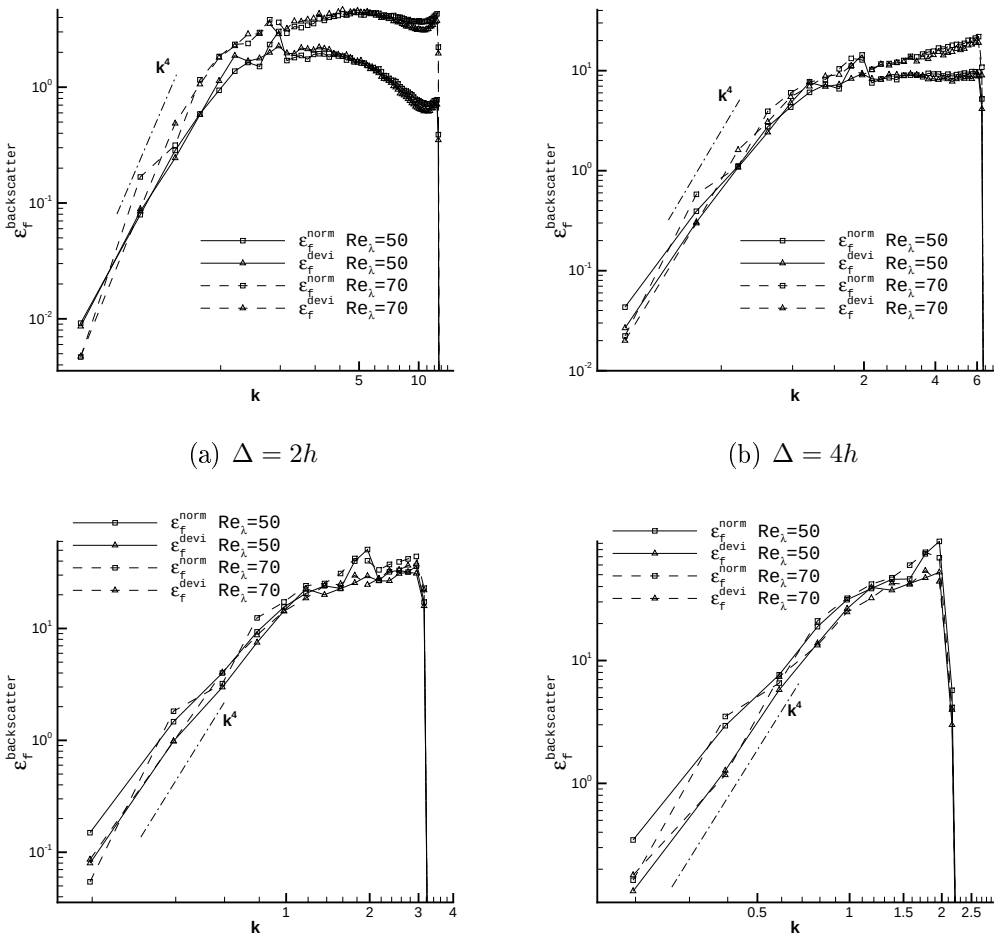

(a) $\Delta = 2h$ (b) $\Delta = 4h$

(c) $\Delta = 8h$ (d) $\Delta = 12h$

Figure 4.9: *A Priori* results of energy backscatter, in homogeneous isotropic turbulence. Filter sizes $\Delta = 2h, 4h, 8h, 12h$. Solid line with symbols: $Re_\lambda = 50$; dashed line with symbols: $Re_\lambda = 70$. Squares: normal component; triangles: deviatonic component.

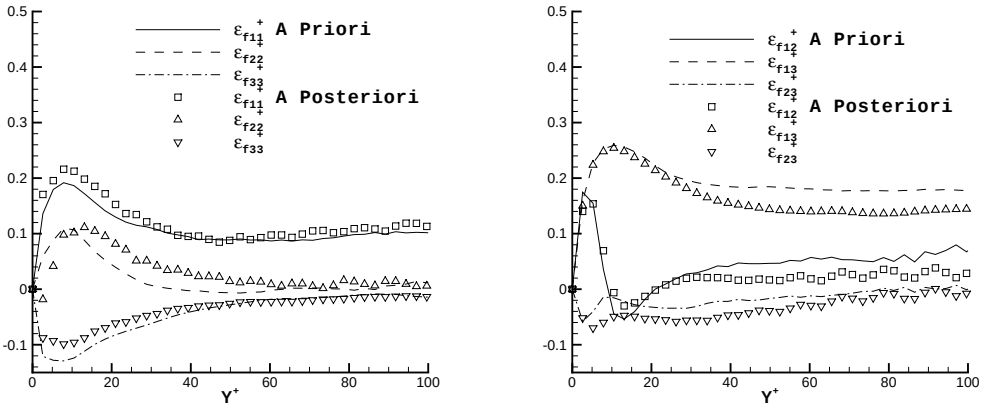

(a) (b)

Figure 4.10: Contributions of components for subgrid energy dissipation, normalized by using equation (4.38). Lines: *A Priori* results; symbols: *A Posteriori* results. (a) Normal components: $\varepsilon^+_{f11}, \varepsilon^+_{f22}$, and ε^+_{f33}. (b) Deviatonic components: $\varepsilon^+_{f12}, \varepsilon^+_{f13}$, and ε^+_{f23}.

most important positive component which leads to the dissipation, while the spanwise components ε_{f33} causes a strong energy backscatter. Compared with Hartel's analysis (see Fig. 9 of [26]), the disagreement only occurs in the $Y^+ < 8$ range, where the slight energy backscatter of ε_{f11} is not shown by our model. It might be caused by the strong inhomogeneity in this region. Among the deviatonic components, the most special component is ε_{f12}, which has the backscatter in the region $10 < Y^+ < 20$ and dissipates in the other ranges. This result is in good agreement with Hartel's analysis, including the peak locations. With each component, both *A Priori* and *A Posteriori* results assert the similar SGS dissipation. The backscatter properties of IVI model could stem from the third order structure function. From equation (4.16) and (4.29), the two-point energy dissipation and subgrid transfer are represented by the third order structure function, which could have different values, either negative or positive, in different directions and in different regions.

4.4 Discussion

The most important improvement in IVI model is to determine the model coefficient C_f by employing the two-pointer energy transfer equation, i.e. KEF. The

dynamic procedure proposed by Brun is based on Taylor expansion, it can be written as:

$$C_f = \frac{1}{\alpha^2}\frac{L_{kk}(\alpha)}{Q_{ii}}, \tag{4.39}$$

in which $L_{ij}(\alpha) = \widehat{u_i^< u_j^<} - \widehat{u_i^<}\,\widehat{u_j^<}$ is the Leonard stress, $\widehat{\bullet}$ is the test filter at size $\alpha\Delta$.

Another method introduced by Brun is to employ the Germano identity $L_{ij}(\alpha) = C_f\left(Q_{ij}(\Delta, \alpha\Delta) - Q_{ij}(\Delta, \Delta)\right)$, by considering C_f as a constant. The coefficient can be then represented as:

$$C_f = \frac{L_{ii}(\alpha)}{Q_{kk}(\Delta, \alpha\Delta) - Q_{kk}(\Delta, \Delta)}. \tag{4.40}$$

Although these methods are introduced with definition (4.3), they can also be applied with our definition (4.14). *A Priori* tests using different methods are shown in Fig. 4.11. The filter size is selected as $\Delta = 2h$, i.e. the LES mesh has $64 \times 64 \times 32$ grids. The values using Taylor expansion are much smaller then other methods, since Taylor expansion can not been employed in large two-point distance. Germano identity yields $C_f \approx 0.5$ in the middle of the channel, which is in agreement with the dynamic IVI model when $n = 2.5$. In the near wall region, differences exist since the anisotropic effect is strong. However, the constant value 0.5 is also acceptably satisfied. In addition, $n = 3$ yields much smaller value than 0.5, and $n = 2.5$ is in better agreement. That is the reason we propose $n = 2.5$ in numerical calculations when utilizing the dynamic formulation (4.33).

A Posteriori results in channel flow are shown in Fig. 4.12, in which the model coefficients are calculated by employing different methods. The parameters in this case are the same as described in the last section. From the figures, both Germano identity and the constant IVI model are better than the method based on Taylor expansion. Both of them are in good agreement with the DNS results, the constant coefficient is as good as the dynamic coefficient using Germano identity. However, the constant value is much less lost and easy to be implemented.

Notice that this IVI model is *time-reversible* since it remains when we change all $\vec{u}^<$ into $-\vec{u}^<$. It is not like some other models, for instance the Smagorinsky model, which is *time-nonreversable*. This issue is particularly discussed in the appendix E. They can represent different properties of turbulence, depending what we want to simulate in LES.

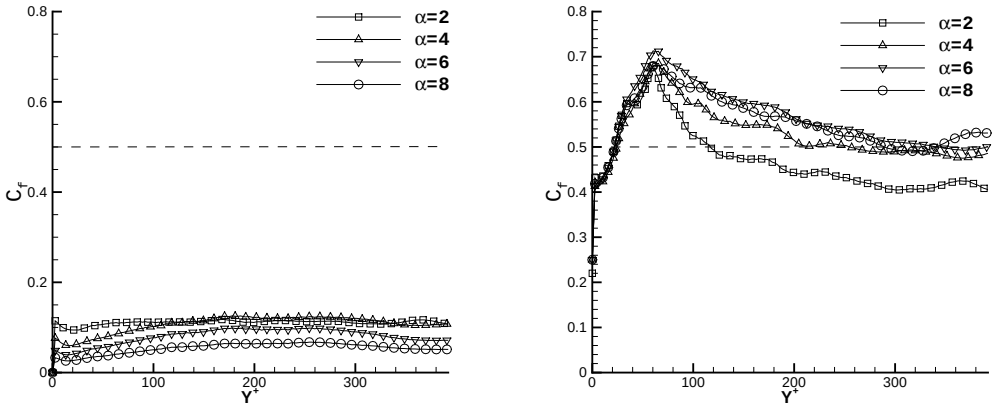

(a) (b)

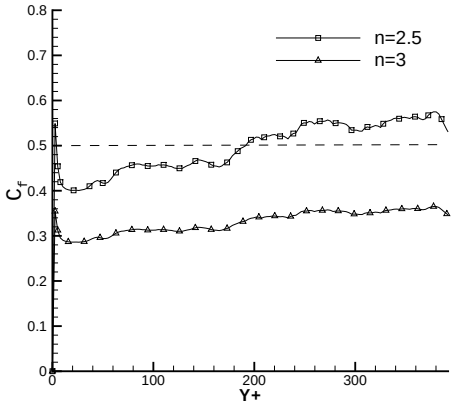

(c)

Figure 4.11: *A Priori* coefficient values using different dynamic methods, in channel flow. Filter size $\Delta = 2h$. (a) Based on Taylor expansion (4.39), with different test filters. (b) Based on Germano identity (4.40), with different test filters. (c) Dynamic formulation of IVI model (4.31), giving the scaling exponent $n = 2.5$ and 3. The dashed line is the constant value in IVI model.

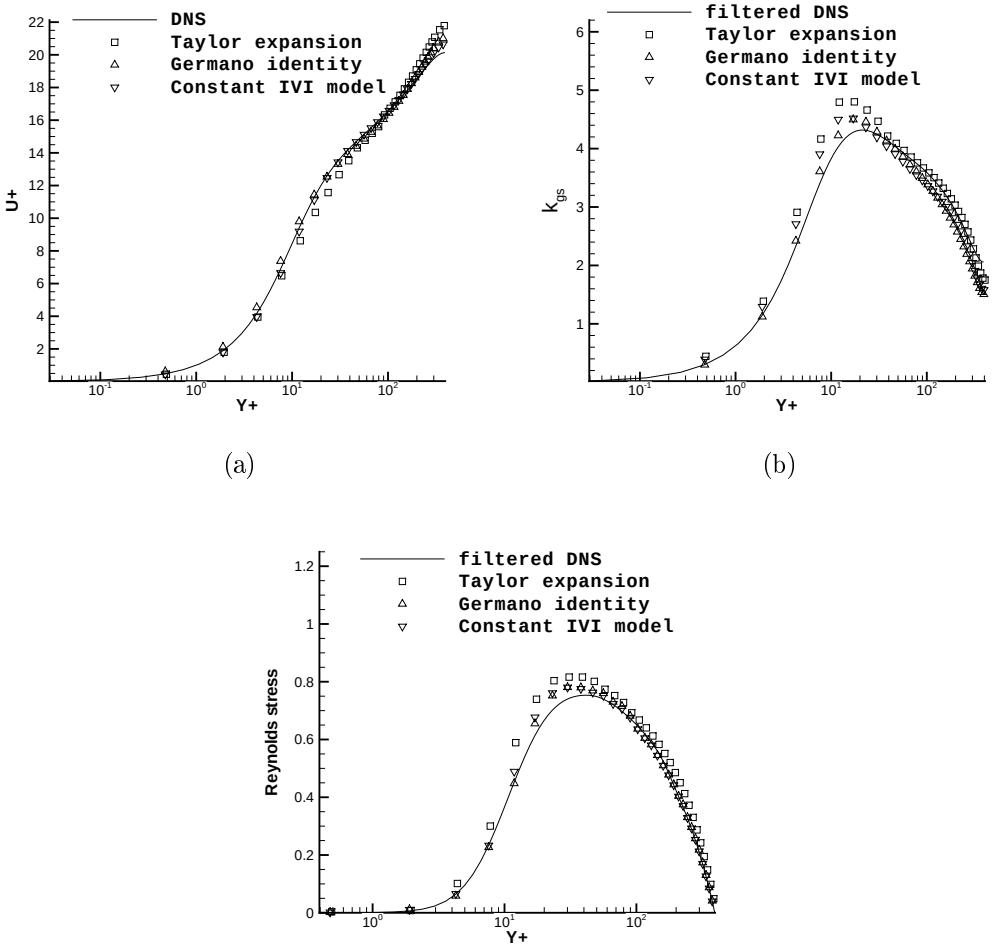

(a) (b)

(c)

Figure 4.12: *A Posteriori* statistical results of channel flow, the model coefficient is determined by different methods. (a) Mean velocity. (b) Resolved-scale turbulence kinetic energy. (c) Resolved-scale Reynolds stress.

Chapter 5

Applying KEF on anisotropic eddy-diffusivity models

The understanding of small-scale fluctuations in scalar fields, such as temperature, pollutant density, chemical or biological species concentration, advected by turbulent flow is of great interest in both theoretical and practical domains [114]. Their dynamical properties have been a subject of very accurate experimental investigations carried out in the last few years both in the atmosphere [115, 116], in the ocean [117] and for laboratory turbulent flow [118, 119]. There are many special behaviors in passive scalar, such as the obvious anisotropy [64, 120, 121]. Many numerical attempts have been performed [122–125]. However, each subgrid model has its limitation in calculation.

In chapter 3, we have discussed the applications of KEF on subgrid eddy-viscosity modeling. Similarly, the KEF formulation of passive scalar (i.e. the Yaglom equation) in homogeneous isotropic turbulence could be derived (see appendix). Zhou introduced a homogeneous isotropic eddy-diffusivity model in his thesis [126]. The eddy diffusivity assumption reads

$$\tau_{\theta j} = -\kappa_t \frac{\partial \theta^<}{\partial x_j}, \tag{5.1}$$

where the subgrid scalar flux is defined as

$$\tau_{\theta j} = (u_j \theta)^< - u_j^< \theta^<. \tag{5.2}$$

Note that in this chapter, we utilize $\tau_{\theta j}$ and τ_{ij} instead of $\tau_{\theta j}^<$ and $\tau_{ij}^<$, but in fact they both represent the same subgrid quantities.

From the homogeneous isotropic formula of KEF (see appendix A), the eddy-diffusivity model could be finally represented as

$$\kappa_t = \frac{-3D^{<}_{l\theta\theta}}{4\left\langle \frac{\partial\theta^{<}}{\partial x_j}\frac{\partial\theta^{<}}{\partial x_j}\right\rangle \xi - 6\frac{\partial D^{<}_{\theta\theta}}{\partial\xi}}. \tag{5.3}$$

This model has been tested in the LES of channel Couette turbulence, but the results are not quite satisfactory.

In this chapter, we do not mention much about this homogeneous isotropic model. Instead, we attempt to study the physical mechanism between mean and fluctuation parts, in inhomogeneous anisotropic scalar turbulence. The scalar variance equation and the scalar flux equation are decomposed into rapid and slow parts. Furthermore, the subgrid transfer of scalar flux contain the interactions between resolved velocity and subgrid scalar, and between subgrid velocity and resolved scalar. DNS database is employed to show *A Priori* results. Finally, KEF is employed in anisotropic model, it is then verified by comparing with the DNS results.

5.1 Basic equations in inhomogeneous anisotropic scalar turbulence

In order to show the exact interactions between velocity and scalar in subgrid transfer, it is necessary to derive the basic equations of inhomogeneous anisotropic scalar turbulence. The filter and the ensemble average operators are defined as the same as in section 2.1. The governing equations of scalar energy and scalar flux are described, respectively.

5.1.1 Governing equations of scalar variance

For a passive scalar θ, the motion equation could be written as

$$\frac{\partial\theta}{\partial t} + u_j\frac{\partial\theta}{\partial x_j} = \kappa\frac{\partial^2\theta}{\partial x_j\partial x_j}. \tag{5.4}$$

Taking ensemble average, the equation becomes

$$\frac{\partial\langle\theta\rangle}{\partial t} + \langle u_j\rangle\frac{\partial\langle\theta\rangle}{\partial x_j} = \kappa\frac{\partial^2\langle\theta\rangle}{\partial x_j\partial x_j} - \frac{\partial}{\partial x_j}\langle u_j'\theta'\rangle. \tag{5.5}$$

$(5.4) - (5.5)$, we could write the equation for fluctuated scalar:

$$\frac{\partial \theta'}{\partial t} + \langle u_j \rangle \frac{\partial \theta'}{\partial x_j} + u'_j \frac{\partial \langle \theta \rangle}{\partial x_j} = \kappa \frac{\partial^2 \theta'}{\partial x_j \partial x_j} - \frac{\partial}{\partial x_j} \left(u'_j \theta' - \langle u'_j \theta' \rangle \right). \tag{5.6}$$

Multiply $\langle \theta \rangle$ to each side of equation (5.5), we could obtain the transfer equation of resolved scalar variance

$$\frac{\partial \langle \theta^2 \rangle}{\partial t} + \langle u_j \rangle \frac{\partial \langle \theta^2 \rangle}{\partial x_j} = 2\kappa \left\langle \theta \frac{\partial^2 \theta}{\partial x_j \partial x_j} \right\rangle - \frac{\partial}{\partial x_j} \left\langle u'_j \left(\theta^2 \right)' \right\rangle. \tag{5.7}$$

Because $(\theta^2)' = 2\langle \theta \rangle \theta' + \theta'^2$, the last term could be expressed as

$$\begin{aligned} -\frac{\partial}{\partial x_j} \left\langle u'_j \left(\theta^2 \right)' \right\rangle &= -\left\langle u'_j \frac{\partial \theta'^2}{\partial x_j} \right\rangle - 2 \left\langle u'_j \frac{\partial \left(\langle \theta \rangle \theta' \right)}{\partial x_j} \right\rangle \\ &= -2 \left\langle u'_j \theta' \frac{\partial \theta'}{\partial x_j} \right\rangle - 2 \left\langle u'_j \theta' \frac{\partial \langle \theta \rangle}{\partial x_j} \right\rangle - 2 \left\langle u'_j \langle \theta \rangle \frac{\partial \theta'}{\partial x_j} \right\rangle \\ &= -2 \left\langle u'_j \theta' \frac{\partial \theta}{\partial x_j} \right\rangle - 2 \langle \theta \rangle \frac{\partial \left\langle u'_j \theta' \right\rangle}{\partial x_j} \\ &= -2 \left\langle u'_j \theta' \right\rangle \frac{\partial \langle \theta \rangle}{\partial x_j} - \frac{\partial}{\partial x_j} \left\langle u'_j \theta' \theta' \right\rangle - 2 \langle \theta \rangle \frac{\partial \left\langle u'_j \theta' \right\rangle}{\partial x_j} \end{aligned} \tag{5.8}$$

From equation (5.6), the transfer equation of fluctuated scalar variance can be written as

$$\frac{\partial \langle \theta'^2 \rangle}{\partial t} + \langle u_j \rangle \frac{\partial \langle \theta'^2 \rangle}{\partial x_j} = -2 \langle u'_j \theta' \rangle \frac{\partial \langle \theta \rangle}{\partial x_j} + 2\kappa \left\langle \theta' \frac{\partial^2 \theta'}{\partial x_j \partial x_j} \right\rangle - \frac{\partial}{\partial x_j} \langle u'_j \theta' \theta' \rangle. \tag{5.9}$$

Multiply $\langle \theta \rangle$ to each side of (5.5), or substract equation (5.7) with (5.9), we could obtain

$$\frac{\partial \langle \theta \rangle^2}{\partial t} + \langle u_j \rangle \frac{\partial \langle \theta \rangle^2}{\partial x_j} = 2\kappa \langle \theta \rangle \frac{\partial^2 \langle \theta \rangle}{\partial x_j \partial x_j} - 2 \langle \theta \rangle \frac{\partial \left\langle u'_j \theta' \right\rangle}{\partial x_j}. \tag{5.10}$$

We can also write the last term as

$$-2 \langle \theta \rangle \frac{\partial \left\langle u'_j \theta' \right\rangle}{\partial x_j} = 2 \left\langle u'_j \theta' \right\rangle \frac{\partial \langle \theta \rangle}{\partial x_j} - 2 \frac{\partial}{\partial x_j} \left(\langle \theta \rangle \langle u'_j \theta' \rangle \right) \tag{5.11}$$

Now consider the energy transfer in LES. The governing equation for the resolved scalar could be written as

$$\frac{\partial \theta^<}{\partial t} + u_j^< \frac{\partial \theta^<}{\partial x_j} = \kappa \frac{\partial^2 \theta^<}{\partial x_j \partial x_j} - \frac{\partial \tau_{\theta j}}{\partial x_j}, \tag{5.12}$$

where $\tau_{\theta j}^{<}$ is the subgrid-scale scalar flux defined as

$$\tau_{\theta j} = (u_j \theta)^{<} - u_j^{<} \theta^{<}. \tag{5.13}$$

The energy transfer of resolved scalar fluctuation could then be written as

$$\begin{aligned} &\frac{1}{2}\frac{\partial \langle \theta'^{<2} \rangle}{\partial t} + \frac{1}{2}\langle u_j^{<} \rangle \frac{\partial \langle \theta'^{<2} \rangle}{\partial x_j} = \\ &\qquad - \langle u_j'^{<} \theta'^{<} \rangle \frac{\partial \langle \theta^{<} \rangle}{\partial x_j} + \kappa \left\langle \theta'^{<} \frac{\partial \theta'^{<}}{\partial x_j \partial x_j} \right\rangle - \left\langle \theta'^{<} \frac{\partial \tau'_{\theta j}}{\partial x_j} \right\rangle - \left\langle \theta'^{<} \frac{\partial}{\partial x_j} \left(u_j'^{<} \theta'^{<} \right) \right\rangle. \end{aligned} \tag{5.14}$$

The term $-\langle u_j'^{<} \theta'^{<} \rangle \frac{\partial \langle \theta^{<} \rangle}{\partial x_j}$ can be regarded as an exchange term between mean and fluctuation scalar variances. And for the last two terms, we have

$$\begin{aligned} - \left\langle \theta'^{<} \frac{\partial \tau'_{\theta j}}{\partial x_j} \right\rangle &= \left\langle \tau'_{\theta j} \frac{\partial \theta'^{<}}{\partial x_j} \right\rangle - \left\langle \frac{\partial}{\partial x_j} \left(\tau'_{\theta j} \theta'^{<} \right) \right\rangle \\ - \left\langle \theta'^{<} \frac{\partial}{\partial x_j} \left(u_j'^{<} \theta'^{<} \right) \right\rangle &= \left\langle u_j'^{<} \theta'^{<} \frac{\partial \theta'^{<}}{\partial x_j} \right\rangle - \left\langle \frac{\partial}{\partial x_j} \left(u'_j \theta' \theta' \right) \right\rangle \end{aligned} \tag{5.15}$$

Similarly, we could write the governing equation for resolved mean scalar variance:

$$\begin{aligned} \frac{1}{2}\frac{\partial \langle \theta^{<} \rangle^2}{\partial t} + \frac{1}{2}\langle u_j^{<} \rangle \frac{\partial \langle \theta^{<} \rangle^2}{\partial x_j} =& \kappa \langle \theta^{<} \rangle \frac{\partial \langle \theta^{<} \rangle}{\partial x_j \partial x_j} + \langle \tau_{\theta j} \rangle \frac{\partial \langle \theta^{<} \rangle}{\partial x_j} \\ &+ \left\langle u_j'^{<} \theta'^{<} \right\rangle \frac{\partial \langle \theta^{<} \rangle}{\partial x_j} - \frac{\partial}{\partial x_j} \left(\langle \tau_{\theta j} \rangle \langle \theta^{<} \rangle \right) - \frac{\partial}{\partial x_j} \left(\left\langle u_j'^{<} \theta'^{<} \right\rangle \langle \theta^{<} \rangle \right) \end{aligned} \tag{5.16}$$

5.1.2 Governing equations of scalar flux

In order to write the governing equation for scalar flux $u_i \theta$, first of all we could write the momentum equation of velocity as

$$\frac{\partial u_i}{\partial t} + u_j \frac{\partial u_i}{\partial x_j} = -\frac{1}{\rho}\frac{\partial p}{\partial x_i} + \nu \frac{\partial^2 u_i}{\partial x_j \partial x_j}. \tag{5.17}$$

With the definition $\tau_{ij} = (u_i u_j)^{<} - u_i^{<} u_j^{<}$, the governing equation for LES could be

$$\frac{\partial u_i^{<}}{\partial t} + u_j^{<} \frac{\partial u_i^{<}}{\partial x_j} = -\frac{1}{\rho}\frac{\partial p^{<}}{\partial x_i} + \nu \frac{\partial^2 u_i^{<}}{\partial x_j \partial x_j} - \frac{\partial \tau_{ij}}{\partial x_j}. \tag{5.18}$$

Taking ensemble average, the averaged equation can be written as

$$\frac{\partial\langle u_i\rangle}{\partial t}+\langle u_j\rangle\frac{\partial\langle u_i\rangle}{\partial x_j}=-\frac{1}{\rho}\frac{\partial\langle p\rangle}{\partial x_i}+\nu\frac{\partial^2\langle u_i\rangle}{\partial x_j\partial x_j}-\frac{\partial}{\partial x_j}\langle u_j'u_i'\rangle, \tag{5.19}$$

and the governing equation of velocity fluctuation is

$$\frac{\partial u_i'}{\partial t}+\langle u_j\rangle\frac{\partial u_i'}{\partial x_j}+u_j'\frac{\partial\langle u_i\rangle}{\partial x_j}=-\frac{1}{\rho}\frac{\partial p'}{\partial x_i}+\nu\frac{\partial^2 u_i'}{\partial x_j\partial x_j}-\frac{\partial}{\partial x_j}\left(u_i'u_j'-\langle u_i'u_j'\rangle\right). \tag{5.20}$$

The governing equation for the fluctuation of scalar flux could be represented as

$$\begin{aligned}\frac{\partial\langle u_i'\theta'\rangle}{\partial t}+\langle u_j\rangle\frac{\partial\langle u_i'\theta'\rangle}{\partial x_j}=&-\left\langle\frac{\theta'}{\rho}\frac{\partial p'}{\partial x_i}\right\rangle+\kappa\left\langle u_i'\frac{\partial^2\theta'}{\partial x_j\partial x_j}\right\rangle\\&+\nu\left\langle\theta'\frac{\partial^2 u_i'}{\partial x_j\partial x_j}\right\rangle-\langle u_j'\theta'\rangle\frac{\partial\langle x_i\rangle}{\partial x_j}-\langle u_i'u_j'\rangle\frac{\partial\langle\theta\rangle}{\partial x_j}-\frac{\partial}{\partial x_j}\langle u_i'u_j'\theta'\rangle.\end{aligned} \tag{5.21}$$

In LES applications, the filtered mean velocity reads

$$\frac{\partial\langle u_i^<\rangle}{\partial t}+\langle u_j^<\rangle\frac{\partial\langle u_i^<\rangle}{\partial x_j}=-\frac{1}{\rho}\frac{\partial\langle p^<\rangle}{\partial x_i}+\nu\frac{\partial^2\langle u_i^<\rangle}{\partial x_j\partial x_j}-\frac{\partial\langle\tau_{ij}\rangle}{\partial x_j}-\frac{\partial}{\partial x_j}\langle u_i'^<u_j'^<\rangle. \tag{5.22}$$

Thus the resolved scalar flux is

$$\begin{aligned}\frac{\partial\langle u_i^<\rangle\langle\theta^<\rangle}{\partial t}+\langle u_j^<\rangle\frac{\partial\langle u_i^<\rangle\langle\theta^<\rangle}{\partial x_j}=&-\frac{1}{\rho}\langle\theta^<\rangle\frac{\partial\langle p^<\rangle}{\partial x_i}+\nu\langle\theta^<\rangle\frac{\partial^2\langle u_i^<\rangle}{\partial x_j\partial x_j}+\kappa\langle u_i^<\rangle\frac{\partial^2\langle\theta^<\rangle}{\partial x_j\partial x_j}\\&-\langle\theta^<\rangle\frac{\partial\langle\tau_{ij}\rangle}{\partial x_j}-\langle u_i^<\rangle\frac{\partial\langle\tau_{\theta j}\rangle}{\partial x_j}-\langle\theta^<\rangle\frac{\partial}{\partial x_j}\langle u_i'^<u_j'^<\rangle-\langle u_i^<\rangle\frac{\partial}{\partial x_j}\langle u_j'^<\theta'^<\rangle\end{aligned} \tag{5.23}$$

Similarly, the governing equation for subgrid scalar flux could be represented as

$$\begin{aligned}\frac{\partial\langle u_i'^<\theta'^<\rangle}{\partial t}+\langle u_j^<\rangle\frac{\partial\langle u_i'^<\theta'^<\rangle}{\partial x_j}=&-\frac{1}{\rho}\left\langle\theta'\frac{\partial p'^<}{\partial x_i}\right\rangle+\kappa\left\langle u_i'^<\frac{\partial^2\theta'^<}{\partial x_j\partial x_j}\right\rangle+\nu\left\langle\theta'^<\frac{\partial^2 u_i'^<}{\partial x_j\partial x_j}\right\rangle\\&-\langle u_i'^<u_j'^<\rangle\frac{\partial\langle\theta^<\rangle}{\partial x_j}-\langle u_j'^<\theta'^<\rangle\frac{\partial\langle u_i^<\rangle}{\partial x_j}-\left\langle u_j'^<\frac{\partial(u_i'^<\theta'^<)}{\partial x_j}\right\rangle\\&-\left\langle u_i'^<\frac{\partial\tau_{\theta j}'}{\partial x_j}\right\rangle-\left\langle\theta'^<\frac{\partial\tau_{ij}}{\partial x_j}\right\rangle\end{aligned} \tag{5.24}$$

5.2 Rapid-and-slow split of subgrid scalar flux

Shao [48] has introduced a method of rapid-and-slow split for subgrid stress. The SGS tensor τ_{ij} is split into two parts: a rapid part that explicitly depends on the mean flow and a remaining slow part. The term "rapid" is used by analogy to the terminology introduced by Rotta [127] and Lumley [128] in the context of Reynolds-averaged modeling, where the component of the pressure–strain term that explicitly depends on the mean velocity gradient is referred to as the rapid part and the remainder as the slow part. Unlike the other researches for the Reynolds-stress transport equation [129–131], the rapid and slow decomposition is applied in LES, and is verified in a turbulent mixing layer by Shao. The classical Smagorinsky model and the scale similarity model are then evaluated. However, subgrid scalar transfer is not analyzed yet.

The subgrid scalar flux $\tau_{\theta j}$ could be split into rapid and slow parts as:

$$\tau_{\theta j} = \tau_{\theta j}^{rapid} + \tau_{\theta j}^{slow}, \tag{5.25}$$

in which

$$\begin{aligned} \tau_{\theta j}^{rapid} &= (\langle u_j\rangle\langle\theta\rangle)^< - \langle u_j\rangle^<\langle\theta\rangle^< + (\langle u_j\rangle\theta')^< - \langle u_j\rangle^<\theta'^< + (u_j'\langle\theta\rangle)^< - u_j'^<\langle\theta\rangle^< \\ \tau_{\theta j}^{slow} &= (u_j'\theta')^< - u_j'^<\theta'^<. \end{aligned} \tag{5.26}$$

In order to describe the effect of rapid and slow components of the SGS stress in the scalar transport process, the rapid and slow parts are furtherly decomposed as:

$$\begin{aligned} \tau_{\theta j}^{rapid} &= \langle\tau_{\theta j}^{rapid}\rangle + \tau_{\theta j}'^{rapid} \\ \tau_{\theta j}^{slow} &= \langle\tau_{\theta j}^{slow}\rangle + \tau_{\theta j}'^{slow} \end{aligned} \tag{5.27}$$

It is clear that the mean rapid part is given by

$$\langle\tau_{\theta j}^{rapid}\rangle = (\langle u_j\rangle\langle\theta\rangle)^< - \langle u_j\rangle^<\langle\theta\rangle^<, \tag{5.28}$$

while the fluctuating rapid part is

$$\tau_{\theta j}'^{rapid} = (\langle u_j\rangle\theta')^< - \langle u_j\rangle^<\theta'^< + (u_j'\langle\theta\rangle)^< - u_j'^<\langle\theta\rangle^< \tag{5.29}$$

Similarly, the mean slow part is

$$\langle\tau_{\theta j}^{slow}\rangle = \langle(u_j'\theta')^< - u_j'^<\theta'^<\rangle \tag{5.30}$$

and the fluctuating slow part is

$$\tau_{\theta j}^{\prime slow} = \tau_{\theta j}^{slow} - \langle \tau_{\theta j}^{slow} \rangle \tag{5.31}$$

5.2.1 Magnitude of the mean rapid subgrid scalar flux

In channel turbulence, the rapid part is produced by the filter in normal direction. In order to study the properties of filters, define the 1-D filter operation in normal direction:

$$\varphi(y)^{<} = \frac{1}{\Delta(y)} \int_a^b G\left(\frac{y'-y}{\Delta(y)}, y\right) \varphi(y') dy' \tag{5.32}$$

where $\Delta(y)$ is the filter width and $G(\eta, y)$ is the location dependent filter function. Let $\eta = \dfrac{y-y'}{\Delta(y)}$, (5.32) can be written as

$$\varphi(y)^{<} = \int_{\frac{y-b}{\Delta(y)}}^{\frac{y-a}{\Delta(y)}} G(\eta, y) \varphi(y - \Delta(y)\eta) d\eta \tag{5.33}$$

Following the processes of Marsden [46] and Vasilyev [45], taking the Taylor series expansion of $\varphi(y - \Delta(x)\eta)$ in powers of Δ, we could obtain

$$\varphi(y)^{<} = \varphi(y) + \sum_{l=n}^{\infty} \frac{(-1)^l}{l!} \Delta^l(y) M^l(y) \mathscr{D}_y^l \varphi(y) \tag{5.34}$$

where

$$M^l(y) = \int_{\frac{y-b}{\Delta(y)}}^{\frac{y-a}{\Delta(y)}} \eta^l G(\eta, y) d\eta$$

$$\text{in which } M^l(y) = \begin{cases} 1, & l = 0 \\ 0, & l = 1, ..., n-1 \end{cases} \tag{5.35}$$

$$\mathscr{D}_y^l = \frac{d^l}{dy^l},$$

in which n could represents a property of the filter. Thus the terms of subgrid scalar flux are expressed as

$$\begin{aligned}\langle\theta\rangle(y)^{<}\langle u_i\rangle(y)^{<} =&\langle\theta\rangle(y)\langle u_i\rangle(y)\\ &+\sum_{l=n}^{\infty}\frac{(-1)^l}{l!}\Delta^l(y)M^l(y)\left(\langle\theta\rangle(y)\mathscr{D}_y^l\langle u_i\rangle(y)+u_i(y)\mathscr{D}_y^l\langle\theta\rangle(y)\right)\\ &+\sum_{l=n}^{\infty}\sum_{r=n}^{\infty}\frac{(-1)^{l+r}}{l!r!}\Delta^{l+r}(y)M^l(y)M^r(y)\mathscr{D}_y^l\langle\theta\rangle(y)\mathscr{D}_y^r\langle u_i\rangle(y)\end{aligned}$$

$$(\langle\theta\rangle(y)\langle u_i\rangle(y))^{<} =\langle\theta\rangle(y)\langle u_i\rangle(y)+\sum_{l=n}^{\infty}\frac{(-1)^l}{l!}\Delta^l(y)M^l(y)\sum_{k=0}^{l}C_l^k\mathscr{D}_y^{l-k}\langle\theta\rangle(y)\mathscr{D}_y^k\langle u_i\rangle(y) \tag{5.36}$$

and the magnitude of the mean rapid part of subgrid scalar flux could be evaluated as:

$$\langle\theta\rangle(y)^{<}\langle u_i\rangle(y)^{<}-(\langle\theta\rangle(y)\langle u_i\rangle(y))^{<}=\begin{cases}O(\Delta^n(y)), & n>1\\ O(\Delta^2(y)), & n=1\end{cases} \tag{5.37}$$

In this chapter, we employ the top-hat filter in physical space, which has $n=1$, and

$$\langle\theta\rangle(y)^{<}\langle u_i\rangle(y)^{<}-(\langle\theta\rangle(y)\langle u_i\rangle(y))^{<}\propto\frac{\partial\langle\theta\rangle}{\partial y}\frac{\partial\langle u_i\rangle}{\partial y}\Delta^2(y) \tag{5.38}$$

It means the mean rapid term is about Δ^2 magnitude. It will be further verified in numerical simulation.

Marsden has given the analysis on the 3-D inhomogeneous filter, and obtained the same conclusion [46]. However, in channel flow, the streamwise and spanwise directions are both homogeneous. We should only consider the effects in normal direction. Thus in the following treatment, all statistical quantities are shown in normal direction.

5.3 A Priori rapid-and-slow decomposition in Couette flow

A DNS case of Couette flow is used in evaluating the rapid and slow parts of scalar transport. The grids number is $192\times384\times96$ in streamwise, normal and spanwise directions respectively, and the corresponding computation domain is $4\pi H\times2H\times$

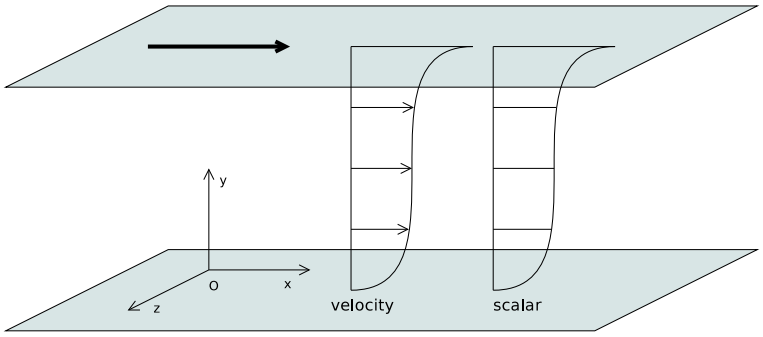

Figure 5.1: Sketch of computational domain, velocity profile and scalar profile.

$2\pi H$. The pseudo-spectral method is employed in calculation. The numerical details can be found from Xu *et al.* [101]. The Reynolds number is $\mathrm{Re}_H = 3200$ based on the bulk velocity U_m and the half width of the channel H, which is equivalent to a Reynolds number of 12800 in Kawamura's DNS results [122]. The scalar value is fixed to be 1 in the upper plane and 0 in the lower plane. The molecular Prandtl number is $\mathrm{Pr} = 0.7$. The sketch of computational domain, velocity profile and scalar profile is shown in Fig. 5.1. The original mesh is inhomogeneous in the normal direction. In order to avoid the non-commutativity described in Sec. 5.1, interpolation is done in normal direction, and a new mesh of $192 \times 300 \times 96$ grids is obtained for the following *A Priori* tests. Tophat filter is employed in physical space. The grid size is denoted as Δ and the filter size is Δ_f, in each direction. Note that the grid sizes of DNS are the same between streamwise direction and spanwise direction, but not the same in normal direction, since normal direction needs more grids in calculation. This limitation may causes the difference of magnitude when comparing the results among the three directions. However, when the filter size is fixed, all results are comparable in normal direction.

Our DNS results are compared with the DNS results of Kawamura [122]. Figure 5.2 shows the comparison between them. The scalar profiles are in quite good agreement, both in the near wall region and the channel center. The scalar variance $\langle\theta^2\rangle$ are also in agreement, except some differences far from wall. This might stem from the lack of grids by employing Chebyshev sample-point method in the normal direction. However, in this section we mainly pay attention to the near wall region, where the inhomogeneous effect could cause the rapid terms.

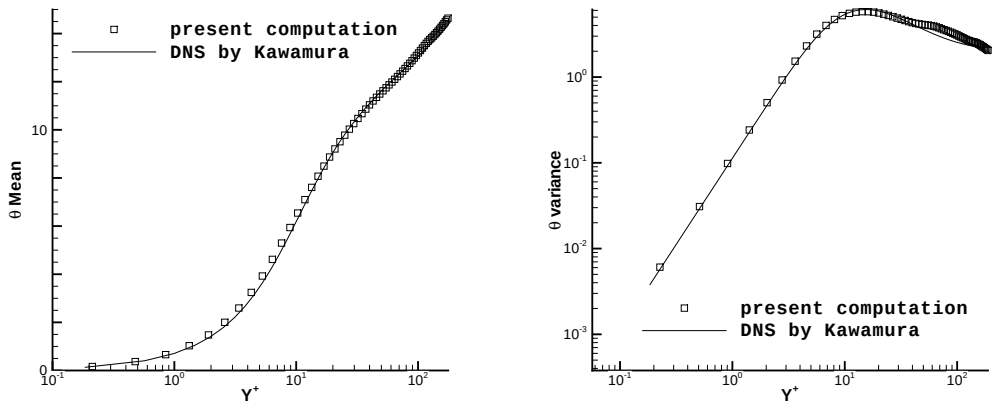

(a) Scalar profile

(b) Scalar variance

Figure 5.2: Comparison between two DNS results. Symbols: DNS with pseudo-spectral method; lines: DNS by Kawamura.

The profiles of scalar flux are shown in Fig. 5.3. In our LES case, the scalar flux is positive in the streamwise direction, and negative in the normal direction. In the spanwise direction it is approximately zero. Note that the sign of the value depends on the direction of the coordinate axis. This figure will be needed in the following parts when we analyze the subgrid flux transfer.

5.3.1 Vector level analysis of rapid-and-slow subgrid scalar flux

In section 5.2, the subgrid scalar flux is split into rapid and slow parts. Furthermore, the mean and fluctuation parts are defined. A simple analysis of the magnitude is shown in section 5.2.1. In the following part, *A Priori* tests are made to show the behavior of rapid-and-slow subgrid scalar flux. In the evaluations, we use the norm of overall slow scalar flux $\Pi_\theta = \|\langle \vec{u}\theta \rangle\|$ to normalize each flux components.

5.3.1.1 Mean subgrid flux magnitude and its anisotropy

Figure 5.4(a) shows the components of subgrid flux in streamwise direction, $\tau_{\theta 1}^{rapid}$ and $\tau_{\theta 1}^{slow}$, for different filter sizes Δ_f varying from 2 to 8 times of the grid size Δ. Note that the rapid part exists mostly in the near-wall region, especially in the region $Y^+ < 25$, where it may have the same magnitude as the slow part. And in the

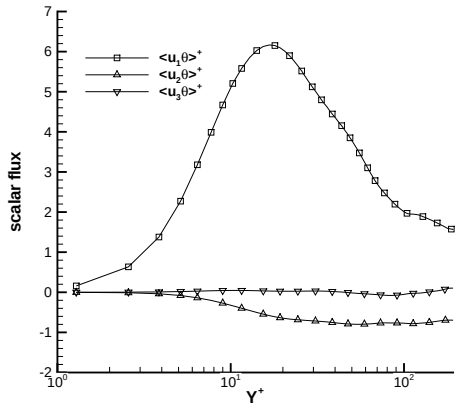

Figure 5.3: Scalar flux profiles.

center part of the Couette flow, the rapid part is negligible because of the nearly homogeneous velocity and scalar fields here.

From equation (5.38), the mean rapid part can be rescaled by the filter size $(\Delta_f/\Delta)^2$, and the results are shown in Fig. 5.4(b). The scaling law of Eq. (5.38) is reasonably satisfied in the $Y \simeq 10$ region, where the normalized curves have the similar values with each other.

Another important fact we should notice is the strong anisotropy of the mean rapid subgrid scalar flux $\langle \tau_{\theta j}^{rapid} \rangle$. This rapid parts in different directions are shown in Fig. 5.5(a). The filter size is fixed as 4 times of grid size, for instance. As mentioned in equation (5.38), the only significant component of the rapid mean SGS flux is $\langle \tau_{\theta 1}^{rapid} \rangle$, and other components are negligibly small. This is simply because of the scalar and velocity profiles are in the x_1 direction. It could also be considered as an example that the large scale structure could give an anisotropic rapid effect on the subgrid scalar flux. This effect is strong in the near-wall region.

The components of the mean slow subgrid scalar flux $\langle \tau_{\theta j}^{slow} \rangle$ are shown in Fig. 5.5(b). The results show the strong anisotropy among the three directions. The differences could also stem from the effect of mean flow and scalar. In streamwise direction, the scalar flux is positive and very strong. In normal direction, the scalar flux is negative and not strong in near-wall region, for instance $Y^+ < 10$. The values in spanwise direction are almost zero. These behaviors are similar as the total scalar flux (Fig. 5.3).

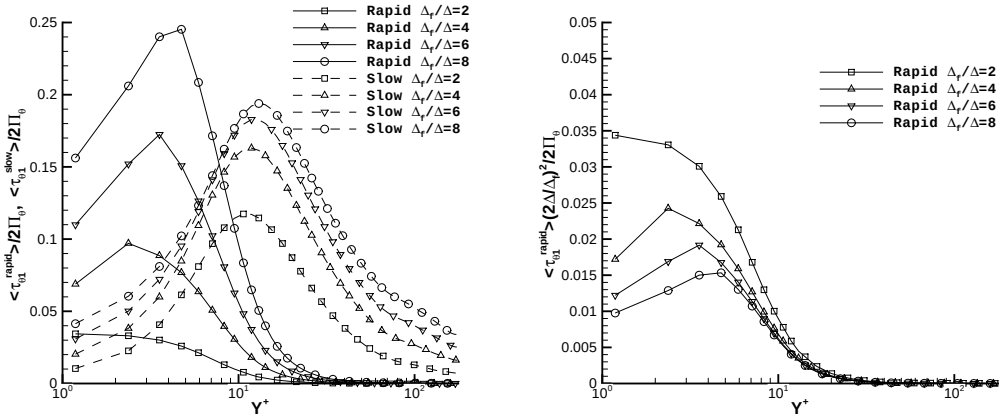

(a) Rapid and slow parts of $\langle \tau_{\theta 1} \rangle$

(b) Rapid part of $\langle \tau_{\theta 1} \rangle$, rescaled by the filter size

Figure 5.4: Normalized mean SGS flux components in streamwise direction, $\langle \tau_{\theta 1}/2\Pi_\theta \rangle$, with $\Delta_f/\Delta = 2, 4, 6$, and 8. Solid lines: rapid parts. Dashed lines: slow parts.

Thus we could say that the mean flow could effect the mean slow subgrid scalar flux mainly in streamwise direction and in $Y^+ < 10$ region. However, in the channel center, there are also anisotropic contributions on the mean slow subgrid scalar flux. The negative values occur in normal direction. Note that the negative subgrid scalar flux do not mean scalar backscatter. The analysis of scalar variance will be shown in section 5.3.2.

5.3.1.2 Fluctuating subgrid scalar flux magnitude and its anisotropy

The root-mean-square (rms) value of the subgrid scalar flux is closely related to the behavior of the small scales. Figure 5.6 shows the rms values of normalized subgrid scalar flux components in streamwise direction. The filter sizes are $2, 4, 6$ and 8 times of grid size, respectively. The magnitude of rms values between rapid and slow parts are compared. Unlike the mean values in Fig. 5.4, the slow parts of rms values are also large in near-wall region, especially when the filter size is large. However, in the center region of the channel ($Y^+ > 20$), different filter sizes yield the same rms magnitude of slow subgrid scalar flux. The near-wall effect could stem from the strong inhomogeneity of velocity and scalar under spatial filters. In addition, the rms values of rapid parts have the similar behavior as in Fig. 5.4.

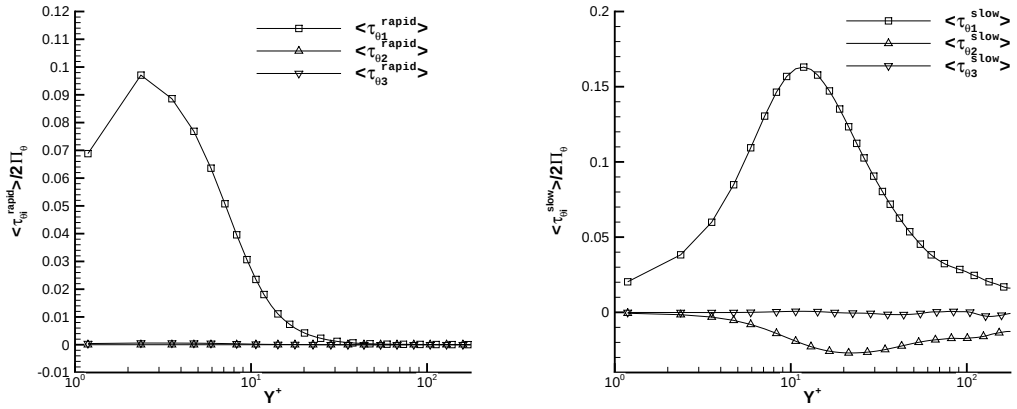

(a) Components of $\langle \tau_{\theta j}^{rapid} \rangle$

(b) Components of $\langle \tau_{\theta j}^{slow} \rangle$

Figure 5.5: Components of the rapid and slow parts of scalar flux, with $\Delta_f/\Delta = 4$

Usually, in the theory of subgrid scalar modeling, the small scales are assumed to be isotropic which allows the use of the isotropic relationship concerning the scalar transport between scales. In the present case, since a spatial filter is employed, the fluctuating part of the SGS motion contains explicitly the mean flow. Therefore, the scalar transport could deviate from isotropy. Figure 5.7 shows the rms values of all components of the rapid and slow subgrid scalar flux, for the case with $\Delta_f/\Delta = 4$. Among the rapid components in Fig. 5.7(a), the most important contribution is in the streamwise direction, and the component in normal direction is almost zero. Comparing with Fig. 5.5(a), there is also the fluctuating contribution in spanwise direction, although the mean value is almost zero. In Fig. 5.7(b), the all three components of rms values of slow subgrid scalar flux are not zero. They have the close values in channel center. In the near-wall region ($Y^+ < 20$), the contributions of both rapid and slow rms values are mainly in the streamwise direction.

5.3.2 Rapid-and-slow scalar dissipation in the equations of scalar variance

In section 5.1.1, the governing equations of scalar variance are already derived. The subgrid scalar flux has interaction with the scalar gradient vector. This inner product could be regarded as subgrid scalar dissipation. In the following part, the

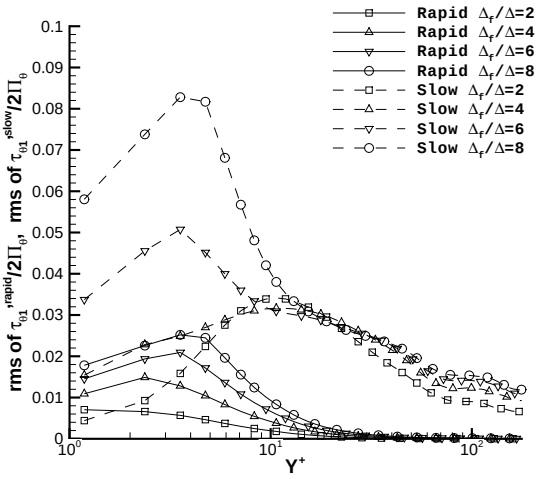

Figure 5.6: Rms of normalized SGS flux components in streamwise direction, $\langle \tau'_{\theta 1}/2k \rangle$, with $\Delta_f/\Delta = 2, 4, 6$, and 8. Solid lines: rapid parts. Dashed lines: slow parts.

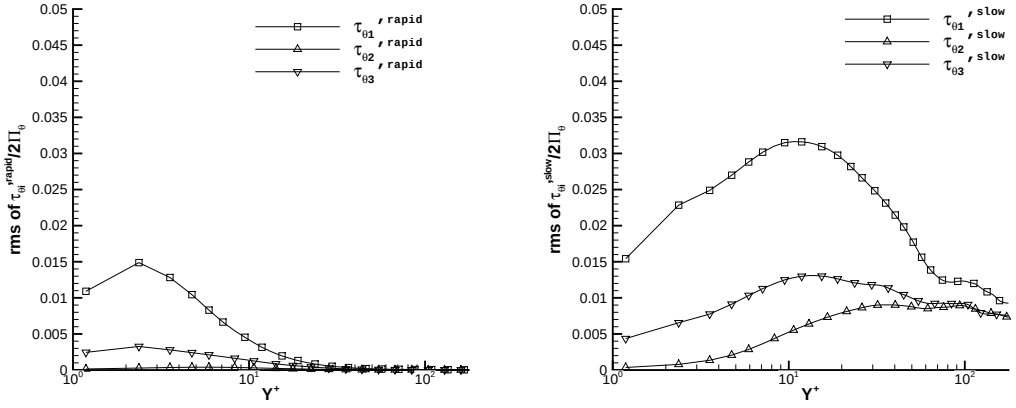

(a) Components of $\tau'^{rapid}_{\theta i}$ (b) Components of $\tau'^{slow}_{\theta i}$

Figure 5.7: Rms of the components of the rapid and slow parts of scalar flux, with $\Delta_f/\Delta = 4$.

rapid and slow parts of subgrid scalar dissipation are studied. The subgrid terms are normalized by using the overall scalar dissipation $\varepsilon_\theta = \kappa \left\langle \frac{\partial \theta}{\partial x_j} \frac{\partial \theta}{\partial x_j} \right\rangle$.

5.3.2.1 Subgrid scalar dissipation of resolved scalar variance

In the governing equation of resolved scalar variance (5.16), the subgrid term could be decomposed into rapid and slow parts:

$$\langle \tau_{\theta j} \rangle \frac{\partial \langle \theta^< \rangle}{\partial x_j} = \left\langle \tau_{\theta j}^{rapid} \right\rangle \frac{\partial \langle \theta^< \rangle}{\partial x_j} + \left\langle \tau_{\theta j}^{slow} \right\rangle \frac{\partial \langle \theta^< \rangle}{\partial x_j}, \tag{5.39}$$

which are shown in Fig. 5.8. The filter sizes are $2, 4, 6$ and 8 times of grid size, respectively. In parallel to the observation at the vector level comparison, the contribution of the mean rapid part, $-\left\langle \tau_{\theta j}^{rapid} \right\rangle \frac{\partial \langle \theta^< \rangle}{\partial x_j}$, is negligibly small compared with the slow part, $-\left\langle \tau_{\theta j}^{slow} \right\rangle \frac{\partial \langle \theta^< \rangle}{\partial x_j}$, because the subgrid flux $\left\langle \tau_{\theta j}^{rapid} \right\rangle$ only has non-zero value when $j = 1$, but the scalar gradient $\frac{\partial \langle \theta^< \rangle}{\partial x_j}$ only has non-zero value when $j = 2$. However, the mean slow part could been generated since $\left\langle \tau_{\theta 2}^{slow} \right\rangle$ is not zero, which is shown in Fig. 5.5(b). Although the value of subgrid scalar flux in normal direction is negative, in Fig. 5.5(b), the value of scalar dissipation is positive, which means that the resolved scalar variance is mainly dissipated is subgrid scale. The larger filter sizes generate the greater mean slow subgrid dissipation.

5.3.2.2 Subgrid dissipation of subgrid scalar variance

In the governing equation of subgrid scalar variance (5.14), the subgrid term could be similarly decomposed as

$$\left\langle \tau'_{\theta j} \frac{\partial \theta'^<}{\partial x_j} \right\rangle = \left\langle \tau'^{rapid}_{\theta j} \frac{\partial \theta'^<}{\partial x_j} \right\rangle + \left\langle \tau'^{slow}_{\theta j} \frac{\partial \theta'^<}{\partial x_j} \right\rangle \tag{5.40}$$

which is shown in Fig. 5.9. The rapid contributions are strong in the near-wall region, i.e. $Y^+ < 10$, and there is little rapid effect in the homogeneous region of channel center. The slow fluctuating subgrid scalar dissipation, however, has special behavior in the buffer layer, i.e. there are negative values in the region $10 < Y^+ < 20$. This means the backscatter in this region. It is in agreement with Friedrich's investigation of velocity field [26], where he found strong effect of backscatter of velocity field also in this region. This phenomenon might stem from the turbulent structures in buffer

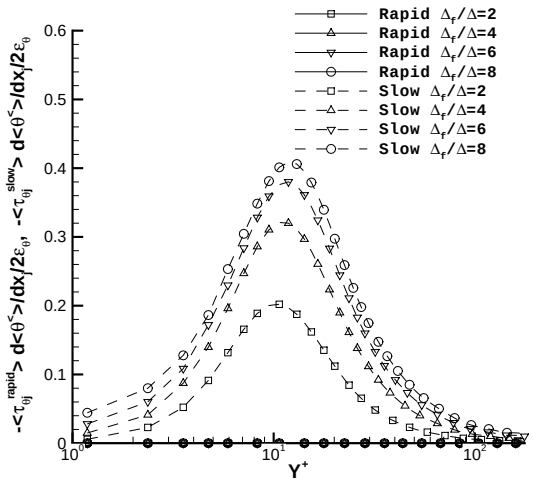

Figure 5.8: Contribution of subgrid dissipation in the transport equation of resolved scalar variance, with $\Delta_f/\Delta = 2, 4, 6$, and 8. Solid lines: rapid parts. Dashed lines: slow parts.

layer. With different filter sizes, the backscatter remains, but the positive peak value and peak location can be different, in the $30 < Y^+ < 70$ region.

5.3.3 Rapid-and-slow scalar transport in the equations of scalar flux

In section 5.1.2, the governing equations of scalar flux are derived. In the governing equations, the subgrid interactions could exist between the subgrid scalar flux and the velocity gradient tensor, or between the subgrid stress tensor and the scalar gradient vector. The former could represent the interaction between GS velocity and SGS scalar; while the latter represents the interaction between GS scalar and SGS velocity. There are already researches on these contributions. Yeung splits the scalar variance transfer term into four parts in spectral space (the superscript $*$ denotes the conjugate) [132]:

1. $\theta^* u^< \theta^<$ is the interaction between GS velocity and GS scalar (GVGS). It causes GS transfer.

2. $\theta^* u^< \theta^>$ is the interaction between GS velocity and SGS scalar (GVSS). It causes SGS transfer.

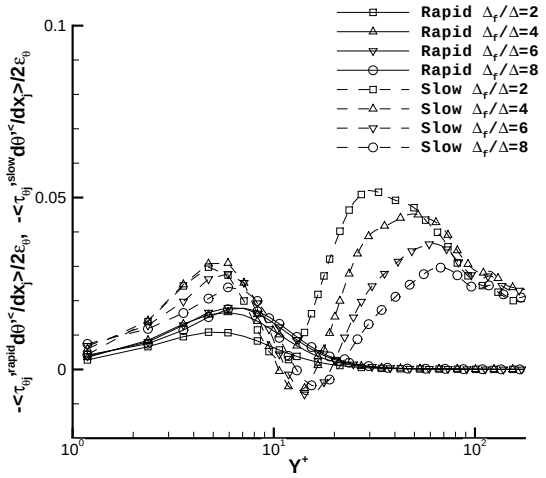

Figure 5.9: Contribution of subgrid dissipation in subgrid scalar transport equation, with $\Delta_f/\Delta = 2, 4, 6$, and 8. Solid lines: rapid parts. Dashed lines: slow parts.

3. $\theta^* u^> \theta^<$ is the interaction between SGS velocity and GS scalar (SVGS). It causes SGS transfer.

4. $\theta^* u^> \theta^>$ is the interaction between SGS velocity and SGS scalar (SVSS). It causes SGS transfer.

In the three parts causing SGS transfer, the interaction between GS velocity and SGS scalar (GVSS) is the main part, which is much more obvious than the other two parts. Especially GVSS has much more contribution than SVGS term has. This phenomenon was verified in isotropic scalar turbulence by Yeung [132] and in anisotropic scalar turbulence by Fang [133]. In the following part, we would like to investigate this behavior in the transport of scalar flux in inhomogeneous anisotropic channel flow, but with a spatial filter in physical space. The subgrid terms are normalized by using the norm of overall scalar flux $\varepsilon_{u\theta} = (\nu + \kappa) \left\| \frac{\partial \vec{u}}{\partial x_j} \frac{\partial \theta}{\partial x_j} \right\|$.

5.3.3.1 Subgrid transport of mean scalar flux

There are two subgrid dissipation terms in the transport equation of mean scalar flux (5.23), which could be denoted as $\langle \tau_{\theta j} \rangle \frac{\partial \langle u_i^< \rangle}{\partial x_j}$ and $\langle \tau_{ij} \rangle \frac{\partial \langle \theta^< \rangle}{\partial x_j}$. They could be

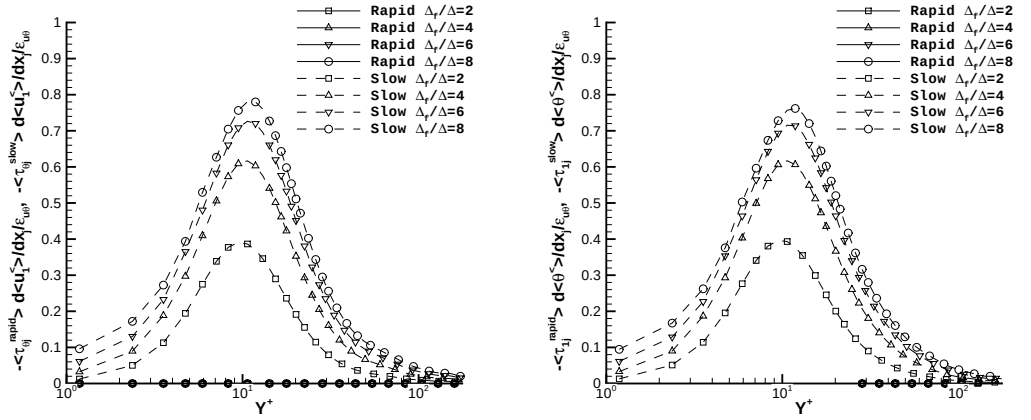

(a) $\left\langle \tau_{\theta j}^{rapid} \right\rangle \dfrac{\partial \langle u_1^< \rangle}{\partial x_j}$ and $\left\langle \tau_{\theta j}^{slow} \right\rangle \dfrac{\partial \langle u_1^< \rangle}{\partial x_j}$ (b) $\left\langle \tau_{1j}^{rapid} \right\rangle \dfrac{\partial \langle \theta^< \rangle}{\partial x_j}$ and $\left\langle \tau_{1j}^{slow} \right\rangle \dfrac{\partial \langle \theta^< \rangle}{\partial x_j}$

Figure 5.10: Contribution of subgrid transport in mean scalar flux equation, at $\Delta_f/\Delta = 2, 4, 6$, and 8. Solid lines: rapid parts. Dashed lines: slow parts.

decomposed into rapid and slow parts, respectively as follows:

$$\begin{aligned} \langle \tau_{\theta j} \rangle \frac{\partial \langle u_i^< \rangle}{\partial x_j} &= \left\langle \tau_{\theta j}^{rapid} \right\rangle \frac{\partial \langle u_i^< \rangle}{\partial x_j} + \left\langle \tau_{\theta j}^{slow} \right\rangle \frac{\partial \langle u_i^< \rangle}{\partial x_j}, \\ \langle \tau_{ij} \rangle \frac{\partial \langle \theta^< \rangle}{\partial x_j} &= \left\langle \tau_{ij}^{rapid} \right\rangle \frac{\partial \langle \theta^< \rangle}{\partial x_j} + \left\langle \tau_{ij}^{slow} \right\rangle \frac{\partial \langle \theta^< \rangle}{\partial x_j}, \end{aligned} \tag{5.41}$$

where the rapid and slow parts of subgrid stress τ_{ij} are defined similar as the subgrid scalar flux $\tau_{\theta j}$. The details could be found in Shao's paper [48].

These four terms are shown in Fig. 5.10. Note that in the mean scalar flux equation, only the component in streamwise direction, $\langle u_1^< \rangle \langle \theta^< \rangle$, is not equal to zero. All the rapid terms have zero values. Between figures 5.10(a) and 5.10(b), the magnitude of the slow terms are almost the same. It shows that the contribution on mean scalar flux of GS velocity and SGS scalar is almost the same as the contribution of SGS velocity and GS scalar. It is reasonable since in Eq. (5.38), the magnitude of rapid subgrid is expressed by the mean gradients of velocity and scalar. We could similarly write the expression for subgrid stress, using the same method as in Sec. 5.2.1, finally the terms are of the same magnitude between Figs. 5.10(a) and 5.10(b). In addition, in both figures the subgrid transfer increases when the filter size increases.

5.3.3.2 Subgrid transport of resolved scalar flux

Similarly, there are two subgrid dissipation terms in the transport equation of resolved scalar flux (5.24), which are $\left\langle \tau'_{\theta j} \frac{\partial u_i'^{<}}{\partial x_j} \right\rangle$ and $\left\langle \tau'_{ij} \frac{\partial \theta'^{<}}{\partial x_j} \right\rangle$. They could be decomposed into rapid and slow parts, respectively:

$$\begin{aligned} \left\langle \tau'_{\theta j} \frac{\partial u_i'^{<}}{\partial x_j} \right\rangle &= \left\langle \tau_{\theta j}'^{rapid} \frac{\partial u_i'^{<}}{\partial x_j} \right\rangle + \left\langle \tau_{\theta j}'^{slow} \frac{\partial u_i'^{<}}{\partial x_j} \right\rangle, \\ \left\langle \tau'_{ij} \frac{\partial \theta'^{<}}{\partial x_j} \right\rangle &= \left\langle \tau_{ij}'^{rapid} \frac{\partial \theta'^{<}}{\partial x_j} \right\rangle + \left\langle \tau_{ij}'^{slow} \frac{\partial \theta'^{<}}{\partial x_j} \right\rangle. \end{aligned} \tag{5.42}$$

These four terms are shown in Fig. 5.11, 5.12 and 5.13, in different directions respectively. The different interactions are both shown. Each figure on the left denotes the interaction between GS velocity and SGS scalar (GVSS), while on the right represents the interaction between SGS velocity and GS scalar (SVGS). Similar as analyzed before, the rapid parts mainly exist in the streamwise direction, and are almost zero in normal and spanwise direction. For the slow parts in the streamwise direction, in the region $10 < Y^+ < 20$ there is also backscatter, it is similar as the analysis of energy variance. Both GVSS and SVGS terms show the same behavior. For the slow parts in the normal direction, GVSS term has negative value while SVGS term is positive in most part of the channel. Since the total scalar flux is negative (see Fig. 5.3), here GVSS term is the forward transfer and SVGS term is backscatter. This behavior of backscatter is quite obvious in the region $Y^+ \approx 20$. For the slow parts in the spanwise direction, all terms are almost zero.

Besides, we can focus at the mostly homogeneous region ($Y^+ > 100$), the principal contribution among the six figures is the GVSS term in streamwise direction, i.e. Fig. 5.11(a). It is much stronger than the SVGS term in the same direction, i.e. Fig. 5.11(b). This phenomenon is in agreement with the results of Yeung [132] and Fang [133]. Thus in the homogeneous anisotropic region, the GVSS term could be considered as the major contribution of subgrid scalar flux.

5.4 A Priori evaluation of subgrid models

From the discussion of the previous sections, it is clear that, through the rapid part, the mean velocity and scalar gradient directly affects the SGS scalar flux and the

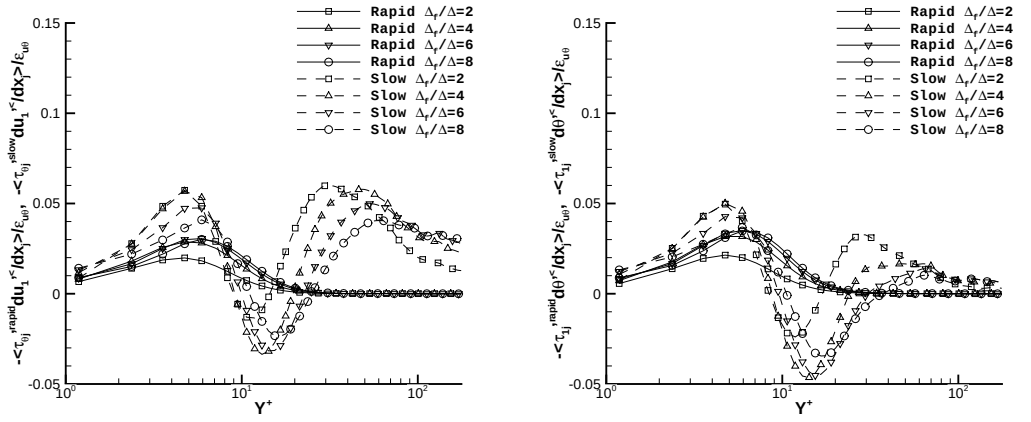

(a) $\left\langle \tau_{\theta j}^{\prime rapid} \dfrac{\partial u_1^{\prime <}}{\partial x_j} \right\rangle$ and $\left\langle \tau\theta j^{\prime slow} \dfrac{\partial u_1^{\prime <}}{\partial x_j} \right\rangle$ (b) $\left\langle \tau_{1j}^{\prime rapid} \dfrac{\partial \theta^{\prime <}}{\partial x_j} \right\rangle$ and $\left\langle \tau_{1j}^{\prime slow} \dfrac{\partial \theta^{\prime <}}{\partial x_j} \right\rangle$

Figure 5.11: The contribution of subgrid transport in resolved scalar flux equation, in the streamwise direction, with $\Delta_f/\Delta = 2, 4, 6$, and 8. Solid lines: rapid parts. Dashed lines: slow parts. (a) GVSS term. (b) SVGS term.

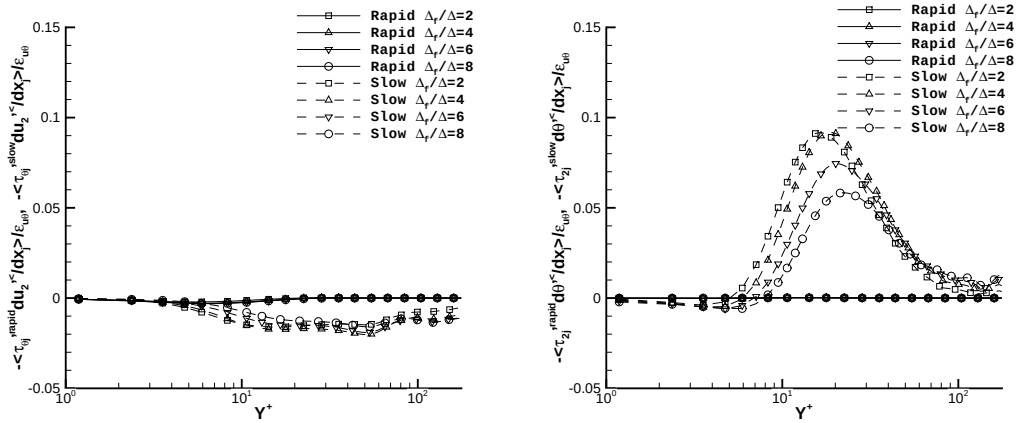

(a) $\left\langle \tau_{\theta j}^{\prime rapid} \dfrac{\partial u_2^{\prime <}}{\partial x_j} \right\rangle$ and $\left\langle \tau\theta j^{\prime slow} \dfrac{\partial u_2^{\prime <}}{\partial x_j} \right\rangle$ (b) $\left\langle \tau_{2j}^{\prime rapid} \dfrac{\partial \theta^{\prime <}}{\partial x_j} \right\rangle$ and $\left\langle \tau_{2j}^{\prime slow} \dfrac{\partial \theta^{\prime <}}{\partial x_j} \right\rangle$

Figure 5.12: The contribution of the subgrid transport in the resolved scalar flux equation, in the normal direction, with $\Delta_f/\Delta = 2, 4, 6$, and 8. Solid lines: rapid parts. Dashed lines: slow parts. (a) GVSS term. (b) SVGS term.

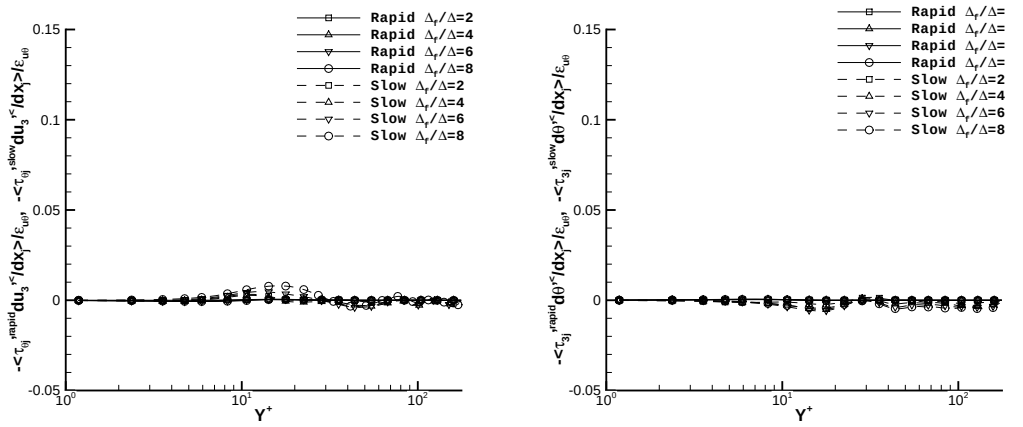

(a) $\left\langle \tau_{\theta j}^{\prime rapid} \dfrac{\partial u_3^{\prime <}}{\partial x_j} \right\rangle$ and $\left\langle \tau\theta j^{\prime slow} \dfrac{\partial u_3^{\prime <}}{\partial x_j} \right\rangle$ (b) $\left\langle \tau_{3j}^{\prime rapid} \dfrac{\partial \theta^{\prime <}}{\partial x_j} \right\rangle$ and $\left\langle \tau_{3j}^{\prime slow} \dfrac{\partial \theta^{\prime <}}{\partial x_j} \right\rangle$

Figure 5.13: The contribution of the subgrid transport in the resolved scalar flux equation, in the span direction, with $\Delta_f/\Delta = 2, 4, 6$, and 8. Solid lines: rapid parts. Dashed lines: slow parts. (a) GVSS term. (b) SVGS term.

associated scalar transfer to the small scales. The question that then arises is whether SGS modeling has to explicitly account for the effect of the mean velocity and scalar gradient manifested by the rapid SGS stress. In fact, because the rapid parts strongly depends on the type of filter, and only exists in inhomogeneous scalar turbulence, it can not be represented by most of the SGS models. In the following part, we follow Shao's conclusion [48], to represent the rapid parts by using the scale-similarity model (SSM):

$$\begin{aligned} \tau_{\theta j}^{\prime rapid} = C_m \left[(\langle\theta\rangle^{<}\langle u_j\rangle^{<})^{<} - \langle\theta\rangle^{<<}\langle u_j\rangle^{<<} + (\langle\theta\rangle^{<}\langle u_j\rangle^{<})^{<} - \langle\theta\rangle^{<<}u_j^{\prime <<} \right. \\ \left. + (\theta^{\prime <}\langle u_j\rangle^{<})^{<} - \theta^{\prime <<}\langle u_j\rangle^{<<} \right], \end{aligned} \tag{5.43}$$

where $C_m = 1$. The second filtering operation is done with a "test" filter that is the same as the original "grid" top-hat filter.

Besides, in order to simulate the slow subgrid scalar dissipation, we apply the Smagorinsky model with constant turbulent Prandtl number, which can be written as

$$\tau_{\theta j}^{\prime slow} = -\kappa_t \frac{\partial \theta^{\prime <}}{\partial x_j}, \qquad \kappa_t = \frac{\nu_t}{\mathrm{Pr}_t}. \tag{5.44}$$

Two classical models are applied to determine the eddy viscosity coefficient. One is the Smagorinsky model $\nu_t = (C_s\Delta)^2(2|S_{ij}^{\prime <}S_{ij}^{\prime <}|)^{1/2}$ with $C_s = 0.1$ and with van

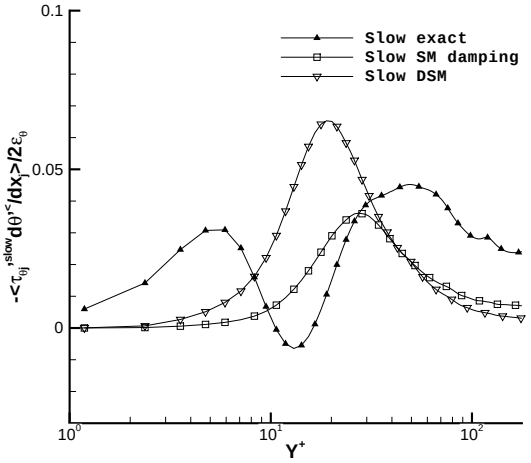

Figure 5.14: Comparison between exact values and model values, of slow subgrid scalar dissipation. $\Delta_f/\Delta = 4$. Smagorinsky model with constant turbulent Prandtl number is applied.

Driest damping function in near-wall region (SM damping) . Another is the Germano Dynamic Smagorinsky model (DSM) [11]. In both cases the turbulent Prandtl number is fixed as $\mathrm{Pr}_t = \mathrm{Pr}$. The comparison with exact slow subgrid scalar dissipation is shown in Fig. 5.14. It is found that these SGS models are not enough dissipated in the channel center, and they can not represent either the backscatter around $Y^+ = 15$, or the scalar dissipation at about $Y^+ = 5$. In order to propose a better SGS model, we choose a recent anisotropic model by Cui *et al.* (Cui Model) [40] to represent the slow parts. Comparing with other SGS models, this anisotropic model explicitly denotes the eddy diffusion as a function of mean velocity and scalar, which can not be analyzed by rapid-and-slow decomposition. We also evaluate the model performance of backscatter performance in near-wall region.

5.4.1 Extended formulation of Cui Model

The original form of scalar model in Ref. [40] did not consider the mean part of scalar. In this section we consider that the turbulence is homogeneous with mean shear γ and mean scalar gradient G, thus the velocity and scalar can be decomposed

to mean and fluctuation as:

$$\begin{aligned} u_i =& u_i' + \gamma x_2 \delta_{i1}, \\ \theta =& \theta' + G x_2. \end{aligned} \tag{5.45}$$

The equation of large eddy simulation for scalar turbulence can then be written as

$$\frac{\partial \theta'^{<}}{\partial t} + \left(u_j'^{<} + \gamma x_2 \delta_{j1}\right)\left(\frac{\partial \theta'^{<}}{\partial x_j} + G\delta_{j2}\right) = \kappa \frac{\partial^2 \theta'^{<}}{\partial x_j \partial x_j} - \frac{\partial \tau_{\theta j}'}{\partial x_j}. \tag{5.46}$$

Following the same process as in Ref. [40], defining the structure functions $D_{\theta\theta}^{<} = \langle \delta\theta'^2 \rangle, D_{j\theta\theta}^{<} = \left\langle \delta u_j'^{<} \delta\theta'^2 \right\rangle$ and $D_{2\theta}^{<} = \langle \delta u_2'^{<} \delta\theta' \rangle$, neglecting the molecular diffusivity, and making average in a local sphere of radius r, finally the SGS eddy diffusivity can be obtained as (Extended Cui Model, denoted as ECM)

$$\kappa_t = \frac{6\left(D_{r\theta\theta}^{<}\right)^A + 6\gamma r \left(D_{\theta\theta}^{<} n_1 n_2\right)^A + \left(D_{2\theta}^{<}\right)^V Gr}{6\left(\frac{dD_{\theta\theta}^{<}}{dr}\right)^A - 4r\left\langle \frac{\partial \theta'^{<}}{\partial x_j}\frac{\partial \theta'^{<}}{\partial x_j}\right\rangle^V} \tag{5.47}$$

in which the notations $(\bullet)^A$ and $(\bullet)^V$ are local surface average and local volume average. We can also divide it into two parts:

$$\begin{aligned} \kappa_t^{fs} =& \frac{6\left(D_{r\theta\theta}^{<}\right)^A}{6\left(\frac{dD_{\theta\theta}^{<}}{dr}\right)^A - 4r\left\langle \frac{\partial \theta'^{<}}{\partial x_j}\frac{\partial \theta'^{<}}{\partial x_j}\right\rangle^V}, \\ \kappa_t^{ms} =& \frac{6\gamma r \left(D_{\theta\theta}^{<} n_1 n_2\right)^A + \left(D_{2\theta}^{<}\right)^V Gr}{6\left(\frac{dD_{\theta\theta}^{<}}{dr}\right)^A - 4r\left\langle \frac{\partial \theta'^{<}}{\partial x_j}\frac{\partial \theta'^{<}}{\partial x_j}\right\rangle^V}, \end{aligned} \tag{5.48}$$

in which κ_t^{fs} represents only the interactions of subgrid scale (fluctuating part), and κ_t^{ms} contains the informations of mean flow and mean scalar (mean part), i.e. γ and G, explicitly. Comparing with the original model formulation in Ref. [40], the mean velocity is additionally considered. Because only homogeneous velocity and scalar fields are considered in Eq. (5.46), we approximately consider that ECM only generates the slow SGS scalar flux. This model formulation shows that the slow SGS scalar flux is not only affected by SGS fluctuations, but also relative with the mean profiles. The model is derived by employing the Yaglom equation of filtered quantities, and the backscatter can also be denoted.

5.4.2 Evaluation of subgrid scalar dissipation

From equation (5.48), the subgrid eddy-diffusivity is split into mean and fluctuating parts. Thus from the eddy-diffusivity assumption, the mean and fluctuating subgrid scalar flux are expressed as [26]:

$$\begin{aligned} \tau_{\theta j}^{\prime ms} &= -\kappa_t^{ms} \frac{\partial \theta'}{\partial x_j}, \\ \tau_{\theta j}^{\prime fs} &= -\kappa_t^{fs} \frac{\partial \theta'}{\partial x_j}. \end{aligned} \tag{5.49}$$

The relative terms of subgrid scalar dissipation read

$$\begin{aligned} \left\langle \tau_{\theta j}^{\prime ms} \frac{\partial \theta'^{<}}{\partial x_j} \right\rangle &= \kappa^{ms} \left\langle \frac{\partial \theta'^{<}}{\partial x_j} \frac{\partial \theta'^{<}}{\partial x_j} \right\rangle, \\ \left\langle \tau_{\theta j}^{\prime fs} \frac{\partial \theta'^{<}}{\partial x_j} \right\rangle &= \kappa^{fs} \left\langle \frac{\partial \theta'^{<}}{\partial x_j} \frac{\partial \theta'^{<}}{\partial x_j} \right\rangle. \end{aligned} \tag{5.50}$$

With an ideal subgrid model, there should be

$$\begin{aligned} \tau_{\theta j}^{\prime slow} &= \tau_{\theta j}^{\prime ms} + \tau_{\theta j}^{\prime fs}, \\ \left\langle \tau_{\theta j}' \frac{\partial \theta'^{<}}{\partial x_j} \right\rangle &= \left\langle \tau_{\theta j}^{\prime ms} \frac{\partial \theta'^{<}}{\partial x_j} \right\rangle + \left\langle \tau_{\theta j}^{\prime fs} \frac{\partial \theta'^{<}}{\partial x_j} \right\rangle. \end{aligned} \tag{5.51}$$

The mean and fluctuating parts of subgrid scalar dissipation are shown in Fig. 5.15, by employing the ECM. The filter sizes are $2, 4, 6$ and 8 times of grid size, respectively. The mean parts have positive values, which means scalar variance could be dissipated by mean velocity and mean scalar. The peak locations is about $Y^+ \simeq 15$. The fluctuating parts also have positive value in most region of channel, which means the subgrid interactions mainly dissipate scalar variance. In the channel center, flow is almost homogeneous, and the subgrid dissipation increases when filter size increases. However, there are also negative values in $Y^+ \simeq 15$ region, i.e. the buffer layer. It means that the scalar backscatter could also be generated by subgrid interactions.

The total slow subgrid scalar dissipation could be calculated by employing the total eddy diffusivity $\kappa = \kappa^{ms} + \kappa^{fs}$. The SSM is used to simulate the rapid subgrid scalar dissipation. With different filter size, the comparisons between exact values and modelled values are shown in Fig. 5.16, respectively.

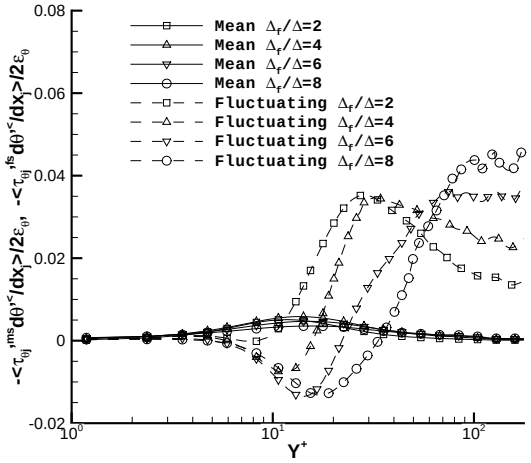

Figure 5.15: Mean and fluctuating parts in the ECM, with $\Delta_f/\Delta = 2, 4, 6$, and 8. Solid lines: mean parts. Dashed lines: fluctuating parts.

For the slow parts of subgrid scalar dissipation, the model results have the similar trend with the exact values. In the channel center, where the turbulence is almost homogeneous, their magnitudes are in good agreement, especially when Δ_f is 4 and 6 times of grid size. In the near-wall region, all the model values are smaller than the exact values, which means that the shear model does not dissipate enough in the viscous sublayer. Comparing with the results of SM and DSM in Fig. 5.14, there is no improvement in this range. It could really be a serious problem for large-eddy simulation [134], which is still not enough studied. However, an advantage could be found in the ECM, that in buffer layer ($Y^+ \simeq 15$), the behavior of scalar backscatter is simulated. The peak locations and values of shear model are in quite good agreement with the exact results, especially when Δ_f is 4 and 6 times of grid size. When the filter size is too large (for instance, $\Delta_f/\Delta = 8$), this scale is probably out of inertial subrange, and there is no good agreement. In brief, both the agreement in channel center and in the range of backscatter could be considered as an great advantage than other scalar models. For the rapid parts, the scale-similarity model simulates quite well the strong dissipation in near-wall region.

Therefore, we propose the ECM to be employed in wall-bounded scalar turbulence. It could represent the behavior of subgrid scalar backscatter. The mean velocity and scalar profiles could affect the subgrid scalar flux explicitly. In addition, in the

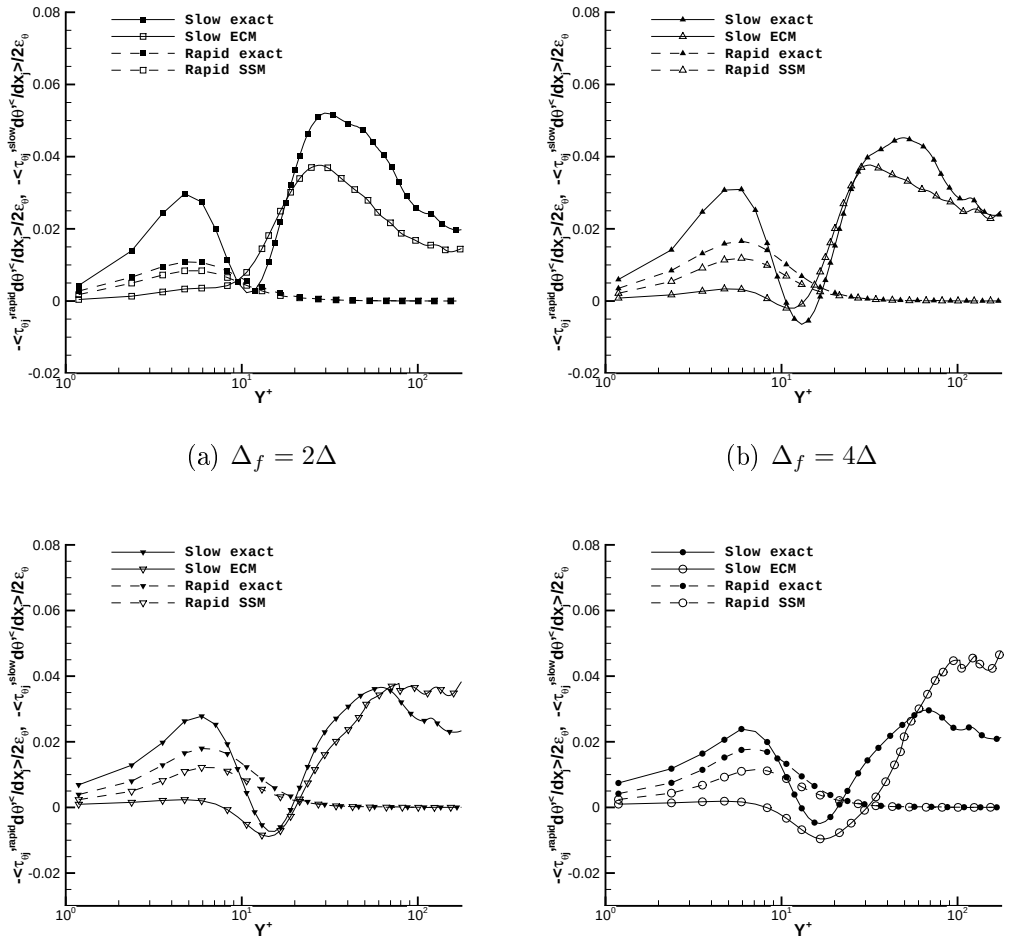

(a) $\Delta_f = 2\Delta$ (b) $\Delta_f = 4\Delta$

(c) $\Delta_f = 6\Delta$ (d) $\Delta_f = 8\Delta$

Figure 5.16: Comparison between exact and model values of scalar dissipation, with $\Delta_f/\Delta = 2, 4, 6$, and 8. Solid line and filled symbols: exact value of slow subgrid scalar dissipation. Solid line and hollow symbols: slow subgrid scalar dissipation by using the shear model. Dashed line and filled symbols: exact value of rapid subgrid scalar dissipation. Dashed line and hollow symbols: rapid subgrid scalar dissipation by using scale-similarity model on the velocity and scalar profiles.

inhomogeneous region, the SSM could be employed on the mean velocity and scalar, to simulate the "rapid" part of subgrid scalar flux and subgrid dissipation.

Chapter 6

Applying KEF on subgrid modeling of magnetohydrodynamic (MHD) turbulence

Many plasmas in turbulent motion observed in astrophysical systems, as well as nuclear fusion devices, and flows of conducting fluids, can be described within the framework of magnetohydrodynamics (MHD). Since MHD turbulence is a vast research area, we will not try to give an exhausting overview of literature on the subject. Rather will we refer to some textbooks on the subject for the reader interested in more details. Initially, interest in MHD focused on the dynamo problem, notably in Batchelor's early paper [135] (see also the book of Moffatt [136] on the subject). The book by Davidson gives a more recent survey of the subject, in particular focusing on the flows of liquid metals [137]. Biskamp's book focuses on turbulence in MHD flows [138].

The interaction of the velocity and magnetic field completely changes the dynamics. For example, the classical scaling theory by Kolmogorov [9] is changed due to the presence of magnetic (Alfvén) waves. A milestone in the fundamental scaling theory was the introduction of the Alfvén effect proposed independently by Iroshnikov [139] and Kraichnan [15]. This describes small-scale turbulent fluctuations as weakly interacting Alfvén waves propagating along the large-scale field. Because of the reduction of the corresponding spectral transfer the energy spectrum was predicted to be somewhat flatter, $k^{-3/2}$ instead of Kolmogorov spectrum $k^{-5/3}$. From the observation side, however, the energy spectrum of solar-wind turbulence was found to be clearly closer to a Kolmogorov law. The solution of the paradox lies in the intrinsic anisotropy of

MHD turbulence emphasized by Goldreich [140] and Vorobev [141], but this remains a subject of active research and debate.

In liquid metal flows most numerical investigations focus on the "Hartmann layer" [142] in channel turbulence. The magnetic field is fixed as a uniform vector $\vec{B}_0$, which is in the normal direction of the wall [143–145].

In astrophysics and geophysics the Reynolds number can become very large so that LES becomes a useful tool. There are already attempts to develop SGS models. In spectral space, models based on EDQNM theory are proposed [146, 147]. In physical space, the most common subgrid model is assuming eddy-viscosity in both velocity and magnetic fields, where the subgrid eddy viscosity and magnetic diffusivity are determined by using either Germano identity [148] or dimensional considerations [149]. However, no physical background exists in these physical-space models. In this chapter, we attempt to derive the homogeneous isotropic formula of KEF in Elsässer variables, and employ them to obtain new physical subgrid models for coupled MHD problems.

6.1 Governing equations of resolved kinetic energy

First of all, the dissipation terms in LES should be derived. The governing equations of filtered quantities in homogeneous isotropic MHD turbulence could be written as

$$\frac{\partial u_i^<}{\partial t} = -\frac{\partial u_i^< u_j^<}{\partial x_j} + \frac{\partial b_i^< b_j^<}{\partial x_j} + \nu \frac{\partial^2 u_i^<}{\partial x_j \partial x_j} - \frac{\partial p^<}{\partial x_i} - \frac{\partial \tau_{ij}^u}{\partial x_j}, \tag{6.1a}$$

$$\frac{\partial b_i^<}{\partial t} = -\frac{\partial b_i^< u_j^<}{\partial x_j} + \frac{\partial u_i^< b_j^<}{\partial x_j} + \eta \frac{\partial^2 b_i^<}{\partial x_j \partial x_j} - \frac{\partial \tau_{ij}^b}{\partial x_j}, \tag{6.1b}$$

in which $\vec{b}$ is the magnetic induction, η is the magnetic diffusivity. The subgrid stress tensors in velocity and magnetic fields read

$$\begin{aligned} \tau_{ij}^u &= \left((u_i u_j)^< - u_i^< u_j^<\right) - \left((b_i b_j)^< - b_i^< b_j^<\right) \\ \tau_{ij}^b &= \left((b_i u_j)^< - b_i^< u_j^<\right) - \left((u_i b_j)^< - u_i^< b_j^<\right). \end{aligned} \tag{6.2}$$

The resolved energies in these fields are then written as

$$\begin{aligned}\frac{1}{2}\frac{\partial u_i^{<^2}}{\partial t} =& -\frac{1}{2}\frac{\partial u_i^< u_i^< u_j^<}{\partial x_j} + \frac{\partial u_i^< b_i^< \partial b_j^<}{\partial x_j} - b_i^< b_j^< \frac{\partial u_i^<}{\partial x_j} \\ &+ \frac{\nu}{2}\frac{\partial^2 u_i^{<^2}}{\partial x_j \partial x_j} - \nu \frac{\partial u_i^<}{\partial x_j}\frac{\partial u_i^<}{\partial x_j} - \frac{\partial p^< u_i^<}{\partial x_i} - u_i^< \frac{\partial \tau_{ij}^u}{\partial x_j},\end{aligned} \tag{6.3a}$$

$$\begin{aligned}\frac{1}{2}\frac{\partial b_i^{<^2}}{\partial t} =& -\frac{1}{2}\frac{\partial b_i^< b_i^< u_j^<}{\partial x_j} + \frac{\partial u_i^< b_i^< \partial b_j^<}{\partial x_j} - u_i^< b_j^< \frac{\partial b_i^<}{\partial x_j} \\ &+ \frac{\eta}{2}\frac{\partial^2 b_i^{<^2}}{\partial x_j \partial x_j} - \eta \frac{\partial b_i^<}{\partial x_j}\frac{\partial u_i^<}{\partial x_j} - b_i^< \frac{\partial \tau_{ij}^b}{\partial x_j}.\end{aligned} \tag{6.3b}$$

Taking ensemble average, we obtain the governing equation of resolved mean kinetic energy:

$$\frac{\partial \langle u_i^{<^2}\rangle}{\partial t} = -2\left\langle b_i^< b_j^< \frac{\partial u_i^<}{\partial x_j}\right\rangle - 2\varepsilon^{u<} - 2\varepsilon_f^u, \tag{6.4a}$$

$$\frac{\partial \langle b_i^{<^2}\rangle}{\partial t} = -2\left\langle u_i^< b_j^< \frac{\partial b_i^<}{\partial x_j}\right\rangle - 2\varepsilon^{b<} - 2\varepsilon_f^b, \tag{6.4b}$$

in which

$$\begin{aligned}\varepsilon^{u<} =& \nu\left\langle \frac{\partial u_i^<}{\partial x_j}\frac{\partial u_i^<}{\partial x_j}\right\rangle, \quad \varepsilon_f^u = -\langle \tau_{ij}^u S_{ij}^<\rangle, \quad S_{ij}^< = \frac{1}{2}\left(\frac{\partial u_i^<}{\partial x_j} + \frac{\partial u_j^<}{\partial x_i}\right), \\ \varepsilon^{b<} =& \eta\left\langle \frac{\partial b_i^<}{\partial x_j}\frac{\partial b_i^<}{\partial x_j}\right\rangle, \quad \varepsilon_f^b = -\langle \tau_{ij}^b J_{ij}^<\rangle, \quad J_{ij}^< = \frac{1}{2}\left(\frac{\partial b_i^<}{\partial x_j} + \frac{\partial b_j^<}{\partial x_i}\right).\end{aligned} \tag{6.5}$$

Add (6.4a) to (6.4b), we eliminate the product terms. Thus we can write

$$\frac{\partial \langle u_i^{<^2}\rangle}{\partial t} + \frac{\partial \langle b_i^{<^2}\rangle}{\partial t} = -2\varepsilon^{u<} - 2\varepsilon_f^u - 2\varepsilon^{b<} - 2\varepsilon_f^b. \tag{6.6}$$

In high Reynolds number turbulence, the terms of resolved dissipation can be neglected. It leads to

$$\frac{\partial \langle u_i^{<^2}\rangle}{\partial t} + \frac{\partial \langle b_i^{<^2}\rangle}{\partial t} = -2\varepsilon_f^u - 2\varepsilon_f^b. \tag{6.7}$$

Similarly, from equation (6.1), we write the following equations:

$$b_i^< \frac{\partial u_i^<}{\partial t} = -b_i^< \frac{\partial u_i^< u_j^<}{\partial x_j} + b_i^< \frac{\partial b_i^< \partial b_j^<}{\partial x_j} + \nu b_i^< \frac{\partial^2 u_i^<}{\partial x_j \partial x_j} - \frac{\partial p^< b_i^<}{\partial x_i} - b_i^< \frac{\partial \tau_{ij}^u}{\partial x_j}, \tag{6.8a}$$

$$u_i^< \frac{\partial b_i^<}{\partial t} = -u_i^< \frac{\partial b_i^< u_j^<}{\partial x_j} + u_i^< \frac{\partial u_i^< \partial b_j^<}{\partial x_j} + \eta u_i^< \frac{\partial^2 b_i^<}{\partial x_j \partial x_j} - u_i^< \frac{\partial \tau_{ij}^b}{\partial x_j}. \tag{6.8b}$$

Add (6.8a) to (6.8b), we write the resolved cross energy as:

$$\begin{aligned}\frac{\partial u_i^< b_i^<}{\partial t} =& -\frac{\partial u_i^< b_i^< b_j^<}{\partial x_j} + \frac{1}{2}\frac{\partial b_i^{<^2} b_j^<}{\partial x_j} + \frac{1}{2}\frac{\partial u_i^{<^2} b_j^<}{\partial x_j} - \frac{\partial p^< b_i^<}{\partial x_i} \\ & -\frac{\partial}{\partial x_j}\left(b_i^< \tau_{ij}^u + u_i \tau_{ij}^b\right) + \nu\mathscr{U} + \eta\mathscr{B} + \tau_{ij}^u J_{ij}^< + \tau_{ij}^b S_{ij}^<,\end{aligned} \tag{6.9}$$

in which $\mathscr{U} = b_i^< \dfrac{\partial^2 u_i^<}{\partial x_j \partial x_j}, \mathscr{B} = u_i^< \dfrac{\partial^2 b_i^<}{\partial x_j \partial x_j}$. Taking ensemble average, equation (6.9) becomes

$$\frac{\partial \langle u_i^< b_i^< \rangle}{\partial t} = \nu\langle \mathscr{U} \rangle + \eta\langle \mathscr{B} \rangle + \langle \tau_{ij}^u J_{ij}^< \rangle + \langle \tau_{ij}^b S_{ij}^< \rangle. \tag{6.10}$$

Since

$$\frac{\partial^2 u_i^< b_i^<}{\partial x_j \partial x_j} = 2\frac{\partial u_i^<}{\partial x_j}\frac{\partial b_i^<}{\partial x_j} + u_i^< \frac{\partial^2 b_i^<}{\partial x_j \partial x_j} + b_i^< \frac{\partial^2 u_i^<}{\partial x_j \partial x_j}, \tag{6.11}$$

we obtain

$$\begin{aligned}\nu\langle \mathscr{U} \rangle =& -2\nu \left\langle \frac{\partial u_i^<}{\partial x_j}\frac{\partial b_i^<}{\partial x_j} \right\rangle - \nu\langle \mathscr{B} \rangle, \\ \eta\langle \mathscr{B} \rangle =& -2\eta \left\langle \frac{\partial u_i^<}{\partial x_j}\frac{\partial b_i^<}{\partial x_j} \right\rangle - \eta\langle \mathscr{U} \rangle.\end{aligned} \tag{6.12}$$

Therefore, equation (6.10) can also be written as

$$\frac{\partial \langle u_i^< b_i^< \rangle}{\partial t} = -2(\nu+\eta)\left\langle \frac{\partial u_i^<}{\partial x_j}\frac{\partial b_i^<}{\partial x_j} \right\rangle - \nu\langle \mathscr{B} \rangle - \eta\langle \mathscr{U} \rangle + \langle \tau_{ij}^u J_{ij}^< \rangle + \langle \tau_{ij}^b S_{ij}^< \rangle. \tag{6.13}$$

Add (6.10) to (6.13), we obtain

$$2\frac{\partial \langle u_i^< b_i^< \rangle}{\partial t} = -2(\nu+\eta)\left\langle \frac{\partial u_i^<}{\partial x_j}\frac{\partial b_i^<}{\partial x_j} \right\rangle + (\nu-\eta)\left(\langle \mathscr{U} \rangle - \langle \mathscr{B} \rangle\right) + 2\langle \tau_{ij}^u J_{ij}^< \rangle + 2\langle \tau_{ij}^b S_{ij}^< \rangle. \tag{6.14}$$

In high Reynolds number turbulence, the terms of resolved dissipation are then neglected. It leads to

$$2\frac{\partial \langle u_i^< b_i^< \rangle}{\partial t} = -2\varepsilon_f^c, \tag{6.15}$$

in which

$$\varepsilon_f^c = -\langle \tau_{ij}^u J_{ij}^< \rangle - \langle \tau_{ij}^b S_{ij}^< \rangle. \tag{6.16}$$

6.2 Kolmogorov equation of filtered quantities

For the Elsässer fields $\vec{z}^{\pm} = \vec{u} \pm \vec{b}$, there is

$$\frac{\partial z_i^{\pm}}{\partial t} + z_i^{\mp}\frac{\partial z_j^{\pm}}{\partial x_j} = -\frac{\partial P}{\partial x_i} + \nu_+\frac{\partial^2 z_i^{\pm}}{\partial x_j \partial x_j} + \nu_-\frac{\partial^2 z_i^{\mp}}{\partial x_j \partial x_j}, \tag{6.17}$$

where $P = p + b^2/2$ is the total pressure, $\nu_{\pm} = (\nu \pm \eta)/2$.

With a given filter, the governing equation of resolved scale fields reads

$$\frac{\partial z_i^{<\pm}}{\partial t} + z_j^{<\mp}\frac{\partial z_i^{<\pm}}{\partial x_j} = -\frac{\partial P^{<}}{\partial x_i} + \nu_+\frac{\partial^2 z_i^{<\pm}}{\partial x_j \partial x_j} + \nu_-\frac{\partial^2 z_i^{<\mp}}{\partial x_j \partial x_j} - \frac{\partial \tau_{ij}^{z\pm}}{\partial x_j}, \tag{6.18}$$

where the subgrid tensor $\tau_{ij}^{z\pm} = (z_i^{\pm} z_j^{\mp})^{<} - z_i^{<\pm} z_j^{<\mp}$. We note the following relations:

$$\tau_{ij}^{z\pm} = \tau_{ij}^{u} \pm \tau_{ij}^{b}. \tag{6.19}$$

Writing equation (6.18) in another point $\vec{x}^*$, and $\vec{\xi} = \vec{x}^* - \vec{x}, \delta\vec{z}^{\pm}(\vec{x}, \vec{\xi}) = \vec{z}^{\pm}(\vec{x}^*) - \vec{z}^{\pm}(\vec{x})$, following the similar process as in section 2.3, we obtain

$$\frac{\partial \delta z_i^{<\pm}}{\partial t} + \delta z_j^{<\mp}\frac{\partial \delta z_i^{<\pm}}{\partial \xi_j} = 2\nu_+\frac{\partial^2 \delta z_i^{<\pm}}{\partial \xi_j \partial \xi_j} + 2\nu_-\frac{\partial^2 \delta z_i^{<\mp}}{\partial \xi_j \partial \xi_j} - \left(\frac{\partial \tau_{ij}^{z\pm *}}{\partial x_j^*} - \frac{\partial \tau_{ij}^{z\pm}}{\partial x_j}\right). \tag{6.20}$$

In high Reynolds number turbulence, it is simplified as

$$\frac{\partial \delta z_i^{<\pm}}{\partial t} + \delta z_j^{<\mp}\frac{\partial \delta z_i^{<\pm}}{\partial \xi_j} = -\frac{\partial \tau_{ij}^{z\pm *}}{\partial x_j^*} + \frac{\partial \tau_{ij}^{z\pm}}{\partial x_j}. \tag{6.21}$$

Multiply equation (6.21) by $\delta z_i^{<\pm}$, it leads to

$$\frac{1}{2}\frac{\partial \delta z_i^{<\pm^2}}{\partial t} + \frac{1}{2}\frac{\partial \delta z_i^{<\pm^2} \delta z_j^{<\mp}}{\partial \xi_j} = -\delta z_i^{<\pm}\frac{\partial \tau_{ij}^{z\pm *}}{\partial x_j^*} + \delta z_i^{<\pm}\frac{\partial \tau_{ij}^{z\pm}}{\partial x_j}. \tag{6.22}$$

Taking ensemble average, in homogeneous isotropic turbulence the right hand side becomes

$$\begin{aligned}
&-\left\langle \delta z_i^{<\pm}\frac{\partial \tau_{ij}^{z\pm *}}{\partial x_j^*} - \delta z_i^{<\pm}\frac{\partial \tau_{ij}^{z\pm}}{\partial x_j}\right\rangle \\
=&-\left\langle \frac{\partial \tau_{ij}^{z\pm *}\delta z_i^{<\pm}}{\partial x_j^*} - \frac{\partial \tau_{ij}^{z\pm}\delta z_i^{<\pm}}{\partial x_j}\right\rangle + \left\langle \tau_{ij}^{z\pm *}\frac{\partial \delta z_i^{<\pm}}{\partial x_j^*} - \tau_{ij}^{z\pm}\frac{\partial \delta z_i^{<\pm}}{\partial x_j}\right\rangle \\
=&-\left\langle \frac{\partial\left(\tau_{ij}^{z\pm *} + \tau_{ij}^{z\pm}\right)\left(z_i^{<\pm *} - z_i^{<\pm}\right)}{\partial \xi_j}\right\rangle + \left\langle \tau_{ij}^{z\pm *}\frac{\partial z_i^{<\pm *}}{\partial x_j^*}\right\rangle + \left\langle \tau_{ij}^{z\pm}\frac{\partial z_i^{<\pm}}{\partial x_j}\right\rangle \\
=&\frac{\partial\left(T_{i,ij}^{z\pm} - T_{ij,i}^{z\pm}\right)}{\partial \xi_j} - 2\varepsilon_f^{z\pm},
\end{aligned} \tag{6.23}$$

in which

$$\begin{aligned} T_{i,ij}^{z\pm}(\xi) =& \langle z_i^{<\pm}(x_1)\tau_{ij}^{z\pm}(x_1+\xi)\rangle, \\ T_{ij,i}^{z\pm}(\xi) =& \langle z_i^{<\pm}(x_1+\xi)\tau_{ij}^{z\pm}(x_1)\rangle, \\ \varepsilon_f^{z\pm} =& -\left\langle \tau_{ij}^{z\pm}\frac{\partial z_i^{<\pm}}{\partial x_j}\right\rangle. \end{aligned} \tag{6.24}$$

In the left hand side of equation (6.22), the time-dependent term vanishes for small distance ξ. Taking ensemble average, the other term is written as

$$\frac{1}{2}\left\langle \frac{\partial \delta z_i^{<\pm^2}\delta z_j^{<\mp}}{\partial \xi_j}\right\rangle = \frac{1}{2}\frac{D_{iij}^{<\pm}}{\partial \xi_j}, \tag{6.25}$$

in which

$$D_{ii,j}^{<\pm} = \langle \delta z_i^{<\pm}\delta z_i^{<\pm}\delta z_j^{<\mp}\rangle. \tag{6.26}$$

In isotropic turbulence, $T_{i,ij}^{z\pm}(\xi) = -T_{ij,i}^{z\pm}(\xi)$, and the third-order tensors can be expressed by using their longitudinal components [51, 138, 150, 151], i.e.

$$\begin{aligned} T_{i,jk}^{z\pm}(\vec{\xi}) =& \frac{T_{l,ll}^{z\pm} - \xi\frac{\partial T_{l,ll}^{z\pm}}{\partial \xi}}{2\xi^3}\xi_i\xi_j\xi_k + \frac{2T_{l,ll}^{z\pm} + \xi\frac{\partial T_{l,ll}^{z\pm}}{\partial \xi}}{4\xi}(\xi_k\delta_{ij} + \xi_j\delta_{ik}) - \frac{T_{l,ll}^{z\pm}}{2\xi}\xi_i\delta_{jk}, \\ T_{n,nl}^{z\pm} =& \frac{1}{4\xi}\frac{\partial}{\partial \xi}\left(\xi^2 T_{l,ll}^{z\pm}\right), \\ D_{ii,k}^{<\pm}(\vec{\xi}) =& D_{ii,l}^{<\pm}\frac{\xi_k}{\xi}, \\ D_{ii,l}^{<\pm} =& \frac{2}{\xi^3}\frac{\partial}{\partial \xi}\left(\frac{\xi^4}{4}\left(D_{ll,l}^{<\pm} - 2C_{ll,l}^{<\pm}\right)\right), \\ C_{ll,l}^{<\pm} =& \langle z_l^{<\pm}(x_1)z_l^{<\pm}(x_1)z_l^{<\mp}(x_1+\xi)\rangle. \end{aligned} \tag{6.27}$$

From equation (6.22), (6.23), (6.25) and (6.27), we obtain

$$\frac{1}{2\xi^2}\frac{\partial}{\partial \xi}\left(\frac{2}{\xi}\frac{\partial}{\partial \xi}\left(\frac{\xi^4}{4}\left(D_{ll,l}^{<\pm} - 2C_{ll,l}^{<\pm}\right)\right)\right) = \frac{2}{\xi^2}\frac{\partial}{\partial \xi}\left(\frac{1}{2\xi}\frac{\partial}{\partial \xi}\left(\xi^4 T_{l,ll}^{z\pm}\right)\right) - 2\varepsilon_f^{z\pm}. \tag{6.28}$$

Integral both sides from 1 to ξ twice, finally we obtain the KEF formulation

$$-\frac{8}{15}\varepsilon_f^{z\pm}\xi = D_{ll,l}^{<\pm} - 2C_{ll,l}^{<\pm} - 4T_{l,ll}^{z\pm}. \tag{6.29}$$

This scaling law is different from the result in a homogeneous isotropic velocity field. Particularly, in the hydrodynamic limit $z^{<\pm} = u^{<}$, we obtain the $-4/5$ law as for the velocity field.

When $\xi \gg \Delta$, as analyzed in section 2.6 and 3.2, the term $T^{z\pm}_{l,ll}$ in equation (6.29) vanishes. Thus the simplified KEF reads

$$-\frac{8}{15}\varepsilon_f^{z\pm}\xi = D^{<\pm}_{ll,l} - 2C^{<\pm}_{ll,l}. \tag{6.30}$$

Noting that $D^{<\pm}_{ll,l} - 2C^{<\pm}_{ll,l} = 4\langle z_l^{<\pm}(x_1) z_l^{<\mp}(x_1) z_l^{<\pm}(x_1+\xi)\rangle$. We write equation (6.30) for $\vec{z}^{<+}$ and $\vec{z}^{<-}$, respectively. Returning to the basic fields, we obtain the following equations:

$$\begin{aligned} -\frac{4}{5}\varepsilon_f^T r =& \langle \delta u_l^{<3}\rangle - 6\langle b_l^{<2}(x_1) u_l^{<}(x_1+\xi)\rangle, \\ -\frac{4}{5}\varepsilon_f^C r =& -\langle \delta b_l^{<3}\rangle + 6\langle u_l^{<2}(x_1) b_l^{<}(x_1+\xi)\rangle, \end{aligned} \tag{6.31}$$

in which

$$\begin{aligned} 2\varepsilon_f^T =& \varepsilon_f^{z+} + \varepsilon_f^{z-}, \\ 2\varepsilon_f^C =& \varepsilon_f^{z+} - \varepsilon_f^{z-}. \end{aligned} \tag{6.32}$$

Comparing with the energy analysis in section 6.1, there are the relations

$$\begin{aligned} \varepsilon_f^T =& \varepsilon_f^u + \varepsilon_f^b, \\ \varepsilon_f^C =& \varepsilon_f^c. \end{aligned} \tag{6.33}$$

6.3 MHD subgrid models in velocity and magnetic fields

The eddy viscosity assumption is applied. Following Agullo [148], the subgrid tensors are modeled by assuming a linear relation:

$$\begin{aligned} \tau_{ij}^u =& -2\nu_t S_{ij}^{<}, \qquad S_{ij}^{<} = \frac{1}{2}\left(\frac{\partial u_i^{<}}{\partial x_j} + \frac{\partial u_j^{<}}{\partial x_i}\right), \\ \tau_{ij}^b =& -2\eta_t J_{ij}^{<}, \qquad J_{ij}^{<} = \frac{1}{2}\left(\frac{\partial b_i^{<}}{\partial x_j} + \frac{\partial b_j^{<}}{\partial x_i}\right). \end{aligned} \tag{6.34}$$

From equations (6.5), (6.16) and (6.33), we obtain

$$\varepsilon_f^T = 2\nu_t\langle S_{ij}^< S_{ij}^<\rangle + 2\eta_t\langle J_{ij}^< J_{ij}^<\rangle, \tag{6.35}$$

$$\varepsilon_f^C = 2(\nu_t+\eta_t)\langle S_{ij}^< J_{ij}^<\rangle. \tag{6.36}$$

From equation (6.31), (6.35) and (6.36), the model coefficient can be described as:

$$\begin{aligned}\nu_t =& \frac{5}{8\xi}\frac{A^T\langle S_{ij}^< J_{ij}^<\rangle - A^C\langle J_{ij}^< J_{ij}^<\rangle}{\langle S_{ij}^< J_{ij}^<\rangle\left(\langle J_{ij}^< J_{ij}^<\rangle - \langle S_{ij}^< S_{ij}^<\rangle\right)},\\ \eta_t =& \frac{5}{8\xi}\frac{A^T\langle S_{ij}^< J_{ij}^<\rangle - A^C\langle S_{ij}^< S_{ij}^<\rangle}{\langle S_{ij}^< J_{ij}^<\rangle\left(\langle S_{ij}^< S_{ij}^<\rangle - \langle J_{ij}^< J_{ij}^<\rangle\right)},\end{aligned} \tag{6.37}$$

in which

$$\begin{aligned}A^T =& \langle \delta u_l^{<^3}(\vec{\xi})\rangle - 6\langle b_l^{<^2}(\vec{x})u_l^<(\vec{x}+\vec{\xi})\rangle,\\ A^C =& -\langle \delta b_l^{<^3}(\vec{\xi})\rangle + 6\langle u_l^{<^2}(\vec{x})b_l^<(\vec{x}+\vec{\xi})\rangle.\end{aligned} \tag{6.38}$$

However, because we can have $E^C \approx 0$, this dynamic method might be not stable in numerical calculation. Therefore, the eddy viscosity is calculated by using CZZS model, assuming that the magnetic field doesn't have affect with the subgrid velocity stress directly. The cross equation (6.36) is ignored. Finally we obtain

$$\begin{aligned}\nu_t =& \frac{-5}{8\xi}\frac{\langle \delta u_l^{<^3}\rangle}{\langle S_{ij}^< S_{ij}^<\rangle},\\ \eta_t =& \frac{5}{8\xi}\frac{6\langle b_l^{<^2}(\vec{x})u_l^<(\vec{x}+\vec{\xi})\rangle}{\langle J_{ij}^< J_{ij}^<\rangle}.\end{aligned} \tag{6.39}$$

A Posteriori test at 64^3 meshes is done in homogeneous isotropic decaying turbulence, by employing model (6.39). The initial velocity and magnetic fields are generated by employing Rogallo's method [54], respectively. It is known since the work by Ting *et al.* [152], that different initial conditions can lead to completely different flows depending on the initial values of $\vec{u}\cdot\vec{b}$, u^2 and b^2. We consider one particular case in which the initial energy spectra are the same, i.e. $E_K = E_M$, and E^C is initially small. The temporal evolution and energy spectra at $t = 16$ are shown in Fig. 6.1. The magnetic energy increases a little before decaying, corresponding to the deformation of the magnetic field lines before the Lorentz force starts to act. The $-5/3$ energy spectrum is approximately obtained for inter in both velocity and magnetic fields. This is only a very simply example to verify the SGS model (6.39).

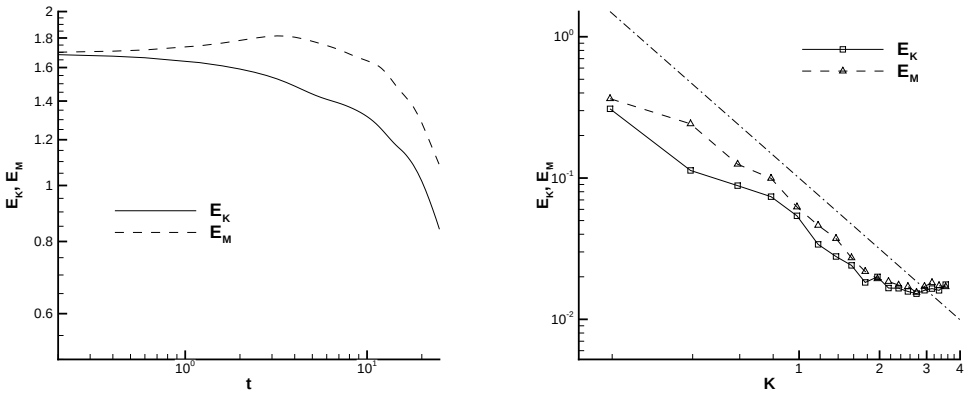

Figure 6.1: Kinetic and magnetic energy in decaying turbulence. Left: temporal evolution. Right: energy spectra.

6.3.1 Discussion in the Elsässer fields

To understand the unstability of (6.37), we discuss the model now expressed in Elsässer variables. In the eddy viscosity assumptions (6.34), the velocity subgrid stress tensor is also affected by magnetic field from definition, but it vanishes in the eddy viscosity assumption. In order to explain it, in this section we directly employ KEF in Elsässer fields. We can also obtain the corresponding subgrid models.

Considering that the subgrid stress tensor take the similar parts as the molecular dissipation, from equation (6.18) we can easily write the eddy viscosity assumption as

$$\tau_{ij}^{z\pm} = -2\nu_t^+ S_{ij}^{<z\pm} - 2\nu_t^- S_{ij}^{<z\mp}, \tag{6.40}$$

in which

$$S_{ij}^{<z\pm} = \frac{1}{2}\left(\frac{\partial z_i^{<\pm}}{\partial x_j} + \frac{\partial z_j^{<\pm}}{\partial x_i}\right) = S_{ij}^{<} \pm J_{ij}^{<}. \tag{6.41}$$

From equation (6.24) and this new eddy viscosity assumption, the subgrid dissipation in Elsässer fields yields

$$\varepsilon_f^{z\pm} = \left\langle \tau_{ij}^{z\pm} S_{ij}^{<z\pm} \right\rangle = 2\nu_t^+ \left\langle S_{ij}^{<z\pm} S_{ij}^{<z\pm} \right\rangle + 2\nu_t^- \left\langle S_{ij}^{<z+} S_{ij}^{<z-} \right\rangle. \tag{6.42}$$

Then from equation (6.30), we obtain

$$-\frac{16}{15}\left(\nu_t^+ \left\langle S_{ij}^{<z\pm} S_{ij}^{<z\pm} \right\rangle + \nu_t^- \left\langle S_{ij}^{<z+} S_{ij}^{<z-} \right\rangle\right)\xi = D_{ll,l}^{<\pm} - 2C_{ll,l}^{<\pm}. \tag{6.43}$$

The eddy viscosities are solved as

$$\begin{aligned}
\nu_t^+ =& \frac{-15}{16\xi}\frac{D_{ll,l}^{<+} - D_{ll,l}^{<-} - 2C_{ll,l}^{<+} + 2C_{ll,l}^{<-}}{\left\langle S_{ij}^{<z+} S_{ij}^{<z+}\right\rangle - \left\langle S_{ij}^{<z-} S_{ij}^{<z-}\right\rangle}, \\
\nu_t^- =& \frac{-15}{16\xi}\frac{\left\langle S_{ij}^{<z+} S_{ij}^{<z+}\right\rangle \left(D_{ll,l}^{<-} - 2C_{ll,l}^{<-}\right) - \left\langle S_{ij}^{<z-} S_{ij}^{<z-}\right\rangle \left(D_{ll,l}^{<+} - 2C_{ll,l}^{<+}\right)}{\left\langle S_{ij}^{<z+} S_{ij}^{<z-}\right\rangle \left(\left\langle S_{ij}^{<z+} S_{ij}^{<z+}\right\rangle - \left\langle S_{ij}^{<z-} S_{ij}^{<z-}\right\rangle\right)}.
\end{aligned} \tag{6.44}$$

Although there is a singular point when the magnetic field vanishes and $z^+ = z^-$, the whole eddy viscosity tends to a limiting value that

$$\nu_t^+ + \nu_t^- \to \frac{-15}{16\xi}\frac{D_{ll,l}^{<} - 2C_{ll,l}^{<}}{\left\langle S_{ij}^{<z} S_{ij}^{<z}\right\rangle}, \tag{6.45}$$

in which $D_{ll,l}^{<} = \frac{1}{2}(D_{ll,l}^{<+} + D_{ll,l}^{<-}), C_{ll,l}^{<} = \frac{1}{2}(C_{ll,l}^{<+} + C_{ll,l}^{<-}), S_{ij}^{<z} = \frac{1}{2}(S_{ij}^{<z+} + S_{ij}^{<z-})$. Alternatively if $\vec{u}\cdot\vec{b} = 0$, we can also obtain $S_{ij}^{<z+} S_{ij}^{<z+} = S_{ij}^{<z-} S_{ij}^{<z-}$ and the same result.

Therefore, if we assume the cross energy is zero, i.e. $\vec{u}\cdot\vec{b} = 0$, and assume $\nu_t^- = 0$, we can obtain the following model

$$\nu_t^+ = \frac{-15}{16\xi}\frac{D_{ll,l}^{<} - 2C_{ll,l}^{<}}{\left\langle S_{ij}^{<z} S_{ij}^{<z}\right\rangle}. \tag{6.46}$$

This model formulation actually implies the eddy viscosity assumption and $\nu_t = \eta_t$.

These results, in fact, are the same as the models expressed in velocity and magnetic fields, which are discussed in the previous section. Considering the eddy viscosity assumptions (6.34), equations (6.32), (6.35) and (6.36) lead to

$$\begin{aligned}
\varepsilon_f^{z+} + \varepsilon_f^{z-} =& 2\varepsilon_f^T = 4\nu_t \langle S_{ij}^{<} S_{ij}^{<}\rangle + 4\eta_t \langle J_{ij}^{<} J_{ij}^{<}\rangle, \\
\varepsilon_f^{z+} - \varepsilon_f^{z-} =& 2\varepsilon_f^C = 4(\nu_t + \eta_t)\langle S_{ij}^{<} J_{ij}^{<}\rangle.
\end{aligned} \tag{6.47}$$

And we can also write equation (6.42) in the following formulations:

$$\begin{aligned}
\varepsilon_f^{z+} + \varepsilon_f^{z-} =& 2\nu_t^+(\langle S_{ij}^{<z+} S_{ij}^{<z+}\rangle + \langle S_{ij}^{<z-} S_{ij}^{<z-}\rangle) + 4\nu_t^- \langle S_{ij}^{<z+} S_{ij}^{<z-}\rangle \\
=& 4(\nu_t^+ + \nu_t^-)\langle S_{ij}^{<} S_{ij}^{<}\rangle + 4(\nu_t^+ - \nu_t^-)\langle J_{ij}^{<} J_{ij}^{<}\rangle, \\
\varepsilon_f^{z+} - \varepsilon_f^{z-} =& 2\nu_t^+(\langle S_{ij}^{<z+} S_{ij}^{<z+}\rangle - \langle S_{ij}^{<z-} S_{ij}^{<z-}\rangle) \\
=& 8\nu_t^+ \langle S_{ij}^{<} J_{ij}^{<}\rangle.
\end{aligned} \tag{6.48}$$

Comparing (6.48) with (6.47), the following relations are obvious:

$$\begin{aligned} \nu_t =& \nu_t^+ + \nu_t^-, \\ \eta_t =& \nu_t^+ - \nu_t^-. \end{aligned} \tag{6.49}$$

Therefore, the models in this section are in fact the same as discussed before. Although two unknown coefficients are solved by two equations (ε_f^T and ε_f^C), the value of ε_f^C can be relatively small, and the numerical solution may be unstable.

6.4 Perspectives

In this chapter we extended the KEF formula to homogeneous isotropic MHD turbulence, and obtained the corresponding SGS models in physical space. The models directly based on the KEF equations, i.e. Eqs. (6.37) and (6.44), are in fact the same as can be seeen by using the relations (6.49). Both of them are not numerical stable if $E^C \approx 0$, i.e. $\vec{u}\cdot\vec{b} \approx 0$. It was shown that, to get a properly working SGS models for MHD turbulence, more physical constraints are needed than the KEF equation only, for instance, in Eq. (6.39) we assume that the magnetic field doesn't have affect with the subgrid velocity stress directly. Better ideas may be employing the scaling law of structure functions, and this topic will be further investigated in the future.

Chapter 7

Conclusion

In subgrid modeling, not only mathematical approach, but also physical properties should be implied. Comparing with plenty of researches in spectral space, there are few works based on energy transfer properties in physical space, in subgrid modeling. This thesis mainly aims on employing Kolmogorov equation of filtered quantities (KEF) in subgrid modeling. It is considered as a general method for any subgrid model assumption. The following results are obtained:

1. Different formulations of KEF are derived, including the forms in velocity field (homogeneous isotropic turbulence, inhomogeneous anisotropic turbulence, homogeneous shear turbulence, homogeneous rotating turbulence), in scalar turbulence and in magnetohydrodynamic turbulence.

2. The anisotropic effect of mean shear in physical space is analyzed. The local isotropic assumption of structure function is queried. Instead, the two-point skewness is proposed to represent the isotropy in small scale.

3. The structure function of filtered velocity is analyzed in physical and spectral spaces, respectively. Results show that in order to satisfy the classical scaling law, the two-point distance of velocity increment must be much larger than the filter size. Otherwise, the classical scaling law can not be directly applied in subgrid modeling.

4. The isotropic formulations of eddy-viscosity models are analyzed. The CZZS model could be simplified in different ways, which yields the one-scale and multi-scale models. Particularly, the skewness-based isotropic formulation is

proposed. Besides, by employing KEF, we could also determine the coefficient of Smagorinsky model dynamically. This dynamic procedure is much less cost then Germano procedure and has clear physical background.

5. The anisotropic formulations of eddy-viscosity models are derived in homogeneous shear turbulence and homogeneous rotating turbulence. *A Posteriori* tests are made to evaluate this model. The most important advantage is that the mean motion is explicitly contained in the formulation of subgrid eddy viscous.

6. With the velocity increment assumption, the improved increment model (IVI) is proposed. In real flow, when scales are not well separated, the model coefficient has a dynamic formulation; in ideal high Reynolds number turbulence, we could obtain a constant coefficient, which is extremely simple and low cost. The IVI model is verified in *A Priori* and *A Posteriori* tests. Wall behavior is well satisfied, and the energy backscatter could be simulated properly.

7. For anisotropic passive scalar field, the transfer processes of scalar energy and scalar flux are mainly investigated. We split the subgrid scalar flux into rapid and slow parts, and do *A Priori* tests on them in a channel Couette flow. The new anisotropic eddy-diffusivity model based on KEF is then verified for its properties of simulating subgrid scalar dissipation. The energy scalar backscatter is well represented. The mean velocity and scalar profiles could effect the subgrid scalar flux explicitly. In addition, during inhomogeneous region, the scale-similarity model could be employed on the mean velocity and scalar, to simulate the "rapid" part of subgrid scalar flux and subgrid dissipation.

8. In magnetohydrodynamic turbulence, the formulation of KEF is derived in the Elsässer fields. Corresponding subgrid models are then founded. However, the present models are not numerical stable when the correlation between velocity and magnitude fields is small. This work is expected to be further investigated.

Résumé

La simulation numérique des grandes échelles (LES) est actuellement un outil prometteur pour la prédiction des écoulements turbulents industriels. Les grandes et petites échelles sont isolées par une opération de filtrage, qui peut être appliquée dans l'espace soit physique soit spectral. Le champ de vitesse filtrée représente le mouvement des grandes échelles et les équations de Navier-Stokes filtrées contiennent le tenseur de sous-maille (SGS) qui résulte des mouvements des petites échelles. [1,2] L'esprit de la LES est de modéliser les petites échelles en utilisant les quantités résolues des grandes échelles, à travers un modèle de sous-maille (SGS). Il y a deux étapes dans chaque modèle de sous-maille :

1. Chaque modèle de sous-maille doit se baser sur une certaine hypothèse de mouvement de sous-maille, c'est-à-dire assumer une formulation pour les quantités de sous-maille (en particulier, le tenseur de sous-maille). Cependant, il y a toujours des facteurs indéterminés dans cette hypothèse.
2. Un modèle de sous-maille complet doit faire appel à certaines méthodes afin de déterminer les facteurs inconnus mentionnés ci-dessus.

Plusieurs hypothèses de tenseur de sous-maille ont été introduites, telles que l'hypothèse de viscosité turbulente [3], la formulation de similitude d'échelle [4], l'hypothèse de gradient de diffusion [5] et la formulation par incréments de vitesse [6]. Pour évaluer les performances de ces propositions, il faudrait définir des critères d'évaluation. Il est impossible de simuler le mouvement "correct" de sous-maille pour chaque point discret, mais au moins deux comportements physiques devraient être impliqués

dans une hypothèse de sous-maille : d'abord, l'hypothèse devrait produire une dissipation appropriée, qui pourrait représenter le comportement dissipatif fort des petites échelles; deuxièmement, l'hypothèse devrait représenter un certain mécanisme physique, à savoir l'interaction entre les échelles résolues et de sous-maille. Des premières hypothèses de sous-maille n'ont pas prêté attention à ces conditions. Par exemple, le modèle de similitude d'échelle [4] approche bien certaines caractéristique des tenseur de sous-maille, mais il ne produit pas assez de dissipation. Puisque la dissipation de sous-maille est très importante dans le calcul numérique, la plupart des travaux sur les modélisations de sous-maille se focalisent sur la dissipation. Cependant, un modèle dissipatif pur, comme le modèle implicite (MILES) [10], ne peut pas représenter le mécanisme physique correct.

Dans ces hypothèses, un type de relation entre les échelles de sous-maille et les mouvements résolus est supposé, mais le mouvement de sous-maille ne peut pas être complètement fixé. Il reste des coefficients à déterminer. Par exemple, la viscosité turbulente peut être calculée par le modèle de Smagorinsky. Dans l'hypothèse d'incréments de vitesse, un coefficient doit aussi être calculé. Essentiellement cela signifie qu'une fois les hypothèses formulées, une autre certaine méthode doit être appliquée pour obtenir une fermeture des équations. Dans cette thèse, nous ne sommes pas intéressés aux différentes hypothèses, mais plutôt aux méthodes de fermeture qui permettent de préciser les coefficients, une fois les hypothèses formulées.

De cette façon, il n'y a aucun "pur" modèle de sous-maille. Pour chaque modèle, on doit déterminer les facteurs indéterminés, tels que la viscosité turbulente. Par exemple, le coefficient du modèle de Smagorinsky pourrait être évalué en utilisant la théorie EDQNM et pourrait aussi être déterminé dynamiquement selon la procédure de Germano. En outre, les différents détails d'une méthode pourraient donner des résultats différents, par exemple beaucoup de travaux fixent la viscosité turbulente par la théorie de EDQNM, mais obtiennent des formulations de modèles différentes, puisque les détails de ces dérivations ne sont pas les mêmes. En fait,

nous préférons considérer ces "modèles" comme "les méthodes différentes de déterminer les facteurs indéterminés de l'hypothèse de viscosité turbulente". Dans cette thèse, nous nous concentrons sur "les méthodes", mais pas sur "les suppositions".

En général, il y a beaucoup de méthodes mathématiques employées dans la modélisation de sous-maille, qui réalisent la fermeture des équations mathématiques. De plus, il y a la théorie dans l'espace spectral présentée par Kraichnan [15,16], qui est employée pour donner beaucoup de modèles SGS spectraux. Dans l'espace physique, la seule théorie est présentée par Kolmogorov [9], dont les différentes échelles sont séparées. Il décrit aussi une loi physique qui devrait être satisfaite dans les simulations des grandes échelles [17]. Cependant, peu de travaux ont été réalisés dans la modélisation de sous-maille. Dans cette thèse, nous employons l'équation de Kolmogorov de quantités filtrées (KEF) dans la modélisation de sous-maille. C'est une méthode pour déterminer les facteurs inconnus de n'importe quelle hypothèse de sous-maille.

Dans le chapitre 2, les formulations diverses de KEF dans des champs de vitesse sont présentées. La formulation en turbulence isotrope homogène, proposés par Meneveau [17] et Cui [38], peut être écrite comme suit:

$$-\frac{4}{5}\epsilon_f\xi - \frac{4}{5}\epsilon^<\xi = D^<_{lll} - 6T_{l,ll} - 6\nu\frac{\partial D^<_{ll}}{\partial\xi}. \tag{7.1}$$

Le budget de l'énergie correspondante dans une turbulence forcée est indiqué dans la Fig. (7.1). Le terme de sous-maille de transfert $T_{l,ll}$ est du même ordre de grandeur que la fonction de structure de la troisième ordre $D^<_{lll}$ lorsque la distance est égale à la taille du filtre, c'est-à-dire $\xi = \Delta$, et tend vers zéro lorsque ξ est grande. Le terme de viscosité est en effet seulement important à très petite distance et peut être négligé quand ξ est du même ordre de grandeur que Δ.

La formulation en turbulence anisotrope inhomogène contient des termes rapides et lents, que l'on pourrait considérer comme une forme complète

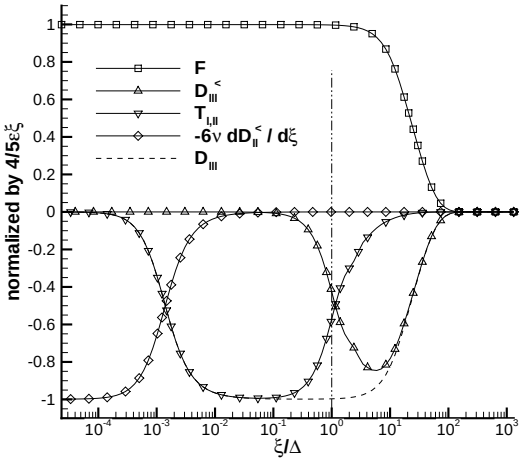

Figure 7.1: Le budget d'énergie en deux points normalisé dans la turbulence forcée avec filtre ($<$) et sans filtre (sans $<$). Calcul EDQNM. La ligne verticale indique la taille de filtre.

de KEF, mais trop complexe pour être appliquée dans la modélisation de sous-maille:

$$\frac{1}{2}\frac{\partial D_{ii}^{<}}{\partial t}+\frac{1}{2}\frac{\partial D_{iij}^{<}}{\partial \xi_j}+\frac{1}{2}\delta\langle u_j\rangle^{<}\frac{\partial D_{ii}^{<}}{\partial \xi_j}+\frac{\partial \delta\langle u_i\rangle^{<}}{\partial \xi_j}D_{ij}^{<}$$

$$=H^{rapid}(\vec{x})+H^{slow}(\vec{x})+\nu\frac{\partial D_{ii}^{<}}{\partial \xi_j\partial \xi_j}-2\varepsilon^{<}$$

$$+\left\langle \delta u_i'^{<}\left(\frac{\partial \tau_{ij}^{slow<}}{\partial x_j}-\frac{\partial \tau_{ij}^{slow<*}}{\partial x_j^*}\right)\right\rangle+\left\langle \delta u_i'^{<}\left(\frac{\partial \tau_{ij}^{rapid<}}{\partial x_j}-\frac{\partial \tau_{ij}^{rapid<*}}{\partial x_j^*}\right)\right\rangle \tag{7.2}$$

La turbulence homogène cisaillée est particulièrement analysée. En comparant avec l'analyse classique pour la fonction de corrélation dans l'espace spectral, nous examinons l'effet du cisaillement dans l'espace physique. Dans la formulation de KEF, les propriétés anisotropes des fonctions de structures entre des directions différentes sont soulignées. Les tests a priori sont réalisés en turbulence de canal, montrant les différences au niveau des fonctions de structures et des valeurs de la di-symétrie (*skewness*).

Parce que les fonctions de structures filtrées existent dans KEF, nous devons examiner la loi d'échelle correspondant. Nous pouvons obtenir la

conclusion que la loi d'échelle classique pour des fonctions de structures non-filtrées peut seulement être utilisée quand la distance est beaucoup plus grande que la taille de filtre dans KEF, c'est-à-dire $\xi \gg \Delta$.

Dans le chapitre 3, les applications de KEF sur des modèles de viscosité sont discutées. Un problème du modèle CZZS original, tient aux hypothèses différentes à des échelles différentes. L'amélioration contient les modèles à une échelle, les modèles multi-échelles dans la sous-gamme inertielle et le modèle de multi-échelle avec les échelles séparées. Les modèles à une échelle ont une formulation tout à fait simple. Nous pouvons aussi présenter le *skewness* en deux points pour améliorer le modèle. On propose aussi le modèle multi-échelle avec les échelles séparées. Il utilise une petite échelle pour l'expansion de Taylor et une grande échelle pour appliquer la loi d'échelle.

L'idée de KEF peut aussi être appliquée dans la détermination du coefficient du modèle Smagorinsky. Dans la sous-gamme inertielle, les valeurs des résultats sont semblables aux valeurs classiques. Tant que nous choisissons la taille de l'incrément appropriée, cette méthode pourrait être appliquée dans LES.

Un autre travail sur le champ de vitesse est le modèle avec viscosité anisotrope, qui s'appuie sur KEF anisotrope inhomogène. La méthode de la moyenne sphérique est employée, et la viscosité turbulente peut être représentée par:

$$\nu_t = \frac{(D^<_{iij} n_j)^S + (\delta U D^<_{ii} n_1)^S + 2V/S \langle \delta u_i'^< \delta s_i^< \rangle^V}{2\left(\frac{\partial D^<_{ii}}{\partial \xi_j} n_j\right)^S - 4V/S \left\langle \frac{\partial u_i'^<}{\partial x_j} \frac{\partial u_i'^<}{\partial x_j} \right\rangle^V}. \tag{7.3}$$

L'avantage principal de ce modèle est que la viscosité turbulente peut être écrite comme une fonction de la moyenne du cisaillement, qui devrait être très important dans la turbulence cisaillée. Ce modèle est vérifié dans la turbulence de rotation et la turbulence de paroi respectivement.

Dans le chapitre 4, on propose un modèle amélioré d'incréments de vitesse (IVI). Une hypothèse très simple a été présentée par Brun:

$$\tau_{ij}^{<} = fQ_{ij}, \qquad Q_{ij} = \delta u_i^{<} \delta u_j^{<}, \tag{7.4}$$

où Q_{ij} est l'incrément de vitesse. C_f est le coefficient dynamique, on peut appliquer KEF pour le déterminer. Dans la turbulence à grand nombre de Reynolds et quand les échelles (la taille de filtre, la taille de l'incrément de vitesse et la distance de deux points dans KEF) sont bien séparées, nous pouvons obtenir la valeur constante :

$$C_f = 1/2. \tag{7.5}$$

Dans la turbulence à nombre de Reynolds modéré, il n'est généralement pas possible de séparer les échelles, et l'on peut obtenir une formule dynamique où les échelles sont fixés de la même façon:

$$C_f = \frac{2D_{lll}^{<}(\xi)}{4\xi \left.\dfrac{\partial D_{lll}^{<}(r)}{\partial r}\right|_{r=\xi} - 4D_{lll}^{<}(\xi) - D_{lll}^{<}(2\xi)}. \tag{7.6}$$

Ces modèles sont vérifiés en turbulence isotrope homogène et dans le cas du canal plan. Les résultats montrent un bon accord avec les résultats de DNS et les expériences. En particulier, la formulation du coefficient constant est tout à fait simple et bon marché. Ce modèle peut être utilisé dans les projets d'ingénierie.

Dans le chapitre 5, nous nous concentrons sur l'étude du mécanisme physique entre des parties moyennées et fluctuantes, dans la turbulence scalaire anisotrope inhomogène. L'équation d'énergie scalaire et l'équation de flux scalaire sont décomposées en parties rapides et lentes. Le phénomène de *backscatter* est observé dans la région $10 < Y^+ < 20$, qui est semblable aux résultats de Hartel *et al.* [26] dans le champ de vitesse. Le transport de flux scalaire est découpé en quatre parties. Dans la région homogène du canal, la partie de GVSS (la vitesse résolue et le scalaire de sous-maille) est beaucoup plus forte que la partie de SVGS (la vitesse de sous-maille et

le scalaire résolu), ce qui est en d'accord avec les résultats d'Yeung [132] et Fang [133].

Il est intéressant de voir si les modèles existants peuvent représenter l'influence de la vitesse et du scalaire moyens. Nous testons la partie lente en utilisant ECM (la modèlisation Cui étendue), dans laquelle on montre explicitement la vitesse et la scalaire moyenne; la partie rapide est dénotée en utilisant SSM (le modèle de similitude d'échelle), à la suite de Shao [48]. Il est trouvé que ECM peut bien représenter la dissipation scalaire lente, de sous-maille, et ceci même sur le backscatter dans $Y^+ \simeq 15$. Le SSM représente bien la partie rapide. Ainsi, on pourrait considérer un modèle mélangeant des parties lentes et rapides dans des applications de LES. Un problème restant est que la dissipation présente près de la paroi, qui existe dans les deux champs scalaires et de la vitesse, ne peut être représentée par aucun modèle de sous-maille. Ce problème devrait être examiné à l'avenir.

Dans le chapitre 6, la formulation de KEF est dérivée dans les champs de Elsässer, pour la turbulence MHD en présence de fluctuation de champ magnétique. Des modèles de sous-maille correspondants sont alors formulés. Cependant, les modèles présents ne sont pas numériquement stables quand la corrélation entre des champs de la vitesse et magnétique est petite. Ce sujet devrait être davantage étudié.

Appendix A

The derivations of the Karman-Howarth equation, Kolmogorov equation and Yaglom equation of filtered velocity and scalar, in homogeneous isotropic turbulence and scalar turbulence

This process of derivation was introduced by Cui *et al.* [38]. We consider the tensors in incompressible homogeneous isotropic turbulence. The second- and third-order correlation functions of resolved velocity fluctuations could be written as

$$\begin{aligned} R_{ij}^{<}(\vec{\xi}) =& \langle u_i^{<}(\vec{x}) u_j^{<}(\vec{x}+\vec{\xi}) \rangle, \\ R_{ij,k}^{<}(\vec{\xi}) =& \langle u_i^{<}(\vec{x}) u_j^{<}(\vec{x}) u_k^{<}(\vec{x}+\vec{\xi}) \rangle. \end{aligned} \tag{A.1}$$

In the following content of this appendix, we use the signals R_{ij} and $R_{ij,k}$ instead of $R_{ij}^{<}$ and $R_{ij,k}^{<}$. They also represent the resolved parts. Another third-order tensor is the correlation between the filtered velocity and subgrid stress:

$$T_{i,jk}(\vec{\xi}) = \langle u_i^{<}(\vec{x}) \tau_{jk}^{<}(\vec{x}+\vec{\xi}) \rangle. \tag{A.2}$$

As suggested by Lumley [128], in homogeneous isotropic turbulence the second-order tensor has only 2 independent components:

$$R_{ij}(\vec{\xi}) = f_1(\xi)\xi_i\xi_j + f_2(\xi)\delta_{ij}, \tag{A.3}$$

and the third-order tensor has 4 independent components:

$$\begin{aligned} R_{ij,k}(\vec{\xi}) =& g_1(\xi)\xi_i\xi_j\xi_k + g_2(\xi)\xi_i\delta_{jk} + g_3(\xi)\xi_j\delta_{ik} + g_4(\xi)\xi_k\delta_{ij}, \\ T_{i,jk}(\vec{\xi}) =& h_1(\xi)\xi_i\xi_j\xi_k + h_2(\xi)\xi_i\delta_{jk} + h_3(\xi)\xi_j\delta_{ik} + h_4(\xi)\xi_k\delta_{ij}. \end{aligned} \tag{A.4}$$

Because of symmetry $R_{ij,k}(\vec{\xi}) = R_{ji,k}(\vec{\xi}), T_{i,jk}(\vec{\xi}) = T_{i,kj}(\vec{\xi})$, we could obtain that

$$g_2 = g_3, \qquad h_3 = h_4. \tag{A.5}$$

The incompressible condition is employed, that

$$\frac{\partial R_{ij}(\vec{\xi})}{\partial \xi_j} = 0, \qquad \frac{\partial R_{ij,k}(\vec{\xi})}{\partial \xi_k} = 0, \qquad \frac{\partial T_{i,jk}(\vec{\xi})}{\partial \xi_k} = 0. \tag{A.6}$$

Notice that there is the relation of transform between Cartesian and Spherical coordinate systems, that for any isotropic vector $\vec{\phi}$, $\dfrac{\partial \phi_i}{\partial x_i} = \dfrac{\partial \phi_r}{\partial r} + \dfrac{2\phi_r}{r}$. Therefore

$$\begin{aligned} \frac{\partial R_{ij}(\vec{\xi})}{\partial \xi_j} &= \left(5f_1 + \xi\frac{df_1}{d\xi}\right)\xi_i + \frac{df_2}{d\xi_i} = 0, \\ \frac{\partial R_{ij,k}(\vec{\xi})}{\partial \xi_k} &= \left(5g_1 + \xi\frac{dg_1}{d\xi} + \frac{2}{\xi}\frac{dg_2}{d\xi}\right)\xi_i\xi_j + \left(2g_2 + 3g_4 + \xi\frac{dg_4}{d\xi}\right)\delta_{ij} = 0, \\ \frac{\partial T_{i,jk}(\vec{\xi})}{\partial \xi_i} &= \left(5h_1 + \xi\frac{dh_1}{d\xi} + \frac{2}{\xi}\frac{dh_3}{d\xi}\right)\xi_i\xi_j + \left(2h_3 + 3h_2 + \xi\frac{dh_2}{d\xi}\right)\delta_{ij} = 0. \end{aligned} \tag{A.7}$$

Finally the correlation functions could be simplified by using the longitudinal components [150]:

$$\begin{aligned} R_{ij}(\vec{\xi}) =& \left(R_{ll} + \frac{\xi}{2}\frac{\partial R_{ll}}{\xi}\right)\delta_{ij} - \frac{\partial R_{ll}}{\partial \xi}\frac{\xi_i\xi_j}{2\xi}, \\ R_{ij,k}(\vec{\xi}) =& \frac{R_{ll,l} - \xi\dfrac{\partial R_{ll,l}}{\partial \xi}}{2\xi^3}\xi_i\xi_j\xi_k + \frac{2R_{ll,l} + \xi\dfrac{\partial R_{ll,l}}{\partial \xi}}{4\xi}\left(\xi_i\delta_{jk} + \xi_j\delta_{ik}\right) - \frac{R_{ll,l}}{2\xi}\xi_k\delta_{ij}, \\ T_{i,jk}(\vec{\xi}) =& \frac{T_{l,ll} - \xi\dfrac{\partial T_{l,ll}}{\partial \xi}}{2\xi^3}\xi_i\xi_j\xi_k + \frac{2T_{l,ll} + \xi\dfrac{\partial T_{l,ll}}{\partial \xi}}{4\xi}\left(\xi_k\delta_{ij} + \xi_j\delta_{ik}\right) - \frac{T_{l,ll}}{2\xi}\xi_i\delta_{jk}. \end{aligned} \tag{A.8}$$

The governing equation of homogeneous isotropic LES could be written as

$$\frac{\partial u_i^<}{\partial t} + u_k^<\frac{\partial u_i^<}{\partial x_k} = -\frac{\partial p^<}{\partial x_i} + \nu\frac{\partial^2 u_i^<}{\partial x_k \partial x_k} - \frac{\partial \tau_{ik}^<}{\partial x_k}. \tag{A.9}$$

In another point $\vec{x}^*$, it leads to

$$\frac{\partial u_j^{<*}}{\partial t} + u_k^{<*}\frac{\partial u_j^{<*}}{\partial x_k^*} = -\frac{\partial p^{<*}}{\partial x_j^*} + \nu\frac{\partial^2 u_j^{<*}}{\partial x_k^* \partial x_k^*} - \frac{\partial \tau_{jk}^{<*}}{\partial x_k^*}. \tag{A.10}$$

(A.9) $\times u_j^{<*}$+ (A.10) $\times u_i^{<}$, and taking ensemble average, we have the equation of correlation R_{ij} as follows:

$$\begin{aligned}
&\frac{\partial R_{ij}}{\partial t} + \frac{\partial \langle u_j^{<*} u_i^{<} u_k^{<} \rangle}{\partial x_k} + \frac{\partial \langle u_i^{<} u_j^{<*} u_k^{<*} \rangle}{\partial x_k^*} = \\
&-\frac{1}{\rho}\left\langle u_j^{<*}\frac{\partial p^{<}}{\partial x_i}\right\rangle - \frac{1}{\rho}\left\langle u_i^{<}\frac{\partial p^{<*}}{\partial x_j^*}\right\rangle + \nu\left\langle u_j^{<*}\frac{\partial^2 u_i^{<}}{\partial x_k \partial x_k}\right\rangle + \nu\left\langle u_j^{<}\frac{\partial^2 u_i^{<*}}{\partial x_k^* \partial x_k^*}\right\rangle \\
&-\left\langle u_j^{<*}\frac{\partial \tau_{ik}^{<}}{\partial x_k}\right\rangle - \left\langle u_i^{<}\frac{\partial \tau_{jk}^{<*}}{\partial x_k^*}\right\rangle.
\end{aligned} \tag{A.11}$$

For homogeneous turbulence it could be further simplified as

$$\begin{aligned}
&\frac{\partial R_{ij}}{\partial t} - \frac{\partial \langle u_j^{<*} u_i^{<} u_k^{<} \rangle}{\partial \xi_k} + \frac{\partial \langle u_i^{<} u_j^{<*} u_k^{<*} \rangle}{\partial \xi_k} = \\
&-\frac{1}{\rho}\left\langle \frac{\partial p^{<} u_j^{<*}}{\partial x_i}\right\rangle - \frac{1}{\rho}\left\langle \frac{\partial p^{<*} u_i^{<}}{\partial x_j^*}\right\rangle + \nu\left\langle \frac{\partial^2 u_i^{<} u_j^{<*}}{\partial \xi_k \partial \xi_k}\right\rangle + \nu\left\langle \frac{\partial^2 u_j^{<} u_i^{<*}}{\partial \xi_k \partial \xi_k}\right\rangle \\
&+\left\langle \frac{\partial \tau_{ik}^{<} u_j^{<*}}{\partial \xi_k}\right\rangle - \left\langle \frac{\partial \tau_{jk}^{<*} u_i^{<}}{\partial \xi_k}\right\rangle.
\end{aligned} \tag{A.12}$$

The pressure-velocity correlation term is vanishing in isotropic turbulence. Thus the correlation equation becomes

$$\frac{\partial R_{ij}}{\partial t} - \frac{\partial R_{ik,j}}{\partial \xi_k} + \frac{\partial R_{i,jk}}{\partial \xi_k} = 2\nu\frac{\partial^2 R_{ij}}{\partial \xi_k \partial \xi_k} + \frac{\partial T_{ik,j}}{\partial \xi_k} - \frac{\partial T_{i,jk}}{\partial \xi_k}. \tag{A.13}$$

Inserting equation (A.8) to equation and applying the same manipulation in derivation of classical Karman-Howarth equation [49], we could then obtain the modified Karman-Howarth equation for resolved-scale turbulence:

$$\frac{\partial R_{ll}}{\partial t} = \frac{1}{\xi^4}\frac{\partial}{\partial \xi}(\xi^4 R_{ll,l}) + 2\frac{\nu}{\xi^4}\frac{\partial}{\partial \xi}\left(\xi^4 \frac{\partial R_{ll}}{\partial \xi}\right) - \frac{1}{\xi^4}\frac{\partial}{\partial \xi}(\xi^4 T_{l,ll}). \tag{A.14}$$

In comparison with the classical Karman-Howarth equation of isotropic turbulence, the last term in the right-hand side is an additional term representing energy transport between resolved- and unresolved-scale turbulence in the modified Karman-Howarth equation.

The second- and third-order correlation functions could be expressed in the second- and third-order structural functions for isotropic turbulence:

$$\begin{aligned} D_{ll}^{<} =& 2\langle u^{<^2}\rangle - 2R_{ll}, \\ D_{lll}^{<} =& 6R_{ll,l}, \end{aligned} \tag{A.15}$$

in which $u^<$ is the longitudinal resolved-scale velocity, $D_{ll}^{<} = \langle (u^<(x+\xi) - u^<(x))^2\rangle$ and $D_{ll}^{<} = \langle (u^<(x+\xi) - u^<(x))^2\rangle$ are the second- and third-order longitudinal structural functions respectively. Replacing correlation function in equation (A.14) by structural functions, we could obtain the following equation for structural functions:

$$\frac{\partial\langle (u_1)^{<2}\rangle}{\partial t} - \frac{1}{2}\frac{\partial D_{ll}^{<}}{\partial t} = \frac{1}{6\xi^4}\frac{\partial}{\partial\xi}(\xi^4 D_{lll}^{<}) - \frac{\nu}{\xi^4}\frac{\partial}{\partial\xi}\left(\xi^4\frac{\partial D_{ll}^{<}}{\partial\xi}\right) - \frac{1}{\xi^4}\frac{\partial}{\partial\xi}(\xi^4 T_{l,ll}). \tag{A.16}$$

This process of derivation of the Yaglom equation of filtered scalar, in homogeneous isotropic scalar turbulence was introduced in Zhou's PhD thesis [126]. The passive scalar is denoted as θ. The governing equation of resolved scalar could be written as

$$\frac{\partial\theta^<}{\partial t} + u_j^<\frac{\partial\theta^<}{\partial x_j} = \kappa\frac{\partial^2\theta^<}{\partial x_j\partial x_j} + \frac{\partial\tau_{\theta j}^<}{\partial x_j}, \tag{A.17}$$

where $\tau_{\theta j}^<$ is the subgrid scalar flux. The correlation functions are defined as

$$\begin{aligned} R_{\theta\theta}^<(\vec{\xi}) =& \langle\theta^<(\vec{x})\theta^<(\vec{x}+\vec{\xi})\rangle, \\ R_{\theta j,\theta}^<(\vec{\xi}) =& \langle\theta^<(\vec{x})u_j^<(\vec{x})\theta^<(\vec{x}+\vec{\xi})\rangle. \end{aligned} \tag{A.18}$$

The second-order correlation function denotes the correlation between filtered scalars, and the third-order correlation function is the mixed function among one velocity and two scalars. In the following part, we use the signals $R_{\theta\theta}$ and $R_{\theta j,\theta}$ instead, respectively. Another third-order correlation function between the resolved scalar and the subgrid scalar flux is denoted as

$$T_{\theta,\theta j}(\vec{\xi}) = \langle\theta^<(\vec{x})\tau_{\theta j}^<(\vec{x}+\vec{\xi})\rangle. \tag{A.19}$$

Write the governing equation (A.17) in another point $\vec{x}^*$, it leads to

$$\frac{\partial\theta^{<*}}{\partial t} + u_j^<\frac{\partial\theta^{<*}}{\partial x_j^*} = \kappa\frac{\partial^2\theta^{<*}}{\partial x_j^*\partial x_j^*} + \frac{\partial\tau_{\theta j}^{<*}}{\partial x_j^*}. \tag{A.20}$$

(A.17) × (A.20), and taking ensemble average, we have the equation of correlation $R_{\theta\theta}$ in homogeneous turbulence:

$$\frac{\partial R_{\theta\theta}}{\partial t} = \frac{\partial}{\partial \xi_j}\left(R_{\theta j,\theta} - R_{\theta,\theta j}\right) + 2\kappa \frac{\partial^2 R_{\theta\theta}}{\partial \xi_j \partial \xi_j}. \tag{A.21}$$

Employing the isotropic condition, the three-order tensors are simplified as

$$\begin{aligned} R_{\theta j,\theta} =& \frac{R_{\theta l,\theta}}{\xi}\xi_j \\ T_{\theta,\theta j} =& \frac{T_{\theta,\theta l}}{\xi}\xi_j \end{aligned} \tag{A.22}$$

where the longitudinal components are

$$\begin{aligned} R_{\theta l,\theta}(\xi) =& \langle \theta^<(x_1) u_1^<(x_1) \theta^<(x_1+\xi)\rangle, \\ T_{\theta,\theta l}(\xi) =& \langle \theta^<(x_1) \tau_{\theta l}^<(x_1+\xi)\rangle. \end{aligned} \tag{A.23}$$

Therefore, equation (A.21) could be rewritten as

$$\frac{\partial R_{\theta\theta}}{\partial t} = 2\left(\frac{\partial}{\partial \xi} + \frac{2}{\xi}\right)\left(R_{\theta l,\theta} + \kappa \frac{\partial R_{\theta\theta}}{\partial \xi} - T_{\theta,\theta l}\right). \tag{A.24}$$

In isotropic scalar turbulence, the second- and third-order correlation functions could be represented by the second- and third-order structure functions:

$$\begin{aligned} D_{\theta\theta}^< =& 2\langle \theta^{<^2}\rangle - 2R_{\theta\theta}, \\ D_{l\theta\theta}^< =& 4R_{\theta l,\theta}, \end{aligned} \tag{A.25}$$

in which

$$\begin{aligned} D_{\theta\theta}^< =& \left\langle \left(\theta^<(x_1+\xi) - \theta^<(x_1)\right)^2 \right\rangle, \\ D_{l\theta\theta}^< =& \left\langle \left(u_1^<(x_1+\xi) - u_1^<(x_1)\right)\left(\theta^<(x_1+\xi) - \theta^<(x_1)\right)^2 \right\rangle. \end{aligned} \tag{A.26}$$

Thus we could obtain the Yaglom equation of filtered scalar for homogeneous isotropic scalar turbulence:

$$\frac{\partial \langle \theta^{<^2}\rangle}{\partial t} - \frac{1}{2}\frac{\partial D_{\theta\theta}^<}{\partial t} = \frac{2}{\xi^2}\frac{\partial}{\partial \xi}\left[\xi^2\left(\frac{D_{l\theta\theta}}{4} - \frac{\kappa}{2}\frac{\partial D_{\theta\theta}}{\partial \xi} - T_{\theta,\theta l}\right)\right]. \tag{A.27}$$

Appendix B

Numerical method for homogeneous isotropic turbulence

Lots of researchers have attempted to simulate homogeneous isotropic turbulence using DNS or LES. One of the recent DNS dababase is a 1024^3 case offered by Meneveau's group [153]. In this thesis, we follow Zhou's methods [126] to generate a homogeneous isotropic turbulence. The DNS cases have 256^3 grids, and the LES cases have 96^3, 64^3 or 48^3 grids.

Governing equation

The governing equations in DNS are

$$\begin{aligned} \frac{\partial u_i}{\partial x_i} &= 0, \\ \frac{\partial u_i}{\partial t} + u_j \frac{\partial u_i}{\partial x_j} &= -\frac{1}{\rho}\frac{\partial p}{\partial x_i} + \nu \frac{\partial^2 u_i}{\partial x_j \partial x_j} + f_i, \end{aligned} \tag{B.1}$$

where f_i is a random forcing introduced to generate stable homogeneous turbulence. The numerical method has been introduced by Eswaran [154] and Overholt [155]. If $f_i = 0$, the turbulence is naturally decaying.

The governing equations in LES are

$$\begin{aligned} \frac{\partial u_i^<}{\partial x_i} &= 0, \\ \frac{\partial u_i^<}{\partial t} + u_j^< \frac{\partial u_i^<}{\partial x_j} &= -\frac{1}{\rho}\frac{\partial p^<}{\partial x_i} + \nu \frac{\partial^2 u_i^<}{\partial x_j \partial x_j} - \frac{\partial \tau_{ij}^<}{\partial x_j} + f_i^<, \end{aligned} \tag{B.2}$$

where $\tau_{ij}^{<}$ is the subgrid stress. The main simulating processes are the same between DNS and LES, thus in the following content, the DNS calculation is principally introduced.

Discretization method

The discretization in physical space could be written as

$$\vec{x} = (x_1, x_2, x_3) = (x, y, z) = (l_1\Delta, l_2\Delta, l_3\Delta), \tag{B.3}$$

in which l_1, l_2, l_3 are integers, $0 \leq l_1, l_2, l_3 \leq N-1$, $\Delta = \dfrac{L}{N}$, L is the length of computing domain, N is the number of grids.

The discretization in spectral space could be written as

$$\vec{k} = (k_1, k_2, k_3) = (m_1 k_{min}, m_2 k_{min}, m_3 k_{min}), \tag{B.4}$$

in which m_1, m_2, m_3 are integers, $-\dfrac{N}{2} \leq m_1, m_2, m_3 \leq \dfrac{N}{2} - 1$, k_{min} is the minimal non-zero wave number, $k_{min} = \dfrac{2\pi}{L}$.

The velocity and pressure could be expressed in spectral space:

$$\begin{aligned} u_i(\vec{x}, t) &= \sum_{\vec{k}} \widehat{u}_i\left(\vec{k}, t\right) e^{\iota\vec{k}\cdot\vec{x}}, \\ p(\vec{x}, t) &= \sum_{\vec{k}} \widehat{p}\left(\vec{k}, t\right) e^{\iota\vec{k}\cdot\vec{x}}, \end{aligned} \tag{B.5}$$

in which $\widehat{\bullet}$ denotes the physical quantity in spectral space. Therefore, the governing equations in spectral space are

$$\begin{aligned} k_i\widehat{u}_i &= 0, \\ \frac{\partial\widehat{u}_i}{\partial t} + \iota k_j\widehat{u_i u_j} &= -\frac{1}{\rho}\iota k_i\widehat{p} + \nu\iota^2 k^2\widehat{u}_i. \end{aligned} \tag{B.6}$$

Initial condition

The initial velocity field is generated in spectral space, by employing Rogallo's method [54]. The initial velocity field should satisfy both the continuous condition and the given energy spectrum. For any wave number vector $\vec{k}$ in spectral space, the

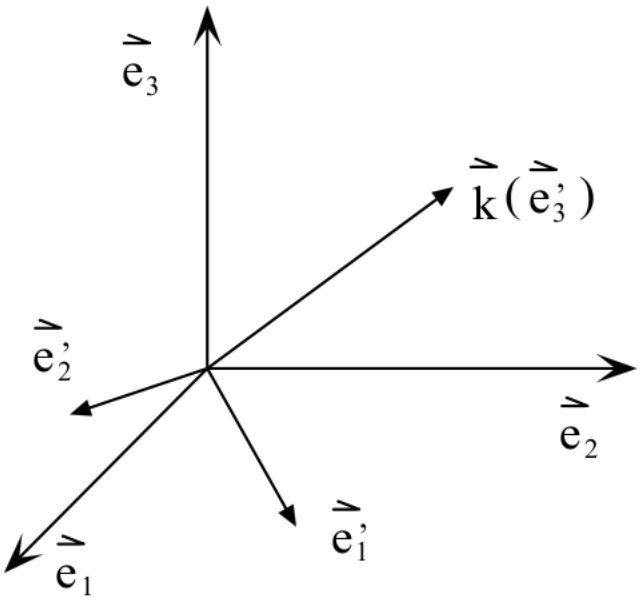

Figure B.1: Coordinate system of initial velocity field in spectral space.

velocity vector must be in the vertical plane, to satisfy the continuous condition (see Fig. B).

For any wave number $\vec{k}$, a coordinate system is set as $\{\vec{e}_1', \vec{e}_2', \vec{e}_3'\}$, in which $\vec{e}_3'$ is parallel to $\vec{k}$, and $\{\vec{e}_1', \vec{e}_2'$ are in the vertical plane of $\vec{k}$. The initial velocity could be written as

$$\vec{u}\left(\vec{k}, 0\right) = \alpha\left(\vec{k}\right)\vec{e}_1' + \beta\left(\vec{k}\right)\vec{e}_2', \tag{B.7}$$

in which α and β are determined by the spectrum conditions, i.e.

$$\oiint_{A(k)} \widehat{u} \cdot \widehat{u}^* dA(k) = E(k), \tag{B.8}$$

where $\widehat{u}^*$ is conjugate to $\widehat{u}$. When the following relations are given, the spectrum condition is satisfied:

$$\begin{aligned} \alpha =& \sqrt{\frac{E(k)}{4\pi k^2}} e^{\iota\theta_1} \cos\phi, \\ \beta =& \sqrt{\frac{E(k)}{4\pi k^2}} e^{\iota\theta_2} \cos\phi, \end{aligned} \tag{B.9}$$

where θ_1, θ_2 and ϕ are random variables satisfying uniform distribution in $(0, 2\pi)$.

The parallel axis $\vec{e}_3'$ is calculated as

$$\vec{e}_3' = \frac{k_1}{k}\vec{e}_1 + \frac{k_2}{k}\vec{e}_2 + \frac{k_3}{k}\vec{e}_3. \tag{B.10}$$

We could simply let $\vec{e}_1' \perp \vec{e}_3$, it leads to

$$\begin{aligned} \vec{e}_1' =& \vec{e}_3' \times \vec{e}_3, \\ \vec{e}_2' =& \vec{e}_3' \times \vec{e}_1'. \end{aligned} \tag{B.11}$$

Therefore, the initial velocity field in spectral space is

$$\vec{u}(k_1,k_2,k_3) = \left(\frac{\alpha k k_2 + \beta k_1 k_3}{k\sqrt{k_1^2+k_2^2}}\right)\vec{e}_1 + \left(\frac{\alpha k_2 k_3 - \beta k k_1}{k\sqrt{k_1^2+k_2^2}}\right)\vec{e}_2 - \left(\frac{\beta\sqrt{k_1^2+k_2^2}}{k}\right)\vec{e}_3. \tag{B.12}$$

The Von-Karman energy spectrum is employed to generate initial velocity field. It could be written as

$$E(k) = E(k_p)2^{17/6}\frac{(k/k_p)^4}{[1+(k/k_p)^2]^{17/6}}, \tag{B.13}$$

where $E(k_p)$ and k_p are the peak value and peak location of energy spectrum, respectively. Different values could lead to homogeneous isotropic turbulence with different characteristic scale and kinetic energy.

Boundary condition

Periodic boundary condition is applied in all directions. It could be written as

$$\begin{aligned} u_i(\vec{x}+\vec{n}L,t) =& u_i(\vec{x},t), \\ p(\vec{x}+\vec{n}L,t) =& p(\vec{x},t), \end{aligned} \tag{B.14}$$

where $\vec{n} = n_1\vec{e}_1 + n_2\vec{e}_2 + n_3\vec{e}_3$, n_1, n_2, n_3 are integers.

Therefore, Fourier transform could be applied in all three directions, and the governing equation could be solved in spectral space.

Temporal integral

The solving process could be simply written as

$$\frac{du}{dt} = f(u,t), \tag{B.15}$$

where $f(u,t)$ contains the convection term, pressure term and viscous term in the governing equation.

Fourth-order explicit Runge-Kutta method in applied in temporal iteration:

$$\begin{aligned} u_{n+1} =& u_n + \frac{\Delta t}{6}(k_1 + 2k_2 + 2k_3 + k_4), \\ k_1 =& f(t_n, u_n), \\ k_2 =& f(t_n + \frac{\Delta t}{2}, u_n + \frac{\Delta t}{2} k_1), \\ k_3 =& f(t_n + \frac{\Delta t}{2}, u_n + \frac{\Delta t}{2} k_2), \\ k_4 =& f(t_n + \Delta t, u_n + \Delta t k_3). \end{aligned} \tag{B.16}$$

The temporal step length should satisfy the stability condition, i.e., CFL condition:

$$|velo|_{\max} \cdot \frac{\Delta t}{\Delta x} = 0.1 < 1, \tag{B.17}$$

where $|velo|_{\max} = \max(|u|_{\max}, |v|_{\max}, |w|_{\max})$.

Parallel algorithm

Parallel calculation is an effective method for extensive numerical simulations. The highest-cost subroutine in the DNS program is Fourier transform. Therefore, Zhou introduced a parallel algorithm to reduce the cost [156]. The existed serial libraries of 1-D Fourier transform are used to implement 3-D parallel Fourier transfer, by dividing regions and exchange messages between computer nodes. Because the Fourier transform of a real function is conjugate symmetrical, we could store up only half of the data. Zhou's algorithm avoids the message exchange of the conjugate symmetrical operations.

Appendix C

Numerical method for channel turbulence

The computer program of channel turbulence used in this thesis was developed by Xu [157]. The scalar part are written by Zhou [126].

Governing equation

In channel flow, the Navier-Stokes equations and the transport equation of passive scalar could be written as

$$\begin{aligned} \frac{\partial \vec{V}}{\partial t} =& \vec{V} \times \vec{\omega} - \nabla \Pi + \nu \nabla^2 \vec{V} - \frac{1}{\rho} \frac{d\overline{p}}{dx} \vec{e}_x, \\ \nabla \cdot \vec{V} =& 0, \\ \frac{\partial \theta}{\partial t} + \vec{V} \cdot \nabla \theta =& \kappa \nabla^2 \theta, \end{aligned} \tag{C.1}$$

where $\vec{V}$ is the velocity vector, θ is the passive scalar, $\vec{\omega} = \nabla \times \vec{V}$ is the vorticity, $\overline{p}$ is the mean pressure, $\frac{d\overline{p}}{dx}$ is the mean pressure gradient in streamwise direction, $\Pi = \frac{p'}{\rho} + \frac{|\vec{V}|^2}{2}$ is the fluctuation part of total pressure. The characteristic velocity is the mean velocity in the cross-section U_m, and the characteristic length is half channel width H. Reynolds number is defined as $\mathrm{Re}_H = U_m H/\nu$, Prandtl number is $\mathrm{Pr} = \nu/\kappa$. The computational domain is shown in Fig. C.1. x, y, z are coordinate axes, u, v, w are velocity components of each axis, respectively.

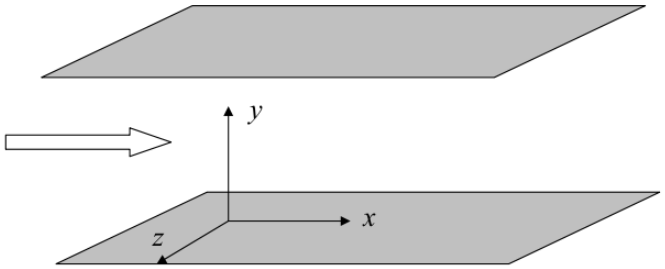

Figure C.1: Computational domain of channel turbulence.

The non-dimensional governing equation and boundary condition could be written as

$$\begin{aligned}
\frac{du}{dt} =& F_x - \frac{\partial \Pi}{\partial x} + \frac{1}{\mathrm{Re}}\nabla^2 u, \\
\frac{dv}{dt} =& F_y - \frac{\partial \Pi}{\partial y} + \frac{1}{\mathrm{Re}}\nabla^2 v, \\
\frac{dw}{dt} =& F_z - \frac{\partial \Pi}{\partial z} + \frac{1}{\mathrm{Re}}\nabla^2 w, \\
\frac{d\theta}{dt} =& F_\theta + \frac{1}{\mathrm{Re}\cdot\mathrm{Pr}}\nabla^2 \theta,
\end{aligned} \tag{C.2}$$

$$F_x = v\cdot\omega_z - w\cdot\omega_y - \frac{1}{\rho}\frac{d\overline{p}}{dx},$$

$$\begin{aligned}
F_y =& w\cdot\omega_x - u\cdot\omega_z, \\
F_z =& u\cdot\omega_y - v\cdot\omega_x,
\end{aligned} \tag{C.3}$$

$$F_\theta = -u\frac{\partial\theta}{\partial x} - v\frac{\partial\theta}{\partial y} - w\frac{\partial\theta}{\partial z},$$

$$\frac{\partial u}{\partial x} + \frac{\partial v}{\partial y} + \frac{\partial w}{\partial z} = 0, \tag{C.4}$$

$$\begin{aligned}
u(x+L_x,y,z,t) =& u(x,y,z,t), \\
v(x+L_x,y,z,t) =& v(x,y,z,t), \\
w(x+L_x,y,z,t) =& w(x,y,z,t), \\
\theta(x+L_x,y,z,t) =& \theta(x,y,z,t),
\end{aligned} \tag{C.5}$$

$$
\begin{aligned}
u(x,y,z+L_z,t) =& u(x,y,z,t),\\
v(x,y,z+L_z,t) =& v(x,y,z,t),\\
w(x,y,z+L_z,t) =& w(x,y,z,t),\\
\theta(x,y,z+L_z,t) =& \theta(x,y,z,t),
\end{aligned}
\tag{C.6}
$$

$$
\begin{aligned}
u(x,1,z,t) =& \begin{cases} 0, & \text{Couette flow},\\ 2, & \text{Poiseuille flow}, \end{cases}\\
v(x,1,z,t) =& w(x,1,z,t) = 0,\\
\theta(x,1,z,t) =& 1,\\
u(x,-1,z,t) =& v(x,-1,z,t) = w(x,-1,z,t) = 0,\\
\theta(x,-1,z,t) =& -1.
\end{aligned}
\tag{C.7}
$$

The governing equations in LES could be written as

$$
\begin{aligned}
\frac{\partial u_i^<}{\partial t} =& F_i^< - \frac{\partial \Pi^<}{\partial x_i} + \nu \frac{\partial^2 u_i^<}{\partial x_j \partial x_j} - \frac{\partial \tau_{ij}^<}{\partial x_j},\\
\frac{\partial u_i^<}{\partial x_i} =& 0,\\
\frac{\partial \theta^<}{\partial t} =& F_\theta^< - \kappa \frac{\partial^2 \theta}{\partial x_j \partial x_j} - \frac{\partial \tau_{\theta j}^<}{\partial x_j}.
\end{aligned}
\tag{C.8}
$$

Spatial discretization

In spatial discretization, the Fourier-Galerkin method and the Chebyshev sample point method are employed. In streamwise the spanwise directions, variables are expanded by Fourier series; in normal direction, variables are expanded by Lagrange interpolation polynomial, in Chebyshev-Gauss-Lobatto sample points. The interpolation polynomial is:

$$
h_j(y) = \frac{2}{N_y} \sum_{p=0}^{N_y} \frac{1}{c_j c_p} T_p(y_j) T_p(y),
\tag{C.9}
$$

where $T_p(y)$ is the p^{th} order Chebyshev polynomial, and

$$
c_j = \begin{cases} 2, & j = 0, N_y,\\ 1, & 1 \le j \le N_y - 1. \end{cases}
\tag{C.10}
$$

The following property is satisfied:

$$h_j(y_k) = \delta_{jk}. \tag{C.11}$$

The derivative could be written as

$$\begin{aligned} h'_j(y) =& \frac{2}{N_y} \sum_{p=0}^{N_y} \frac{1}{c_j c_p} T_p(y_j) T'_p(y), \\ h''_j(y) =& \frac{2}{N_y} \sum_{p=0}^{N_y} \frac{1}{c_j c_p} T_p(y_j) T''_p(y). \end{aligned} \tag{C.12}$$

If $\phi(x, y, z, t)$ is any physical quantity, it could be expanded as

$$\phi(x, y, z, t) = \sum_{m=-\frac{N_x}{2}}^{\frac{N_x}{2}-1} \sum_{n=-\frac{N_z}{2}}^{\frac{N_z}{2}-1} \sum_{p=0}^{N_y} \phi(m, p, n, t) \exp(\iota \alpha m x + \iota \beta n z) h_p(y). \tag{C.13}$$

Temporal discretization

Each temporal step is divided into three substeps:

1) Non-linear substep:

$$\begin{aligned} \frac{\vec{u}^{s+1/3} - \sum_{q=0}^{J_i-1} \alpha_q \vec{u}^{s-q}}{\Delta t} &= \sum_{q=0}^{J_e-1} \beta_q N(\vec{u}^{s-q}), \\ \frac{\theta^{s+1/3} - \sum_{q=0}^{J_i-1} \alpha_q \theta^{s-q}}{\Delta t} &= \sum_{q=0}^{J_e-1} \beta_q N_\theta(\theta^{s-q}). \end{aligned} \tag{C.14}$$

2) Pressure substep:

$$\begin{aligned} \frac{\vec{u}^{s+2/3} - \vec{u}^{s+1/3}}{\Delta t} =& - \nabla \Pi^{s+1}, \\ \nabla \cdot \vec{u}^{s+2/3} =& 0. \end{aligned} \tag{C.15}$$

3) Viscosity substep:

$$\begin{aligned} \frac{\gamma_0 \vec{u}^{s+1} - \vec{u}^{s+2/3}}{\Delta t} =& \frac{1}{Re} \nabla^2 \vec{u}^{s+1}, \\ \frac{\gamma_0 \theta^{s+1} - \theta^{s+2/3}}{\Delta t} =& \frac{1}{Re\, Pr} \nabla^2 \theta^{s+1}. \end{aligned} \tag{C.16}$$

In equation (C.14), N and N_θ are linear operators, $\vec{n}$ is unit vector in the vertical direction of wall. The non-linear term is calculated explicitly with J_e order precision; other terms are treated implicitly with J_i order precision. We employ the third-order temporal precision, the corresponding constant are

$$\begin{aligned} \gamma_0 =& \frac{11}{6}, \\ \alpha_0 =& 3,\ \alpha_1 = -\frac{3}{2},\ \alpha_2 = \frac{1}{3}, \\ \beta_0 =& 3,\ \beta_1 = -3,\ \beta_2 = 1. \end{aligned} \tag{C.17}$$

Appendix D

Corrections for the scaling of the second-order structure function in isotropic turbulence

The scaling law of structure functions is a basic problem in the study of turbulence. The second and third order longitudinal structure function of the velocity $\boldsymbol{u}$ are respectively defined as

$$D_{ll}(r) = \langle (u(x_1 + r) - u(x_1))^2 \rangle \tag{D.1}$$

$$D_{lll}(r) = \langle (u(x_1 + r) - u(x_1))^3 \rangle \tag{D.2}$$

with u the velocity component in the x_1-direction and $\langle \cdot \rangle$ denoting an ensemble average. In the inertial range of high Reynolds number turbulence, these structure functions were proposed to scale as [9, 158]:

$$D_{ll}(r) \sim (\varepsilon r)^{2/3} \tag{D.3}$$

$$D_{lll}(r) \sim \varepsilon r, \tag{D.4}$$

with the dissipation defined as

$$\varepsilon = \nu \left\langle \frac{\partial u_i}{\partial x_j} \frac{\partial u_i}{\partial x_j} \right\rangle, \tag{D.5}$$

and ν the kinematic viscosity. Later, Kolmogorov proposed a correction to the scaling of $D_{ll}(r)$, taking into account the increasingly intermittent character of the energy flux ε when the scale r is decreased. This correction is however small and disputed.

For example, Qian argued that the anomalous scaling (as observed experimentally by *e.g.* [79]) may stem from a finite Reynolds number effect [159], and he proposed that the 2/3 law may be satisfied when the Reynolds number tends to infinity. The second relation is an exact relation, which can be derived from the Navier-Stokes equations, be it only in the limit of very large Reynolds number. Indeed, for stationary isotropic incompressible turbulence one can derive

$$D_{lll}(r) = 6\nu \frac{dD_{ll}(r)}{dr} - \frac{4}{5}\varepsilon r. \tag{D.6}$$

For scales much larger than the viscous scale, the first term on the right hand side vanishes so that (D.4) is obtained. Equation (D.6) relates the second and third order structure functions. So if $D_{lll}(r)$ or the skewness $S_k(r) = D_{lll}(r)/\left(D_{ll}(r)\right)^{3/2}$ is known, the second order structure function can be computed using (D.6). A first attempt is substituting a constant Skewness, as was proposed by Obukhov [160] (see also [94], chapter 22, or [161]). Indeed, in the inertial range, from (D.3) and (D.4) it is clear that the skewness of the longitudinal velocity increment should be a constant (in the absence of intermittency corrections). For $r \ll \eta$, with η the viscous cut-off scale, the flow can be considered as smooth, so that the velocity increments scale linearly with the separation distance. This gives the trivial scaling

$$D_{ll}(r) \sim r^2 \tag{D.7}$$

$$D_{lll}(r) \sim r^3 \tag{D.8}$$

so that also at small scales the skewness should be a constant. Around η, the skewness is however not constant, since the plateaus at small and large r do not have the same value, as sketched in Figure D.1. Let us call these two values $S_k(0)$ and $S_k(\infty)$. By coincidence, these two values are relatively close, differing by approximately a factor two.

In order to well represent the transition of the scaling exponent from 2 to 2/3, Batchelor proposed an interpolation formula for the structure function [162], and this result has been widely applied [163, 164]:

$$\frac{D_{ll}(r)}{v^2} = \frac{2(r/\eta)^{2/3}}{\left[1 + (C\eta/r)^2\right]^{2/3}}, \tag{D.9}$$

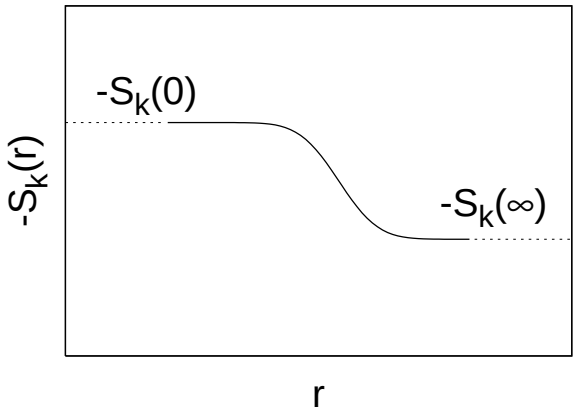

Figure D.1: Schematic of the velocity increment skewness in isotropic turbulence. Two plateaus are expected at very large Reynolds number: one for $r \ll \eta$ the other for $\eta \ll r \ll L$

with $v = (\nu\varepsilon)^{1/4}$ the characteristic velocity, $\eta = \nu^{3/4}\varepsilon^{-1/4}$ is the Kolmogorov scale, and C is a constant. This form was proposed because of its simplicity, not because of any underlying physics. It is in reasonable agreement with experiments.

In the present communication we present results on the transition region of the second-order structure function between the inertial range and the viscous range. The method is based on an extension of the work by Obukhov. Indeed, we use the assumption of a constant skewness for for $r \ll \eta$ and $\eta \ll r \ll L$ as a zeroth order solution. Then, starting from the inertial range we apply a perturbation method to evaluate the influence of the viscous damping. In the viscous range, we use Taylor-expansions to obtain an approximation of the influence of the non-constant skewness. Analytical expressions for the scaling exponent in both ranges are obtained. Results are compared to the Batchelor formula, and small quantitative modifications of the latter are proposed.

D.1 Analytical solutions

In homogeneous isotropic turbulence, The Kolmorogov equation (D.6), can be written as a function of $D_{ll}(r)$ and the skewness:

$$S_k(r)D_{ll}(r)^{3/2} = 6\nu\frac{dD_{ll}(r)}{dr} - \frac{4}{5}\varepsilon r. \tag{D.10}$$

We will in this section consider the two regions in which the skewness is constant at high Reynolds numbers, and compute analytically the corrections to the scaling of $D_{ll}(r)$, when r approaches η.

D.1.1 Corrections for the scaling in the dissipative range

In dissipative range, we can define $r_\eta = r/\eta, D_\eta(r_\eta) = D_{ll}(\eta r_\eta)/v^2, D'_\eta(r_\eta) = dD_\eta(r_\eta)/dr_\eta$, and Eq. (D.10) leads to

$$6D'_\eta - \frac{4}{5}r_\eta - S_k(r_\eta)D_\eta^{3/2} = 0. \tag{D.11}$$

Suppose $S_k(r_\eta) = S_k(0)$ in dissipative range, and let $w = D_\eta^{1/2}$, it can be rewritten as

$$12ww' - \frac{4}{5}r_\eta - S_k(0)w^3 = 0. \tag{D.12}$$

When r_η tends to zero, from Taylor expansion we have

$$w = \sum_{i=0}^{\infty} a_i r_\eta^i, \tag{D.13}$$

in which a_i are unknown coefficients. Then the terms in Eq. (D.12) can be expressed:

$$ww' = a_1^2 r_\eta + 3a_1a_2r_\eta^2 + (4a_1a_3 + 2a_2^2)r_\eta^3 + (5a_1a_4 + 5a_2a_3)r_\eta^4 + ... \tag{D.14}$$

$$w^3 = a_1^3 r_\eta^3 + 3a_1^2a_2r_\eta^4 + (3a_1a_2^2 + 3a_1^2a_3)r_\eta^5 + ... \tag{D.15}$$

Substituting Eqs. (D.14) and (D.15) into (D.12), and comparing the same order terms of r_η, finally we have

$$w = \frac{1}{\sqrt{15}}r_\eta + \frac{S_k(0)}{720}r_\eta^3 + \frac{\sqrt{15}S_k(0)^2}{345600}r_\eta^5 + \frac{S_k(0)^3}{11059200}r_\eta^7 + \frac{133S_k(0)^4}{47775744000\sqrt{15}}r_\eta^9 ...., \tag{D.16}$$

and the structure function is

$$D_\eta(r_\eta) = \frac{1}{15}r_\eta^2 + \frac{S_k(0)}{360\sqrt{15}}r_\eta^4 + \frac{S_k(0)^2}{129600}r_\eta^6 + \frac{S_k(0)^3}{3317760\sqrt{15}}r_\eta^8 + \frac{67S_k(0)^4}{89579520000}r_\eta^{10} ... \tag{D.17}$$

The scaling exponent n is defined that $D_\eta(r_\eta) \propto r_\eta^n$, i.e. $n = \dfrac{d\log D_\eta}{d\log r_\eta} = \dfrac{dD_\eta}{dr_\eta}\dfrac{r_\eta}{D_\eta}$. Thus the solution of 4^{th} order precision can be written as:

$$n \approx 2\left(\frac{\frac{1}{15} + \frac{S_k(0)}{180\sqrt{15}}r_\eta^2 + \frac{S_k(0)^2}{43200}r_\eta^4 + \frac{S_k(0)^3}{829440\sqrt{15}}r_\eta^6 + \frac{67S_k(0)^4}{17915904000}r_\eta^8}{\frac{1}{15} + \frac{S_k(0)}{360\sqrt{15}}r_\eta^2 + \frac{S_k(0)^2}{129600}r_\eta^4 + \frac{S_k(0)^3}{3317760\sqrt{15}}r_\eta^6 + \frac{67S_k(0)^4}{89579520000}r_\eta^8}\right). \tag{D.18}$$

D.1.2 Corrections for the scaling in the inertial range

From Eq. (D.10), the constant skewness can also yield

$$\frac{dS_k(r)}{dr} = \frac{d}{dr}\left(D_{ll}(r)^{-3/2}\left(6\nu\frac{dD_{ll}(r)}{dr} - \frac{4}{5}\varepsilon r\right)\right) = 0. \tag{D.19}$$

Introducing the Taylor micro-scale $\lambda = u_0\sqrt{15\nu/\varepsilon}$, where $u_0 = \sqrt{k^2/3}$ is the characteristic velocity, and $r_\lambda = r/\lambda, D_\lambda(r_\lambda) = \dfrac{D_{ll}(\lambda r_\lambda)}{u_0^2}, D'_\lambda(r_\lambda) = \dfrac{dD_\lambda(r_\lambda)}{dr_\lambda}$, it leads to

$$30\left(\frac{\eta}{\lambda}\right)^2 D_\lambda D''_\lambda - 45\left(\frac{\eta}{\lambda}\right)^2 D'^2_\lambda + 6r_\lambda D'_\lambda - 4D_\lambda = 0. \tag{D.20}$$

Considering the Reynolds number

$$\mathrm{Re}_\lambda = \frac{u_0\lambda}{\nu} = \frac{1}{\sqrt{15}}\left(\frac{\lambda}{\eta}\right)^2, \tag{D.21}$$

we could rewrite Eq. (D.20) as

$$30\frac{\sqrt{15}}{\mathrm{Re}_\lambda} D_\lambda D''_\lambda - 45\frac{\sqrt{15}}{\mathrm{Re}_\lambda} D'^2_\lambda + 6r_\lambda D'_\lambda - 4D_\lambda = 0. \tag{D.22}$$

When Reynolds number is large, i.e. $\delta = \sqrt{15}/\mathrm{Re}_\lambda \ll 1$, the perturbation method can be applied, the differential equation (D.22) is rewritten as

$$30\delta D_\lambda D''_\lambda - 45\delta D'^2_\lambda + 6r_\lambda D'_\lambda - 4D_\lambda = 0, \tag{D.23}$$

and the general solution can be expanded using δ:

$$D_\lambda = \sum_{n=0}^{\infty} \delta^n D_{\lambda n}. \tag{D.24}$$

Substituting (D.24) into (D.23), the 0^{th} order equation for δ is

$$6r_\lambda D'_{\lambda 0} - 4D_{\lambda 0} = 0, \tag{D.25}$$

the general solution can be found that

$$D_{\lambda 0}(r_\lambda) = A_0 r_\lambda^{2/3}. \tag{D.26}$$

The coefficient A_0 can be determined by employing the skewness value when $r_\lambda \to \infty$. We can easily obtain

$$A_0 = 15^{1/6}\mathrm{Re}_\lambda^{1/3} C_0, \tag{D.27}$$

in which

$$C_0 = \left(\frac{-4}{5S_k(\infty)}\right)^{2/3} \tag{D.28}$$

is a constant which does not depend on Reynolds number. Note that the value of skewness $S_k(\infty)$ is usually not the same as $S_k(0)$.

Similarly, we can write the 1^{st} order equation for δ:

$$30D_{\lambda 0}D''_{\lambda 0} - 45D'^2_{\lambda 0} + 6r_\lambda D'_{\lambda 1} - 4D_{\lambda 1} = 0. \tag{D.29}$$

From the solution of $D_{\lambda 0}$, i.e. Eq. (D.26), the solution of $D_{\lambda 1}$ can be obtain:

$$D_{\lambda 1}(r_\lambda) = -\frac{10A_0^2}{3r_\lambda^{2/3}} + A_1 r_\lambda^{2/3}. \tag{D.30}$$

Since $D_{\lambda 1}$ should tend to 0 when $x \to \infty$, we have the coefficient $A_1 = 0$, thus

$$D_{\lambda 1}(x) = -\frac{10A_0^2}{3r_\lambda^{2/3}}. \tag{D.31}$$

Note that when $x \to 0$, this 1^{st} order solution can not been applied. It means the perturbative solution is not correct when the two-point distance r is very small, i.e. in the dissipative range.

Therefore, the general solution with 1^{st} order precision can be written as

$$D_\lambda(r_\lambda) = A_0 r_\lambda^{2/3} - \frac{10}{3}A_0^2 r_\lambda^{-2/3}. \tag{D.32}$$

We can also write this equation as the formulation r_η:

$$D_\eta(r_\eta) = C_0 r_\eta^{2/3} - \frac{10}{3}C_0^2 r_\eta^{-2/3}. \tag{D.33}$$

This formula does not depend on Reynolds number any more.

Higher order solutions can also been solved using the same method. For instance the solution with 4^{th} order precision is

$$D_\eta(r_\eta) = C_0 r_\eta^{2/3} - \frac{10}{3}C_0^2 r_\eta^{-2/3} - \frac{125}{9}C_0^3 r_\eta^{-2} - \frac{4750}{27}C_0^4 r_\eta^{-10/3} - \frac{290000}{81}C_0^5 r_\eta^{-14/3}. \tag{D.34}$$

The scaling exponent with 4^{th} order precision is

$$n = \frac{2}{3}\left(\frac{1 + \frac{10}{3}C_0 r_\eta^{-4/3} + \frac{125}{3}C_0^2 r_\eta^{-8/3} + \frac{23750}{27}C_0^3 r_\eta^{-12/3} + \frac{2030000}{81}C_0^4 r_\eta^{-16/3}}{1 - \frac{10}{3}C_0 r_\eta^{-4/3} - \frac{125}{9}C_0^2 r_\eta^{-8/3} - \frac{4750}{27}C_0^3 r_\eta^{-12/3} - \frac{290000}{81}C_0^4 r_\eta^{-16/3}}\right) \tag{D.35}$$

The scaling exponent is always larger than 2/3, and tends to 2/3 when $x \to \infty$. It is in agreement with Barenblatt's viewpoint. However in Barenblatt's paper, only a general expression is derived by using nondimensional analysis, in which the coefficients are not determined. Comparing with his work, this section shows an analytic scaling law considering the effect of molecular viscosity.

D.2 Comparison of the corrections with existing results

D.2.1 Comparison with the approximation of a constant skewness

In order to verify the analytical solutions, we compare them with the exact numerical solution of the original differential equation (D.11), i.e. the approximation of a constant skewness.

The comparisons in the dissipative range are shown in Fig. (D.2). The skewness value is fixed as $S_k(0) = -0.45$. The structure functions and the scaling exponents are shown respectively. Different orders of precision are shown. When r is small, the analytical solutions are in good agreement with the numerical solution. The 1^{st} order solution is satisfied in the range about $0 < r_\eta < 6$, and for the 4^{th} order solution it is about $0 < r_\eta < 10$.

Figure D.3 shows comparisons between the numerical solution and the perturbative solutions when $r \gg \eta$. The skewness value is fixed as $S_k(0) = -0.2$. The perturbative solutions are also in good agreement with the numerical solution. The solution of 1^{st} order precision is in good agreement when $r/\eta > 60$, and the solution of 4^{th} order precision is in good agreement when $r/\eta > 25$.

Note that these parameters are changeable with different values of skewness. The skewness value in dissipative range $S_k(0)$ can be obtained from spectral theory or experimental results, but there is no analytical result for the transition between dissipative range and inertial range. Tatarskii suggested an interpolation formula between this skewness value and the skewness in inertial range [161]. However, we do not know if his interpolation model is physical. In sum, we do not know the precise physical relations in the transition range. And in dissipative range and inertial range, seperately our analytical solutions are in good agreement.

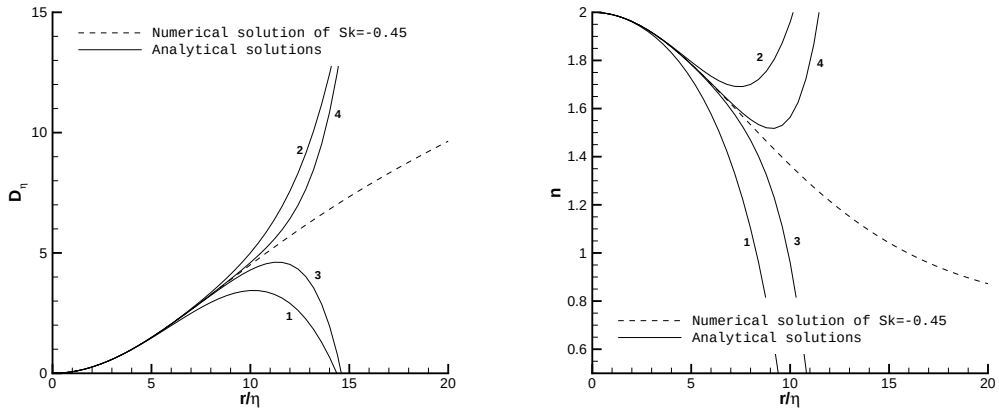

Figure D.2: Comparisons between the numerical solution and the analytical solutions in dissipative range. In each figure, the perturbative solutions have 1^{st} to 4^{th} order precisions, the numbers in the figure denote the orders respectively. (a) Structure functions. (b) Scaling exponents.

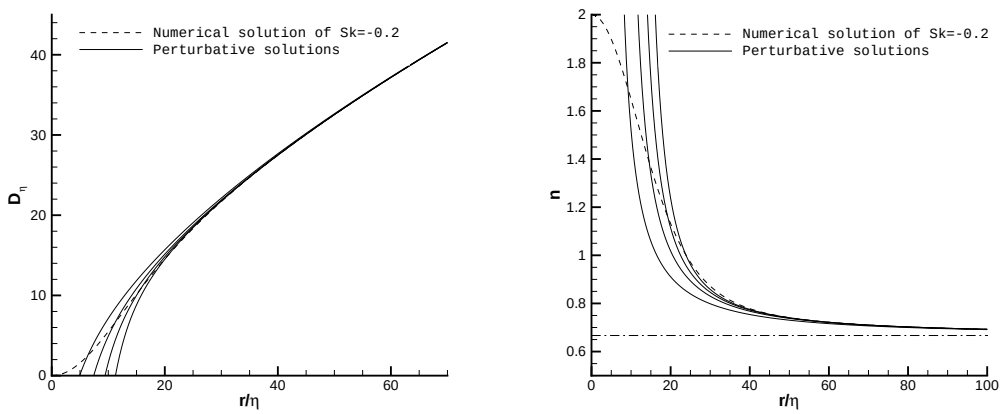

Figure D.3: Comparisons between the numerical solution and the perturbative solutions when $r \gg \eta$. In each figure, the perturbative solutions have 1^{st} to 4^{th} order precisions, from left to right respectively. (a) Structure functions. (b) Scaling exponents. The horizontal line is constant 2/3.

D.2.2 Comparison with Batchelor's formula

When r_η is small, Batchelor's formula (D.7) can be expanded using Taylor series:

$$D_\eta = 2C^{-4/3}r_\eta^2 - \frac{4}{3}C^{-4/3}r_\eta^4 + \frac{10}{9}C^{-16/3}r_\eta^6 - \frac{80}{81}C^{22/3}r_\eta^8 + ... \tag{D.36}$$

Comparing Eq. (D.36) with (D.17), the r^2 terms yields $2C^{-4/3} = 1/15$, i.e. $C = 30^{3/4} \approx 13$. This formula with constant value $C = 13$ has been applied widely in many researches [163, 164]. Indeed this constant value satisfies well the behavior of D_η, however, in this section we focus on the performance of scaling exponent n by using Batchelor's formula, which has not been investigated before.

Comparing Eq. (D.36) with the analytical solution of scaling exponent D.18, and ignoring the high-order terms, we can obtain:

$$\frac{6C^2 - 8r_\eta^2}{3C^2 - 2r_\eta^2} = \frac{48\sqrt{15} + 4S_k(0)r_\eta^2}{24\sqrt{15} + S_k(0)r_\eta^2}, \tag{D.37}$$

and the constant value C can be solve:

$$C = 4\sqrt{-\frac{\sqrt{15}}{S_k(0)}}. \tag{D.38}$$

If $C = 13$, we should have $S_k(0) \approx -0.38$. However, there is no proof that the value of $S_k(0)$ is always -0.38. In fact it can change with different Reynolds numbers [71]. For example in this paper we use $S_k(0) = -0.45$, and from Eq. (D.38) we obtain $C \approx 11.7$.

In Fig. D.4, Batchelor's interpolation formula (D.7) is compared with the numerical and analytical solutions of constant skewness. In the dissipative range we fix $S_k = -0.45$ and in inertial range $S_k = -0.2$. Both results of $C = 13$ and $C = 11.7$ are shown, and $C = 11.7$ is in better agreement with the $S_k = -0.45$ solutions in dissipative range (see the enlarged subfigure). From Fig. D.4 (a), we can find that Batchelor's formula denote a transition between the solutions of different values of skewness. The formula with $C = 11.7$ is in good agreement with the $S_k = -0.45$ solution in dissipative range, and also in agreement with the $S_k = -0.2$ solution in the range $r/\eta > 30$, i.e. the inertial range. Also our analytical solutions are good enough in these two ranges respectively, which are shown in Fig. D.4 (b).

The comparisons of the structure functions between Batchelor's formula the analytical solutions of constant skewness are shown in Fig. D.5. There is slight difference

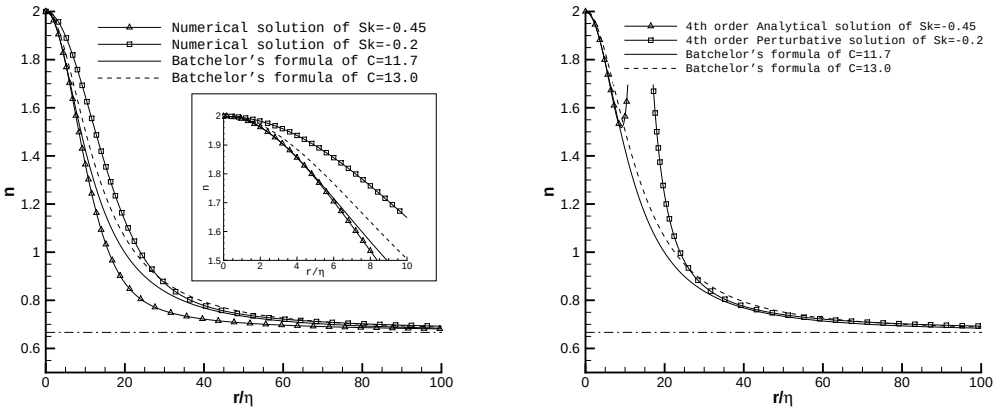

Figure D.4: Comparisons between Batchelor's formula and: (a) numerical solutions of constant skewness. (b) analytical solutions of constant skewness. The horizontal line is constant 2/3.

in small scales, since we changed the value of C and the relation $D_\eta \approx r_\eta^2/15$ is no longer satisfied. It means Batchelor's formula can not well simulate both the structure function and the scaling exponent. When we need the formula for structure function, $C = 13$ may be a good approach, but when representing the scaling exponent, $C = 11.7$ will be better and it can be determined by Eq. (D.38) if $S_k(0) \neq -0.45$.

Furthermore, in Fig. D.6 we can also find the agreement in inertial range is not perfect. In fact, Bathelor's formula is more closed as $S_k = -0.2$ solution in the range $30 < r/\eta < 80$, and almost equals to $S_k = -0.45$ solution when $r/\eta \approx 130$. It decreases much faster than the solutions of constant skewness, when r is large (for instance $r/\eta > 150$). It means Batchelor's formula does not strictly provide a constant skewness in inertial range. Thus we suggest the perturbative solutions of $S_k = -0.2$ in inertial range instead.

In brief, Bathelor's formula is an interpolation expression, which is not accurate enough to simulate both the structure function and the scaling exponent. In applications if the scaling exponent is needed, we propose Eq. (D.38) to obtain a better result.

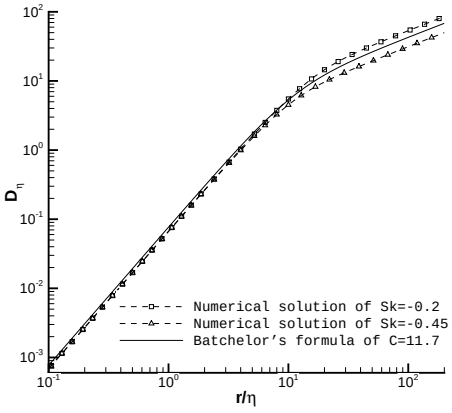

Figure D.5: Comparisons of the structure functions, between Batchelor's formula the numerical solutions of constant skewness.

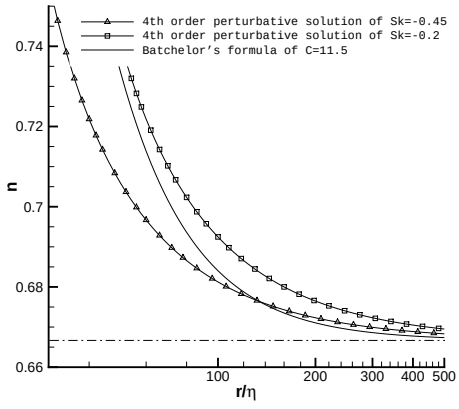

Figure D.6: Comparisons between Batchelor's formula the analytical solutions of constant skewness, in inertial range. The horizontal line is constant 2/3.

Appendix E

Time-reversibility of Navier-Stokes turbulence and its implication for subgrid-scale models

The complexity of turbulence is due to a wide range of nonlinearly interacting scales. The numerical simulation of a turbulent flow can in most practical application not take into account the full range of scales, due to limitations in computational resources. The principle of Large Eddy Simulation (LES) is that only the largest scales are computed directly. The influence of the scales smaller than a certain scale are modeled as a function of the resolved scales. To develop efficient subgrid models, criteria are needed, based on numerical stability and physical principles. It is important that these criteria are well defined and generally accepted. The purpose of this part is to investigate one of these criteria, which is the time-reversibility of a sub-grid model, when the sign of the velocity is inversed, *i.e.*, under the transformation $\boldsymbol{u} \rightarrow -\boldsymbol{u}$.

In the absence of viscosity, the dynamics of the Navier-Stokes equations (which reduce to the Euler equations), are time-reversible under the transformation $\boldsymbol{u} \rightarrow -\boldsymbol{u}$. This means that the flow will evolve backwards in time until the initial condition is reached. This can be understood since the nonlinear interactions, which govern the cascade of energy, are triple velocity correlations. The sign of these triple products is changed when the velocity is reversed, so that the nonlinear energy transfer proceeds in the opposite direction. This symmetry is broken as soon as viscous dissipation is introduced. Indeed, the conversion of kinetic energy to heat through the action of viscous stresses is an irreversible process within the macroscopic (continuum) description of turbulence.

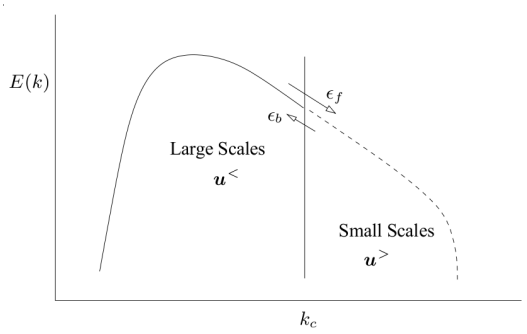

Figure E.1: Schematic representation of the LES approach. The large scales are resolved and the small scales as well as the spectral fluxes have to be modeled. Figure a modifier et a completer

If we consider LES, and we reverse the resolved velocity, it is not known what the subgrid-model is supposed to do. For certain models, the reversal of the velocity leads to a reversal of the subgrid-stress tensor, for others not. Indeed, the dynamic model [11] is time-reversible, in the sense that the direction of the energy flux at the filter-size reverses when the resolved velocity is reversed, whereas for the Smagorinsky [3] model this is not the case. For the latter model, the net flux of energy to the subgrid-scales ($\epsilon_f - \epsilon_b$, see Fig. E.1) cannot become negative. The time-reversibility property of, for example the dynamic model, is sometimes seen as a weakness, since the model becomes more easily (numerically) unstable. However it is well known that the backscatter of energy ϵ_b, to the resolved scales is a physical property, which should be taken into account in a correct model of the subgrid dynamics (see *e.g.* reference [165]). The amount of backscatter ϵ_b is not necessarily constrained to be inferior to the forward flux ϵ_f. A negative energy flux should therefore not *a priori* be excluded by a model. The problem with the dynamic model is that the total amount of energy which can flow back to the resolved scales is not constrained, so that an unphysical amount of energy can flow back into the large scales. Ghosal *et al.* [166] remedied this problem by basing the flux of energy to the small scales on the subgrid-scale energy, which was computed using a transport equation for the Reynolds averaged subgrid scales. This procedure implicitly assumes that the net energy flux from the resolved scales to the subgrid-scales is determined by the subgrid energy. This is one of the assumptions we will verify.

	$\boldsymbol{u}^< + \boldsymbol{u}^>$	$-\boldsymbol{u}^< - \boldsymbol{u}^>$	$-\boldsymbol{u}^< + \boldsymbol{u}^>$	$-\boldsymbol{u}^< + 0$
DNS cases	NN	RR	RN	RZ

Table E.1: The short names of different DNS cases.

In this appendix we will consider by direct numerical simulation (DNS) the dynamics of subgrid and resolved scale energy after transformation $\boldsymbol{u} \to -\boldsymbol{u}$. We will define a resolved velocity field, $\boldsymbol{u}^<$ and a subgrid velocity $\boldsymbol{u}^>$ (see Fig. E.1). In the DNS both velocities are computed and distinction between the two velocities is made by introducing a cut-off wavenumber k_c in Fourier-space, corresponding to the use of a low-pass filter. In LES the small scales are not known. It is therefore important to know how the resolved scales can be affected by different subgrid scale dynamics. We therefore compare three distinct cases with a freely decaying turbulent flow. In all three cases we apply $\boldsymbol{u}^< \to -\boldsymbol{u}^<$. The subgrid scales are transformed to first, $\boldsymbol{u}^> \to -\boldsymbol{u}^>$, second, $\boldsymbol{u}^> \to \boldsymbol{u}^>$ and third, $\boldsymbol{u}^> \to 0$. In each case we will study the evolution of the resolved scale energy.

Numerical results A group of DNS cases are implemented and shown in Table E.1 with spectral method. The computation domain has 256^3 grid. All cases simulate a free-decaying process from the same initial field, but at a certain time ($t = 0.81$ in our case): the Normal-Normal (NN) case keeps the velocity decaying without reversed; the Reverse-Reverse (RR) case reverses all scales; the Reverse-Normal (RN) case only reverses the resolved scale part and keeps the subgrid part; the Reverse-Zero (RZ) case reverses the resolved scale part and sets the subgrid part to be zero. The location of the filter can be found in Fig. E.2, in which the energy spectrum at the time of reversing is also shown.

The evolution of grid-scale energy is shown in Fig. E.3 (a). The time t is normalized by the turn-over time. The values of energy of the reversed cases are larger than the NN case after reversed, then they decay faster. The original NN case has a decaying rate at about $t^{-1.2}$, while the other cases have about t^{-2} when $t > 5$. This change of decaying rate is stem from the change of the shape of energy spectrum. The corresponding spectra at $t = 4.0$ are shown in Fig. E.4. The main difference between the reversed cases and the NN case is in the large scale $k < 8$. This difference of the

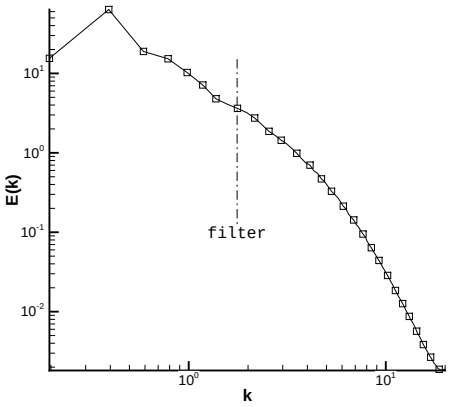

Figure E.2: Energy spectrum at the time of reversing $t = 0.81$. The vertical line is the location of filter.

energy-containing scale can affect the decaying rate [99]. It also means that all the reversed cases have strong energy backscatter, which transfers the energy from small to large scales.

In order to investigate the difference among the reversed cases, Fig. E.3 (b) shows the evolution of grid-scale energy around the reversing time. The RR case reverses all scales, as if the time is reversed, and the line is nearly symmetrical with the NN case when $0.81 < t < 1$. The grid-scale energy of the RR case then decreases because of the viscosity effect. The RN and RZ cases have quite similar behaviors after reversed, the grid-scale energy is nearly constant in that time range. It means that when the large scales are reversed, the unchanged small scales can neither drain energy from them nor produce energy to them anymore. It is just like if the were absent.

The evolution of subgrid-scale energy is shown in Fig. (E.5). The differences exist mainly in the range $0.81 < t < 2$. The RR and RN cases decrease very fast after reversed, since the grid-scale energy is reversed and provide less energy to the subgrid-scale part. However there is still the energy forward scatter, and the RZ case has increased subgrid energy.

Conclusion The thought-experiment in which the velocity at each point in a turbulent flow is reversed can be carried out in numerical simulations, and this is what we performed in this thesis. The general response of a turbulent flow on such a reversal is that the energy decay rate decreases temporarily. When only the large scales are

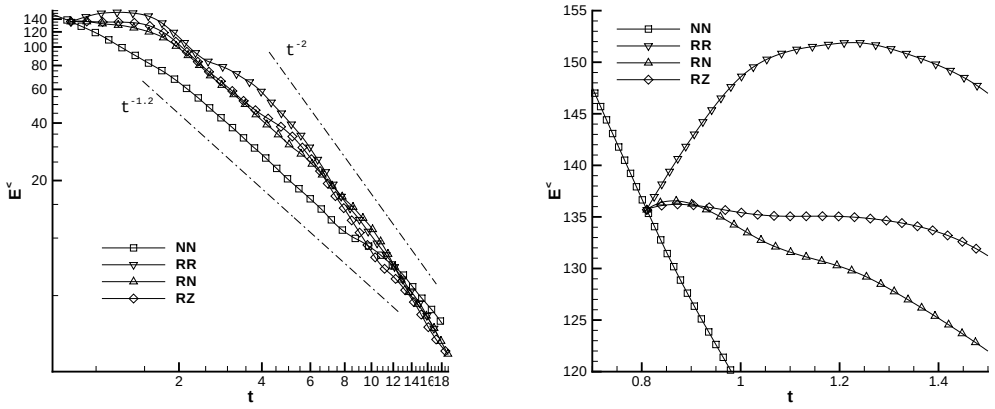

(a) (b)

Figure E.3: Evolution of grid-scale energy: (a) in the whole calculation. (b) around the point of reversing.

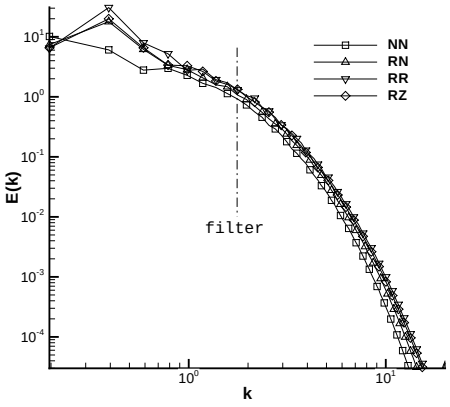

Figure E.4: Energy spectra of different cases at $t = 4.0$. The vertical line is the location of filter.

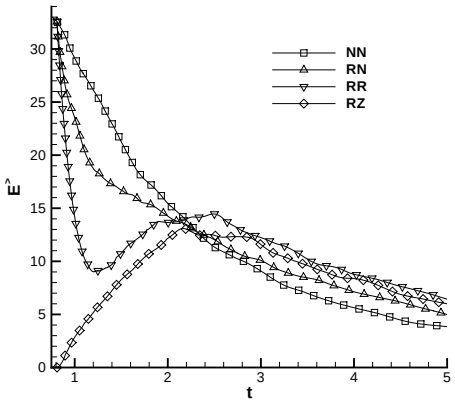

Figure E.5: Evolution of subgrid-scale energy.

considered, the dynamics depend to a certain extend on what happens at the small scales. In LES these scales are not known. The thought experiment described here can therefore not serve as a strict criterion on subgrid-scale models. It should be decided by the developer or user of a subgrid model, what he expects from the model. If he expects the model to work in the different test-cases described here, he should give some input about the unknown scales to the model.

Appendix F

A rapid algorithm for Tophat filter operator in discrete field

Tophat filter operator is widely applied in many sciences. However, when the filter size is large, the filter operator is of low efficiency. We design a rapid algorithm on the tophat filter in discrete field, and the algorithm details are shown in 3-D and 2-D cases respectively. For 3-D filters, the algorithm complexity is reduced from $O(n^3\Delta^3)$ to $O(n^3)$; for 2-D filters, the algorithm complexity is reduced from $O(n^2\Delta^2)$ to $O(n^2)$. Thus from the rapid algorithm, the complexity is independent of the filter size, but only related with the size of filtered field.

We take the 3-D case as example. Let a_{xyz} represents the original physical value at coordinate (x, y, z), and $\overline{a}_{xyz}$ represents the filtered value. A discrete Tophat filter with filter size 2Δ could be defined as

$$\overline{a}_{xyz} = \frac{1}{8\Delta^3} \sum_{i=x-\Delta}^{x+\Delta} \sum_{j=y-\Delta}^{y+\Delta} \sum_{k=z-\Delta}^{z+\Delta} a_{ijk}. \tag{F.1}$$

In order to make a filter operation on the whole $n \times n \times n$ field, the algorithm complexity is $O(n^3\Delta^3)$. When Δ is large, this algorithm costs too much. Similarly, 2-D discrete Tophat filter could be written as

$$\overline{a}_{xy} = \frac{1}{4\Delta^2} \sum_{i=x-\Delta}^{x+\Delta} \sum_{j=y-\Delta}^{y+\Delta} a_{ij}. \tag{F.2}$$

A filter operation on a $n \times n$ field costs $O(n^2\Delta^2)$ time.

Simple Moving Average and its 1-D applications

Moving average is a statistical technique used to analyze a set of data points by creating an average of one subset of the full data set at a time. It has different formulations, with different types of weights. A simple moving average (SMA) is the unweighted mean of the previous n data points. For example, a n-day simple moving average of price is the mean of the previous n days' prices:

$$\mathrm{SMA} = \frac{1}{n} \sum_{i=M-n+1}^{M} p_i, \tag{F.3}$$

where p_i is the price of the i^{th} day. When calculating successive values, a new value comes into the sum and an old value drops out, meaning a full summation each time is unnecessary:

$$\mathrm{SMA}_{M+1} = \mathrm{SMA}_M - \frac{p_{M-n+1}}{n} + \frac{p_{M+1}}{n}. \tag{F.4}$$

SMA is often used in technical analysis of financial data, like stock prices, returns or trading volumes. It is also used in economics to examine gross domestic product, employment or other macroeconomic time series.

The similar method could be applied to simplify the discrete Tophat filter. Taking 3-D case as example, we consider any direction (for instance, x direction) as a time series, and could obtain

$$\overline{a}_{(x+1)yz} - \overline{a}_{xyz} = \frac{1}{8\Delta^3} \left(\sum_{j=y-\Delta}^{y+\Delta} \sum_{k=z-\Delta}^{z+\Delta} a_{(x+1+\Delta)jk} - \sum_{j=y-\Delta}^{y+\Delta} \sum_{k=z-\Delta}^{z+\Delta} a_{(x-\Delta)jk} \right). \tag{F.5}$$

Therefore, at any straight line in x direction, only one $\overline{a}_{xyz}$ value is needed to be calculated, and other values could be obtained using this recursive relation. However, the time complexity is $O(n^3\Delta^2)$ and should be further optimized.

Rapid algorithm for 3-D Tophat filter operator in the whole discrete field

We define

$$b_{xyz} = 8\Delta^3 \overline{a}_{xyz}. \tag{F.6}$$

This time complexity of calculating the b_{xyz} value at one point is $O(\Delta^3)$. According to equation (F.1), the following relations of dimensionality reduction are satisfied:

$$\delta^{(x)}_{xyz} = b_{(x+1)yz} - b_{xyz} = \sum_{j=y-\Delta}^{y+\Delta}\sum_{k=z-\Delta}^{z+\Delta} a_{(x+1+\Delta)jk} - \sum_{j=y-\Delta}^{y+\Delta}\sum_{k=z-\Delta}^{z+\Delta} a_{(x-\Delta)jk} \tag{F.7a}$$

$$\delta^{(y)}_{xyz} = b_{x(y+1)z} - b_{xyz} = \sum_{i=x-\Delta}^{x+\Delta}\sum_{k=z-\Delta}^{z+\Delta} a_{i(y+1+\Delta)k} - \sum_{i=x-\Delta}^{x+\Delta}\sum_{k=z-\Delta}^{z+\Delta} a_{i(y-\Delta)k} \tag{F.7b}$$

$$\delta^{(z)}_{xyz} = b_{xy(z+1)} - b_{xyz} = \sum_{i=x-\Delta}^{x+\Delta}\sum_{j=y-\Delta}^{y+\Delta} a_{ij(z+1+\Delta)} - \sum_{i=x-\Delta}^{x+\Delta}\sum_{j=y-\Delta}^{y+\Delta} a_{ij(z-\Delta)} \tag{F.7c}$$

The time complexity of calculating the $\delta^{(x)}_{xyz}, \delta^{(y)}_{xyz}, \delta^{(z)}_{xyz}$ values at one point is $O(\Delta^2)$. Therefore, the complexity at single point is reduced. Similarly we could obtain

$$\begin{aligned}
\delta^{(xy)}_{xyz} =& \delta^{(x)}_{x(y+1)z} - \delta^{(x)}_{xyz} = \delta^{(y)}_{(x+1)yz} - \delta^{(y)}_{xyz} \\
=& \sum_{k=z-\Delta}^{z+\Delta} a_{(x+1+\Delta)(y+1+\Delta)k} - \sum_{k=z-\Delta}^{z+\Delta} a_{(x+1+\Delta)(y-\Delta)k} \\
&- \sum_{k=z-\Delta}^{z+\Delta} a_{(x-\Delta)(y+1+\Delta)k} + \sum_{k=z-\Delta}^{z+\Delta} a_{(x-\Delta)(y-\Delta)k}
\end{aligned} \tag{F.8a}$$

$$\begin{aligned}
\delta^{(xz)}_{xyz} =& \delta^{(x)}_{xy(z+1)} - \delta^{(x)}_{xyz} = \delta^{(z)}_{(x+1)yz} - \delta^{(z)}_{xyz} \\
=& \sum_{j=y-\Delta}^{y+\Delta} a_{(x+1+\Delta)j(z+1+\Delta)} - \sum_{j=y-\Delta}^{y+\Delta} a_{(x+1+\Delta)j(z-\Delta)} \\
&- \sum_{j=y-\Delta}^{y+\Delta} a_{(x-\Delta)j(z+1+\Delta)} + \sum_{j=y-\Delta}^{y+\Delta} a_{(x-\Delta)j(z-\Delta)}
\end{aligned} \tag{F.8b}$$

$$\begin{aligned}
\delta^{(yz)}_{xyz} =& \delta^{(y)}_{xy(z+1)} - \delta^{(y)}_{xyz} = \delta^{(z)}_{x(y+1)z} - \delta^{(z)}_{xyz} \\
=& \sum_{i=x-\Delta}^{x+\Delta} a_{i(y+1+\Delta)(z+1+\Delta)} - \sum_{i=x-\Delta}^{x+\Delta} a_{i(y+1+\Delta)(z-\Delta)} \\
&- \sum_{i=x-\Delta}^{x+\Delta} a_{i(y-\Delta)(z+1+\Delta)} + \sum_{i=x-\Delta}^{x+\Delta} a_{i(y-\Delta)(z-\Delta)}
\end{aligned} \tag{F.8c}$$

Finally

$$\begin{aligned}\delta_{xyz}^{(xyz)} =& \delta_{xy(z+1)}^{(xy)} - \delta_{xyz}^{(xy)} = \delta_{x(y+1)z}^{(xz)} - \delta_{xyz}^{(xz)} = \delta_{(x+1)yz}^{(yz)} - \delta_{xyz}^{(yz)} \\ =& a_{(x+1+\Delta)(y+1+\Delta)(z+1+\Delta)} - a_{(x-\Delta)(y+1+\Delta)(z+1+\Delta)} \\ & - a_{(x+1+\Delta)(y-\Delta)(z+1+\Delta)} - a_{(x+1+\Delta)(y+1+\Delta)(z-\Delta)} \\ & + a_{(x-\Delta)(y-\Delta)(z+1+\Delta)} + a_{(x-\Delta)(y+1+\Delta)(z-\Delta)} \\ & + a_{(x+1+\Delta)(y-\Delta)(z-\Delta)} - a_{(x-\Delta)(y-\Delta)(z-\Delta)}\end{aligned} \tag{F.9}$$

Notice that every former equation contains two relations: the recursive relation between two dimensions, for instance $\delta_{xyz}^{(z)} = b_{xy(z+1)} - b_{xyz}$, from which we could obtain the results of higher dimension by knowing whole field of lower dimension and one point of higher dimension; another relation is the equation for calculating in certain dimension, for instance $\delta_{xyz}^{(z)} = \sum_{i=x-\Delta}^{x+\Delta} \sum_{j=y-\Delta}^{y+\Delta} a_{ij(z+1+\Delta)} - \sum_{i=x-\Delta}^{x+\Delta} \sum_{j=y-\Delta}^{y+\Delta} a_{ij(z-\Delta)}$. Notice that the complexity of calculating $\delta_{xyz}^{(x)}$, $\delta_{xyz}^{(y)}$, $\delta_{xyz}^{(z)}$ at one point is $O(n^2)$, the complexity of calculating $\delta_{xyz}^{(xy)}$, $\delta_{xyz}^{(xz)}$, $\delta_{xyz}^{(yz)}$ at one point is $O(n)$, and the complexity of calculating $\delta_{xyz}^{(xyz)}$ at one point is $O(1)$. Therefore, we could calculate the $\delta_{xyz}^{(xyz)}$ values in the whole field only at zero-dimension, and calculate a part of values at higher dimensions, and obtain the other values from the recursive relations.

According these analysis, the algorithm for 3-D Tophat filter operator in the whole discrete field could be described as:

1) Calculate the variables needed for recursive iterations.

- From equation (F.9): calculate the $\delta_{xyz}^{(xyz)}$ values in the whole field.
- From equation (F.8): calculate the $\delta_{xyz}^{(xy)}$ values in any $x-y$ plane; calculate the $\delta_{xyz}^{(xz)}$ values in any $x-z$ plane; calculate the $\delta_{xyz}^{(yz)}$ values in any $y-z$ plane.
- From equation (F.7): calculate the $\delta_{xyz}^{(x)}$ values in any straight line at x direction; calculate the $\delta_{xyz}^{(y)}$ values in any straight line at y direction; calculate the $\delta_{xyz}^{(z)}$ values in any straight line at z direction.
- From equation (F.1) and (F.6): calculate the b_{xyz} value at any point.

The time complexities of these operations are no more than $O(n^3)$.

2) Recursive calculations.

- Calculate the $\delta_{xyz}^{(xy)}$ values in the whole field, according to the recursive relation in equation (F.9), the $\delta_{xyz}^{(xyz)}$ values in the whole field and the $\delta_{xyz}^{(xy)}$ values at a $x-y$ plane, which are obtained in the last step. Similarly we could calculate the $\delta_{xyz}^{(xz)}$ and $\delta_{xyz}^{(yz)}$ values in the whole field.

- Calculate the $\delta_{xyz}^{(x)}$ values in the whole field, according to the recursive relation in equation (F.8), the $\delta_{xyz}^{(xy)}$ and the $\delta_{xyz}^{(xz)}$ values in the whole field and the $\delta_{xyz}^{(x)}$ values at a straight line of x direction, which are obtained in the last step. Similarly we could calculate the $\delta_{xyz}^{(y)}$ and $\delta_{xyz}^{(z)}$ values in the whole field.

- Calculate the b_{xyz} values in the whole field, according to the recursive relation in equation (F.7), the $\delta_{xyz}^{(x)}$, $\delta_{xyz}^{(y)}$ and $\delta_{xyz}^{(z)}$ values in the whole field and the b_{xyz} values at a point, which are obtained in the last step.

The time complexities of these operations are $O(n^3)$.

3) From equation (F.6) calculate the $\overline{a}_{xyz}$ values in the whole field.

Therefore, the algorithm is $O(n^3)$. When the filter size if large, the calculation efficiency is improved.

Rapid algorithm for 2-D Tophat filter operator in the whole discrete field

The algorithm of 2-D case is similar with the 3-D case. Thus here we only write the steps of the algorithm. All the variables are named as the same as in 3-D case. $b_{xy} = 4\Delta^2 \overline{a}_{xy}$.

1) Calculate the variables needed for recursive iterations.

- Calculate the $\delta_{xy}^{(xy)}$ values in the whole field.

- Calculate the $\delta_{xy}^{(x)}$ values in any straight line at x direction; calculate the $\delta_{xy}^{(y)}$ values in any straight line at y direction.

- Calculate the b_{xy} value at any point.

2) Recursive calculations.

- Calculate the $\delta_{xy}^{(x)}$ values in the whole field, according to the recursive relation, the $\delta_{xy}^{(xy)}$ values in the whole field and the $\delta_{xy}^{(x)}$ values at a straight line of x direction, which are obtained in the last step. Similarly we could calculate the $\delta_{xy}^{(y)}$ values in the whole field.

- Calculate the b_{xy} values in the whole field, according to the recursive relation, the $\delta_{xy}^{(x)}$ and $\delta_{xy}^{(y)}$ values in the whole field and the b_{xy} values at a point, which are obtained in the last step.

3) Calculate the $\overline{a}_{xy}$ values in the whole field.

Therefore, the algorithm is $O(n^2)$. When the filter size if large, the calculation efficiency is improved.

Bibliography

[1] S. Pope. *Turbulent Flows*. Cambridge University Press, 2000.

[2] P. Sagaut. *Large eddy simulation for imcompressible flows*. Springer, 2006.

[3] J. Smagorinsky. General circulation experiments with primitive equation. *Monthly Weather Review*, 91:99, 1963.

[4] J. Bardina, J. Ferziger, and W.C. Reynolds. Improved subgrid-scale models for large-eddy simulation. *AIAA paper*, pages 80–1357, 1987.

[5] A. Leonard. Energy cascade in large-eddy simulations of turbulent flows. *Advances in Geophysics*, A18:237, 1974.

[6] C. Brun, R. Friedrich, and C.B. da Silva. A non-linear SGS model based on the spatial velocity increment. *Theoretical and Computational Fluid Dynamics*, 20:1, 2006.

[7] C. Meneveau and J. Katz. Scale-invariance and turbulence models for large-eddy simulation. *Annual Reviews in Fluid Mechanics*, 32:1–32, 2000.

[8] M. Lesieur. *Turbulence in Fluids*. Kluwer Academic, Dordrecht, 1997.

[9] A. N. Kolmogorov. The local structure of turbulence in incompressible viscous fluid for very large reynolds number. *Proceedings: Mathematical and Physical Sciences*, 30:301, 1941.

[10] J.P. Boris, F.F. Grinstein, E.S. Oran, and R.J. Kolbe. New insights into large-eddy simulation. *Fluid Dynamics Research*, 10:199–228, 1992.

[11] M. Germano, U. Piomelli, P. Moin, and W.H. Cabot. A dynamic subgrid-scale eddy viscosity model. *Physics of Fluids A*, 3(7):1760–1765, 1991.

[12] M. Germano. Turbulence. the filtering approach. *Journal of Fluid Mechanics*, 238:325–336, 1992.

[13] Bernard J. Geurts. Inverse modeling for large-eddy simulation. *Physics of Fluids*, 9(12):3585–3587, 1997.

[14] B. J. Geurts and D. Holm. Regularization modeling for large-eddy simulations of turbulence. *Journal of Computational Physics*, 15:L13–L16, 2003.

[15] R. H. Kraichnan. Inertial range spectrum in hydromagnetic turbulence. *Physics of Fluids*, 9:1728, 1965.

[16] R.H. Kraichnan. Inertial ranges in two-dimensional turbulence. *Physics of Fluids*, 10(7):1417–1423, 1967.

[17] C. Meneveau. Statistics of turbulence subgrid-scale stresses: Necessary conditions and experimental tests. *Physics of Fluids*, 6(2):815–833, 1994.

[18] S. Liu, C. Meneveau, and J. Katz. On the properties of similarity subgrid-scale models as deduced from measurements in a turbulent jet. *Journal of Fluid Mechanics*, 275:83, 1994.

[19] A.W. Cook. Determination of the constant coefficient in scale similarity models. *Physics of Fluids*, 9:1485–1487, 1997.

[20] M. Germano. Ten years of the dynamic model. In *Modern simulation strategies for turbulent flow*, 2001.

[21] M. Germano. Fundamentals of large-eddy simulation. In *Advanced turbulent flows computations*, 1998.

[22] J. A. Domaradzki and D. D. Holm. The Navier-Stokes-alpha model: LES equations with nonlinear dispersion. In *Modern simulation strategies for turbulent flow*, 2001.

[23] F. Waleffe. The nature of triad interactions in homogeneous turbulence. *Physics of Fluids A*, 4(2):350–363, 1992.

[24] U. Piomelli, W.H. Cabot, P. Moin, and S. Lee. Subgrid backscatter in turbulent and transitional flows. *Physics of Fluids A*, 3:1766, 1991.

[25] J.A. Domaradzki and E.M. Saiki. A subgrid-scale model based on the estimation of unresolved scales of turbulence. *Physics of Fluids*, 9(2):2148–2164, 1997.

[26] C. Hartel, L. Kleiser, F. Unger, and R. Friedrich. Subgrid-scale energy transfer in the near-wall region of turbulent flows. *Physics of Fluids*, 6(9):3130–3143, 1994.

[27] S.A. Orszag. Analytical theories of turbulence. *Journal of Fluid Mechanics*, 41(2):363–386, 1970.

[28] J.P. Chollet and M. Lesieur. Parametrization of small scales of three-dimensional isotropic turbulence utilizing spectral closures. *Journal of the Atmospheric Sciences*, 38:2747–2757, 1981.

[29] O. Métais and M. Lesieur. Spectral large-eddy simulation of isotropic and stably stratified turbulence. *Joural of Fluid Mechanics*, 239:157–194, 1992.

[30] J. P. Bertoglio. A stochastic subgrid model for sheared turbulence. In *Proceedings of macroscopic modelling of turbulent flows, Lecture notes in physics, Vol.230*, pages 100–119, 1985.

[31] A. M. Yaglom. On the local structure of temperature field in a turbulent flow. *Dokl. Akad. Nauk. SSSR*, 69:743, 1949.

[32] R. Benzi, G. Paladin, G. Parisi, and A. Vulpiani. On the multifractal nature of fully developed turbulence and chaotic system. *Journal of Physics A*, 17:3521, 1984.

[33] C. Meneveau and K.R. Sreenivasan. Simple multifractal cascade model for fully developed turbulence. *Physics Review Letters*, 59:1424, 1987.

[34] Z. S. She and E. Leveque. Universal scaling law in fully developed turbulence. *Physics Review Letters*, 72:336, 1994.

[35] U. Frisch, P. Sulem, and M. Nelkin. A simple dynamical model of intermittent fully developed turbulence. *Journal of Fluid Mechanics*, 87:719, 1978.

[36] Roberto Benzi, Sergio Ciliberto, Cristophe Baudet, and G.R. Chavarria. On the scaling of three-dimensional homogeneous and isotropic turbulence. *Physica D*, 80:385–398, 1995.

[37] G.I. Barenblatt, A.J. Chorin, and V.M. Prostokishin. Comment on the paper "on the scaling of three-dimensional homogeneous and isotropic turbulence" by benzi et al. *Physica D*, 127:105–110, 1999.

[38] G.X. Cui, H.B. Zhou, Z.S. Zhang, and L. Shao. A new dynamic subgrid eddy viscosity model with application to turbulent channel flow. *Physics of Fluids*, 16(8):2835–2842, 2004.

[39] L. Shao, J. P. Bertoglio, G. X. Cui, H. B. Zhou, and Z. S. Zhang. Kolmogorov equation for LES and its use for subgrid modeling. In *Direct and Large-Eddy Simulation V*, 2004.

[40] G.X. Cui, C.X. Xu, L. Fang, L. Shao, and Z.S. Zhang. A new subgrid eddy-viscosity model for large-eddy simulation of anisotropic turbulence. *Journal of Fluid Mechanics*, 582:377–397, 2007.

[41] L. Fang, J. Boudet, and L. Shao. Les échanges inter-echelles en simulation des grandes échelles. 18^e *Congrés Français de Mécanique*, 2007.

[42] L. Fang, L. Shao, J.P. Bertoglio, G. Cui, C. Xu, and Z. Zhang. An improved velocity increment model based on kolmogorov equation of filtered velocity. *Physics of Fluids*, 21(6):065108, 2009.

[43] L. Fang, L. Shao, J.P. Bertoglio, G.X. Cui, C. X. Xu, and Z.S. Zhang. An improvement of increment model by using kolmogorov equation of filtered velocity. In *DLES 8*, 2008.

[44] S. Ghosal and P. Moin. The basic equations of large eddy simulation of turbulent flows in complex geometry. *Journal of Computational Physics*, 118:24, 1995.

[45] O.V. Vasilyev, T.S. Lund, and P. Moin. A general class of commutative filters for LES in complex geometries. *Journal of Computational Physics*, 146:82–104, 1998.

[46] A.L. Marsden and O.V. Vasilyev. Commutative filters for LES on unstructured meshes. *Center for Turbulence Research, Annual Research Briefs*, pages 389–402, 1999.

[47] S. Leonard, M. Terracola, and P. Sagaut. Commutation error in LES with time-dependent filter width. *Computers and Fluids*, 36(3):513–519, 2007.

[48] L. Shao, S. Sarkar, and C. Pantano. On the relationship between the mean flow and subgrid stresses in large eddy simulation of turbulent shear flows. *Physics of Fluids*, 11(5):1229–1248, 1999.

[49] G. K. Batchelor. *The theory of homogeneous turbulence*. Cambridge University Press, 1953.

[50] O. M. Phillips. Shear-flow turbulence. *Annual Review of Fluid Mechanics*, 1:245–264, 1969.

[51] Hinze. *Turbulence*. McGraw-Hill, 2 edition, 1975.

[52] J. L. Lumley. Spectral energy budget in wall turbulence. *Physics of Fluids*, 7:190–196, 1964.

[53] J. L. Lumley and H. A. Panofsky. The structure of atmospheric turbulence. In *Interscience Monographs and Texts in Physics and Astronomy, New York*, 1964.

[54] R.S. Rogallo. *Numerical experiments in homogeneous turbulence*. NASA TM 81315, 1981.

[55] P. Gualtieri, C.M. Casciola, R. Benzi, and R. Piva. Preservation of statistical properties in large-eddy simulation of shear turbulence. *Journal of Fluid Mechanics*, 592:471–494, 2007.

[56] D.J. Thomson. A stochastic model for the motion of particle pairs in isotropic high-reynolds-number turbulence, and its application to the problem of concentration variance. *Joural of Fluid Mechanics*, 210:113–153, 1990.

[57] P.S. Bernard and A.L.Rovelstad. On the physical accuracy of scalar transport modeling in inhomogeneous turbulence. *Physics of Fluids*, 6(9):3093–3108, 1994.

[58] A. N. Kolmogorov. A refinement of previous hypotheses concerning the local structure of turbulence. *Journal of Fluid Mechanics*, 13:82:85, 1962.

[59] A. M. Obukhov. Turbulence in thermally inhomogeneous atmosphere. *Trudy Inst. Teor. Geophys. Acad. Nauk*, 1:95, 1946.

[60] Stanley Corrsin. On the spectrum of isotropic temperature field in isotropic turbulence. *Journal of Applied Physics*, 22:468, 1951.

[61] A. A. Townsend. Local isotropy in the turbulent wake of a cylinder. *Australian Journal of Scientific Research, Series A*, 1:161, 1948.

[62] M. S. Uberoi. Equipartition of energy and local isotropy in turbulent flows. *Journal of Applied Physics*, 28(10):1165, 1957.

[63] A. A. Townsend. *The Structure of Turbulent Shear Flow*. Cambridge University Press, 1980.

[64] P. Mestayer. Local isotropy and anisotropy in a high-reynolds-number turbulent boundary layer. *Journal of Fluid Mechanics*, 125:475–503, 1982.

[65] I. Arad, B. Dhruva, S. Kurien, V. S. L'vov, I. Procaccia, and K. R. Sreenivasan. Extraction of anisotropic contributions in turbulent flows. *Physical Review Letters*, 81:5330–5333, 1998.

[66] I. Arad, V. S. L'vov, and I. Procaccia. Correlation functions in isotropic and anisotropic turbulence: The role of the symmetry group. *Physical Review E*, 59(6):6753–6765, 1999.

[67] L. Biferale and M. Vergassola. Isotropy vs anisotropy in small-scale turbulence. *Physics of Fluids*, 13:2139, 2001.

[68] S. Kurien and K. R. Sreenivasan. Anisotropic scaling contributions to high-order structure functions in high-reynolds-number turbulence. *Physical Review E*, 62(2):2206, 2000.

[69] X. Shen and Z. Warhaft. Longitudinal and transverse structure functions in sheared and unsheared wind-tunnel turbulence. *Physics of Fluids*, 14:370, 2002.

[70] E. Lévêque, F. Toschi, L. Shao, and J.P. Bertoglio. Shear-improved Smagorinsky model for large-eddy simulation of wall-bounded turbulent flows. *Journal of Fluid Mechanics*, 570:491–502, 2007.

[71] C. W. Van Atta and R. A. Antonia. Reynolds number dependence of skewness and flatness factors of turbulent velocity derivatives. *Physics of Fluids*, 23(2):252–257, 1980.

[72] R. J. Driscoll and L. A. Kennedy. Spectral transfer and velocity derivative skewness equation for a turbulent velocity field. *Physics of Fluids*, 24:1428–1430, 1981.

[73] P. Tabeling, G. Zocchi, F. Belin, J. Maurer, and H. Willaime. Probability density functions, skewness, and flatness in large reynolds number turbulence. *Physical Review E*, 53(2):1613–1621, 1996.

[74] S. Cerutti, C. Meneveau, and O. M. Knio. Spectral and hyper eddy viscosity in high-reynolds-number turbulence. *Journal of Fluid Mechanics*, 421:307–338, 2000.

[75] C. Cambon, N. N. Mansour, and F. S. Godeferd. Energy transfer in rotating turbulence. *Journal of Fluid Mechanics*, 337:303, 1997.

[76] L. Jacquin, O. Leuchter, C. Cambon, and J. Mathieu. Homogeneous turbulence in the presence of rotation. *Journal of Fluid Mechanics*, 220:1, 1990.

[77] C. Cambon, R. Rubinstein, and F. S. Godeferd. Advances in wave turbulence: rapidly rotating flows. *New Journal of Physics*, 6:73, 2004.

[78] L. Shao, Z. S. Zhang, G. X. Cui, and C. X. Xu. Subgrid modeling of anisotropic rotating homogeneous turbulence. *Physics of Fluids*, 17(11):115106.1–115106.7, 2005.

[79] F. Anselmet, Y. Gagne, E.J. Hopfinger, and R.A. Antonia. High-order velocity structure functions in turbulent shear flows. *Journal of Fluid Mechanics*, 140:63, 1984.

[80] C. Meneveau and K.R. Sreenivasan. The multifractal nature of energy dissipation. *Journal of Fluid Mechanics*, 224:429, 1991.

[81] Y. Gagne. *Etude experimentale de l'intermittence et des singularities dans le plan complexe en turbulence developpe.* PhD thesis, Universite de Grenoble, 1987.

[82] G. Strolovitzky, P. Kailasnath, and K.R. Sreenivasan. Kolmogorov refined similarity hypothesis. *Physics Review Letters*, 69:1178, 1992.

[83] M. Germano. A direct relation between the filtered subgrid stress and the second order structure function. *Physics of Fluids*, 19(3):038102, 2007.

[84] S. A. Orszag. *Lectures on the statistical theory of turbulence.* 1974.

[85] M. Lesieur and O. Metais. New trends in large-eddy simulations of turbulence. *Annual Reviews in Fluid Mechanics*, 28:45–82, 1996.

[86] D. K. Lilly. *The representation of small scale turbulence in numerical simulation experiments. Lecture notes on turbulence.* World Scientific, 1987.

[87] R.A. Clark, J.H. Ferziger, and W.C. Reynolds. Evaluation of subgrid-scale models using an accurately simulated turbulent flow. *Journal of Fluid Mechanics*, 91:1, 1979.

[88] J. W. Deardoff. A numerical study of three-dimensional turbulent channel flow at large reynolds numbers. *Journal of Fluid Mechanics*, 41:453–465, 1970.

[89] J. O'Neil and C. Meneveau. Subgrid-scale stresses and their modelling in a turbulent plane wake. *Journal of Fluid Mechanics*, 349:253, 1997.

[90] W. D. McComb. *The physics of fluid turbulence.* Clarendon Press, Oxford, 1990.

[91] A. Yoshizawa. Eddy-viscosity-type subgrid-scale model with a variable smagorinsky coefficient and its relationship with the one-equation model in large eddy simulation. *Physics of Fluids*, 3(8):2007–2009, 1991.

[92] R.D. Moser, J. Kim, and N.N. Mansour. Direct numerical simulation of turbulent channel flow up to $\mathrm{Re}_\tau = 590$. *Physics of Fluids*, 11:943, 1999.

[93] V. M. Canuto and Y. Cheng. Determination of the smagorinsky-lilly constant cs. *Physics of Fluids*, 9(5):1368–1378, 1997.

[94] A. S. Monin and A. M. Yaglom. *Statistical Fluid Mechanics. Mechanics of Turbulence, Vol 2.* MIT Press, 1975.

[95] R. J. Hill. Exact second-order structure function relationship. *Journal of Fluid Mechanics*, 468:303, 2002.

[96] C.M. Casciola, P. Gualtieri, R. Benzi, and R. Piva. Scale-by-scale budget and similarity laws for shear turbulence. *Journal of Fluid Mechanics*, 476:105–114, 2003.

[97] X. Yang and J. A. Domaradzki. Large eddy simulation of decaying turbulence. *Physics of Fluids*, 16(11):4088, 2004.

[98] L. Skrbek and S. R. Stalp. On the decay of homogeneous turbulence. *Physics of Fluids*, 12(8):1997, 2000.

[99] H. Touil, J.P. Bertoglio, and L. Shao. The decay of turbulence in a bounded domain. *Journal of Turbulence*, 3(1):49, 2002.

[100] H. Kawamura, H. Abe, and Y. Matsuo. DNS of turbulent heat transfer in channel flow with respect to reynolds and prandtl number effects. *International Journal of Heat and Fluid Flow*, 20:196–207, 1999.

[101] C. X. Xu, Z. S. Zhang, and F. T. M. Nieuwstadt. Origin of high kurtosis in viscous sublayer. *Physics of Fluids*, 8:1938–1942, 1996.

[102] K. Horiuti. Transformation properties of dynamic subgrid-scale models in a frame of reference undergoing rotation. *Journal of Turbulence*, 7:1, 2006.

[103] B. J. Geurts. *Elements of Direct and Large-Eddy Simulation*. Edwards, 2004.

[104] C. Brun and R. Friedrich. Modelling the SGS tensor Tij: An issue in the dynamin approach. *Physics of Fluids*, 13(8):2373–2385, 2001.

[105] M. V. Salvetti and F. Beux. The effect of the numerical scheme on the subgrid-scale term in large-eddy simulation. *Physics of Fluids*, 10:3020, 1998.

[106] G. S. Winckelmans, A. A. Wray, O. V. Vasilyev, and H. Jeanmart. Explicit-filtering large-eddy simulation using the tensor-diffusivity model supplemented by a dynamic smagorinsky term. *Physics of Fluids*, 13(5):1385–1403, 2001.

[107] V. Borue and S. A. Orszag. Local energy flux and subgrid-scale statistics in three-dimensional turbulence. *Journal of Fluid Mechanics*, 366:1–31, 1998.

[108] U Frisch. *Turbulence. The legacy of A. N. Kolmogorov*. Cambridge University Press, 1995.

[109] B. Vreman, B. Geurts, and H. Kuerten. Large-eddy simulation of the temporal mixing layer using the clark model. *Theoretical and Computational Fluid Dynamics*, 8(4):309–324, 1996.

[110] G. Comte-Bellot and S. Corrsin. The use of contraction to improve the isotropy of grid generated turbulence. *Journal of Fluid Mechanics*, 25:657, 1966.

[111] D. C. Leslie and G. L. Quarini. The application of turbulence theory to the formulation of subgrid modeling procedures. *Journal of Fluid Mechanics*, 91:75, 1979.

[112] C. E. Leith. Stochastic backscatter in a subgrid-scale model: Plane shear mixing layer. *Physics of Fluids A*, 2:297, 1990.

[113] J.R. Chasnov. Simulation of the kolmogorov inertial subrange using an improved subgrid model. *Physics of Fluids*, 3:188–200, 1991.

[114] B. I. Shraiman and E. D. Siggia. Scalar turbulence. *Nature*, 405:639, 2000.

[115] F. Dalaudier, C. Sidi, M. Crochet, and J. Vernin. Direct evidences of "sheets" in the atmospheric temperature field. *Journal of the Atmospheric Sciences*, 51:237, 1994.

[116] E. E. Gossard, J. E. Gaynor, R. J. Zamora, and W. D. Neff. Finestructure of elevated stable layers observed by sounder and in situ tower sensors. *Journal of the Atmospheric Sciences*, 42:2156, 1985.

[117] M. C. Gregg. Microstructure patches in the thermocline. *Journal of Physical Oceanography*, 10:915, 1980.

[118] C. H. Gibson, C. A. Freihe, and S. O. McConnell. Skewness of temperature derivatives in turbulent shear flows. *Physics of Fluids*, 20:S156, 1977.

[119] L. Mydlarski and Z. Warhaft. Passive scalar statistics in high-Peclet-number grid turbulence. *Journal of Fluid Mechanics*, 358:135, 1998.

[120] K. R. Sreenivasan. On local isotropy of passive scalars in turbulent shear flows. *Proceedings of the Royal Society: Mathematical and Physical Sciences*, 434(1890):165–182, 1991.

[121] A. Celani, A. Lanotte, A. Mazzino, and M. Vergassola. Fronts in passive scalar turbulence. *Physics of Fluids*, 13:1768, 2001.

[122] H. Kawamura, H. Abe, and K. Shingai. DNS of turbulence and heat transport in a channel flow with different Reynolds and Prandtl numbers and boundary conditions. *Turbulence, Heat and Mass Transfer*, 2000.

[123] F. Jaberi and P. Collucci. Large eddy simulation of heat and mass transport in turbulent flows. part 2: scalar field. *International Journal of Heat and Mass Transfer*, 46:1827–1840, 2003.

[124] I. Calmet and J. Magnaudet. Large-eddy simulation of high-schmidt number mass transfer in a turbulent channel flow. *Physics of Fluids*, 9(2):438–455, 1997.

[125] W. P. Wang and R. Pletcher. On the large eddy simulation of a turbulent channel flow with significant heat transfer. *Physics of Fluids*, 8(12):3354–3366, 1997.

[126] H. B. Zhou. *Numerical study of scalar turbulence (in Chinese)*. PhD thesis, Tsinghua University, 2003.

[127] J. Rotta. Statistische theorie nichthomogener turbulenz. *Zeitschrift für Physik A Hadrons and Nuclei*, 129:547–592, 1951.

[128] J.L. Lumley. Computational modeling of turbulent flows. *Advances in applied mechanics*, 18:123, 1978.

[129] P. Y. Chou. On velocity correlations and the solutions of the equations of turbulent fluctuation. *Quart. Appl. Math.*, 3:38–54, 1945.

[130] S. V. Poroseva. New approach to modeling the pressure-containing correlations. In *Proc. 3rd Int. Symp. on Turbulence, Heat and Mass Transfer*, 2000.

[131] S.V. Poroseva. Modeling the "rapid" part of the velocity/pressure-gradient correlation in inhomogeneous turbulence. *Center of Turbulence Research, Annual Research Briefs*, pages 367–374, 2001.

[132] P.K. Yeung. Spectral transfer of self-similar passive scalar fields in isotropic turbulence. *Physics of Fluids*, 7:2245, 1994.

[133] L. Fang, G. X. Cui, C. X. Xu, and Z. S. Zhang. Multi-scale analysis of energy transfer in scalar turbulence. *Chinese Physics Letters*, 22(11):2877–2880, 2005.

[134] P. R. Spalart, W. H. Jou, M. Strelets, and S. R. Allmaras. Comments on the feasibility of les for wings, and on a hybrid rans. *Advances in DNS/LES*, page 137, 1997.

[135] G. K. Batchelor. On the spontaneous magnetic field in a conducting liquid in turbulent motion. *Proceedings of the Royal Society of London. Series A*, 201:405, 1950.

[136] H. K. Moffatt, North Atlantic Treaty Organization, Institute for Theoretical Physics, and Scientific Affairs Division. *Topological aspects of the dynamics of fluids and plasmas*. Kluwer Academic Publishers Boston, 1992.

[137] Peter Alan Davidson. *An introduction to magnetohydrodynamics*. Cambridge University Press, 2001.

[138] D. Biskamp. *Magnetohydrodynamic Turbulence*. Cambridge University Press, 2003.

[139] P. S. Iroshnikov. Turbulence of a conducting fluid in a strong magnetic field. *Soviet Astronomy*, 7:566, 1964.

[140] P. Goldreich and S. Sridhar. Toward a theory of interstellar turbulence. ii. strong alfvenic turbulence. *The Astrophysical Journal*, 438:763, 1995.

[141] A. Vorobev, O. Zikanova, P. A. Davidson, and B. Knaepen. Anisotropy of magnetohydrodynamic turbulence at low magnetic Reynolds number. *Physics of Fluids*, 17:125105, 2005.

[142] J. Hartmann and F. Lazarus. Experimental investigations on the flow of mercury in a homogeneous magnetic field. *Det. Kgl. Danske Videnskabernes Selskab.(Math.—Fys. Medd.)*, 15(7):1–45, 1937.

[143] D. Lee and H. Choi. Magnetohydrodynamic turbulent flow in a channel at low magnetic reynolds number. *Journal of Fluid Mechanics*, 439:367–394, 2001.

[144] E. V. Votyakov, E. Zienicke, and A. Thess. Mhd-channel flow of liquid metal under an inhomogeneous magnetic flield. part 2: Direct numerical simulation. In 15^{th} *Riga and* 6^{th} *PAMIR Conference on Fundamental and Applied MHD*.

[145] T. Boeck, D. Krasnov, and E. Zienicke. Numerical study of magnetohydrodynamic turbulence in channel flow. In *The 5th International Symposium on Electromagnetic Processing of Materials*, 2006.

[146] T. Gomez, P. Sagaut, O. Schilling, and Y. Zhou. Large-eddy simulation of very large kinetic and magnetic reynolds number isotropic magnetohydrodynamic turbulence using a spectral subgrid model. *Physics of Fluids*, 19:048101, 2007.

[147] J. Baerenzung, H. Politano, Y. Ponty, and A. Pouquet. Spectral modeling of magnetohydrodynamic turbulent flows. *Physical Review E*, 2008.

[148] O. Agullo, W.C. Muller, B. Knaepen, and D. Carati. Large eddy simulation of decaying magnetohydrodynamic turbulence with dynamic subgrid-modeling. *Physics of Plasmas*, 8(7):3502–3505, 2001.

[149] W. C. Müller and D. Carati. Large-eddy simulation of magnetohydrodynamic turbulence. *Computer Physics Communications*, 147:544–547, 2002.

[150] R.J. Hill. Applicability of Kolmogorov's and Monin's equations of turbulence. *Journal of Fluid Mechanics*, 353:67–81, 1997.

[151] H. Politano and A. Pouquet. Dynamical length scales for turbulent magnetized flows. *Geophysical Research Letters*, 25(3):273–276, 1998.

[152] A.C. Ting, W.H. Matthaeus, and D. Montgomery. Turbulent relaxation processes in magnetohydrodynamics. *Physics of Fluids*, 29:3261, 1986.

[153] Y. Li, E. Perlman, M. Wan, Y. Yang, R. Burns, C. Meneveau, S. Chen, A. Szalay, and G. Eyink. A public turbulence database cluster and applications to study lagrangian evolution of velocity increments in turbulence. *Journal of Turbulence*, 9(31), 2008.

[154] V. Eswaran and S. B. Pope. An examination of forcing in direct numerical simulations of turbulence. *Computers and Fluids*, 16(3):257–278, 1988.

[155] M. R. Overholt and S. B. Pope. A deterministic forcing scheme for direct numerical simulations of turbulence. *Computers and Fluids*, 27(1):11–28, 1998.

[156] H. B. Zhou, G. X. Cui, and J. W. Shu. Parallel calculation for direct numerical simulation of turbulence (in Chinese). *Journal of Nanjing University (Natural Sciences)*, 37:190–194, 2001.

[157] C. X. Xu. *Direct numerical simulation of channel turbulence (in Chinese)*. PhD thesis, Tsinghua University, 1995.

[158] A.N. Kolmogorov. Dissipation of energy in locally isotropic turbulence. *Dokl. Akad. Nauk. SSSR*, 30:16, 1941.

[159] J. Qian. Normal and anomalous scaling of turbulence. *Physical Review E*, 58(6):7325–7329, 1998.

[160] A. M. Obukhov. The local structure of atmospheric turbulence. *Dokl. Akad. Nauk. SSSR*, 67:643, 1949.

[161] V. I. Tatarskii. Use of the 4 / 5 kolmogorov equation for describing some characteristics of fully developed turbulence. *Physics of Fluids*, 17:035110, 2005.

[162] G. K. Batchelor. Pressure fluctuations in isotropic turbulence. *Proc. Cambridge Philos. Soc.*, 47:359, 1951.

[163] D. Lohse and A. Muller-Groeling. Bottleneck effects in turbulence: scaling phenomena in r versus p space. *Physical Review Letters*, 74(10):1747, 1995.

[164] C. Meneveau. Transition between viscous and inertial-range scaling of turbulence structure functions. *Physical Review E*, 54(4):3657, 1996.

[165] U. Schumann. Stochastic backscatter of turbulence energy and scalar variance by random subgrid-scale fluxes. *Proc. R. Soc. Lond. A.*, 451:293, 1995.

[166] S. Ghosal, T.S. Lund, P. Moin, and K. Akselvoll. A dynamic localization model for large-eddy simulation of turbulent flows. *Journal of Fluid Mechanics*, 286:229, 1995.